



UTS

**UNIVERSITY
OF TECHNOLOGY
SYDNEY**

Faculty of Engineering & Information Technology

**A Mild Hybrid Vehicle Control Unit Capable
of Torque Hole Elimination in Manual
Transmissions**

A thesis submitted for degree of
Doctor of Philosophy

Mohamed Mahmoud Zakaria Awadallah

December 2017



UTS

**UNIVERSITY
OF TECHNOLOGY
SYDNEY**

School of Mechanical and Mechatronic Engineering (MME)
Faculty of Engineering & Information Technology (FEIT)

**A Mild Hybrid Vehicle Control Unit Capable of Torque
Hole Elimination in Manual Transmissions**

Research Centre: The UTS Centre for Green Energy and Vehicle
Innovations (GEVI)

Done by: Mohamed Mahmoud Zakaria Awadallah

Supervisor: Prof. Nong Zhang

Co-supervisors: Dr. Paul Walker
Peter Tawadros

Course code: C02018

Subject Number: 49986 Doctor of Philosophy (PhD)

Date: 01/07/2013 to 20/12/2017

University of Technology Sydney (UTS)
P.O. Box 123, Broadway, Ultimo, N.S.W. 2007
Australia

CERTIFICATE

I certify that the work in this thesis has not previously been submitted for a degree nor has it been submitted as part of requirements for a degree except as fully acknowledged within the text.

I also certify that the thesis has been written by me. Any help that I have received in my research work and the preparation of the thesis itself has been acknowledged. In addition, I certify that all information sources and literature used are indicated in the thesis.

Signature of Student:

Production Note:
Signature removed prior to publication.

Date: 31 July 2018

Acknowledgements

بِسْمِ اللَّهِ الرَّحْمَنِ الرَّحِيمِ
فَإِنَّ مَعَ الْعُسْرِ يُسْرًا (٥) إِنَّ مَعَ الْعُسْرِ يُسْرًا (٦) (سورة الشرح)

For indeed, with hardship {will be} ease (5). Indeed, with hardship {will be} ease (6).
{Quran, The Soothing/ash-Sharh 94}

First and foremost, my sincere thanks to Allah, who endowed me to complete this PhD degree.

I would like to sincerely thank my supervisor Professor Nong Zhang, thank you for all your guidance, support and the opportunities you have presented to me. Your managerial skills and uncompromising quest for excellence always motivated me to present the best of what I can. Dr Paul Walker, my Co-supervisor, thank you for all the hours of collaboration, insightful ideas and constant pursues of research output. Together with Prof. Nong Zhang, you have been both a source of inspiration that continued to support me to achieve the research goals.

I wish to acknowledge the support of the following people Dr Paul Walker and Mr Peter Tawadros for their assistance and support my research during my candidature. Thanks also extend to my UTS colleagues whose advice, humour and knowledge have helped me focus and provided entertainment through this journey.

Special thanks must go to my parents for their continuous support, prayers, encouragement and for motivating me to seek a high reduction. I would also like to sincerely thank my family who was always there to support me and making it easy for me to concentrate on my research.

Financial support for this project is provided jointly by the Australian Research Council

(Linkage ID number LP0775445) moreover, The UTS Centre for Green Energy and Vehicle Innovations (GEVI).

Abstract

This thesis describes a new technique for eliminating the “torque hole” in conventional manual transmission-equipped vehicles (CV). This technique involves designing a hybrid control system for a hybridized powertrain, which was used in the development of the new control techniques. To develop a mild hybrid electric vehicle (MHEV) that is both relatively cheap to manufacture, and offers smooth torque transfer during a gear change, as well as a degree of damping against torque oscillation. It needs a small electric motor (EM) at the transmission output, in addition, clutch position measurement, and optionally, automatic actuation. The function of the motor is to eliminate or reduce the torque hole during gear changes by providing a tractive force when the clutch is disengaged, and also provide damping, particularly during gear changes and take-off. In another instance, the electric motor may act as a motor or generator in certain driving situations. The MHEV requires only a single EM in its powertrain to function as an electric motor or generator in different time intervals controlled by an energy management strategy (EMS). In other words, the motor of the vehicle act as an accelerator during acceleration to assist Internal combustion engine (ICE) and act as a generator during deceleration. This powertrain uses electric energy sources in the form of battery or ultracapacitors pack.

In this work, through a power flow analysis of the powertrain, the main vehicle components were sized according to the vehicle parameters, specifications and performance requirements to meet the expected power requirements for the steady-state velocity of an average typical small 5-passenger light vehicle. After the sizing process, the components were selected based on the simulation, which was based on a 1990 Mazda MX-5 (Miata). Then, the model of individual components that make up the overall structure of the MHEV powertrain, are

developed in Simscape/Simulink environment and the Simscape and SimDriveline tool boxes environment to study their operational performance in various drive cycles measured under real-life conditions. The accuracy of the model is verified and validated by a comparison between the simulation results from the CV and the Advanced Vehicle Simulator (ADVISOR) codes during a number of standard drive cycles.

This project aims to develop a low-cost electric hybrid drive system for small vehicles as a proof of concept. The hybrid drive system being developed is such that in a mass-manufacturing situation the total extra cost of the system should not exceed 5% over the expense of the base vehicle as manufacture cost for hybridization to include motor, inverter, and battery. Such a system would be suitable for low-end cars typically sold in developing nations and would serve both to reduce fossil-fuel dependency in these regions as well as improve air pollution characteristics, which are typically poor owing to urban particulate matter. Extensive analysis has been conducted on the fuel economy, greenhouse gas (GHG) emissions, electrical consumption, operation cost and total lifetime cost computed for different standard drive cycles.

Dynamic investigations of the system with numerous degrees of freedom are conducted in this thesis, and the resulting sets of equations of motion are written in an indexed form that can easily be integrated into a vehicle model. Lumped stiffness-inertia torsional models of the powertrain will be developed for different powertrain states to investigate transient vibration. The mathematical models of each configuration, using eight degrees of freedom (DOF) for the MHEV, compared to seven degrees of freedom for a CV. Free vibration analysis is undertaken to compare the two powertrain models and demonstrate the similarities in natural frequencies and mode shapes.

The impact of motor power on the degree of torque hole compensation is also investigated, keeping in mind the practical limits to motor specification. This investigation uses both the

output torque, vehicle speed as well as vibration dose value (VDV) to evaluate the quality of gearshifts at different motor sizes.

A credible conclusion is gained, through different simulation phases in the form of Software-in-the-loop (SIL), Rapid prototyping, and hardware-in-the-loop (HIL) to support the MHEV scenario in the development. The strategies proposed in this thesis are shown to not only achieve shifting performance, driving comfort and energy recovery rate during all conditions but also to significantly reduce cost in both the short and long terms.

Keywords — Automotive; Battery; BLDC; Constraint modeling; Driveability; Driving cycle; Dynamic programming; Dynamics; Emissions; Fuel economy; Gearshift strategy; Hardware-in-the-loop (HIL); Hybrid powertrain architectures; Life cycle assessment; Manual transmission; Mild Hybrid Electric Vehicle (MHEV); Model-Based Design; Operation cost; Optimal control; Passenger vehicles; Rapid Prototyping; Simulation; Torque-fill; Torque-hole; Whole-life costing;

Contents

CERTIFICATE.....	I
ACKNOWLEDGEMENTS	II
ABSTRACT.....	III
CONTENTS.....	VI
LIST OF FIGURES	IX
LIST OF TABLES	XI
ACRONYMS AND ABBREVIATIONS.....	XII
CHAPTER 1: INTRODUCTION.....	1
1.1 Statement.....	1
1.2 Objectives	2
1.3 Scope.....	4
1.4 Outline of the thesis	5
1.5 Publications and Achievements	9
CHAPTER 2: BACKGROUND AND LITERATURE REVIEW	10
2.1 Background.....	10
2.1.1 Environmental protection.....	12
2.2 Literature Review.....	16
2.2.1 Vehicle propulsion systems	17
2.2.2 Hybrid electric vehicle.....	18
2.2.3 Classification based on topology	19
2.2.4 Parallel HEV classification.....	21
2.2.5 Mild HEV.....	24
2.2.6 Automotive transmissions.....	27
2.2.7 Torque hole & shift process analysis.....	31
2.3 Summary.....	32
CHAPTER 3: MHEV PARAMETERS, SPECIFICATIONS AND REQUIREMENTS	
37	
3.1 Motor specifications.....	40
3.1.1 Power calculations	41
3.1.2 Motor type selection	43
3.1.3 BLDC / PMSM	45
3.1.4 The motor ordered.....	47
3.2 Mild hybrid powertrain configuration	49
CHAPTER 4: DYNAMIC MODELING OF A POWERTRAIN.....	52
4.1 Powertrain lumped model formulation	53
4.2 Free vibration analysis	59
4.3 Summary and contributions	63
CHAPTER 5: MHEV MODEL DEVELOPMENT.....	65
5.1 The overall structure of the powertrain model.....	65
5.1.1 Modeling environment.....	66
5.1.2 Vehicle torque model.....	67
5.1.3 Engine model	67
5.1.4 Single dry clutch model	68
5.1.5 Gears model	70
5.1.6 Motor model.....	70
5.2 Transmission actuation and driver model.....	72
5.2.1 Throttle and brake control.....	73

5.2.2	Shift-control strategies for mild HEV	74
5.2.3	Energy management strategy	80
5.2.4	Other drive conditions	83
5.3	Mass constraints	84
5.4	Simulation results	84
5.5	Motor selection	89
5.6	Shift quality	91
5.7	Drive cycles	94
5.8	Summary	98
CHAPTER 6: MODEL VERIFICATION WITH FUEL AND EMISSIONS ANALYSIS 100		
6.1	Survey and discussion of the choice simulation tool for verification	101
6.2	Validation conventional vehicle model	103
6.3	Analysis of fuel economy and electricity consumption	104
6.3.1	Physical performance benchmarking and torque-hole elimination	105
6.4	Direct emissions	107
6.5	Low and high-density traffic patterns drive cycles	109
6.6	Driver classification	117
6.7	Summary	120
CHAPTER 7: A COMPARATIVE STUDY OF BATTERY AND ULTRA-CAPACITORS 123		
7.1	NiMH battery	125
7.2	Battery SOC	126
7.2.1	SOC battery model	126
7.3	Impact of regenerative braking on the SOC of the battery during the example of high congestion drive cycle	128
7.4	Ultracapacitor SOC	130
7.4.1	Capacity calculation	132
7.5	Summary	134
CHAPTER 8: COST ANALYSIS 136		
8.1	Production Cost	137
8.1.1	Electric propulsion system (EPS) Cost	138
8.1.2	Battery cost	140
8.2	Payback period	140
8.3	Ultracapacitor cost	141
8.4	Vehicles daily and annual operation cost	142
8.5	Summary	143
CHAPTER 9: MODEL-BASED DESIGN OF AN AUTOMOTIVE MHEV 145		
9.1	Design and system definition	147
9.1.1	Simulation model	149
9.2	Prototyping and deployment	150
9.2.1	EPS architecture	151
9.2.2	Traction motor	154
9.2.3	Supervisory controller	154
9.2.4	EPS control panel	156
9.2.5	Motor control	159
9.2.6	Protoshield kit and relay shield board	160
9.2.7	Mechanical coupling	160
9.2.8	Shaft	162
9.2.9	Companion flange	162

9.2.10	Validation.....	163
9.2.11	Testing results	167
9.3	HIL phase.....	168
9.3.1	System structure and integration.....	170
9.3.2	Test rig model	177
9.3.3	Control panel.....	178
9.3.4	Electric drive interface levels.....	179
9.4	Test scenario	181
9.5	Summary	185
CHAPTER 10:	THESIS CONCLUSIONS.....	188
10.1	Contributions.....	193
10.2	Future research.....	196
Appendix A	: Internet multimedia.....	197
A.1	Simulink model.....	197
A.2	Thesis softcopy	197
A.3	Presentation.....	197
A.4	Thesis figures	197
A.5	Lab videos and photos	197
Appendix B	: List of publications and achievements.....	198
B.1	Journal Papers	198
B.2	Journal papers under reviewing.....	198
B.3	Conference proceedings.....	198
B.4	Special sessions.....	200
B.5	Awards	200
Appendix C	: Vehicle parameters	201
Appendix D	: HIL test rig.....	202
D.1	EPS.....	202
D.2	IM and ABB.....	202
D.3	Sensors	202
D.4	Eddy brake (AS706)	202
D.5	Couplers	203
D.6	Break-out box.....	203
Appendix E	: Internal combustion engine (ICE) Data.....	205
Appendix F	: Dynamics Calculations	207
Appendix G	: Posters.....	208

List of figures

Figure 1-1: System Architecture	5
Figure 2-1. The global temperature for both the annual and 5-year means [2].	10
Figure 2-2. Greenhouse emissions distribution.	11
Figure 2-3: Energy consumption statistics in different sectors [5].	12
Figure 2-4: Carbon-dioxide emission statistics in different sectors [5].	12
Figure 2-5. Fuel economy standards for new passenger vehicles by country.	14
Figure 2-6: Comparison of global CO ₂ regulations for passenger cars, in terms of NEDC gCO ₂ /km [15].	16
Figure 2-7: Conceptual illustration of an automobile powertrain.	17
Figure 2-8: Forecast for the progress of different drivetrain concepts [20].	19
Figure 2-9: Classifications of HEVs [21].	19
Figure 2-10: HEV architectures based on the position of the motor.	22
Figure 2-11: Different Mild Hybrid Powertrains Architecture [26].	27
Figure 2-12: a. Effect of torque-fill on half shaft torque – torque-fill is shown below	32
Figure 3-1. General powertrain layout with hybridization.	39
Figure 3-2: (a)-(c). NYC cycle analysis.	43
Figure 3-3: Mars 0913 PMSM/BLDC motor.	47
Figure 3-4: Electric motor test facility at UTS.	48
Figure 3-5: Generalised powertrain layout with hybridization (only one gear/synchro pair shown).	49
Figure 3-6: Clutch assembly [58].	50
Figure 4-1: Lumped parameter model for a mild HEV equipped powertrain.	55
Figure 4-2: Natural frequencies of each gear ratio	63
Figure 5-1: A high-level view of the powertrain of the mild HEV model in Simulink.	66
Figure 5-2: Engine map.	68
Figure 5-3: Driver control unit.	73
Figure 5-4: Driver model for throttle and brake.	74
Figure 5-5: Up-shift process.	77
Figure 5-6: Gearshifting schedule.	77
Figure 5-7: The flowchart of an Up-shift process.	78
Figure 5-8: Transmission control unit (TCU).	79
Figure 5-9: EM modes of operation.	82
Figure 5-10: (a)-(b). Rural Drive Cycle simulation for both conventional and mild hybrid vehicles.	86
Figure 5-11: Shift process analysis.	86
Figure 5-12: 0-100 km/h acceleration in ICE and Mild HEV models.	88
Figure 5-13: Output shaft torque profile during 0-100km/h acceleration cycle.	88
Figure 5-14: (a)-(d). Mild hybrid manual transmission performance study with different motor powers.	91
Figure 5-15: Shift-optimized.	93
Figure 5-16: Speed and Torque profile for the NEDC, UDDS and NYCC.	98
Figure 6-1: Benchmarking test: vehicle speed and acceleration profile.	107
Figure 6-2: The speed profile of INDIAN URBAN Drive Cycle.	110
Figure 6-3: The speed profile of the HWFET Drive Cycle.	110
Figure 6-4. Cumulative distribution of daily driving distance in Australia [103].	114
Figure 6-5: The low-density traffic pattern drive cycle.	114
Figure 6-6: The high-density traffic pattern drive cycle.	115

Figure 6-7: Speed and torque profile depending on drive style.....	120
Figure 7-1. Specific energy and power of the main battery technologies [107].....	124
Figure 7-2: Battery SOC calculation in the Simulink environment.....	127
Figure 7-3. SOC profile.	128
Figure 7-4. SOC 50% profile.	128
Figure 7-5: Battery SOC and Speed of High Congestion Drive Cycles.....	130
Figure 7-6: General Powertrain layout with an ultracapacitor.....	131
Figure 7-7: Supercapacitor bank.	133
Figure 7-8: SOC of ultracapacitors with regenerative braking on the NEDC Drive Cycle...	134
Figure 9-1: Model-Based Design Adoption Grid.	146
Figure 9-2: V-Cycle for automotive system design.	147
Figure 9-3: MHEV Powertrain.	148
Figure 9-4: A high-level view of the powertrain of the mild HEV model in Simulink.....	149
Figure 9-5: Automotive Development Process.....	150
Figure 9-6: The functional block diagram of an electric propulsion system.	153
Figure 9-7: System architecture of an electric propulsion system.	154
Figure 9-8: Modeling control design.	157
Figure 9-9: EPS control panel.	158
Figure 9-10: Eddy-current dynamometer and its characteristic curve [140].	160
Figure 9-9-11: Motor Mount.....	161
Figure 9-12: Shaft installation and line drawing (Hardy Spicer, 2014).....	162
Figure 9-13: Companion Flange	163
Figure 9-14: Efficiency map of the electric propulsion system.....	166
Figure 9-15: EPS test facility at UTS.	166
Figure 9-16: Torque and Power vs Speed of the motor at different throttles.	167
Figure 9-17: System structure schematic.....	170
Figure 9-18: Plan view of the test rig.....	171
Figure 9-19: System in the loop.....	171
Figure 9-20: Torque sensors.	172
Figure 9-21: B-DAQ Torque Sensor Calibration.....	173
Figure 9-22: Real torque on the shaft VS Labview display Bluetooth DAQ.	173
Figure 9-23: Induction Motor and ABB ACS355 assembly.....	174
Figure 9-24: Eddy current brake Eaton Dynamatic.	175
Figure 9-25 Kubler Encoder.	176
Figure 9-26: Power supply assembly.....	176
Figure 9-27: The top level of the RTI-Simulink blocks used for the Test Rig.....	177
Figure 9-28: Test rig modeling control design.	178
Figure 9-29: PC display panel for data acquiring, variables changing in ControDesk.....	179
Figure 9-30: HIL Interface Levels.	180
Figure 9-31: shows the torque and rotation speed output of a gearshift from 2 nd to 3 rd gear.	183
Figure 9-32: HIL torque profile.	185

List of tables

Table 2-1: Hybrid classification based on functionalities.....	21
Table 2-2: Existing MHEV with its hybridization factor of various and fuel economy.....	25
Table 2-3: Gearbox Type	29
Table 3-1: Level of hybrid assistance.	37
Table 3-2: Vehicle global specifications.....	39
Table 3-3: Qualitative comparison of commercial electric motors	44
Table 3-4: Selected motor parameters and specifications.....	47
Table 3-5: Mars 0913(Etek Comparable) PMSM/BLDC motor.	47
Table 4-1: Model parameters	59
Table 4-2: Parameters	59
Table 4-3: Damped free vibration results of ICE powertrain and mild HEV in first gear.	62
Table 4-4. Natural frequencies of each gear ratio	62
Table 5-1: VDV profile.....	94
Table 5-2: Characteristic parameters of different driving cycles.....	95
Table 6-1. The reported consumption L/100 km.	104
Table 6-2. Comparison chart for all vehicles tested Fuel and electricity consumption of the modelled vehicles.....	105
Table 6-3. Fuel Economics for conventional and Mild HEV.	105
Table 6-4. Comparison chart for configurations tested through the acceleration event 0-100 km/h	107
Table 6-5. GHG Emissions for conventional and Mild HEV.....	108
Table 6-6: Characteristic parameters of different driving cycles.....	109
Table 6-7: Fuel economy and emissions for INDIAN URBAN drive cycle.	111
Table 6-8. Fuel economy and emissions for HWFET drive cycle.....	111
Table 6-9. Fuel economy and emissions comparison for the composite drive cycles.	112
Table 6-10. The characteristics of low and high-density traffic patterns drive cycles.	115
Table 6-11. Fuel economy and emissions during the developed low and high-density traffic patterns drive cycles.....	115
Table 6-12. Fuel Economics for conventional and Mild HEV by three driver styles.	120
Table 7-1. Battery Specifications.....	126
Table 8-1: Payback period of years.	141
Table 8-2: Vehicle and components parameters and specifications.	142
Table 8-3: Vehicles daily and annual fuel cost under same distance.	143
Table 9-1: KHB1260124.....	159
Table 9-2: EPS test results	168
Table 9-3: McCOLL 180M IM motor.	174

Acronyms and abbreviations

ACG	Auto code generation
ADC	Analog to digital converter
ADVISOR	Advanced vehicle simulator
AGO	Australian greenhouse office
AMT	Automated manual transmission
AT-PZEV	Advanced technology partial zero-emissions vehicle
AWD	All-Wheel Drive
B-DAQ	Bluetooth data acquisition
BLDC	Brushless dc electric motor
BSA	Belt starter alternator
BSG	Belt starter generator
CAFE	Corporate average fuel economy
CAGR	Compound annual growth rate
CAN	Control area network protocol
CO	Carbon monoxide
CO ²	Carbon dioxide
CSHVR	City-suburban heavy vehicle route
CV	Conventional vehicle
CVT	Continuously variable transmission
DAC	Digital to analog converter
DAI	Data acquisition interface
DCT	Dual-clutch transmissions
DOF	Degree-of-freedom
ECU	Engine control unit
EM	Electric machine
EMC	Energy management controller
EMF	Electromotive force
EMS	Energy management strategy
EPA	Environmental Protection Agency
EPS	Electric-propulsion system
ESC	Electronic speed control
EV	Electric vehicles
FEAD	Front-end accessory drive
FOC	Field Oriented Control
GHG	Greenhouse gas emissions
HC	Hydrocarbons
HEV	Hybrid electric vehicles
HIL	Hardware-in-the-loop
I/O	Digital inputs and outputs
ICE	Internal combustion engine
IM	Induction motor
ISG	Integrate Starter-Generator
Li-ion	Lithium-ion
MBD	Model-based design
MHEV	Mild hybrid electric vehicle
MT	Manual transmission
NEDC	New European drive cycle
NiMH	Nickel metal hydride
NO _x	Oxides of nitrogen
NVH	Noise, vibration, and harshness
NYC	New York cycle
NYCDDS	New York city dynamometer drive schedule
OECD	Organization for economic co-operation and development

OEM	Original equipment manufacturer
PC	Personal computer
PID	Proportional–integral–derivative
PM	Permanent magnet motor
PMSM	Permanent magnet synchronous motor
PWM	Pulse width modulation
PZEV	Partial zero-emissions vehicle
RBM	Rigid body mode
RCO	Relative cost of ownership
RCP	Rapid control prototyping
RDC	Rural driving cycle
RPM/rpm	Revolutions per minute
RTI	The real-time interface
RTP	Real-time processor unit
SIL	Software-in-the-loop
SOC	The state of charge
SPF	Sale price factor
SRM	Switched reluctance motor
SULEV	Super ultra-low emissions vehicle
TCO	Total cost of ownership
TCU	Transmission control unit
UDDS	Dynamometer drive schedule
ULEV	Ultra-low emissions vehicle
VDV	Vibration dose value
ZEV	Zero-emissions vehicle

Chapter 1: Introduction

Gear-shifting is one of the most significant concerns in transmission systems since it influences passenger comfort, dynamic performance and efficiency, besides drivability. Automotive transmission technology today revolves around three main technologies. These are the manual transmission (MT), the automatic transmission, and the continuously variable transmission. Each of these categories of technology has their derivatives (for instance, the automated manual transmission (AMT), the dual-clutch transmission, the toroidal CVT, cone CVT and IVT). Of these, the manual transmission is the cheapest to manufacture and offers the highest power transfer efficiency, but also faces drawbacks in terms of customer acceptance (particularly in the North American and Australian markets), and shift quality. In particular, the traditional manual transmission architecture offers very little damping of torque oscillations through the driveline (as compared to other types of transmission architecture), and is incapable of transmitting torque during a gear change. These results in a torque hole which is felt by passengers as “stilted” progress as compared to the relatively smooth delivery of automatic and Conventional Vehicle (CV) transmissions.

This research aims to eliminate the transient transmission torque response in a manual transmission with a mild hybrid technique. It presents a detailed investigation into the torque hole of a typical manual transmission.

1.1 Statement

The development of computationally efficient models of an MHEV equipped with a manual transmission for eliminating of its torque hole, including the characterization and analysis of the hybridization of a conventional vehicle with the electric drive unit. The three most significant and novel aspects of this research are: (1) Modeling and control of a Conventional Vehicle (CV) with hybrid technique, (2) The detailed study of dynamics and vibration

analysis as a part of transmission, and (3) The fuel economy, emissions, and cost computed based on different types of analysis under a wide range of operating conditions.

1.2 Objectives

The recent growing interest in hybrid electric vehicles (HEV) demands an efficient, reliable and economical integrated motor drive and transmission system for propulsion. However, identifying suitable power management technologies and balanced system configurations becomes quite involved when vehicle dynamics and system architecture are considered. This thesis makes an in-depth investigation on developing a manual architecture that is both relatively cheap to manufacture, and offers smooth torque transfer during a gear change, as well as a degree of damping against torque oscillation.

A mild hybrid electric vehicle architecture is proposed incorporating a small electric motor at the transmission output. In addition, clutch position measurement, and optionally, automatic actuation is considered. The purpose of which is to provide the superior Noise/Vibration/Harshness (NVH) characteristics of a vehicle equipped with an automatic transmission, coupled with the fuel economy, and cost benefits of a manual gearbox. The small electric motor at the transmission power output serves multiple purposes:

1. Elimination of the torque hole during gear changes, therefore providing continuous torque during acceleration and avoiding the “stilted” progress commonly associated with manual gearboxes.
2. Active damping of torque oscillations due to harsh clutch engagement, commonly known as “bunny-hopping”.
3. Providing assistive motive power in conjunction with the engine, or loading the engine where necessary, in order to control the engine operating point towards the best possible fuel-efficiency. If the system is run as a mild parallel hybrid (to boost peak performance)).

4. Assisting friction brakes and recapturing braking energy through the driveline, by operating as a generator during braking events.
5. Improving fuel economy by
 - a. “power-buffering” techniques – assisting the engine when it is in low-efficiency regions, and an acceleration demand is high or loading the engine when it is in low-efficiency regions, and acceleration demand is low.
 - b. Improving fuel-economy by regenerative braking technique – generating energy during a braking event whilst assisting friction braking effort.
 - c. Improving fuel-economy by idle-stop and low-speed EV modes.

To achieve these results a detailed model of the MHEV powertrain components and the overall structure with a 5-speed MT was derived. The behaviour of the proposed powertrain was simulated in the Matlab/Simulink environment using a forward-looking modeling approach for different types of analysis. The results were verified and compared the simulation results with advanced vehicle simulator (ADVISOR) codes. Including a comparative study conducted between MHEV and CV powertrains analysing fuel economy, emissions, operation cost and total lifetime cost during the standard drive cycles to investigate the influence of initial and target the state of charge (SOC) of the battery, and effectiveness of the developed EPS.

The proposed system offers significantly decreased complexity over traditional hybrid vehicles, whilst capturing the majority of the benefits. In the case of the driver-actuated clutch mechanism, in order to avoid safety issues related to learned driver behaviour, the torque fill-in function may be turned off or may operate at reduced effectiveness. The other functions of the system would continue to operate as normal. This is not an issue when using automated clutch actuation.

1.3 Scope

This research is focused on the developing a methodology for eliminating the torque hole of the manual transmission in conventional powertrain and improving the fuel economy and emissions by using the mild hybrid technique with low cost. It is explored the functionality of the powertrain in improving drivability, with particular reference to active damping of torque oscillations due to clutch engagement characteristics (the elimination of “bunny-hopping”), as well as regenerating electricity during braking events for fuel-saving, and finally, whether it is advantageous to control the motor in parallel with the engine for electric-assist.

An Energy Management Controller (EMC) is designed for a specific purpose, which is to allow for the MHEV powertrain to act as both an electric generator or motor respectively at different times and having a battery pack for energy storage to capture the regenerative braking as shown in Figure 1-1.

The powertrain parameters and specifications are selected based on a 1990 Mazda MX-5 (Miata) parameters, specifications and performance requirements. After that, a detailed modeling of each component and the overall structure is developed and simulated in the Matlab/Simulink environment in order to predict the behaviour of a real system during the standard and developed drive cycles. Then, the code verification process of the powertrain is conducted by comparing its simulation results with an existing simulation tool, which is the ADVISOR code, pros and cons are discussed. This research also intends to investigate the fuel economy, emissions, operation cost and total lifetime cost of the MHEV powertrain during the different standard and developed drive cycles.

Physical modeling of the major components of mild and conventional powertrains uses Newtonian methods, lumped parameter models and dynamics. The scope includes free and forced vibration analysis of powertrains models.

Finally, to validate the simulation hardware-in-the-loop (HIL) experimental system is utilised to evaluate shift control performance with and without torque compensation. The HIL test rig is used to simulate the output torque of a manual transmission equipped vehicle, with particular reference replicating the torque hole. A secondary electric motor is then used to compensate for this hole on a test bench. This enables verification of the shift control stage of this project.

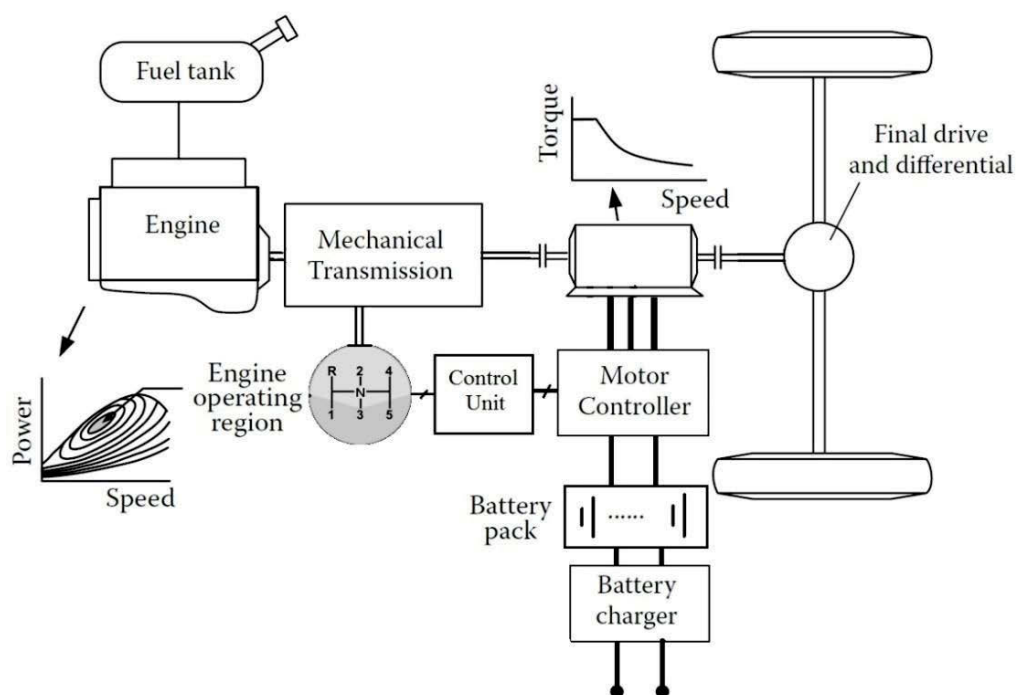


Figure 1-1: System Architecture

1.4 Outline of the thesis

Detailed modeling and analysis methods in this thesis are introduced to sufficiently represent powertrain and component dynamics to aid the reader in their understanding of the procedures applied, and provide clarity and continuity of research. This thesis is divided into ten chapters. Contents of the chapters are subdivided into subsections to maintain the flow of the chapters. The main topics of each chapter are introduced in the following sections.

Chapter 2

This chapter provides the framework for the research of this thesis. Initially, it provides an introduction to the problem in addition to background information, including environmental impacts and vehicle powertrains architectures, such as ICE powered vehicles, electric vehicles (EVs), HEVs and hybrid development trends. This is followed by a detailed literature review examining the required background information on relevant aspects of automotive powertrains, which is presented to introduce the topics for research. Focusing the search on increasingly relevant aspects, manual transmission (MT) equipped MHEV is presented to introduce the topics for research. This is followed by a detailed literature review which identifies the state-of-the-art in MHEV powertrain and major components as well as a review of some studies from the past and other research about the existing vehicle models and simulation tools. To complement this work, a brief exploration of literature is performed in each relevant chapter to identify the important aspects of relevant research, as necessary.

Chapter 3

In this chapter, the details of the powertrain are explained. These include the procedure of components sizing and selection for EM, ICE and battery in order to fulfil the vehicle specifications, parameters and performance requirements. The principles, characteristics and applications of switched reluctance motor, brushed DC motor, induction motor, and permanent magnetic synchronous motor are carefully analysed. Selection is made after the comparison of cost, reliability, controllability, efficiency and power density within above traction motor options.

Chapter 4

The thesis now moves on to the development of the powertrain model and its control. This section presents the mathematical models of each configuration, using eight degrees of

freedom for the mild HEV powertrain, compared to seven degrees of freedom for a conventional powertrain. The specifics of lumped spring-inertia modeling are discussed here, including free vibration results. Finally, the different torque models are introduced. This includes an engine torque model, a clutch model, transmission model, and vehicle resistance torques. Additionally, the fuel-saving oriented shifting schedules for MT are discussed.

Chapter 5

The overview of the MHEV powertrain development is discussed. The power flow management under various drive conditions is explained in this chapter. EM operating tracks are presented under a variety of driving conditions. A general predictive backwards-facing model, which includes the components model system and driving cycles profiles, is applied to Matlab/Simulink to investigate the economic benefit and dynamic performance achievement of the hybrid technique.

Chapter 6

Chapter 6 shows the results of performance analysis, sensitivity study and model verification. Different tests, such as acceleration, gradability and range are simulated using the MHEV powertrain model. A sensitivity study is also conducted on the MHEV powertrain to analyse driving styles. The validation procedure is conducted by comparing the results of standard drive cycles, which are the NEDC, UDDS and NYCC of the CV and the ADVISOR codes. The simulation results from each component are also compared. An analysis of the fuel economy and emissions are compared.

Chapter 7

This chapter aims to develop a mild hybrid system for such markets with a focus on energy storage. A comparison and analysis are undertaken, of both storage system options: a NiMH battery, and an ultra-capacitor with the incorporation of components required for the mild

hybrid system. These were undertaken by running simulation models using Matlab and Simulink. The simulations assessed the powertrains in specific driving conditions, with observations made of the advantages of MHEV over conventional drivetrains.

Chapter 8

The economic benefit is presented, regarding the manufacturing and maintenance cost saving. It focuses on a comparative analysis of vehicle operating cost and total lifetime cost. A comparative study on the total lifetime cost of the MHEV and a CV are estimated calculated in order to present the significant improvement of the MHEV powertrain. After that, the operation cost of fuel under different driving characteristics is calculated.

Chapter 9

This chapter covers the experimental validation of the simulation. It is divided into two parts. The first part is devoted to the rapid prototyping and validation of Mars 0913 Brushless Motor to develop EM for MHEV. The second part discusses developing an HIL simulation to a manual powertrain that offers torque transfer during a gear change, as well as a degree of damping against torque oscillation. The configuration of the lab powertrain testing rig is presented. Torque sensors are carefully calibrated to measure the torque hole. Vehicle control unit comprising a dSPACE prototyping system and the self-designed electric control panel is demonstrated. Parameters are set in the dynamometer to provide the dynamic vehicle resistance on the road.

Chapter 10

The concluding chapter reviews and summarizes this thesis with a general summary of the contributions each of the previous chapters, presenting significant and novel results of this thesis as well as identifying the important areas for further research.

1.5 Publications and Achievements

All Publications details and achievements added in Appendix B.

Chapter 2: Background and literature review

2.1 Background

The world today is facing problems as a result of oil depletion and the rise in earth's surface temperature (global warming). This is a result of the greenhouse gas (GHG) emissions induced by the presence of carbon dioxide and other gases. Figure 2-1 shows the global temperature for both the annual and 5-year means from 1880 to 2010. Based on the global measurements the global temperature pattern is fluctuating, but the overall average temperature trend keeps rising and has resulted in the global warming issues [1].

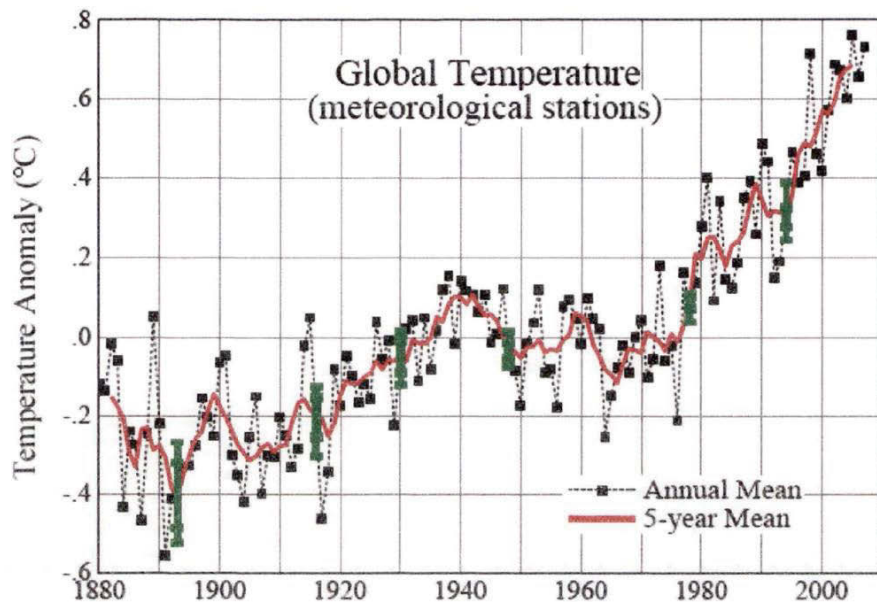


Figure 2-1. The global temperature for both the annual and 5-year means [2].

The primary sources of GHG emissions, and specifically, carbon dioxide, is the combustion of hydrocarbon (HC) fuels and coal. Heat and combustion products are yielded by the ignited reaction of HC fuel in combustion engines. An energy transformation from heat to mechanical power is facilitated by the engine, resulting in atmospheric deposits of combustion products. GHG emissions as contributed by industry can be observed in Figure 2-2. Fossil fuels have become a huge resource of reliance for the present global transportation sector. Unfortunately, this use has contributed to the detrimental effects of ozone layer

depletion and air pollution – or global warming factors. Additionally, excessive usage of fossil fuel in vehicles is a reason behind dwindling of underground petroleum resources. The transportation sector is clearly now the major contributor about one-third of the emissions produced each year. It consumes about 49% of oil resources. Following the current trends of oil consumption and crude oil sources, the world’s oil resources are predicted to be depleted by 2038 [3].

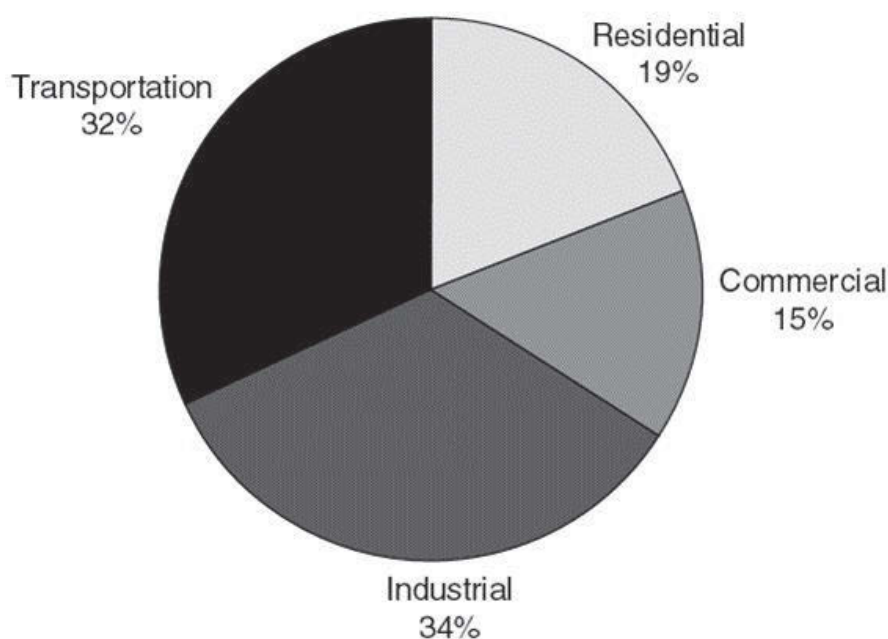


Figure 2-2. Greenhouse emissions distribution.

Both energy consumption and carbon dioxide emissions as contributed by different sectors in more modern times can be observed in Figure 2-3 and Figure 2-4. There is also an extrapolation of predicted figures for future times. Current population trends show growth from 6-10 billion in the next 50 years. Along with this, an estimated increase of 700 million to 2.5 billion will be seen with vehicle ownership and usage. On the assumption that most of these vehicles employ Internal Combustion Engines (ICE’s), this raises many concerns about the sustainability of the source of energy (i.e. oil) and the harsh effects seen by their usage (i.e. emissions). These potential problems and the desire for a sustainable future create the motivation for society to find alternate solutions for road transportation [4].

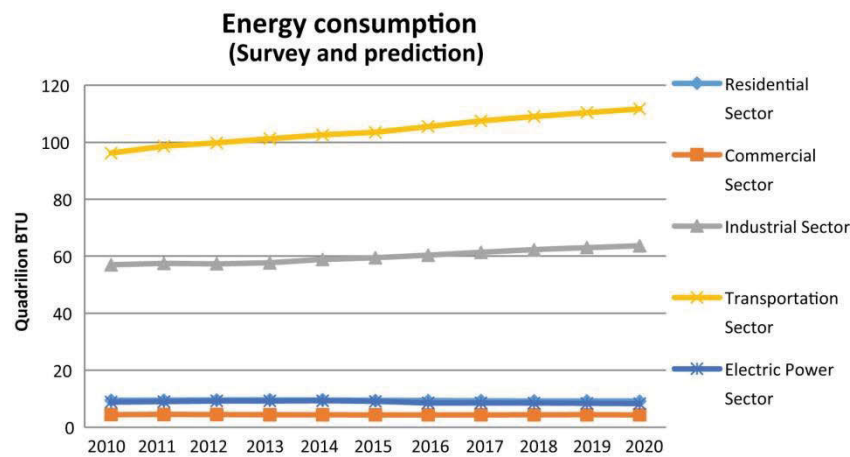


Figure 2-3: Energy consumption statistics in different sectors [5].

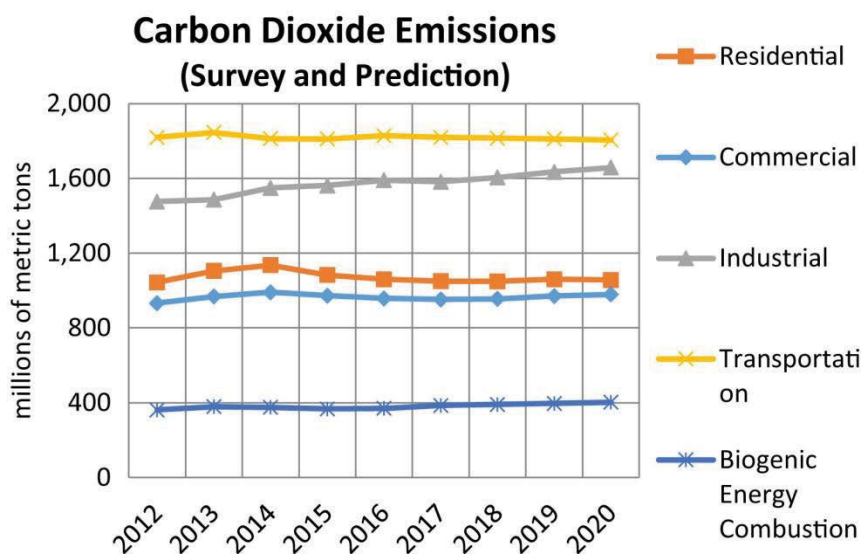


Figure 2-4: Carbon-dioxide emission statistics in different sectors [5].

2.1.1 Environmental protection

To protect the environment on individual, an organisation controlled or governmental levels that have been recognised, governments have begun placing restraints on activities that cause environmental degradation through agreements and standards by government agencies to create awareness of the various environmental issues. Agencies are essential in having both a foundation and continuation of upholding required standards of environmental sustainability and the ability of the environment to sustain life. Formal environmental protection in the USA is through the Environmental Protection Agency (EPA) agency, responsible for writing and enforcing regulations based on laws passed by Congress. Elements of the controlled

GHG emissions include Nitrogen Oxides (NO_x), Hydro Carbons (HC), Carbon Monoxide (CO), and particulate matter (PM). One of the major contributors to urban air pollution is the emissions in the transportation sector. In Australia, the environmental protection portfolio is regulated by the Australian Greenhouse Office (AGO) and membership the Environment Committee of the Organisation for Economic Co-operation and Development (OECD). The OECD is an intergovernmental economic organisation with 35-member countries.

In the face of ever-tightening emissions regulations, automotive researchers and OEMs the world over are racing to develop new, complex control methods of multi-modal hybrid powertrain architectures [6, 7] or eke minuscule but repeatable gains in efficiency out of a vehicle through careful and painstaking review of construction and optimization [8, 9]. This activity is a recognition of the significant impact the transportation sector has in worldwide energy consumption and GHG emissions, accounting for some 27% of worldwide energy consumption and 33.7% of GHG emissions [10]. The developed markets of the US, Japan, and Europe, as well as other OECD countries, are primary buyers of ULEV (Ultra-Low Emissions Vehicle), SULEV (Super-ULEV) PZEV (Partial Zero-Emissions Vehicle), AT-PZEV (Advanced Technology PZEV) or ZEV (Zero-Emissions Vehicle) vehicles and see their direct benefit. According to the OECD [11], many of the member countries have consistently achieved reductions in atmospheric pollutant levels since 2005. However, the world still faces problems of climate change and oil depletion, and the uptake of modern vehicle technology has altered the distribution of air pollution. If we are to inspect the distribution of air pollution levels in cities worldwide, it is no longer these developed regions that are the problem. A clear trend describing increasing mortality in the developing, low-income cities of the world is emerging [12]. The inhabitants of these cities, whether they are limited by circumstance or availability, are also those least likely to be able to purchase a new low-emissions vehicle. A new problem has therefore emerged for engineers to solve. That is:

how can we bring the benefits of low-emissions technology to the people who need it the most, but can afford it the least?

This question will be explored through the framework of a prototype vehicle, which is designed to bring the benefits of hybrid vehicle architecture to developing markets at an attractive price-point, and with attractive low-cost features suitable for these particular markets. A financial analysis is conducted in which the vehicle production cost and total operating cost are estimated. This is accomplished by breaking the mild hybrid vehicle and conventional vehicle down into major components or systems and accounting for the price difference between the conventional vehicle and the hybrid. By examining the difference in price rather than the absolute cost of ownership of each vehicle, variations in energy costs are highlighted and quantified [13]. Further development potential and improvements in the economy through optimisation of the electrified powertrain are also discussed.

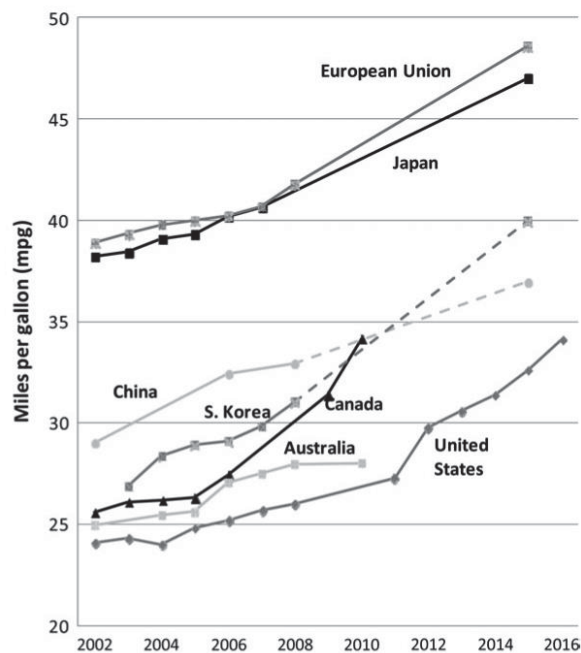


Figure 2-5. Fuel economy standards for new passenger vehicles by country.

Corporate Average Fuel Economy (CAFE) standards were enacted to improve the average fuel economy of cars and light trucks. Every country has its own test method to measure the CAFE standards and also the implementation requirements. Figure 2-5 summarises the fuel

economy standards for passenger cars model by countries that have similar programs in miles per gallon (mpg). The automakers required to follow the CAFE standards and keep the total emissions below specified levels. Otherwise, they may face penalties for failing to meet those standards [14].

The relationship between EU CO² passenger car standards alongside other comparable global regulations can be seen in Figure 2-6. Europe proves to be superior in regards to the legislation it has put in place for emissions. This is defined by its projected goal of 95g of CO²/Km in 2021, signifying 27% and 50% decrease from 2015 and 2010 levels respectively. The US has intended to decrease its 2010 level by approximately 50%, represented by its 2020 target of 109g of CO²/Km. Analogous trends have been observed in Asian countries, with the following target values: China to meet 117g CO²/Km and Japan to meet 105g CO²/Km both by 2020, and India to meet 113g CO²/Km by 2021. It has proven to be a challenging task to comfortably reach these standards. In order to both decrease the loss of energy, while improving efficiency in regards to the internal combustion engine and vehicle powertrain system, novel technologies must be taken on board and implemented. Some methods have been presented by research and industry sectors over the last two decades to tackle this problem. These include the implementation of turbochargers with the intent to increase fuel efficiency or the use of catalytic converters served with the purpose of removing detrimental gases. These implementations have already proven beneficial in the automotive industry. However, they have not been able to combat the growing threat of increased emission levels due to the direct relationship of growing vehicles on the road. As such, it is necessary to find an overwhelmingly effective solution through novel technologies. Many automotive manufacturers to produce alternative vehicles such as Hybrid Electric Vehicles (HEVs), Electric Vehicles (EVs), and Plug-in Hybrid Electric vehicles (PHEVs), which are more environmentally friendly and fuel-efficient without sacrificing the comfort and drive

performance of current ICE powered vehicles. New types of clean and energy efficient vehicle powertrains are urgently needed in order to boost vehicle fuel economy, and at the same time mitigate the harmful emissions. The next section presents an overview of existing vehicle powertrain architectures also describes a trend of hybrid development by a few major car manufacturers.

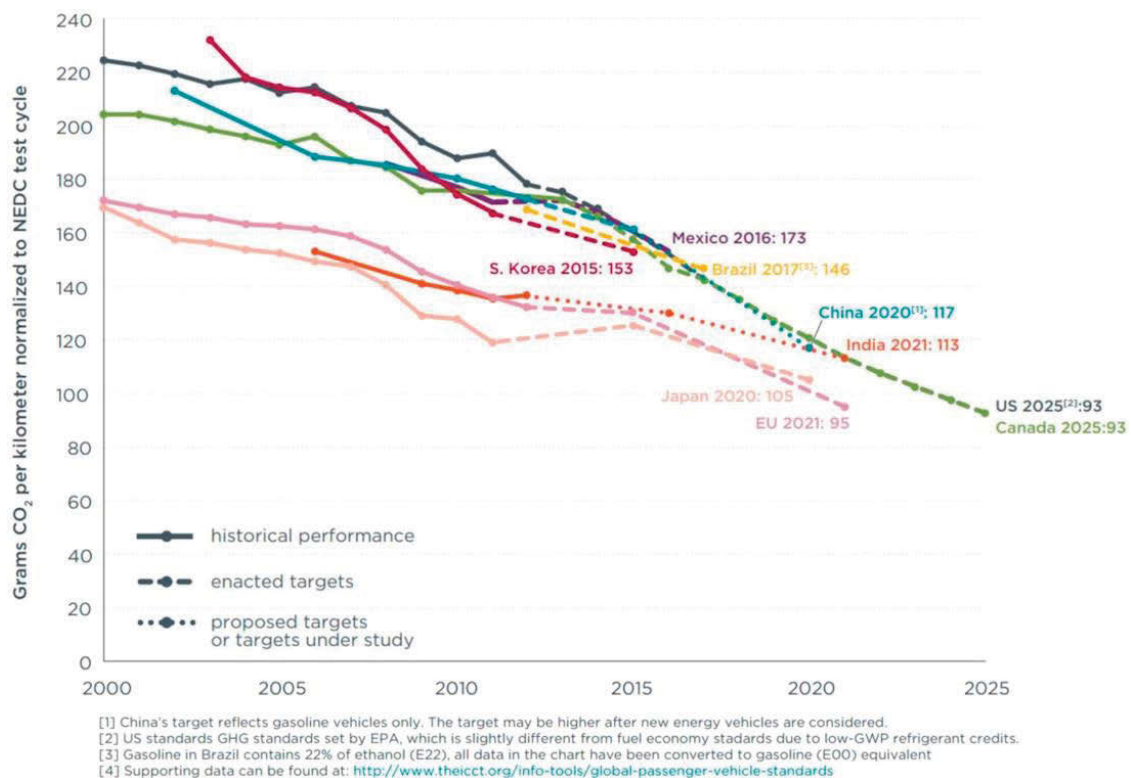


Figure 2-6: Comparison of global CO₂ regulations for passenger cars, in terms of NEDC gCO₂/km [15].

2.2 Literature Review

An automotive powertrain has many components that serve a certain purpose for its overall function. This system can be visualised in Figure 2.7. The main components that comprise this system include a power plant (either an engine or electric motor), a clutch or torque converter (depending on manual or automatic transmission respectively) and the gearbox (which defines the nature of the transmission type). Along with these components are included the final drive, differential, drive shaft and the propelled wheels. The power plant provides both torque and rotating speed that directly drives the wheels. In manual transmissions, the purpose of the clutch is to couple/decouple the gearbox from the power

plant. In an automatic transmission, the torque converter is by its nature a hydrodynamic device. It has a continuously variable rotation ratio but serves the same role as a clutch would in a manual transmission system.

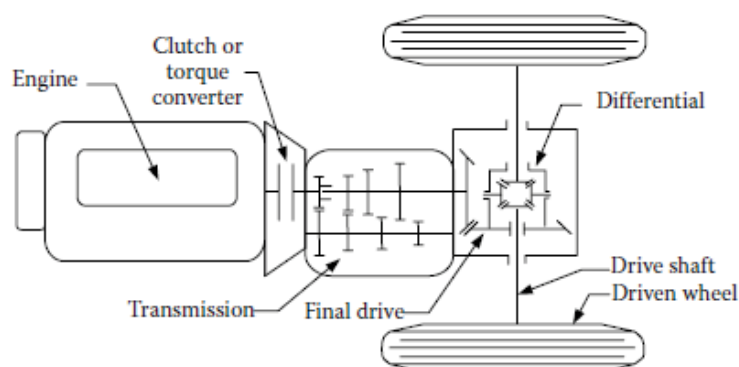


Figure 2-7: Conceptual illustration of an automobile powertrain.

An efficient vehicle powertrain system has a general purpose that it is required to fulfil. These principles are mainly (1) deliver a standard of desired vehicle performance by providing appropriate power, (2) support the longevity of vehicle driving and usage by adequate onboard energy, (3) provide increased efficiency, and (4) minimise the contribution of pollutants to the environment. It is possible that a vehicle may employ more than one powertrain in its system if the powertrain is defined by the source of energy it utilises with the power converter it employs for a power source. Examples of these systems include gasoline (or diesel) heat engine, hydrogen fuel cell-electric motor, and chemical battery-electric motor. The term used for vehicles that are defined as having these combination powertrains are known as hybrid vehicles. Vehicles with an electrical powertrain system are known as Hybrid Electric Vehicles (HEV). The culmination of all of the different powertrains employed in a vehicle system is referred to as the drivetrain.

2.2.1 Vehicle propulsion systems

Due to the high energy density properties of petroleum fuels, conventional vehicles with internal combustion engines can deliver both increased levels of performance and duration of

the operation. With these advantages, there are also disadvantages, which include inefficient fuel economy and adverse environmental contributions. In comparison, Electric Vehicles (EV's) have almost reversed characteristics in terms of their advantages and disadvantages. They are found to have much higher energy efficiency, and detrimental environmental tailpipe emissions are non-existent. However, due to the inferior energy density of batteries when compared to gasoline, both performance and operation range per battery charge compare poorly to IC engine systems. It can be safely assumed that IC engines will continue to dominate the vehicular market in the near future. In saying this, the utilization of Hybrid Electric Vehicles (HEV's) that use two power sources (primary and secondary power sources) allow for a compromise between each powertrain's advantages coupled with the compensation of their respective disadvantages. More specifically, they provide higher fuel efficiency and lower emissions through the combination of the conventional internal combustion engine coupled with electric machines in varying degrees of hybridization [16]. According to Figure 2-8, the market share of hybrid vehicles will significantly increase by the year 2022. Conventional ICE's will likely still retain the majority of the market share, but HEV's will likely become far more competitive in the market [17].

2.2.2 Hybrid electric vehicle

The decline in worldwide oil reserves as well as increasingly stringent emissions legislation has made improvements in fuel economy and efficiency ever more critical. Industry, engineers and scientists have all raced to develop new solutions and innovations to address this need. Hybrid Electric Vehicles (HEV's) are one such development, able to address the problem by introducing powertrains into vehicles with additional propulsion systems and bi-directional energy flows, reducing reliance on fossil fuels. The major types of hybrid systems being used in hybrid vehicles currently on the market are shown in Figure 2-9, according to the power flow within the powertrain [18, 19].

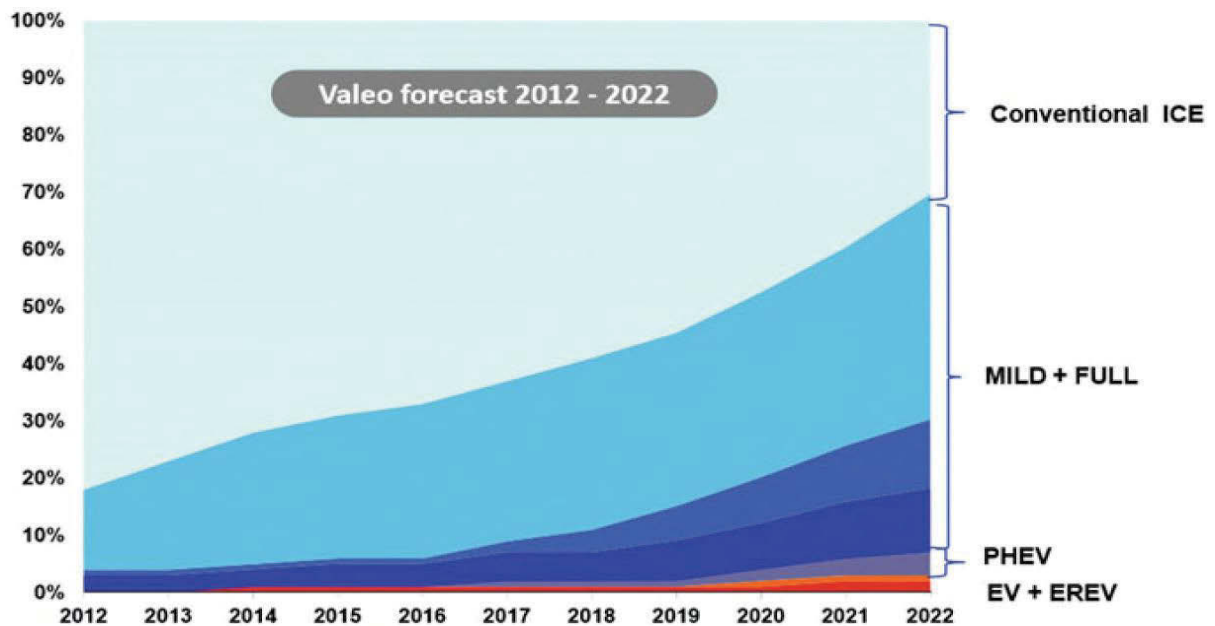
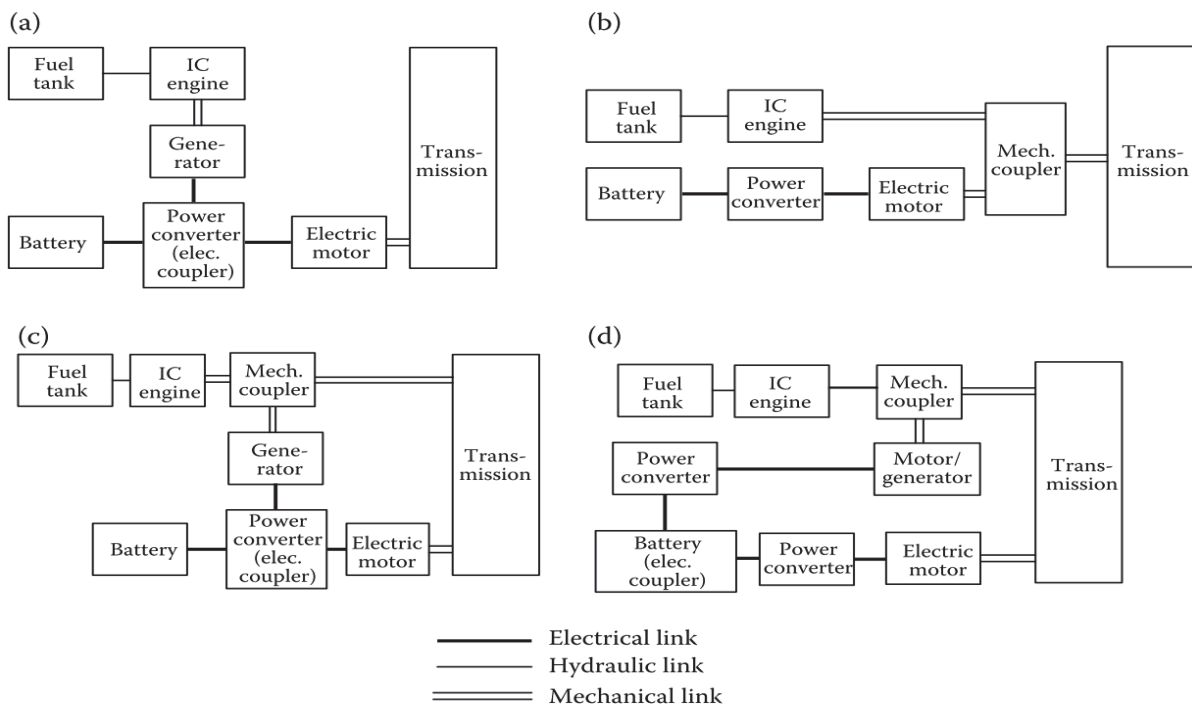


Figure 2-8: Forecast for the progress of different drivetrain concepts [20].



(a) Series, (b) parallel, (c) series-parallel, and (d) complex.

Figure 2-9: Classifications of HEVs [21].

2.2.3 Classification based on topology

1. Series hybrid system

The engine powers a generator, which in turn delivers energy to power an electric motor responsible for turning the wheels. Such a system is referred to as a series hybrid system due to the nature of the relationship starting from engine power, to motor power, to power

transmitted to the wheels. This series hybrid system has demonstrated the ability to output steadily efficient power within a defined operating range, with adequate output to both power the motor and charge the battery. Two electric motors are employed. However one of these motors acts as a generator to provide electricity to the other motor. An example of this system usage can be seen in the Coaster Hybrid by Toyota. This design results in a simple mechanical connection to the wheels and control strategy compared to the parallel HEV and allows more freedom in the component placement. This can provide excellent fuel economy, even under the varying loads during urban drives. On the other hand, the major weakness is the higher weight and cost because the ICE, generator and motor are arranged in series and must all have full capacity.

2. Parallel hybrid system

Just like the series hybrid system, a parallel hybrid system is so called due to the nature of the relationship between the engine and electric motor in driving the wheels. In this case, both these components can provide direct power to the wheels, dependent on the most suitable conditions for their implementation. The electric motor can act as a generator to charge the battery, or as an electric motor to drive the wheels (with power from the battery). However, it can only serve one of these functions at a time. The ICE operation can be optimized, with the electric motor sharing the power flow to the wheel in parallel. A parallel HEV usually can provide better highway fuel economy, due to its efficient ICE loading at steady highway speeds, and possibly less mass. It also provides the ability to withstand long uphill grades. The control strategy and transmission in a parallel HEV powertrain configuration is complex, and a full-size ICE is required.

3. Series/Parallel hybrid System (Split Powertrain)

Once again, the name suggests a combination between both series and parallel component configurations in driving the wheels. This allows for a sharing of the benefits arising from

both systems. It comprises of two motors, with one motor driving the wheels alone or in combination with the engine (depending on the most efficient mode of operation) and the other motor acting as a generator to charge the battery. This means that there can be simultaneous electrical charging and electrically-powered driving.

4. Plug-In hybrid system

A plug-in hybrid vehicle (PHEV's) can employ either hybrid configurations, with an external power source to charge the battery (i.e. external established power grid). This means that the vehicle can spend more time operating under a solely electric mode. The batteries can be easily charged via an AC outlet power source or at designated power stations set up for such vehicles. Allowing for the possibility for external charge has made a big contribution to the development of hybrid vehicle technology.

2.2.4 Parallel HEV classification

1. Classification based on levels of powertrain hybridization

Table 2-1 shows the degree to which hybridisation can be achieved and integrated into a system. Elements like engine stop/start operation, regenerative braking, modification of engine operation points and differing degrees of hybrid electric propulsion assist all determine and define the overall system of hybridisation that can be employed in an HEV. On the other hand, such measures involve different levels of powertrain hybridization, including micro, mild, and full HEV [22].

Table 2-1: Hybrid classification based on functionalities

Hybrid System type	Engine Start/Stop	Regenerative braking	Motor Assist	Electric drive	Motor Main Power	Power grid (recharge)	System Voltage	Trend
Micro HEV	YES	No	No	No	No	No	~12V	Citroen C3 VW Passat BlueMotion
Mild HEC	YES	YES	Modest	No	No	No	~42V	Honda Insight, Civic
Full HEV	YES	YES	YES	Modest	No	No	~144V	Toyota Prius
Plug-in HEV	YES	YES	YES	YES	YES	YES	>200V	Chevrolet Volt Honda Accord

2. Classification based on the position of the secondary energy converter

Where full and mild hybrid architectures are concerned, the position of the electric motor (EM) within the powertrain is fundamental to the capabilities that are possible to design into the powertrain, as well as the ease with which the powertrain may be modified from a conventional (IC-only) base vehicle. The choice of which topological configuration must be made bearing in mind the strengths and weaknesses of each possibility. These possibilities are described below, using the position of the electric motor relative to the internal combustion engine as a reference Figure 2-10 [23, 24].

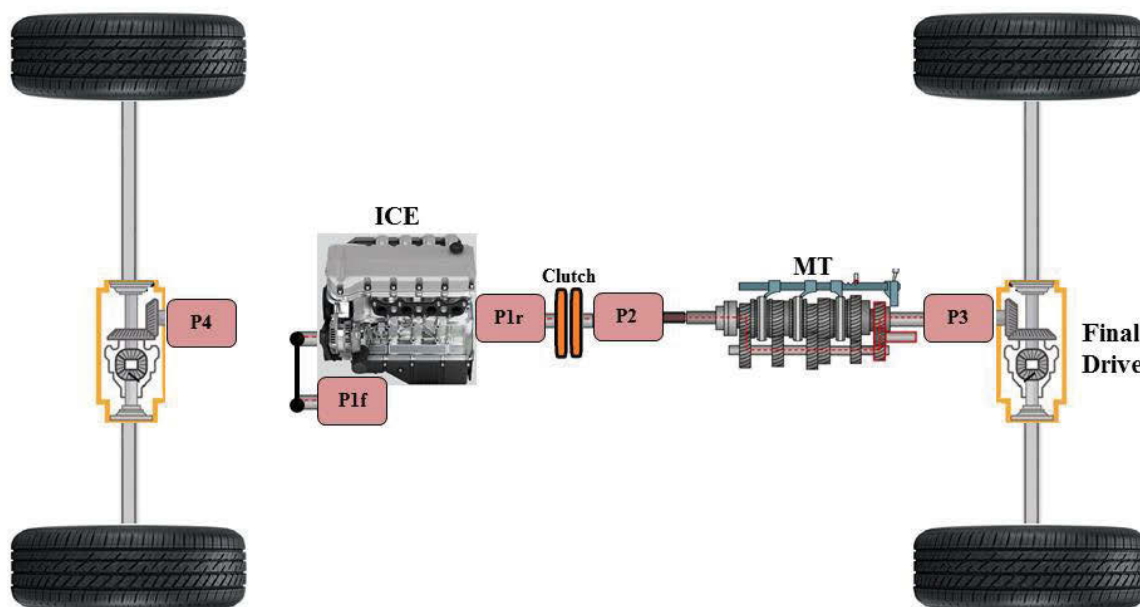


Figure 2-10: HEV architectures based on the position of the motor.

A. P1-front (P0)

The P1 configuration entails an electrical machine placed on the front-end accessory drive (FEAD) of the engine. This machine can drive accessories independently of the engine as well as assisting the engine to propel the vehicle. The configuration can also be used for regenerative braking. However, the efficiency in this mode is quite low, as parasitic losses occur along the entire driveline, through the final drive, transmission, engine, and belt. Because of space constraints, high power density is required, and therefore the electric machine must rotate at high velocity (typically, 15-18,000 RPM) with a large gear reduction

in order to develop appropriate torque and power. However, the design provides a high degree of cost-effectiveness.

These systems are typically described as belt starter-alternator (BSA), or belt starter generator (BSG) systems.

B. P1-rear

This configuration sees the electric machine located on the output of the engine crankshaft, ahead of the drivetrain. The electric machine is often integrated with the flywheel to improve transient torque response. This configuration can be harder to package and requires motor characteristics exhibiting high torque density. The benefits include better regenerative braking performance and relatively simple design.

C. P2

ICE - dependent in previous configurations, the P2 configuration decouples the electric motor from the engine by placing it behind the clutch plate. This configuration allows the independent operation of both devices, which provides greater opportunity for optimization as well as possibilities such as a pure electric drive mode. This also reduces drive losses by placing the electric motor downstream of engine pumping losses and inertia. The motor is still constrained by size due to its location at the transmission bell-housing. P2 can be an Integrate Starter-Generator (ISG).

D. P3

Continuing to move the electric machine downstream, this configuration sees the electric motor placed at the driven shaft of the transmission. This configuration has the same characteristics as the P2 configuration but for further increased efficiency and regenerative braking is, in this case, maximized, due to the location of the electric motor closer to the driven wheels, which eliminates losses through the transmission and clutch assembly. P3 does allow for torque fill on gear change.

E. P4

This configuration places the IC engine on one axle and drives the second axle using an independent electric powertrain. The two powertrains are linked electrically, but there is no mechanical connection. Usually, this is provided by using the IC engine to drive a charging generator to charge a traction battery, and/or supplementing this power with plug-in charging capability. The electric motor connects to two wheels on a single axle, usually through a mechanical differential, although two electric motors may be used to drive each wheel independently, eliminating the mechanical differential. This configuration generally provides the highest flexibility and efficiency, by eliminating any complex componentry between the wheels and motor. P4 has the potential to perform the All-Wheel Drive (AWD) function.

2.2.5 Mild HEV

Full hybrid drivetrains have vast differences in configuration and component relationship when compared to drivetrains with a more conventional system. HEV's (regardless of their specific configuration) are more efficient in optimising engine operation with the added benefit of regenerative braking. This efficiency comes at the ironic expense of needing an inefficient power source like a battery, which may be both heavy and cumbersome. The implications of their usage include spatial complications in fitting the system within the body of the vehicle, a decrease in loading capacity and the loss of energy from the loaded tyres. Time, money and determination are essential factors in diverting away from conventional drivetrains and more toward full hybrid vehicles. A strategy to aid in this is to provide a solution that allows for a conversion of conventional drivetrains to hybrid technology that is both cost-effective and increases efficiency. In a practical sense, one way this could be achieved is by employing a small electric motor behind the engine that operates as both an engine starter and an electrical generator. Another added benefit of this motor is that it can provide on-demand power to the drivetrain when needed and gain extra power through the

use of regenerative braking. The implementation of such a system is referred to as a mild/soft hybrid electric drivetrain. Mild hybrid vehicles represent a compromise between the high cost of fully hybridized vehicles and the high emissions and fuel consumption of conventional internal combustion engine (ICE) powered vehicles. This fundamental observation suggests that mild hybrid vehicles may be well-suited to developing regions. These regions are often price-sensitive but also are most often in need of low-emissions technology. The greater goal of the work described herein is to investigate this identified market need and propose a vehicle that could fulfil the dual goals of having a remarkably low manufacturing cost, but also delivering reasonable emissions performance.

The most significant variation that can be seen between different Mild hybrid powertrain architectures is in the transmission systems, but there are also various energy storage options, with batteries by far the most popular. This small motor can potentially replace the clutch or the torque converter, which is inefficient when operating with a high slip ratio. Several of the most popular automakers around the world, particularly Honda Motor Company, Toyota Motor Company, GM Company, BMW and Nissan Motor Company, are making great efforts to introduce and produce MHEV into the automotive market. Table 2-2 lists the existing MHEV design from the Hybrid development trends. Production examples of mild hybrids include the Honda Civic HEV and Honda Insight as well as the Toyota Crown Royale with a parallel type of powertrain configuration [10].

Table 2-2: Existing MHEV with its hybridization factor of various and fuel economy.

Name of the vehicle	Hybridization ratio (hp) (P_{EM}/P_{total})	Hybridization factor (HF)	EPA fuel economy (mpg)
BMWActiveHybrid 7 2012	15/455	0.03	20
Honda Insight 2012	13/111	0.12	42
Honda Civic Hybrid 2012	23/110	0.21	44

Honda stands out as a pioneer of Mild Hybrid technology with its Integrated Motor Assist (IMA) system. Honda offers the IMA architecture in its Civic, CR-Z, Insight and Jazz hybrid models. Honda CR-Z is one of the most typical representatives for mild HEV. The working principle of mild HEV is summarized as follows: when the vehicle starts, the electric generator comes alive while the petrol engine is shut down. Subsequently, all the working equipment will rely solely on the electric motor. When the brake pedal is released, and the vehicle is accelerated, the petrol engine will start and continuously provides the entire propulsion under fast speeds. These processes result in a significant feature: the engine should be shut down once the vehicle stops, which is known as an idle stop-start feature. The battery is primarily recharged when the vehicle is either decelerating and/or braking. The design of ISG requires both engine and electric motor to work collaboratively when heavy acceleration is required [25]. The General Motors offers eAssist system can be seen in the Buick LaCrosse and Regal models and the Chevrolet Malibu Eco. The real difference between the eAssist and IMA systems is that the former couples the motor to the engine's crankshaft through a belt, whereas the latter couples them directly. The eAssist system uses an induction motor, where permanent magnet synchronous motors are used in most hybrid powertrains. Figure 2-11(a) displays an overview of the powertrain architecture from the current Civic Hybrid model. It assisted by a 10 kW permanent magnet synchronous (PMS) motor attached to the crankshaft and powered by a 144 V NiMH battery pack. The Honda CR-Z is marketed as a sporty hybrid and contains the same electrical architecture but offers a choice of CVT with paddle shifters or manual 6-speed transmission as shown in Figure 2-11b. Daimler and BMW offer very similar systems in the Mercedes-Benz S400 Hybrid and BMW ActiveHybrid 7 models but with standard automatic transmissions (Figure 2-11c). The Buick LaCrosse with the eAssist system and 2.4 L gasoline engine and automatic transmission, as shown in Figure 2-11d.

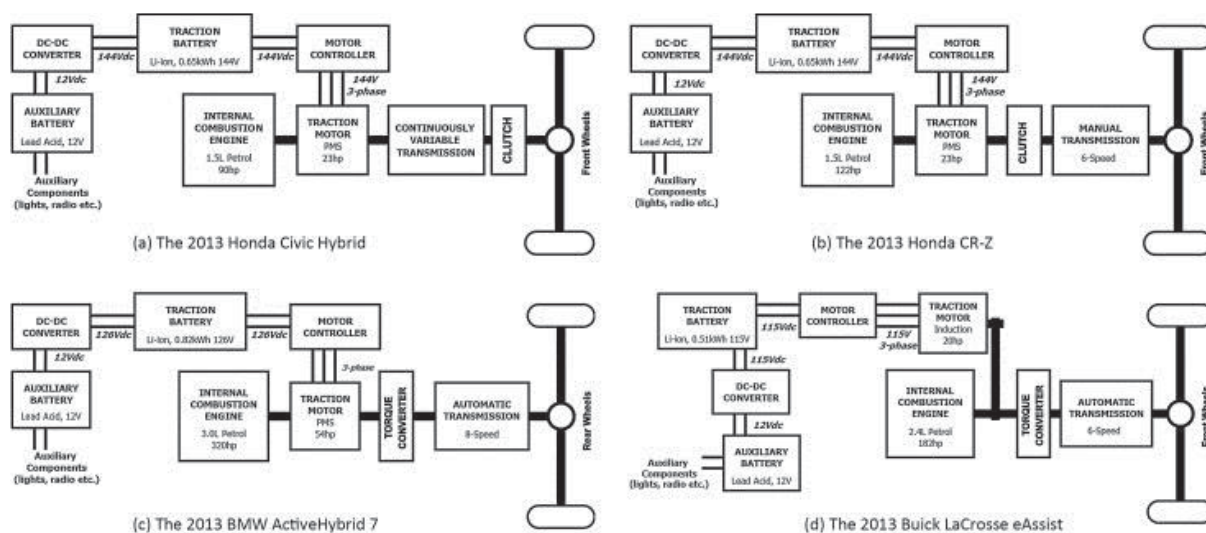


Figure 2-11: Different Mild Hybrid Powertrains Architecture [26].

Both Mild-HEV and micro-HEV systems share the same advantages, with the motor in mild-HEV having a rated continuous mechanical power output of 7-20 kW, and ability, in conjunction with ICE, to operate the car. Due to the fact that they share the same shaft, this configuration does not allow for it to run without ICE (acting as the primary power). In saying this, the size of the ICE can be made smaller coupled with fuel efficiency increases of up to 30%. High stored energy capacity is not needed for a mild hybrid electric drivetrain, due to the small power rating of the electric motor that it uses. In implementing a mild hybrid system in a conventional vehicle, most of the components involved in the system do not need much alteration. One of the main energy losses in this system is in braking, which is most highlighted by the stop-go nature of driving in urban areas. A small motor integrated into this system would be able to utilise part of the energy lost during braking. Another effect of driving patterns resultant of urban areas is the impact on the transmission. Frequent acceleration results in a low-speed ratio in the torque converter, reducing efficiency in operation.

2.2.6 Automotive transmissions

The transmission is a primary component of the powertrain, the function of which is to convert and deliver power to the road. These are torsional systems consisting of many

lumped inertias, such as differentials, and long flexible shafts. The essential function of a modern transmission is to deliver torque to the road-tyre interface while providing high efficiency, and excellent ride quality [27]. System design, and in particular, engine and transmission control design are the primary tools available to deliver these requirements. The control systems, including hydraulic clutch control, must provide ideal control of engine and transmission speed and torque, to achieve the best possible results during the shift period.

During the shift period, shift transients are the result of discontinuities in speed, torque, and inertia present during shifting. These discontinuities must be minimised to reduce the transient response of the powertrain [28]. Certain technologies form the basis of present-day automotive transmission technology as shown in Table 2-3. Some of these include manual transmission (MT) and Automatic Transmission (AT), with the dual clutch transmission (DCT), automatic manual transmission (AMT) and continuously variable transmission (CVT) forming the semi-automatic transmission type. Many of these technologies are designed to minimise shift transients.

The MT is very easy to manufacture having few parts. It is reliable and easy to maintain. AMT's and DCT's were developed in response to the growing need for an efficient alternative to the automatic transmission, in order to meet the twin targets of increasingly tightened emissions legislation and increasing consumer expectations in terms of driveline comfort.

Measuring transmission shift quality has aspects that may be defined empirically, analytically, objectively as well as subjectively. An example of this is apparent when the longitudinal acceleration of a vehicle is measured. Quantitative values can be attained for longitudinal acceleration during a gearshift. Also along this quantitative sense, there is a measurable torque interruption to the wheels during a standard upshift in a manual transmission. The figure shown demonstrates this concept clearly. From a subjective

viewpoint, a user observation can be made about the behaviour of the vehicle, typically seen as pitching of the front end, or by a characteristic behaviour referred to as a ‘head nod.’ Once again, user observation can be a marker of measurement, ranging from slight rider discomfort all the way to uncontrollable handling and poor manoeuvrability.

The oscillations through a drivetrain can be considered a source of noise, vibration, and harshness (NVH). In these cases, damping against NVH is sourced from torsional vibration absorbers and parasitic losses in clutches, transmission components and the differential. As a consequence of eliminating the torque converter from the powertrain system damping is reduced [29, 30]. However, whilst the AMT offers the efficiency of the manual architecture with automatic operation, it is usually inferior to a skilled driver with a traditional manual transmission in terms of ride quality. The DCT eliminates the “torque hole” and offers the same, or marginally better efficiency than traditional MT’s, however it is costly to produce, and shift quality is often described as “harsh”. Table 2-3 is presented below, qualitatively assessing the primary options for gearbox type [31].

Table 2-3: Gearbox Type

Automatic Transmission (AT)	High manufacturing cost Smooth gear-change characteristics – no need for supplementary torque fill
Continuously Variable Transmission (CVT)	Cheaper than Automatic but lower torque capacity No discrete gear changes – no need for supplementary torque fill
Dual Clutch Transmission (DCT)	Relatively high manufacturing cost Constant meshing eliminates torque hole
Automated Manual Transmission (AMT)	Lower manufacturing cost – clutch and shift hub actuators may be incorporated into the hybrid architecture Poorest gear change characteristics The motor must be placed after the first reduction
Manual Transmission (MT)	Lowest manufacturing cost The motor can only be placed after the first reduction

The MT was selected for this project for a number of strong reasons. Firstly, the MT still offers the best efficiency/cost ratio of any transmission. It has proven to be superior in terms of its efficiency. Consequently, the vehicles in which they are installed demonstrate

favourable fuel consumption. In saying this, the load applied on the manual transmission plays a big role in the level of this efficiency. A value of up to 97% efficiency can be reached over a typical drive cycle. This advantage is important because of the price-sensitive nature of the intended markets. These markets also typically do not have a high penetration of AT vehicles, and even lower penetration of electrification, principally due to the high-cost sensitivity. It, therefore, made sense to offer a product with which these markets are familiar. However, it was also recognised that an incentive is required to entice consumers in these regions to pay a small (unavoidable) premium for a hybrid vehicle. Because the cost of petrol in these regions is often quite cheap, minimised running cost was seen as only one of a variety of unique selling points of the proposed architecture.

In developing the other selling points, it was recognised that AT-equipped vehicles are often an aspirational purchase in these regions. Therefore, being able to deliver “AT-like” performance for MT money appeared to be a strong development target. However, this is countered by many disadvantages. From a user point of view, there is a reduced customer uptake and a poorer quality in shifting. From an operational sense, there is lessened damping of torque oscillations or step-changes through the driveline when assessed alongside alternate transmission architectures. In addition to this, there is an inability to transmit torque when changing gears. However, in the context of a mild hybrid vehicle, many of these disadvantages may be remedied.

The biggest weakness of the MT is the torque hole during gear change. It became apparent that exploring this weakness to develop methods to eliminate the problem while maintaining a cost advantage would yield a significant benefit to the project. As such, it became a project goal to improve MT drivability by exploring and reducing vibration characteristics, in order to approach the continuous torque delivery (“smoothness”) of an AT.

2.2.7 Torque hole & shift process analysis

Shift process analysis is essential for MT shift quality control. The process involves the disengagement and engagement of a single clutch connecting the transmission to the power source. The shift process may be divided into three phases. The first phase involves the disengagement of the clutch, where the driver depresses the clutch pedal, but gear ratio remains constant. The engine is decoupled from the gearbox, so vehicle speed decreases due to internal friction, rolling resistance, and aerodynamic drag and is characterised by a rapid reduction in torque transmission to zero. The second phase is the gear selection phase and is characterised by a fully disengaged clutch, torque hole as well as minor torque oscillation from the synchronisation of the selected gear, where the driver selects the next gear for engagement. The final phase is the inertia phase and is characterised by a significant torque oscillation as the clutch slips during re-engagement, where the clutch pedal is released, engine throttle is opened to apply torque to the transmission. When a constant speed ratio is achieved, the speed of the powertrain is proportional to the speed of the vehicle, and the clutch is fully engaged [32]. Various factors may influence the shift process, including the magnitude of transmitted torque before and after the gear change, and the speed of clutch disengagement and engagement. Figure 2-12 shows an example of actual vehicle data for half-shaft torque (with torque fill during shifts) [33]. During clutch disengagement, a speed differential is introduced between the clutch friction faces, and the output torque varies sharply, the discontinuity is called torque hole or torque gap. The torque hole is defined by its width, which is the time interval of entire shift process. A larger torque hole results in more significant deceleration of the vehicle. The torque hole is also characterized by torque oscillation at its extreme ends, which reflect the smoothness of clutch disengagement and engagement, related to the shock and vibration of the gearshift [34]. In a traditional manual/ICE powertrain, the depth of the torque hole is equivalent to the torque value

immediately before the initiation of the gearshift. Reducing the torque hole introduces a torque value somewhere between zero and the torque value immediately before the gearshift, to smooth the shift process. This architecture calls for a low-powered electric motor mounted on the manual transmission output shaft, coupled to a controlled power source. This configuration allows for increased functionality of the powertrain along with a reduction in the torque hole during gear changes, improving driving performance. High-quality shift control is critical to minimising the gear-shift torque hole and vibration of the powertrain [35].

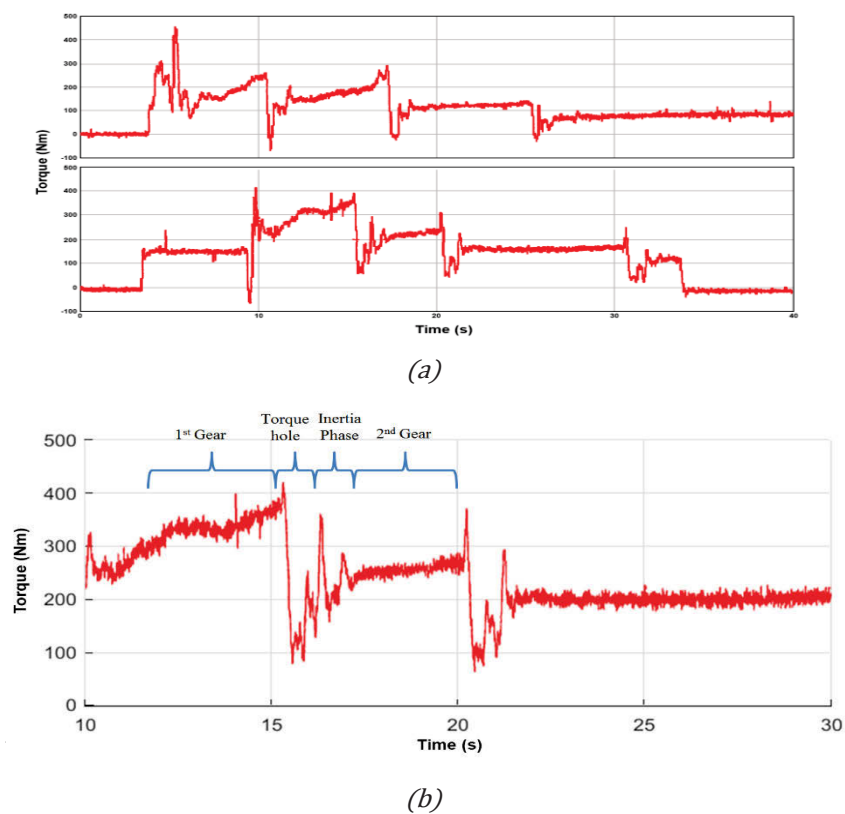


Figure 2-12: a. Effect of torque-fill on half shaft torque – torque-fill is shown below
 b. Actual measured half shaft torque with fill-in, showing the different phases of the gear change [36].

2.3 Summary

Major trends in the hybrid automotive industry are aimed at improving gearshift quality and increasing hybridization or electrification of the powertrain. Improved shift quality without the use of hydrodynamic torque converters is achieved through the application of precise transient clutch control technologies. Vehicles in which hydrodynamic power couplings are

not used are increasingly susceptible to driveline oscillations that are perceived by the driver as poor driving quality.

A number of recent studies have been conducted into the application of hybridized and electrified power shifting transmission systems. For a conventional vehicle Galvagno [35] designed a power shifting AMT by replacing the synchronizer mechanism on the highest gear ratio with a friction clutch, thus enabling power on up and down shifts for the system. In electric vehicles, Gao [37] designed an inverse AMT for electric vehicles, with the clutch on the low-speed section. Clutchless Automated Manual Transmissions (CAMT) have also been viewed as cost-effective transmission systems for electric and hybrid vehicles [38]. Such designs typically increase the torque and speed capabilities of the EV at the cost of overall efficiency in comparison to a single speed EV. Not dissimilar to the powertrain prototype proposed in this research is a dual motor hybrid vehicle, proposed in [39]. This topology uses a combination of synchronizers, gears and large electric motors upstream of the transmission to achieve similar functions for shift control as described in this research, but with an increased complexity of the system and for its control.

The approach undertaken in this thesis is to deliver a low-cost, low-tech mild-hybrid powertrain, with unique power delivery features designed to appeal to price-sensitive, but aspirational consumers. This strategy is designed to result in a vehicle marketable in developing regions where atmospheric pollutant levels are relatively high, and fleet electrification is low. The powertrain is a simple post-transmission parallel hybrid configuration. It utilises a low-powered four-cylinder engine coupled to a five-speed manual transmission through a robotically actuated clutch. The design is designed to be easily upgradeable to an AMT as development work progresses, which is a goal of this body of work. The secondary power source, in the form of an electric motor (EM), is rigidly coupled to the MT output shaft, in line with the prop shaft and prior to the final drive system. The

rigid coupling allows a high degree of fidelity when calibrating the torque-hole filling algorithm, and simplifies the kinematic model.

Prior literature includes some similar architectures to that proposed herein [36, 40-42]. Of these, Baraszu [36] most closely resembles the architecture proposed herein. However, the proposed architecture is simpler still, by the omission of the motor clutch. Moreover, the primary focus of the broader research is as much about the socio-environmental impact of the technology as it is on the technical development. The literature also includes research into the control of gearshifts in automated manual transmissions [43-45].

The project constraints are derived from the fundamental goal of bringing hybrid technology to developing nations with high mortality rates attributed to environmental pollution. The novelty arises out of the use of low-voltage, low-power hybridization together with low-cost mechanical hardware, coupled with innovative control methods to deliver powertrain architecture specifically designed for regions. These regions typically do not have a high penetration of AT vehicles and even lower penetration of hybrid/low-emission/zero-emission vehicles, due to high cost-sensitivity.

Literature mainly focuses on the study of control during the shift for optimization of: comfort, the speed of shift, and fuel economy. It appears there is some novelty in the investigation of a shift control strategy for the proposed post-transmission hybrid architecture. By identifying this market need, it may begin to see OEMs actively working in this niche to solve the identified socio-environmental problem. This focus compares well with the literature, which typically focuses on the technological aspect without significant reference to its social context.

With the use of manual transmission (MT) gear trains, a high-efficiency transmission is realised. In Hybrid Electric Vehicles (HEV) powertrains the electric machine (EM) output

torque may be controlled to suppress powertrain transients rapidly. This control technique is commonly known as “anti-jerk”. Modeling and analysis for control of vehicle powertrains have been critical to the development of transmissions in recent years. Prior research at UTS has resulted in the development of a detailed powertrain model of a mild hybrid electric vehicle [46]. These results have been used as a foundation upon which has been developed an integrated powertrain and vehicle optimization model, as is presented herein. The model and comprehensive analysis of MHEV component selection process for the whole vehicle is presented in this thesis in the following parts:

- 1- Motor characteristic evaluation and motor selection based on vehicle performance requirements.
- 2- Dynamics and control of MHEV and Deployment of detailed lumped inertia powertrain models.
- 3- Comparison of simulation results concerning energy consumption and motor efficiency in driving cycles.
- 4- Bench testing for MHEV in different driving cycles.
- 5- The relative selling prices based on CVs are calculated. The cost saved in manufacturing, particular driving range and lifetime mileage are presented.

Most of the previously discussed studies focused on eliminating torque hole but neglected the vibration and comfort issues introduced by the addition of a hybrid system. Although some papers discussed the control and stability of MHEV systems, they did not address the details of vibration distribution, the kinetic energy recovery ability, or the short and long-term economic benefits. It is often overlooked that purpose-designed drivers mode testing is vital in assessing performance in varying environments. The inclusion of multi-speed gearboxes (AT, DCT, CVT) in complex powertrain architectures can enhance both gearshifting and driving range with the implementation of well-developed algorithms. These algorithms would

ensure the safety and effectiveness of the configuration. Thus, this thesis presents a comprehensive evaluation of a novel MHEV system in terms of:

- Transient behaviour during shift control
- Integrated system design
- Efficiency and performance analysis, and
- Comparative cost evaluation.

Furthermore, some of the major technical outcomes, particularly shift control and behaviour, are verified using HIL simulation of an exemplary powertrain system.

Chapter 3: MHEV parameters, specifications and requirements

In developing a drivetrain architecture that is relatively cheap to manufacture, and offers both smooth torque transfer during the gear change, as well as a degree of damping against torque oscillation, a number of options may be considered. The cost-effectiveness must be balanced against the performance criteria required. Principally, there are options related to the type of gearbox, the magnitude of hybrid assistance, and the electric motor placement. The placement of the motor also affects the required motor speed and torque characteristics. Table 3-1 is presented below, the level of hybrid assistance [31]. Qualitatively, Table 2-3 and Table 3-1 can be seen that a mild hybrid coupled with an AMT or MT represents the greatest opportunity for improved drivability at the lowest manufacturing cost.

Table 3-1: Level of hybrid assistance.

Sub-mild hybrid (<10% electric assist)	Mild hybrid (10%<electric assist<20%)	Full hybrid (20% or more electric assist)
Limited benefit – torque hole may not be eliminated in many cases, and hybrid assist is not strong	Higher cost but may eliminate torque hole in most cases. Can also be used for anti-jerk	Highest cost – but offers no benefit compared to power split devices and is not economically sound. The packaging of motor and battery difficult

Powertrains provide torque over a large range of operating speeds and deliver it to the road. Therefore, the driving torque, gear reduction and vehicle resistance torque must be considered to model the powertrain accurately. The powertrain is a simple post-transmission parallel hybrid configuration. It utilises a low-powered four-cylinder engine coupled to a five-speed manual transmission through a robotically actuated clutch. The electric motor is connected to the transmission output shaft, before the final drive. The advent of a mild hybrid electric powertrain represents the greatest opportunity for improvement of driving comfort, shifting quality, fuel economy and improved driveability with low manufacturing costs. The

vehicle type selected for the mild HEV is a B-segment five-passenger lightweight sedan, which is typical of the majority of passenger vehicles on the road [47, 48]. The electrified side of the powertrain can serve multiple functions, including engine start-stop, motor-assist, as well as regenerative braking. The hybrid configuration specified in this research is based on a low-powered, output shaft-mounted electric motor, connected to the output shaft of an MT and powered with a controlled power source. The motor is mounted after the gearbox, over-rev protection is not required. Instead, the engine rev limiter and appropriate gearing ratios are used to limit motor speed naturally.

The design is established based on a typical ICE powertrain with manual transmission were taken from a 1990 model Mazda MX-5 (Miata) [49]. This vehicle model was selected as its characteristics (notwithstanding the convertible body) are highly representative of many vehicles being sold new in developing regions. It uses a low-tech 4-cylinder with power output and other physical characteristics typical of most B- and C-segment vehicles, and shares similar weight with these vehicles. In addition to this, the lightweight and simple body and rear drive powertrain, as well as the easy and cheap availability of parts in Australia made this vehicle choice appropriate as a basis for the later development of the physical prototype. It was expected to be substantially simpler to modify the rear-drive powertrain and open-top body for hybridization than would be a more typical B/C-segment front-drive hatchback, which is the only other vehicle configuration widely available in Australia that approaches the desired characteristics. The system is divided into numerous elements to develop the model; these elements are detailed in Figure 3-1. Elements of the engine, flywheel and pressure plate, clutch plate, transmission gears, shaft, differential, driveshaft, wheels, and vehicle inertia are included. More detailed specific features are shown in Table 3-2. The size and capacity of each mild hybrid component such as the battery, EM, and control unit are then determined through analysis accordingly to meet these requirements.

Each component or system on the vehicle is sized appropriately using well-established analysis methods, in order to meet benchmark requirements. A model is also implemented for the driver, capturing unique, modifiable characteristics.

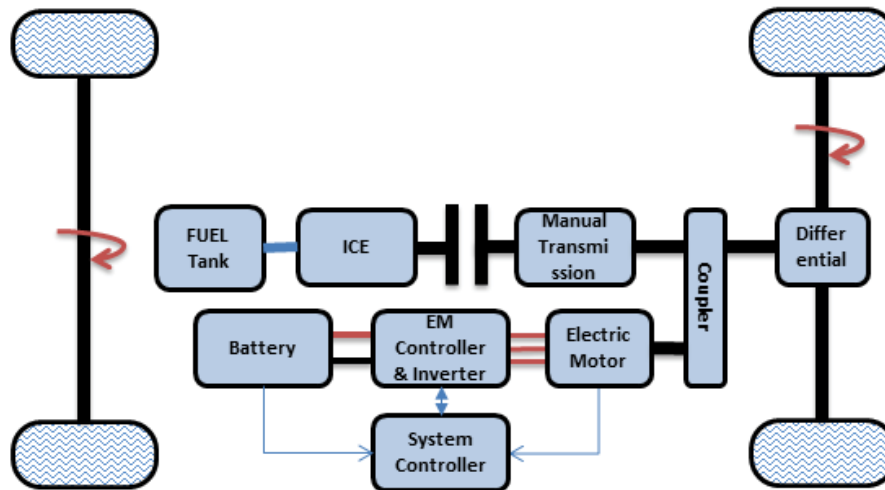


Figure 3-1. General powertrain layout with hybridization.

Table 3-2: Vehicle global specifications

Component	Parameter	SI Units
Vehicle	Mass	1100 kg
	Frontal area	3 m ²
	Drag coefficient	0.4
	Distance from CG to front axle	1.4 m
	Distance from CG to rear axle	1.6 m
	CG height	0.5 m
	Air density	1.2 kg/m ³
	Gravitational acceleration	9.81 m/s ²
	Tire rolling radius	0.312 m
	Rolling resistance coefficient	0.015
	Mass as hybrid	1200 kg
Engine	Type	Spark-Ignition
	Maximum power	70 kW
	Speed at maximum power	5000 rpm
	Maximum speed	7000 rpm
	Idling speed	800 rpm
	Cylinders	4
Gear ratio	Type	Manual, 5 forward 1 reverse, fully synchronised
	First	3.581
	Second	2.022
	Third	1.4
	Fourth	1.03
	Fifth	0.94
Clutch	Final drive ratio	4.06
	Type	single dry-plate clutch
	Friction coefficient	0.3

3.1 Motor specifications

Electric motors have many advantages over internal combustion engines. The efficiency of the conversion from electrical to mechanical energy is high at between 70% and 95%. They have high torque and power density and better torque characteristics at low speed. Moreover, it is possible to use electric motors as generators during braking to recover energy. The drivers appreciate the fact that they are quiet and offer a rapid and smooth acceleration. The choice of the electric motor (EM) needs careful consideration for a hybrid propulsion system. It has been an ongoing challenge for the automotive industry to find the best selection method for the electric-propulsion system (EPS) for both hybrid electric vehicles (HEV's) and electric vehicles (EV) respectively. The factors that contribute to this selection mainly revolve around efficiency, reliability and cost. As mentioned, this choice is not without careful consideration, and it is vital that this be done at the system level. In terms of more specific requirements for the selection of EPS for HEV's, considerations to driver expectation, vehicle constraint and energy source play a big role. Other target requirements may include noise, vibration and harshness (NVH), drivability, or other quality characteristics. There is extensive literature in the field of designing EPS to particular constraints [50-52]. It can be observed that the overall motor operating point is not framed in a specific definition, especially when considering the above. This is what makes it difficult to select the best EPS for an HEV. For a vehicular traction application, being able to find an appropriate machine format requires much thought, especially in the absence of adequate definition. Previous studies and literature in the field of EV/HEV for EM selection include torque density, inverter size, extended speed range-ability, energy efficiency, safety and reliability, thermal cooling and cost. Both vehicle dynamics and system architecture have an effect on the extended range of speed and how energy efficient the system is. Since this is the

case, the choice for traction drives for a specific vehicle architecture (EV, series and parallel HEV, etc.) need to take these motor drive features into consideration [53].

3.1.1 Power calculations

The electric motor in the proposed mild hybrid is designed to be mechanically connected directly to the propshaft. A mechanical input power of up to 10 kW is provided for the system. It is intended to provide acceleration assistance but no, or highly limited all-electric driving mode [26, 54]. The motor output is mainly used for accelerating and starting. The Rural Driving cycle (RDC) was used to investigate the effect of the torque-fill system on gear changes. Its simplicity and the requirement to select all available gears to fulfil the speed profile made it ideal as a base for investigating transient torque characteristics shown above. However, it is not representative of the everyday stop-start driving and heavy congestion in many developing capital cities, which are the target market for this powertrain. Therefore, it could not be used to select appropriate motor characteristics.

Quantitative measured values of aspects like fuel consumption do not reflect attained values under real-world driving conditions. As such, these conditions have been simulated in the form of drive cycles to reflect real-world examples. Some of these include EPA FTP75 urban and highway, LA92, ECE-15, and Japan1015 among others. The drive cycles mainly characterize vehicle speed and driving time. By using the urban and highway drive cycles of EPA FTP75 used in the New York City as a reference. To select an appropriate electric motor, an analysis of the vehicle architecture under the New York City Dynamometer Drive Schedule (NYCDDS, or NYC Cycle) was conducted. The NYC cycle was selected as the most appropriate representation of the target market for this proposed vehicle architecture. The analysis used a speed trigger to determine the number of gearshift events over the course of the cycle. In some sections of the NYC cycle, the speed profile fluctuates quickly. This

rapid fluctuation resulted in the speed trigger identifying a number of shifts in quick succession. Where shifts that were not required to maintain the cycle profile were identified, or where the profile could be better maintained by holding a gear longer, superfluous shifts were deleted. For instance, a shift pattern of 3-2-3 in a period of fewer than ten seconds suggests that gear three could be held. Therefore, the superfluous 2-downshift and 3-upshift are deleted. Likewise, a shift pattern of 1-2-1-2-3 in rapid succession indicates that second gear may be held longer, eliminating the downshift and subsequent upshift.

For the total cycle length of 598 seconds, 42 gearshifts were required. Ignoring downshifts, the average power required at upshift was calculated to be 9.47 kW, with only five upshift events requiring over 10 kW (see Figure 3-2 a). A similar plot can be produced for motor output torque using the target speed at each projected gear change. As the motor is placed after the first reduction ratio, it is independent of this variable, and the output torque is, therefore, a simple function of the target speed and required power. All but four gear change events are found to require less than 130 Nm output torque for torque fill-in (see Figure 3-2 c). The motor speed and torque characteristics can then be determined by plotting these variables for each gear change event.

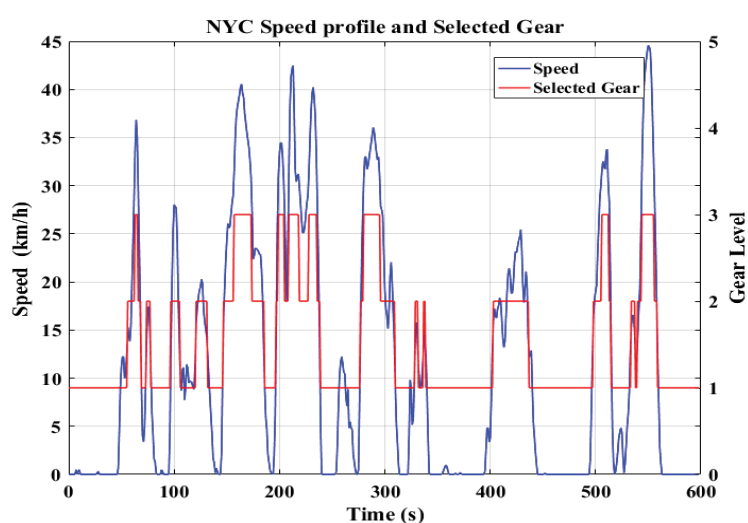


Figure (a). NYC Cycle speed profile with selected gear superimposed.

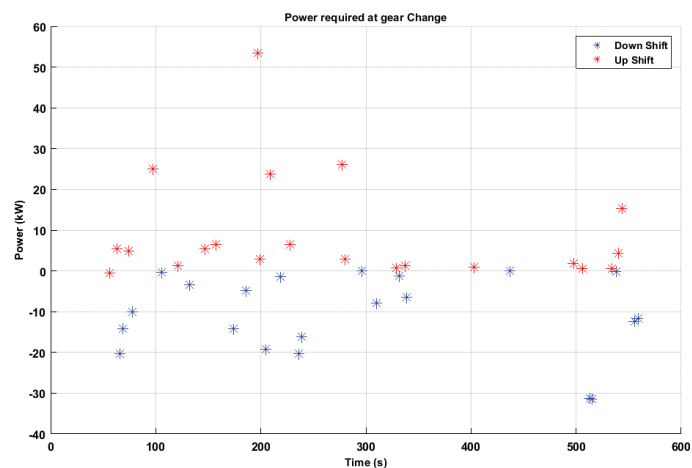


Figure (b). Power required for gear change, NYC Cycle.

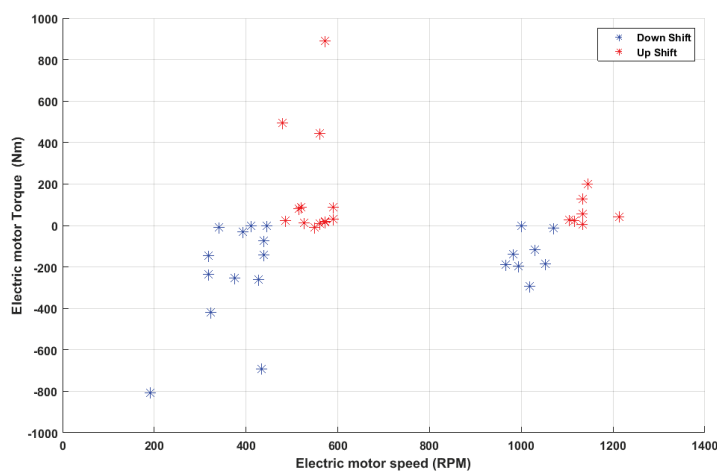


Figure (c). Electric motor torque and speed required at gear change.

Figure 3-2: (a)-(c). NYC cycle analysis.

3.1.2 Motor type selection

Extended speed range and efficiency contour are two aspects that need to be heavily considered when selecting traction motors. Some of these motors have the ability to run with superior extended speeds. There are many options for EV drive-trains. These can be: permanent magnet motor (PM), induction motor (IM), switched reluctance motor (SRM) and brushed DC motor (DC). Using the separately excited DC motor as a representative example, issues that arise from its use are the commutators and brushes that reduce the motor's maximum speed, along with much spark creation and frequent maintenance. An increased speed range along with field-oriented control can be attained by using an induction motor (IM). IM's are frequently used in EV-HEV applications as it is a technology that is both well

understood and has established manufacturing infrastructure. In saying this, aspects such as the nonlinearity of the dynamic IM model and the dependency on motor parameters prove difficult for motor control. When looking at the switched reluctance motor (SRM), it demonstrates the lowest weight and generates series type torque-speed characteristics. It also has the capability of boosting the torque above the baseline speed by ‘phase advancing.’ Just as the prior example, the control involved is non-linear and machine dependent. A quantitative value of 6x in 1hp rating (demonstrating a wide speed range) has been documented in a prior publication. Considering this, it would be an appropriate consideration for SRM to qualify for use for EV, series HEV and low hybridised parallel HEV applications. Table 3-3 is an evaluation of most commercial electric motors for vehicular propulsion systems [52, 55, 56]. The evaluation grades six major characteristics of each motor on a scale from 1 (worst performance) to 5 (best). PM brushless motors are most capable of competing with IMs for the electric propulsion of HEVs are more attractive for OEMs. It is also true that the renowned automotive manufacturer has taken these HEV’s on board. The motors have proven to excel in many areas, some of which include: 1) High power density – Weight and volume both at decreased values for a specified output power; 2) increased efficiency; 3) Efficient heat dissipation into the environment. In saying this, it does need to be considered that due to the effect the motor’s limited field weakening ability, the motors have a consequential short constant-power region. This is also resultant from the PM field, with speed range limited due to their fixed nature.

Table 3-3: Qualitative comparison of commercial electric motors

	PMSM	IM	Brushed DC Motor	SRM
Cost	3.0	5.0	4.0	4.0
Power density	5.0	3.5	2.5	3.5
Maturity	4.0	5.0	5.0	4.0
Efficiency	5.0	3.5	2.5	3.5
Reliability	4.0	5.0	3.0	5.0
Controllability	4.0	5.0	5.0	3.0
Total	25.0	27.0	22.0	23.0

3.1.3 BLDC / PMSM

The major advantages of PMSM motor include high efficiency, low maintenance, good longevity and reliability, low noise emissions, and low cogging torque. Importantly, the control of a PMSM motor is also considerably cheaper than other suitable candidates (eg., IM, and SRM). PMSM has proven itself an adequately proficient motor for a 50% hybridized car. This is based on many preliminary studies conducted by the author on wide speed range ability and energy efficiency. It was shown that it demonstrated superior efficiency in a constant torque regime. The disadvantages to its use include cost, safety and cooling. One cost that proved to be expensive were the large magnets for high-power PMSM. They also have a sensitivity to high temperature. In addition to this, there remain unfortunate consequences caused by the permanent field in the instance of short circuit faults. If measures are not implemented to cool the magnet, a decline in motor efficiency is observed. More manufacturers take the PMSM as the primary option for their EVs and HEVs, such as Chevrolet Spark EV, BMW i3, VW e- Golf, Mercedes B250e, Nissan Leaf, Toyota Prius, Honda Insight and so on.

Generally, PMSM can be classified into two types by the control methods, i.e. brushless DC (BLDC), or brushless AC (BLAC). Low-cost hall sensors are used a lot for BLDC drives where the phase currents only have to be commutated on and off. Expensive resolvers or encoders need to be used for BLAC drives where the phase current waveforms require finely specific control. More recently, methods that do not require sensors are currently being tested and implemented for both of these drives. Regardless, it is a vital requirement that motors be provided with alternating current. Otherwise, they would not be able to rotate.

Despite the name that a Brushless DC motor (BLDC) suggests, it is considered an AC motor. Its function can be described by concentrated coil windings on the stator working together

with surface mounted magnets on the rotor to create a closely uniform flux density in the airgap. Through this, a constant DC voltage allows the stator coils to be driven, switching from one stator coil to the next (commutation) – this is what gives this motor the name brushless DC. Commutation is electronically synchronized to the rotor angular position. An AC voltage waveform resembling a trapezoidal shape is resultant of this. The BLDC motor is absent of arcing issues that are seen with brushed DC motors since it does not use brushes or commutator. Essentially, the brushless DC electric motor can be considered and described as a brushless AC motor – containing an integrated power inverter and rectifier, sensor and inverter control electronics.

The Permanent Magnet Synchronous Motor (PMSM) can be described as an electrically powered rotating mechanism where the stator represents a classic three-phase stator – similar to the structure of an IM. However, the rotor has permanent magnets. PM motors can be designed to operate efficiently by allowing permanent magnets to create a considerable air gap magnetic flux. This can also be achieved in newer designs by using concentrated stator windings and a modified rotor structure. To achieve the lowest torque ripple, rotor magnets can be mounted on the surface. For increased saliency, which in turn escalates the reluctance torque of the machine, the rotor magnets can be installed deep within the rotor. To control these motors, it is vital that the rotor angular position is known accurately, using what is referred to as Field Oriented Control (FOC).

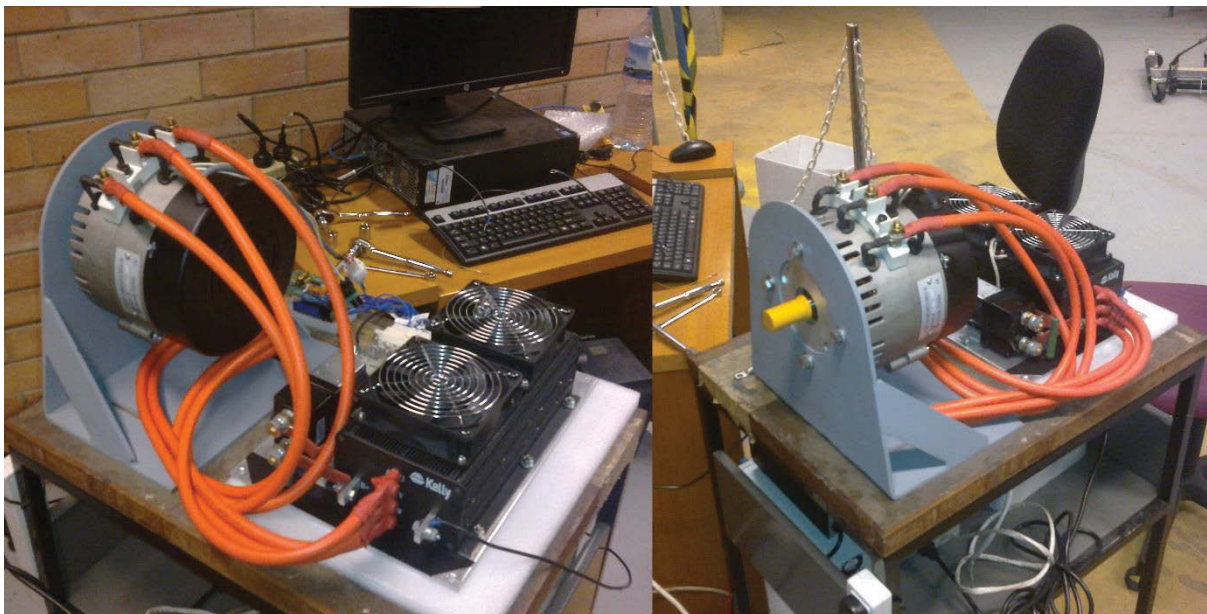
Considering the primary purpose of this thesis is to design a proper powertrain system for MHEV, and controllability for manual transmission PMSM, as the mainstream product on the HEV market, is selected as a propulsion motor for further study. The selected EM parameters and specifications are listed in Table 3-4.

Table 3-4: Selected motor parameters and specifications

Parameter	Specification
Motor type	Brushless DC Motor
Continuous Output Power	12 KW
Peak Power	30 KW
Max speed	5000RPM

3.1.4 The motor ordered

Based on the NYC cycle analysis, a 10 kW / 30 kW pk. electric motor was found to satisfy requirements. The Motenergy ME0913 is listed in Table 3-5 and (see Figure 3-3). The motor was selected as a suitable off-the-shelf motor for initial testing. The manufacturer quotes a thermal efficiency of 85% at its full continuous power, which translates to 10.2 kW mechanical output. Although its peak torque is somewhat lower than ideal, it is the closest off-the-shelf solution to meet the required hardware needs. The characteristics of the selected motor in combination with the matching inverter KHB1260124 are demonstrated in Figure 3-4. Bench-testing yields characteristic curves, which are included in the Simulink model. The complete testing and validation process is described in Chapter 9.

*Figure 3-3: Mars 0913 PMSM/BLDC motor.**Table 3-5: Mars 0913(Etek Comparable) PMSM/BLDC motor.*

Parameter	SI Units
Continuous Output Power	12 KW
Peak Power at 96 volts	30 KW
Voltages range	0 to 96 VDC
AC Continuous current	125 A
DC Continuous current	180 A
AC Peak current	420 A
DC Peak current	600 A
Efficiency	92% (at voltages between 24 to 96 VDC)
Winding resistance	0.013 Ohms (Phase to Phase)
Maximum speed	5000 RPM
Torque constant	0.15 Nm / Amp
Peak Stall Torque	90 Nm
Cooling	Fan Cooled motor
Weight	15.8 Kg
Inductance	0.10 m Henry (Phase to Phase)
	28 turns per phase
Armature Inertia	45 Kg Cm ²
Number of poles and magnets	4 pole motor (8 magnets)
Electric Connection	3-phase, Y-connected
Axial rotor motor	Axial air gap
Sensors	3 Hall sensors (at 120 degrees electrical timing)
Stators	Two stators with a rotor in the centre

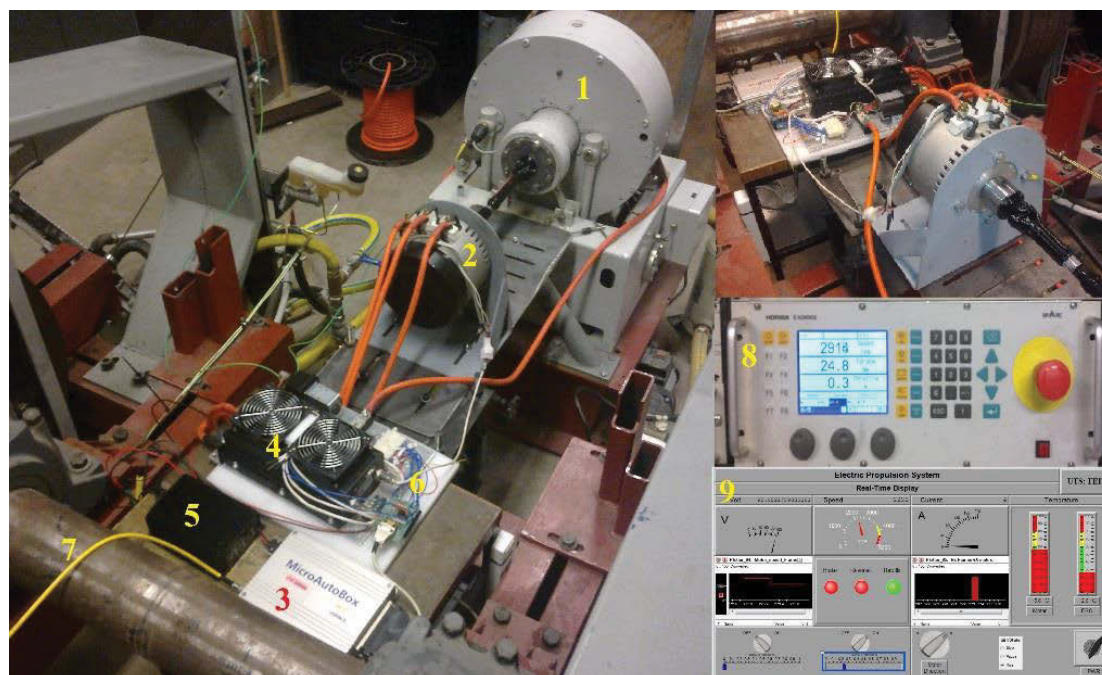


Figure 3-4: Electric motor test facility at UTS.

1- Dynamometer WT190. 2- Mars 0913 PMSM/BLDC. 3- MicroAutoBoxII. 4- KHB1260124. 5- Step-down 96v/13.5v. 6- Relays Board. 7- PC host interface. 8- SPARC control (Dyno stand controller). 9- Control Desk.

3.2 Mild hybrid powertrain configuration

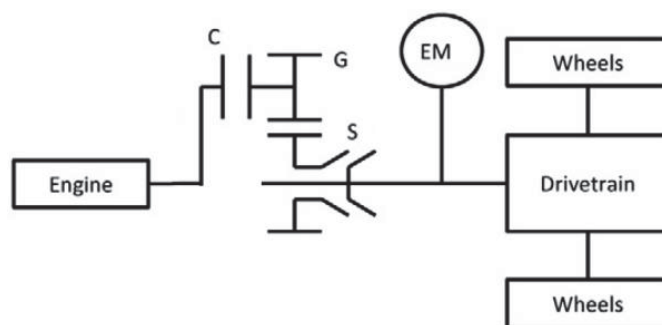


Figure 3-5: Generalised powertrain layout with hybridization (only one gear/synchro pair shown).

Figure 3-5 presents a basic mild hybrid powertrain. The powertrain is a post-transmission parallel hybrid type, utilising an electric machine (EM) permanently coupled to the transmission output shaft. This configuration allows the EM to drive the wheels directly. As the motor is downstream of the transmission, it, therefore, has a fixed constant speed ratio to the wheels, via the final drive. In the transmission model, gears, 1, 2, 3, 4, and 5 (G) are connected to the input and output shafts and are driven through the closed clutch (C). The synchronizer is denoted as S. In a traditional manual transmission it is necessary to release the clutch before synchronisation, isolating the synchroniser from engine inertia. The nature of the powertrain requires a single dry-plate clutch interfacing between the engine and transmission, shown in Figure 3-6. The damping sourced from this coupling must be recognised in the system. This damping is related to the torsionally-mounted coil springs which connect the segments of the clutch disc, as well as the friction between the various segments as they move past each other [57]. A pressure plate consisting of a pre-tensioned (normally closed) diaphragm spring clamps the disc to the engine output, and the friction plate is independently splined to the transmission input shaft. In this model gears, one to five are connected to the input and output shafts, where they can be individually selected with synchronizer mechanisms, and are driven through the closed clutch. In a traditional manual transmission, the primary clutch is opened before synchronisation, isolating the synchronizer from engine inertia and torque.

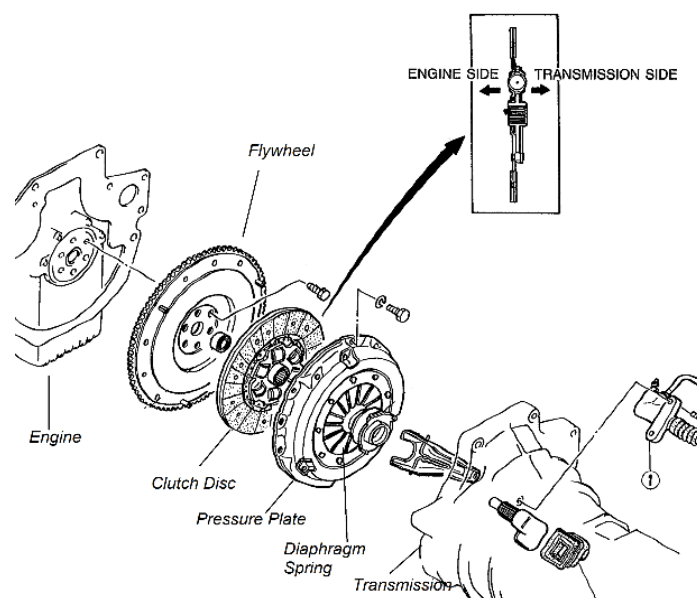


Figure 3-6: Clutch assembly [58].

Suggesting that the most suitable EM for this low-cost HEV is a Brushless DC Motor (BLDC), with a rated continuous mechanical power output of 10 kW (30 kW peak). Because the intended use profile involves short pulses of high power for torque-filling, the peak mechanical power figure is as significant a consideration as the continuous output. A 10 kW electric machine was found to satisfy most requirements for torque-fill in during gear change. It is also sufficiently powerful to be implemented for secondary functions to improve the powertrain efficiency. These secondary functions may include torque supplementation under high demand or low engine efficiency conditions [59] or energy recovery during braking events.

The obvious limitation of this vehicle configuration is that it is not possible to isolate the EM from the wheels, and therefore there are incidental losses while the motor is freewheeling. Speed synchronisation during gearshifting is accomplished using standard synchronizers that are popular in manual transmissions, having low cost and high reliability. It is recognised that due to the nature of the mild HEV system proposed, material savings may be found by removal of the synchronizers, instead of using electronic throttle control to accomplish speed synchronisation. However, these savings assume that speed synchronisation may be achieved

with a very high degree of accuracy, where the inclusion of synchronizers means that the accuracy of the speed synchronisation may be reduced, improving system response. Further, the savings do not translate into lower cost due to the current economies of scale. For these reasons, they are therefore not pursued.

Chapter 4: Dynamic modeling of a powertrain

In this chapter investigates the dynamics of a wheel drive mild hybrid electric powertrain. A comprehensive analysis of the system with numerous degrees of freedom is proposed, and the resulting sets of equations of motion are written in an indexed form that can easily be integrated into a vehicle model. Lumped stiffness-inertia torsional models of the powertrain will be developed for different powertrain states to investigate transient vibration. These models include those capable of shift transient studies, combining major components of the powertrain into a single model. To make a complete study of system response, the study must be extended to consider the vibration of the powertrain, as well as control of clutch and motor. The powertrain model is divided into subsections. These are: the engine model, motor model, the powertrain inertia model, and vehicle resistance torques model. These models are presented in the next chapter. The major powertrain components - such as engine, flywheel, transmission, and differential - are lumped as inertia elements, interconnected with torsional stiffness and damping elements to represent a multi-degree of freedom model of the powertrain [60, 61]. This chapter presents the mathematical models of each configuration, using eight degrees of freedom for the mild HEV powertrain, compared to seven degrees of freedom for a conventional powertrain. Powertrain system torques are also presented for these models, including mean engine torque, a piecewise clutch model, vehicle resistance torque, and motor torque models. Free vibration analysis is undertaken to compare the two powertrain models and demonstrate the similarities in natural frequencies and mode shapes.

This chapter is then divided into five sections covering the development of a lumped mass model of the powertrain. The first section is devoted to the introduction of modeling theory and free vibration analysis. In the second section, the different states of the powertrain are identified through the combination of open and closed clutches. Next, in section three, the

lumped inertial powertrain is presented, and specific assumptions regarding the model development are identified. In section four, the model matrices and free vibration analysis are presented for the states that are studied during the transient period. Section five presents mathematical models of the applied torques to the powertrain. Finally concluding remarks are made.

4.1 Powertrain lumped model formulation

The generalised Newton's second law is used to derive the models. The aim of modeling the powertrain is to identify possible improvements when using the electric drive unit. The mild hybrid powertrain is compared with a traditional manual transmission driveline. The analysis is focused on the lower gears. The reason for this is that in lower gears, the torque transferred to the drive shaft is greater, as is the deflection in the shaft. This greater deflection means the shaft torsion is higher at lower gear ratios, yielding larger oscillations.

The application of the torsional lumped inertia models to complex structures such as vehicle powertrains is a popular method for determining powertrain characteristics such as damped natural frequencies and modal shapes or studying the transient response of the powertrain under different operating scenarios. The application of lumped parameter methods for higher order powertrain models makes use of powertrain characteristics of shaft stiffness and rotating inertia, in conjunction with the physical layout to produce representative models for different powertrain configurations.

The lumped parameter model is then constructed using the procedures, for applying these modeling techniques can be found in many sources of literature, such as Rao [62]. For inertial elements, the equations of motion are derived from Newton's Second Law. Presented mathematically, with i as the i^{th} element in a structure consisting of n degrees of freedom, as:

$$\Sigma M_i = I_i \ddot{\theta}_i \quad (4.1)$$

where M is the applied moment, I is the inertia, and $\ddot{\theta}$ is angular acceleration.

To apply this method to a powertrain, components are reduced to a series of lumped inertias connected via torsional stiffness and dampers. For example, the differential is conveniently modelled as a lumped inertia; the propeller shaft combines both mass and stiffness. Thus it is possible to provide a reasonable approximation of the response of the powertrain system through the use of lumped inertia multi-degree of freedom models. The complex nature of powertrains, structured with multiple branches and gear pairs are all defined using interconnected elements. For transient analysis, loading exists in the form of externally applied torques from engine, clutches, synchronisers, and vehicle resistance. The first assessment of any powertrain system model is the free vibration analysis of the system. The natural modes of any system characterise the response under generalised forcing conditions. Typical methods for determining the free vibration response of a powertrain system include undamped or damped free vibration analysis.

The equation of motion may be used for free vibration and forced vibration analysis. Idling gears are lumped as additional inertia on gears targeted for shifting. Backlash in gears is ignored as frequencies excited in lash are generally significantly higher than the main powertrain natural frequencies of 3 to 100 Hz and are unlikely to impact on synchroniser engagement [63]. The generalised equation of motion is:

$$I\ddot{\theta} + C\dot{\theta} + K\theta = T \quad (4.2)$$

Where I is the inertia matrix in $\text{kg}\cdot\text{m}^2$, C is the damping matrix in $\text{Nm}\cdot\text{s}/\text{rad}$, K is the stiffness matrix in Nm/rad , T is the torque vector in Nm , and θ is the rotational displacement in rad , $\dot{\theta}$ is the angular velocity in rad/s and $\ddot{\theta}$ is the angular acceleration in rad/s^2 .

The powertrain is modelled using torsional lumped parameters to capture the shift characteristics of the system. Inertia elements represent the major components of the

powertrain, such as engine, flywheel, clutch drum, clutch plate, synchroniser with final drive gears, shafts, differential, electric motor, wheels and vehicle inertia. These are subjected to various loads such as rolling resistance and air drag. Torsional shaft stiffness is represented by spring elements connecting principal components, and losses are represented as damping elements. To model the powertrain economically several simplifications can be made to the transmission and powertrain, thereby reducing the degrees of freedom. For the transmission, the idling gears not targeted for synchronisation or shifting can be grouped as a single lumped inertia on the primary shaft, added to engaged gear inertia. The propeller shaft is divided into one inertia, while symmetry in the wheels and hubs pair the lumped inertias. As a result, the lumped mass model is reflected in Figure 4-1. Where θ is angular displacement, $\dot{\theta}$ is angular velocity, T is torque, and subscripts e is Engine, F is flywheel, and for clutch respectively.

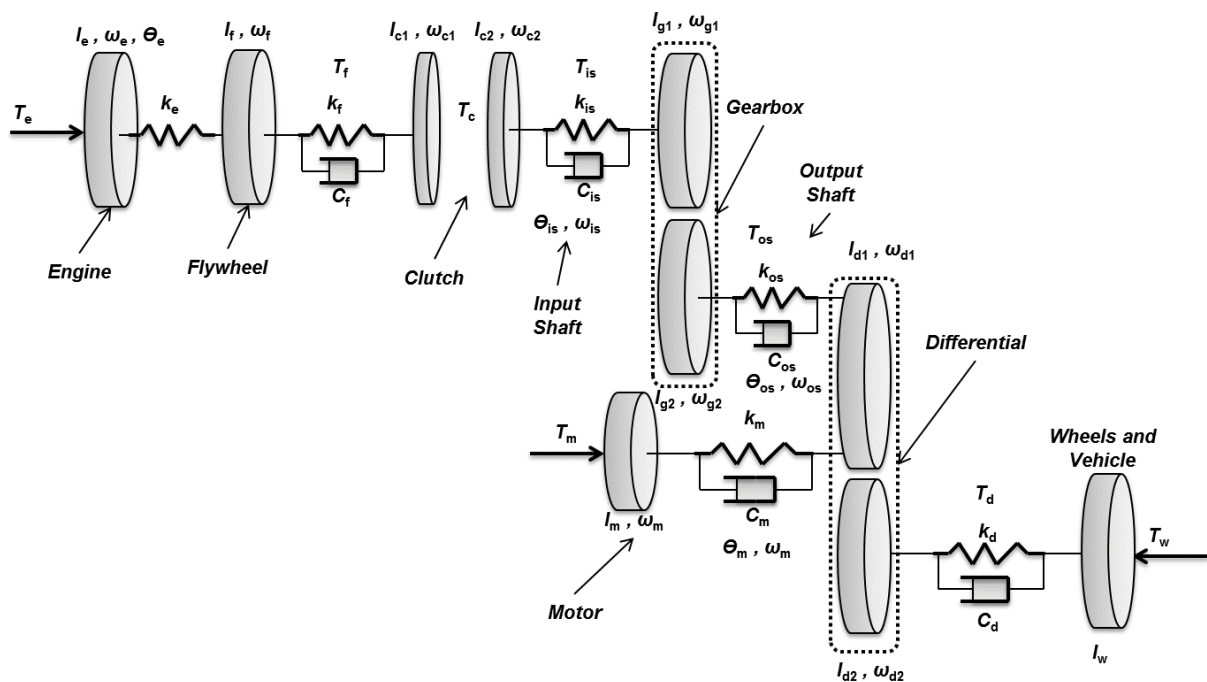


Figure 4-1: Lumped parameter model for a mild HEV equipped powertrain.

The model layout of a motor mounted on an output shaft. Assumptions can be applied to reduce the complexity of the powertrain. The first is to lump inertia of idling gears in the

transmission, and primary gear and synchroniser inertias, thus eliminating numerous transmission components. It is then assumed that there is no backlash in the gears, nor engaged synchronisers, eliminating high stiffness elements in the model. This assumption reduces computational demand. Finally, symmetry in the wheels and axle results in the ability to group these inertias together, as a single element. Additional losses in transmission and differential are modelled with grounded damping elements.

For general simulations, the engine is modelled as a single degree of freedom with input torque from a lookup table. This ignores engine harmonics, as it is a more convenient method when considering engine control during shift transients. Though it is possible to replace the flywheel with a clutch drum inertia only, to study the dynamic effects during shifting. Thus for the initial simulations flywheel stiffnesses are a representative of the output shaft stiffness without hysteresis damping. Within the transmission model clutch hubs, gears and the synchronisers are modelled as lumped inertias and shafts as stiffness elements. Damping is associated with the drag torques that results from system losses. The final drive components are reduced to single inertia that links transmission lay shafts and the drive shaft by assuming no backlash in the gears. The differential and axle splits the drive torque to both rear wheels, in this case, a one to one ratio as the final drive is incorporated in the transmission. The differential is modelled as a lumped mass with damping to the ground as a result of its efficiency loss. Stiffness elements connect driveshaft and axles to the differential. The wheel model integrates the hub and tyre inertia with the flexural rigidity of the tyre wall. Moreover, the tyre inertia receives torque from the rolling resistance of the vehicle, and the tyre must also include the vehicle inertia to accurately reflect the load on the transmission. This inertia is typically several orders of magnitude larger than that of any other powertrain component.

In creating these models, assumptions have employed. I.e.:

- Ignore backlash in the gear mesh

- Ignore temperature dependence of the powertrain and particularly transmission
- Simplifying branched symmetrical axles and tyres to one branch of the powertrain
- Reduce the idling gears to reflected inertia at the active gear.

These assumptions have allowed the development of a simplified powertrain model while still capturing the important characteristics of the powertrain, particularly with regard to transient vibration, and damping of the powertrain system.

Equations of motion for each element are:

$$I_e \ddot{\theta}_e - K_e(\theta_F - \theta_e) = T_e \quad (4.3)$$

$$I_F \ddot{\theta}_F + K_e(\theta_F - \theta_e) - K_F(\theta_{C1} - \theta_F) - C_F(\dot{\theta}_{C1} - \dot{\theta}_F) = 0 \quad (4.4)$$

$$I_{C1} \ddot{\theta}_{C1} + K_F(\theta_{C1} - \theta_F) + C_F(\dot{\theta}_{C1} - \dot{\theta}_F) = -(T_C) \quad (4.5)$$

$$I_{C2} \ddot{\theta}_{C2} - K_{is}(\theta_{g1} - \theta_{C2}) - C_{is}(\dot{\theta}_{g1} - \dot{\theta}_{C2}) = T_C \quad (4.6)$$

$$\begin{aligned} \ddot{\theta}_{g1}(\gamma_1^2 I_{g2} + I_{g1}) + K_{is}(\theta_{g1} - \theta_{C2}) + C_{is}(\dot{\theta}_{g1} - \dot{\theta}_{C2}) - \gamma_1 K_{os}(\theta_{d1} - \gamma_1 \theta_{g1}) \\ - \gamma_1 C_{os}(\dot{\theta}_{d1} - \gamma_1 \dot{\theta}_{g1}) = 0 \end{aligned} \quad (4.7)$$

$$\begin{aligned} \ddot{\theta}_{d1}(\gamma_2^2 I_{d2} + I_{d1}) + K_{os}(\theta_{d1} - \gamma_1 \theta_{g1}) + C_{os}(\dot{\theta}_{d1} - \gamma_1 \dot{\theta}_{g1}) \\ - \gamma_2 K_d(\theta_W - \gamma_2 \theta_{d1}) - \gamma_2 C_d(\dot{\theta}_W - \gamma_2 \dot{\theta}_{d1}) = 0 \end{aligned} \quad (4.8)$$

$$\begin{aligned} \ddot{\theta}_{d1}(\gamma_2^2 I_{d2} + I_{d1}) + K_{os}(\theta_{d1} - \gamma_1 \theta_{g1}) + C_{os}(\dot{\theta}_{d1} - \gamma_1 \dot{\theta}_{g1}) + K_m(\theta_{d1} - \theta_m) \\ + C_m(\dot{\theta}_{d1} - \dot{\theta}_m) - \gamma_2 K_d(\theta_W - \gamma_2 \theta_{d1}) - \gamma_2 C_d(\dot{\theta}_W - \gamma_2 \dot{\theta}_{d1}) \\ = 0 \end{aligned} \quad (4.9)$$

$$I_W \ddot{\theta}_W + K_d(\theta_W - \gamma_2 \theta_{d1}) + C_d(\dot{\theta}_W - \gamma_2 \dot{\theta}_{d1}) = T_W \quad (4.10)$$

$$I_m \ddot{\theta}_m + K_m(\theta_m - \theta_{d1}) - C_d(\dot{\theta}_{d1} - \dot{\theta}_m) = -T_m \quad (4.11)$$

Gear ratios are represented as γ for the transmission reduction pairs, and final drive pairs. If the clutch is engaged, equations (4.5) and (4.6) are unified, and the inertias of the clutch members combine. Equation (4.12) is the resulting equation of motion. With the clutch engaged the total number of degrees of freedom of the system decreases. If the clutch is disengaged, then the system has eight degrees of freedoms, while if the clutch is engaged, there are only seven degrees of freedom.

$$\begin{aligned} (I_{C2} + I_{C1})\ddot{\theta}_C + K_F(\theta_C - \theta_F) + C_F(\dot{\theta}_C - \dot{\theta}_F) - K_{is}(\theta_{g1} - \theta_C) - C_{is}(\dot{\theta}_{g1} - \dot{\theta}_C) \\ = 0 \end{aligned} \quad (4.12)$$

The flexibility of hybrid vehicles allows many choices of engine/electric machine configuration. This flexibility in configuration enables the study of the effect of different configurations on vehicle performance and transient vibration suppression. In the proposed configuration as presented in Figure 4-1, the electric machine will be positioned on the transmission output shaft, using a constant gear ratio for power conversion. The powertrain configuration for hybrid vehicle powertrains is dependent on a range of design considerations which ultimately determine the layout, interconnection, and sizing of components. The model parameters of the powertrain (inertia, damping, and stiffness) are listed in Table 4-1 and Table 4-2 and are sourced from known data or estimated based on published literature. When looking at a mild hybrid powertrain equation (4.11) is introduced, and equation (4.9) is used instead of equation (4.8) which is used when analysing a conventional powertrain.

Table 4-1: Model parameters

Name	Symbol	Units
Torque	T	Nm
Equivalent Inertia	I	Kg m ²
Speed	ω	rad/s
Displacement	Θ	rad
Torsional stiffness	K	Nm/rad
Friction Coefficient	C	Nms/rad

Component	Symbol
Engine	e
Flywheel	F
Clutch drum	C1
Clutch hub	C2
Input Shaft	is
Gearbox	g
Output shaft	os
Differential	d
Motor	m
Vehicle with tire	W

Table 4-2: Parameters

Parameter	Inertia (kg-m ²)
I_e	0.4
I_F	0.2
I_{c1}	0.0072
I_{c2}	0.0125
I_{g1}	0.0006
I_{g2}	0.0013
I_{d1}	0.16
I_{d2}	1.6
I_m	0.0045
I_w	167.558

Parameter	Stiffness (Nm/rad)
K_e	95000
K_F	2000
K_{is}	5600
K_{os}	4700
K_m	9500
K_d	65000

Parameter	Damping (Nm/rad)
C_F	2
C_c	0.049
C_{is}	0.0044
C_{os}	0.1
C_d	0.1
C_m	0.0045

4.2 Free vibration analysis

Damped free vibration analysis is used to determine the vehicle modes, damping ratios, and natural frequencies. This method requires the representation of the model in state-space form. The externally applied torques are assigned as a zero value for free vibration. The equations are then presented in matrix form, as:

$$\mathbf{I}\ddot{\theta} + \mathbf{C}\dot{\theta} + \mathbf{K}\theta = 0 \quad (4.13)$$

The system matrix is taken from equation (4.13) and used to perform damped free vibration analysis. The application of the eigenvalue problem can be used to determine natural frequencies and damping ratio. The system matrix is:

$$\mathbf{A} = \begin{bmatrix} \mathbf{0} & \bar{\mathbf{I}} \\ \mathbf{I}^{-1}\mathbf{C} & \mathbf{I}^{-1}\mathbf{K} \end{bmatrix} \quad (4.14)$$

where A is the system matrix, and \bar{I} is the identity matrix.

Where 0 represents a zero matrix of size n by n , where n is the degrees of freedom, and I is the identity matrix. The solutions to the eigenvalue problem provide then matrices for the eigenvalues, representing paired damped natural frequencies with real and imaginary components, and eigenvectors, paired columns representing the modal shape corresponding to a particular natural frequency. From the eigenvalues, it is then possible to retrieve the natural frequencies, damped natural frequencies, and damping ratio for the system. Where the natural frequency can be taken as the absolute value of a particular eigenvalue, or for the eigenvalue $= a + ib$, the natural frequency is:

$$\omega_n = \sqrt{a^2 + b^2} \quad (4.15)$$

The damping ratio is then:

$$\xi = \frac{|a|}{\omega_n} \quad (4.16)$$

Moreover, the damped natural frequency is:

$$\omega_d = \omega_n \sqrt{1 - \xi^2} \quad (4.17)$$

where ω_n is natural frequency, ω_d is damped natural frequency, and ξ is damping ratio. To complete the analysis the eigenvectors are then studied. Taken as part of the result of the eigenvalue problem, a paired column of eigenvectors represents the modal shape of a particular natural frequency, or, more generally, the relative displacements of inertial elements from the neutral point. Thus it is possible to define many of the important characteristics of a dynamic system and associate natural frequencies with particular modal responses.

Previously the equations of motion were derived for each element of the powertrain. These included elements from the engine, dual mass flywheel, transmission, differential, output shafts and wheels. These equations of motion must be integrated into inertia, stiffness and damping matrices in conjunction with vectors for input torques, and angular displacement, velocity and acceleration to provide suitable tools for analysis.

The natural frequencies and damping ratios are presented in Table 4-3. With the clutch open there are effectively two rigid body modes as the two separate powertrain halves are effectively not coupled. Further, each of the open natural frequencies is associated with the two separate bodies, the higher frequency for the engine and clutch disc with high stiffness and relatively small inertia, and the lower frequency for the transmission and vehicle body. With the clutch closed, however, the damping ratios are essentially identical, and the natural frequencies are reasonably close, consistent with the change in effective inertia experienced by the locked drum and transmission inertias coupled via reduction gear pairs. The damped free vibration of the powertrain is completed using state-space methods. Matrices for I , C , K are developed and merged into the system matrix, and the eigenvalue problem is solved for the damped natural frequencies of the system. Real and imaginary components are utilised to identify the un-damped natural frequency and damping ratio.

Free vibration analysis is used here to compare powertrain models with and without a motor. Damped free vibration analysis is applied to both models, with natural frequencies and damping ratios presented for each. Modal shapes are then used to identify the relationship of natural frequency to the model. Damped free vibration results provide the essential characteristics of the powertrain. Damping ratio results demonstrate the lightly damped nature of the powertrain, where no damping ratio exceeds 10% (Table 4-4). Light damping provides more opportunities for excitation in the powertrain resulting from nonlinearities that can contribute to the initiation of high-frequency vibration in the propshaft. For the mild

hybrid vehicle model with primary clutch closed free vibration analysis results in one rigid body mode of the powertrain and six natural frequencies with corresponding damping ratios. Solutions to the eigenvalue problem resulted in 7 paired solutions with real and imaginary components. For each solution, the real component of the eigenvalue was negative, indicating a mathematically stable system, and zeros have been omitted from matrices for clarity. The natural frequency of the rigid body mode (RBM) included a small imaginary component as a result of the use of grounded damping elements; this does not affect the stability of the system. In both powertrain models for the open clutch case, two RBM are present, while, for each of the closed clutch models only one RBM is present.

Table 4-3: Damped free vibration results of ICE powertrain and mild HEV in first gear.

	ICE Model	
Frequency number	Natural frequency ω_n (Hz)	Damping ratio ζ (%)
1	312.6261	1.901
2	134.9499	0.62
3	96.3400	8.41
4	10.1634	0.07
5	7.7347	1.71
6	0	-

	Mild HEV Model	
Frequency number	Natural frequency ω_n (Hz)	Damping ratio ζ (%)
1	312.6261	1.901
2	231.2795	0.03
3	134.9499	0.62
4	96.3400	8.41
5	10.1620	0.07
6	7.7347	1.71
7	0	-

Table 4-4. Natural frequencies of each gear ratio

	Original Drivetrain				
Mode	1 st	2 nd	3 rd	4 th	5 th
1	312.62	328.15	347.12	369.53	390.57
2	134.94	134.95	134.96	134.96	134.97
3	96.34	90.87	84.76	78.25	72.71
4	10.16	10.19	10.23	10.28	10.32
5	7.73	7.53	7.25	6.86	6.43
6	0	0	0	0	0

Mild HEV					
Mode	1 st	2 nd	3 rd	4 th	5 th
1	312.62	328.15	347.12	369.53	390.57
2	231.27	231.27	231.27	231.27	231.27
3	134.94	134.95	134.96	134.96	134.97
4	96.34	90.87	84.76	78.25	72.71
5	10.16	10.19	10.23	10.28	10.32
6	7.73	7.53	7.25	6.86	6.43
7	0	0	0	0	0

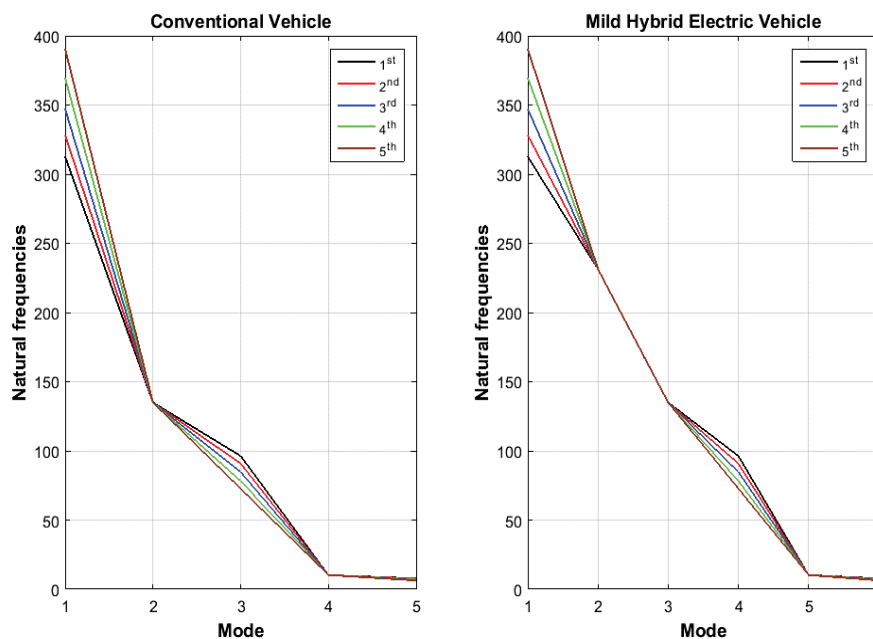


Figure 4-2: Natural frequencies of each gear ratio

Compared with the original drivetrain, the design system has one more degree of freedom, so there is one more state of natural frequency; the high-frequency response is higher than the original drivetrain. For lower frequency response, there is no significant difference. Therefore, it can be concluded that inserting an electric motor with additional inertia does not have a significant effect on low-frequency response. Indeed, it can be observed in Figure 4-2 that with the addition of the motor a single new frequency at 231 Hz is introduced to the system. It is otherwise unaffected.

4.3 Summary and contributions

The focus of this chapter was the development of a model of a manual transmission equipped powertrain compared with MHEV for use in transient gearshift simulations. The powertrain

is characterised as a rear wheel drive, dry clutch to engage gears for shifting. Multiple n-degree of freedom powertrain models have been developed to CV and MHEV using different arrangements of the one powertrain model.

The adoption of an electric motor has required the development of vehicle shift-control strategies to improve the performance of powertrain system damping, by actively controlling the electric motor output during the transient vibration resulting from gearshifting. The torque-fill drivetrain can be used equally successfully with automated manual, and traditional manual gearboxes. Due to the intermittent operation, it is also possible to safely operate the components beyond their rated continuous output and yield greater benefit.

Chapter 5: MHEV model development

Due to the nature of the relationship and dynamic interaction between system components, it becomes highly difficult to emulate varying driving cycles for different vehicles. Accuracy and repeatability are vital aspects of ensuring the most appropriate simulation for any given system. This is also without consideration to result in validity, playing an essential role in selecting an appropriate simulation platform. These attributes are characterised and embodied in the Matlab/Simulink software platform. This chapter describes the overall structure of the powertrain model and its components in detail. The physical vehicle parameters on which the simulation is based were taken from a 1990 model Mazda MX-5 (Miata) [49]. This vehicle model was selected as its characteristics (notwithstanding the convertible body) are highly representative of many vehicles being sold new in developing regions. It uses a low-tech 4-cylinder with power output and other physical characteristics typical of most B- and C-segment vehicles, and shares similar weight with these vehicles. In addition to this, the lightweight and simple body and rear drive powertrain, as well as the easy and cheap availability of parts in Australia made this vehicle choice appropriate as a basis for the later development of the physical prototype. It was expected to be substantially simpler to modify the rear-drive powertrain and open-top body for hybridization than would be a more typical B/C-segment front-drive hatchback, which is the only other vehicle configuration widely available in Australia that approaches the desired characteristics.

5.1 The overall structure of the powertrain model

Figure 5-1 demonstrates the overall structure of the powertrain model is implemented in the Matlab/Simulink environment. Each component model has been connected to create the entire MHEV system. A complete MHEV system must be designed to meet the power requirements according to the vehicle parameters, specifications and performance

requirements. The complete MHEV powertrain model is built using a forward-looking modeling approach, which was chosen for model verification, comparative analysis and optimization benefits. The forward-looking approach works by modeling the input of the driver to develop the appropriate throttle and braking commands to meet the desired vehicle speed.

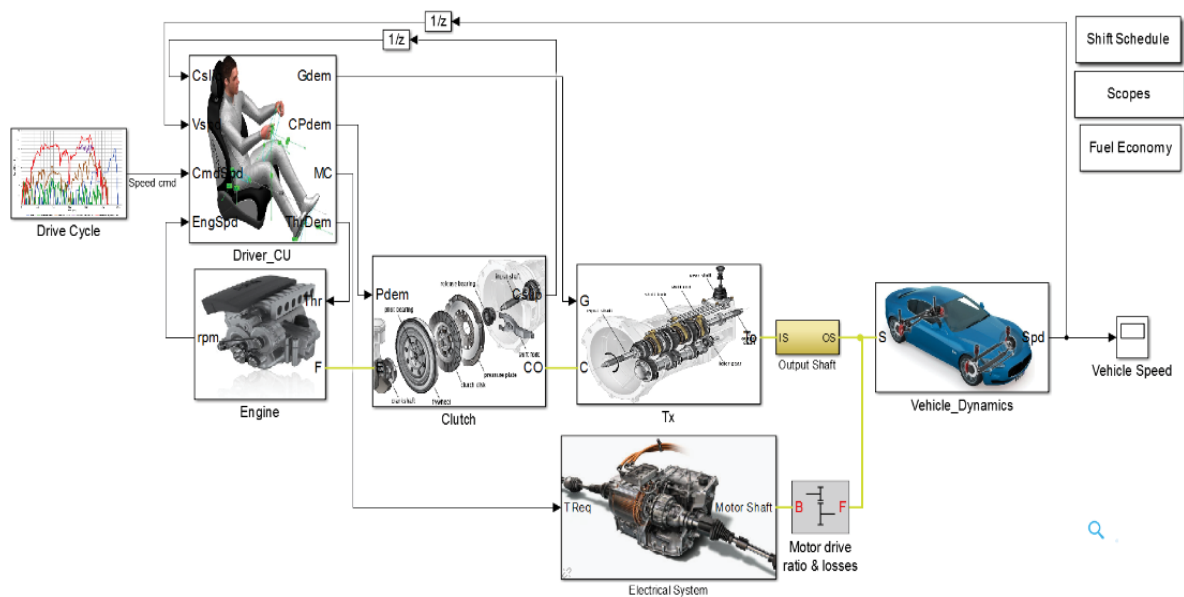


Figure 5-1: A high-level view of the powertrain of the mild HEV model in Simulink.

5.1.1 Modeling environment

A complete vehicle model, including physical and control components, was developed in the Simscape/Simulink environment and the SimDriveline and Simscape toolboxes. Given the complexity of the model, solvers were implemented and configured to optimise ensure both simulation accuracy without compromising the speed of these simulations [64]. The simulation uses the velocity profile of the assigned driving schedule as an input. From this, torque and power demands are generated and distributed by component characteristics and selected operating strategies. The block diagram of the vehicle model can be seen in Figure 5-1.

The model was implemented using the relevant Simscape toolbox component block. The model is forward-facing (an up-bottom modeling strategy). The force-generating systems such as tires, powertrain, brakes, suspension, and aerodynamics are taken into account in the model. The driver is modelled using a proportional–integral–derivative (PID) controller, with adaptations to determine acceleration/braking requirements. Gear change is determined according to a two-dimensional shift schedule.

5.1.2 Vehicle torque model

The vehicle block represents the overall vehicle body and its associated characteristics such as mass distribution, aerodynamic drag, longitudinal motion and gradeability factors. This model is integrated with differential and tyre models. With the tyre model including rotating inertia, rolling resistance and contact models with the road [65, 66]. Again these are implemented from the Simscape toolbox in Matlab as equation (5.1).

$$T_v = (f_R M_v g \cos \phi + M_v g \sin \phi + \frac{1}{2} C_D \rho A_v V_v^2) r_w \quad (5.1)$$

Where T_v is vehicle torque, V_v , m , A_v are the speed, mass and frontal area of the vehicle, r_w is the wheel radius, f_R is the rolling resistance (friction) coefficient, c_D and ρ are the drag coefficient and air density, ϕ is the road grade and g is gravitational , cceleration [65, 66].

5.1.3 Engine model

The physical simulation models of engine and control were established within the Simscape environment. Because the engine model is only required to provide torque and speed in response to a given throttle command, the ‘Generic Engine’ component in the SimDriveline package offers sufficient functionality for our needs. This development strategy has been successfully used in the prior literature [67, 68]. Figure 5-2 shows the engine map and the maximum torque line of the engine.

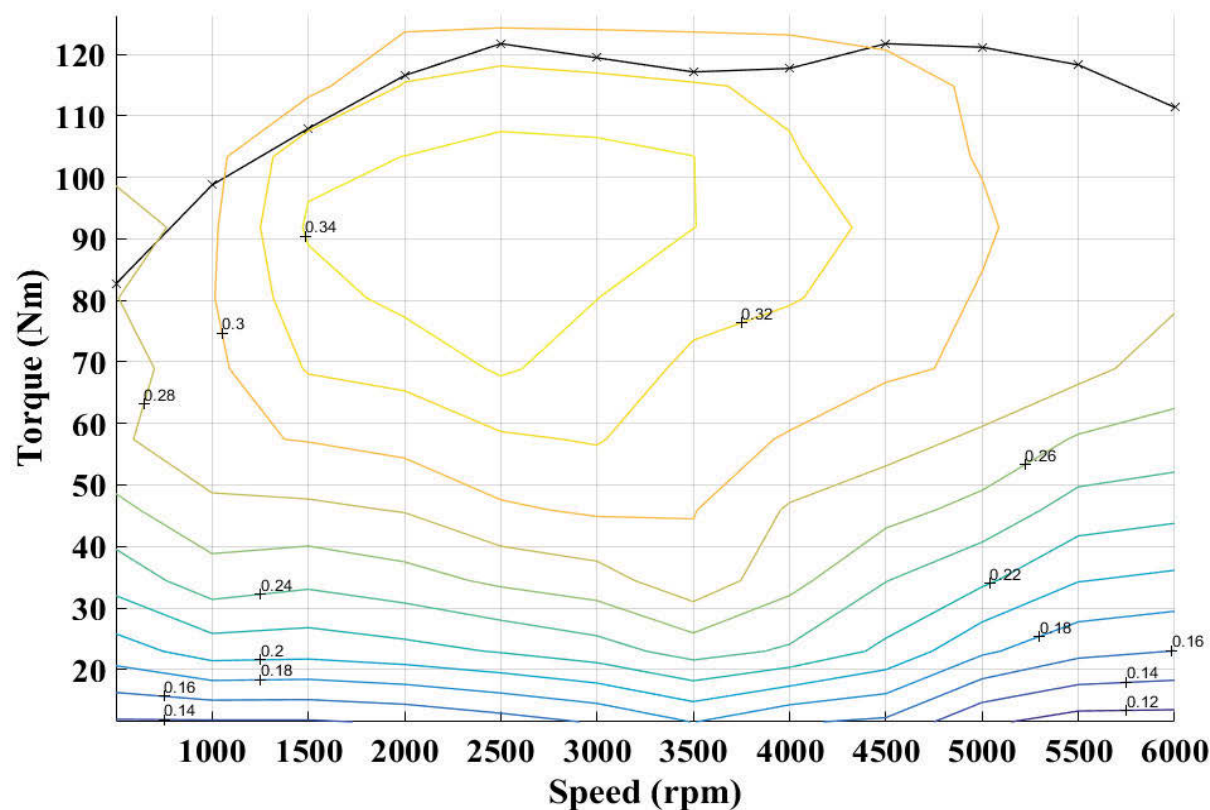


Figure 5-2: Engine map.

5.1.4 Single dry clutch model

The main weakness of a manual transmission is that it is not easy to drive as it requires the driver to provide the actuation force for the clutch and gear selector. As a result, gearshifts are sometimes not smooth which causes jerk or jolt on the vehicle body and affects driving comfort for passengers who will notice an interruption of engine torque to the wheels. Analysis of the shift process is essential for ensuring shift quality control. It requires release and re-engagement of a single friction clutch between the prime mover and transmission. Within this, there are additional phases. First, there is the clutch disengagement. Disengagement is characterised by a rapid reduction in torque to the transmission as the prime mover is isolated. Second gear selection occurs. With the clutch open, alternative synchronizers are released and engaged to select the target gear. At this point, there is no traction load to the road, and a substantial torque hole is generated. There can also be some transient response as synchronizers are released and engaged. Finally, there is the inertia

phase. It involves friction loading of the clutch to synchronise speeds and is characterised by large torsional vibrations during clutch slip and lockup. When speeds are synchronised lockup is achieved, and the clutch is fully engaged. There are many factors that impact on the shift process, such as the magnitude of transmitted torque before and after the gear change, and the rate of clutch disengagement and engagement.

The preferred model describes the system in a piece-wise manner, with one equation describing the slipping phase and another describing the sticking phase of the clutch. The torque through the clutch while slipping is given by equation (5.2). The sticking of the clutch is sustained as long as the torque transmitted through clutch (T_c) remains below the maximally transmittable torque T_c^{max} , which is given by equation (5.3) [57, 69, 70].

$$T_c = -F_n \mu R_a \text{sign}(\omega_e - \omega_c) \quad (5.2)$$

$$T_c^{max} = F_n \mu_{stick} R_a \text{sign}(T_c) \quad (5.3)$$

The active radius of clutch calculated given by equation (5.4), which is detailed in [71].

$$R_a = \frac{2}{3} \left(\frac{r_o^3 - r_i^3}{r_o^2 - r_i^2} \right) \quad (5.4)$$

In equations (5.2), (5.3), (5.4): μ is the dynamic friction coefficient of the clutch-facing material with opposing surfaces, ω_e, ω_c represent the rotational speed of the clutch disc and transmission input shaft respectively, R_a is the active radius of the clutch plates. The clutch actuator produces the normal force F_n as pressure load on the clutch and with this force the clutch torque T_c that is transferred to the driveline is controlled. Simplifying assumptions are made regarding variation in dynamic friction according to clutch face pressure, interface temperature, and slip speed. The pressure is assumed uniform across the clutch face in this model, and, for simulation purposes the clutch, is assumed to be non-varying in temperature.

Generally speaking, the friction coefficient is expected to vary somewhat with both temperature and wear. Whilst these variables will have some impact on experimental work, for the purposes of this investigation it is sufficient to assume that friction is independent of these variables. The static friction coefficient μ_{stick} is applied to the normal force across the clutch when the clutch is locked. μ_{stick} must be larger than μ . Based on the available literature [72, 73], μ_{stick} has been assumed to be 0.3, and is 20% higher than μ (that is, $\mu_{stick} = 1.2(\mu)$). Furthermore, the term $sign(T_c)$ is non-positive in the case of vehicle (engine) braking and positive in all other cases. r_o is external diameter the of clutch friction plate and r_i is inner diameter of clutch frictionthe plate. When modeling a dry clutch system, the stick-slip frthe iction model is detailed in [72, 73].

5.1.5 Gears model

The gearbox consists of different gears which transmit speed and torque of the ICE to the differential (final drive). The torque and speed from the ICE model enter the gearbox model. Here the torque and speed are manipulated according to the gear and the respective gear ratio depending on the control system. These inputs will be manipulated to obtain the output torque and speed. Gearshift process is modelled in order to reveal all 5 phases during torque hole by Simscape Driveline. Each gear pair is modelled: cone synchronizers with dog clutches are explicitly modelled to mimic the detailed process of gear disengagement, speed synchronization and engagement of new gear. The ratios for each gear of the gearbox and differential are listed in Table 3-2. The differential is a constant gear reduction ratio between the transmission and the wheels.

5.1.6 Motor model

To simplify the system model, a DC equivalent motor model is used to represent the electric prime mover. This simplification reduces the three-phase permanent magnet motor to a

simple two degree of freedom model and allows direct control of input voltage without consideration of power electronics for these simulations. The complexity of simulating power electronics is eliminated, and the direct voltage control of the motor is now possible. The differential equation for the electric circuit is defined in equation (5.5).

$$V = IR + K_e \dot{\theta} + L \frac{dI}{dt} \quad (5.5)$$

Where I is the line current, L is the line inductance, K_e is the back emf constant, R is the line resistance, and V is line voltage. The electromagnetic torque produced in the motor is defined as follows:

$$T_{em} = K_t \dot{\theta} \quad (5.6)$$

Where K_t is the torque constant and T_{em} is the electromagnetic torque. These two equations represent the electrical component of the model equations of motion, and should be considered in conjunction with the equations of motion presented [74].

Modeling the electric machine for vehicular powertrains is somewhat different to traditional engine modeling. Generally, electric machine models use only a maximum output torque with an integrated efficiency map and the supplied battery power to determine the driving load delivered to the wheels. For the electric machine, it is assumed that the demanded power from the controller is supplied to the motor (P_s), this is combined with motor speed and efficiency to determine the actual motor output torque. The motor output torque is calculated as follows for the motor.

$$T_m = \eta_m \frac{P_s}{\dot{\theta}} \quad (5.7)$$

Where P_s is the supplied power, T_m is the output torque of the motor, and η_m is the motor efficiency. It is important to note here that the maximum torque available from the motor is limited by the rated power.

5.2 Transmission actuation and driver model

The shift-control strategy utilises a supervisory controller which is a master to the engine control module (slave 1) and the motor controller (slave 2). The supervisory controller passes control to slave 1 under most driving conditions, taking control during gearshifting events or during hybrid operation. During the gearshift event, the supervisory controller is responsible for the actuation and detection of clutch and gear position, prediction of torque demand at the end of the gear change event, and synchronizing engine and motor torque to minimise the torque hole. To execute this function the controller synchronises the load increase of the electric motor with the load decrease of the engine, disengaging the clutch at the optimum time, such that the torque removed by clutch disengagement is immediately compensated by the EM. At the time the clutch is fully disengaged, the mechanical gear selection is accomplished, and the throttle, electric power, and clutch engagement are modulated synchronously so as to minimise the step change in torque. A comparative analysis of conventional and torque-fill drivetrain simulation models was undertaken. [75].

A Driver and vehicle control unit are used to provide engine and the electric machine (EM) with required torque signals. Figure 5-3 illustrates the block diagram for the driver model. It contains the main three models to control vehicle. Th_ctrl is driver model, Shift_state is shift control unit, and EM_Managment is Electric Machine unit / Energy Management unit. As the system is based on a conventional manual transmission, the actuation process is relatively simple. It is divided into four stages:

- A. Release throttle and open primary clutch
- B. Disengage current gear

- C. Select and engage target gear
- D. Close primary clutch and restore engine power.

These results demonstrated a reduced shifting time and improved shifting performance in terms of transient vibrations for the proposed mild hybrid vehicle. For the purpose of this research linkages and actuators have been replaced with ideal force inputs. This simplifies the modeling process without losing the desired characteristics of the powertrain.

Primary input signals to the motor controller are: clutch position, ICE load (calculated from speed and throttle angle), and selected gear. The function of the electric machine is to eliminate or reduce the torque hole during gear changes by providing a tractive force when the clutch is disengaged, and also, provide damping for torque oscillation, particularly during gear changes and take-off (anti-jerk). The electric motor may also act as a generator under certain driving situations

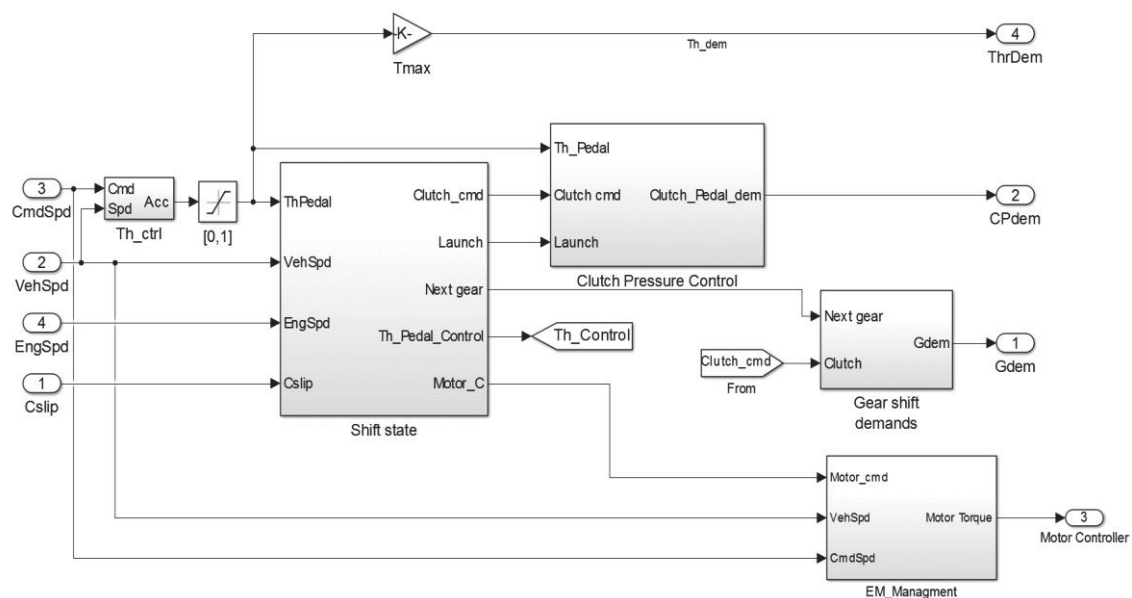


Figure 5-3: Driver control unit

5.2.1 Throttle and brake control

By controlling the ICE throttle in conjunction with the mechanical brakes, the driver model has an ability to determine the desired vehicle speed. Vehicle speed acts as the input variable for

the driver model. The difference between intended and measured speed is fed into the driver controller, which outputs the error data into a proportional-integral (PI) controller. As the behaviour of a PI controller would suggest, a negative error value results in the application of vehicle braking, with a positive error value resulting in driving the throttle pedal. Figure 5-4 illustrates the driver model in the Simulink environment.

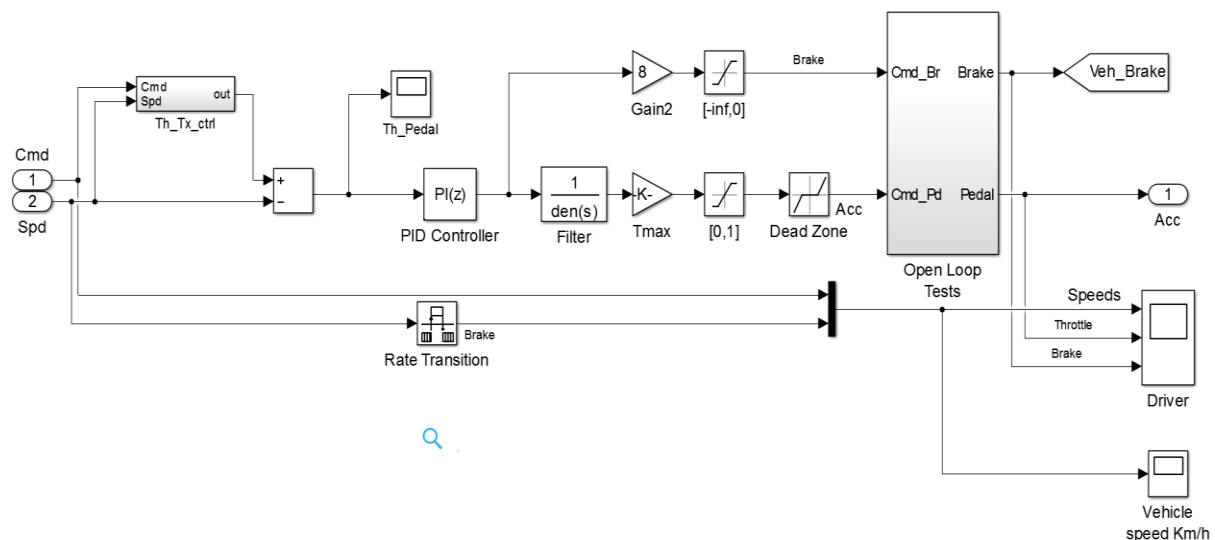


Figure 5-4: Driver model for throttle and brake.

5.2.2 Shift-control strategies for mild HEV

Modern hybrid powertrains aim to deliver excellent ride quality and high efficiency through smooth tractive torque delivery. To this end, some powertrains employ continuously variable transmissions, eliminating shift transients, but introducing other limitations and increasing cost. Good system design can maximise efficiency and ride quality, but it is the powertrain control systems which must provide optimal control of transmission and engine speeds and torques to achieve the best possible results during the transient (shift) periods. Powertrain transient vibration during and after gearshift are the results of discontinuities in torque, speed, and inertia (typically resulting from ratio change and power decoupling). Transient control of the powertrain aims to reduce these discontinuities to a minimum so as to restrict the dynamic response to desirable levels. The mild hybrid structure used in this paper employs a low

voltage electric motor coupled to the transmission output shaft. Input signals for motor control include (i) clutch position, (ii) ICE load (typically from engine map), and (iii) engaged the gear. The electric motor achieves three outcomes. First, it should minimise the torque hole during gearshift by supplying an output torque to the wheels when the clutch is open. Second, it should provide some capacity for damping out torsional vibration during launch and gear change. Third, it will assist the ICE during launch and provide some regenerative braking capacity during braking.

There are many considerations required for implementing the control strategy and its integration with gearshift control. These considerations include clutch position, gear state, engine speed, throttle position, and propshaft speed. A robotized clutch and gear actuator would be applied to the final system, allowing control of both target gear and shift time. This hardware simplifies the control problem immensely and improves the quality of the solution. However, for proof of concept, a predictive model is established based on a known drive cycle. For simplicity, clutch and gear actuation may be controlled using driver-in-loop or open-loop electronic control. Either method is time- and cost-efficient, and provides valid results, that may be simply applied to a robotized system with little modification. Gear state and clutch engagement are electronically detected by a control unit, which drives the motor assembly integrated into the transmission output shaft. The discussion of shift-control strategies below assumes a robotized gear and clutch actuator. There are three control regimes. The first is ICE-start, which is used when starting the vehicle from rest. The second and third are shift-up and shift-down. During the ICE-start regime, the vehicle may be powered in three modes: by the engine alone, by the engine and motor, or by the motor alone. In the first (engine-only) mode, the first gear is engaged, and the clutch is open; thereby no torque is transferred to the wheels. When the clutch begins to engage, thanks to an axial load

acting on its friction surface, a progressive torque transfer to the first gear set takes place through the input shaft. The system then passes control to the “shift-up” regime.

Under limited circumstances, the motor-only mode of ICE-start may be engaged. These circumstances include suitable high-SOC, idle start-stop has stopped the engine and, low torque request from the driver. In this case, second gear is engaged at zero speed, and the clutch is open so that it does not cause the engine to be driven by the motor. The motor supplies 100% of the requested torque until the shift schedule indicates a shift into second gear is required, or a low-SOC causes the engine to fire. At this point, the engine is fired, and the system switches to the “shift-up” control mode, having already preselected the required gear. In the case of a high torque request from the driver, the ICE-start regime may engage both engine and motor to propel the vehicle from rest. Because at high torque, the 1-2 torque hole will not be able to be completely filled by the motor, it may be minimised by operating the motor at peak torque until the completion of the 1-2 shift. This strategy ensures swift progress while maximising drivability.

Figure 5-5 outlines the process involved in shift-up. The shift-up regime is used whenever a higher gear is required than that currently selected. It is described in the flowchart presented in Figure 5-7 Likewise, shift-down controls the system when a shorter gear is needed. The two regimes are very similar in operation, and both are called depending on a shift schedule that is illustrated in Figure 5-6 [76]. Because the proof-of-concept will be tested according to specified drive cycles, robotized gear and clutch actuation is not strictly necessary for the development of the torque hole compensation function. Target torques and speeds may be programmed instead, and the control strategy is initiated using a clutch switch. This development programme also presents an interesting opportunity to study the performance of the system with and without automatic shifting, which may present further cost savings.

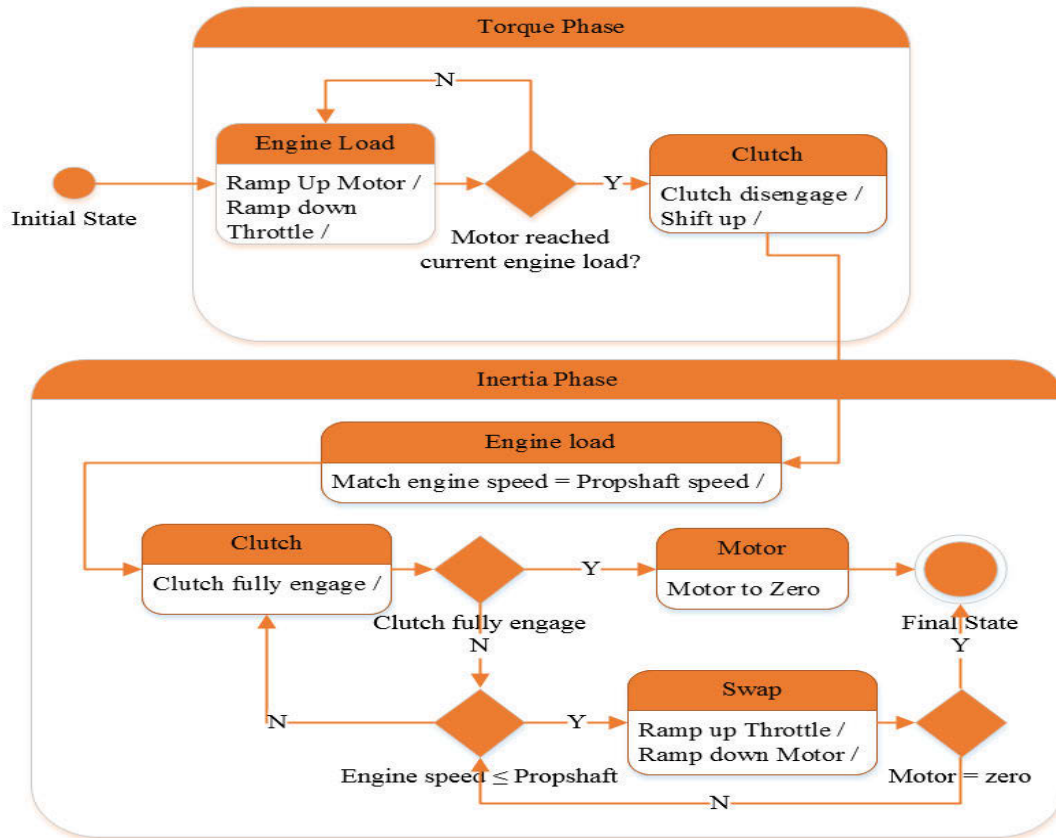


Figure 5-5: Up-shift process.

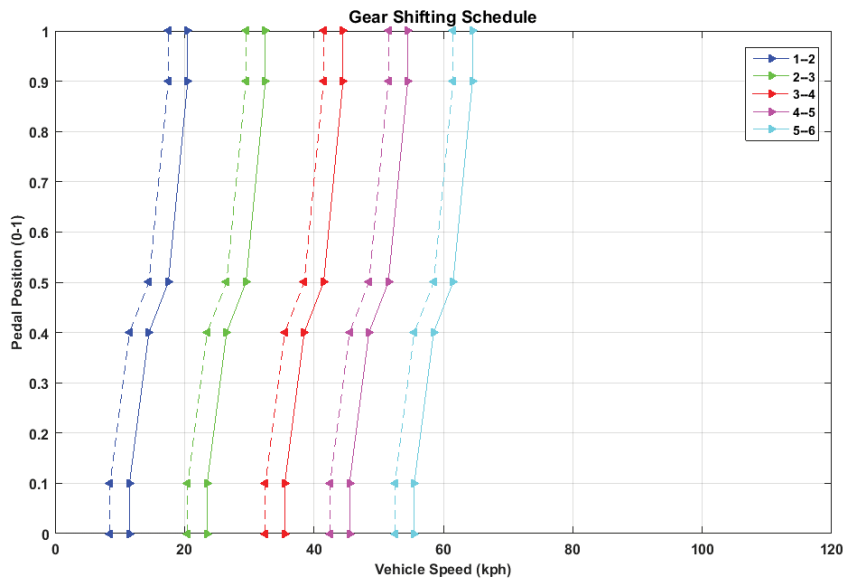


Figure 5-6: Gearshifting schedule.

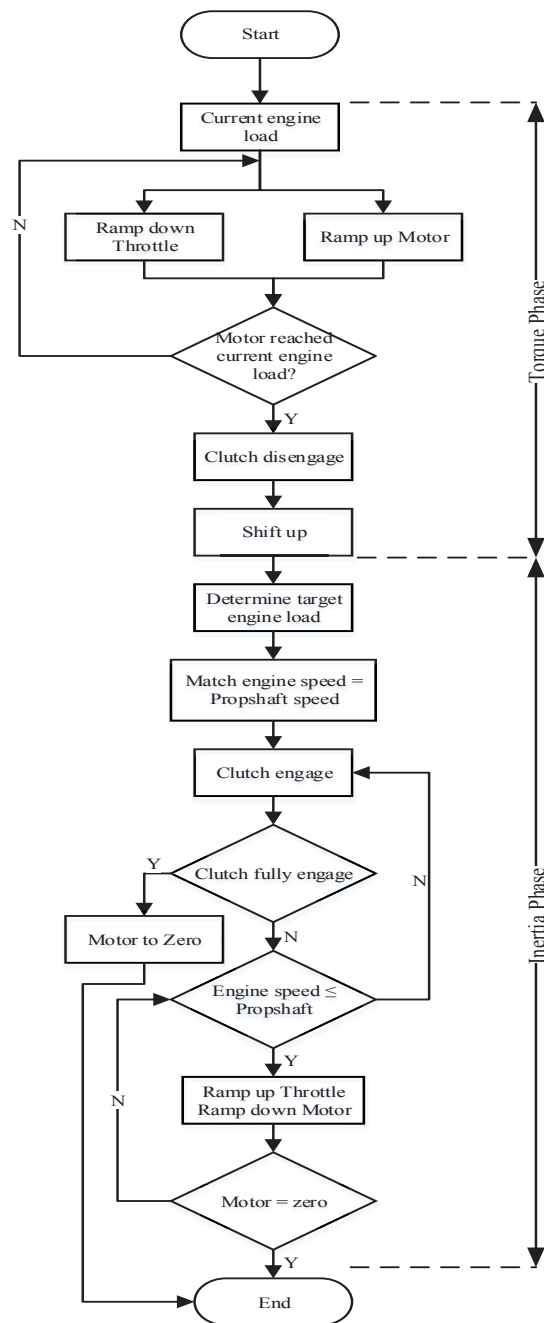


Figure 5-7: The flowchart of an Up-shift process

Manual transmission synchronizers are used to match speeds with the target gear and physically lock it to the shaft. The synchronizer consists of a dog-clutch and a cone. The dog-clutch is engaged after the cone and brings the gear up to the speed of the shaft. This hardware compensates for the normal dynamic limits of manual transmission [77], eliminating the need to accelerate each gear as it is engaged (“double de-clutching”). Synchronizers grant better performance in accelerating the vehicle and more comfortable

driving in the absence of continuous torque transmission during gearshifts [78]. When synchronisers are combined with the electric torque-fill, the hardware will ideally result in no loss of tractive torque to the road, as well as reduced maintenance by reducing wear of the clutch friction lining through better synchronisation of the engine speed to the in-gear road speed.

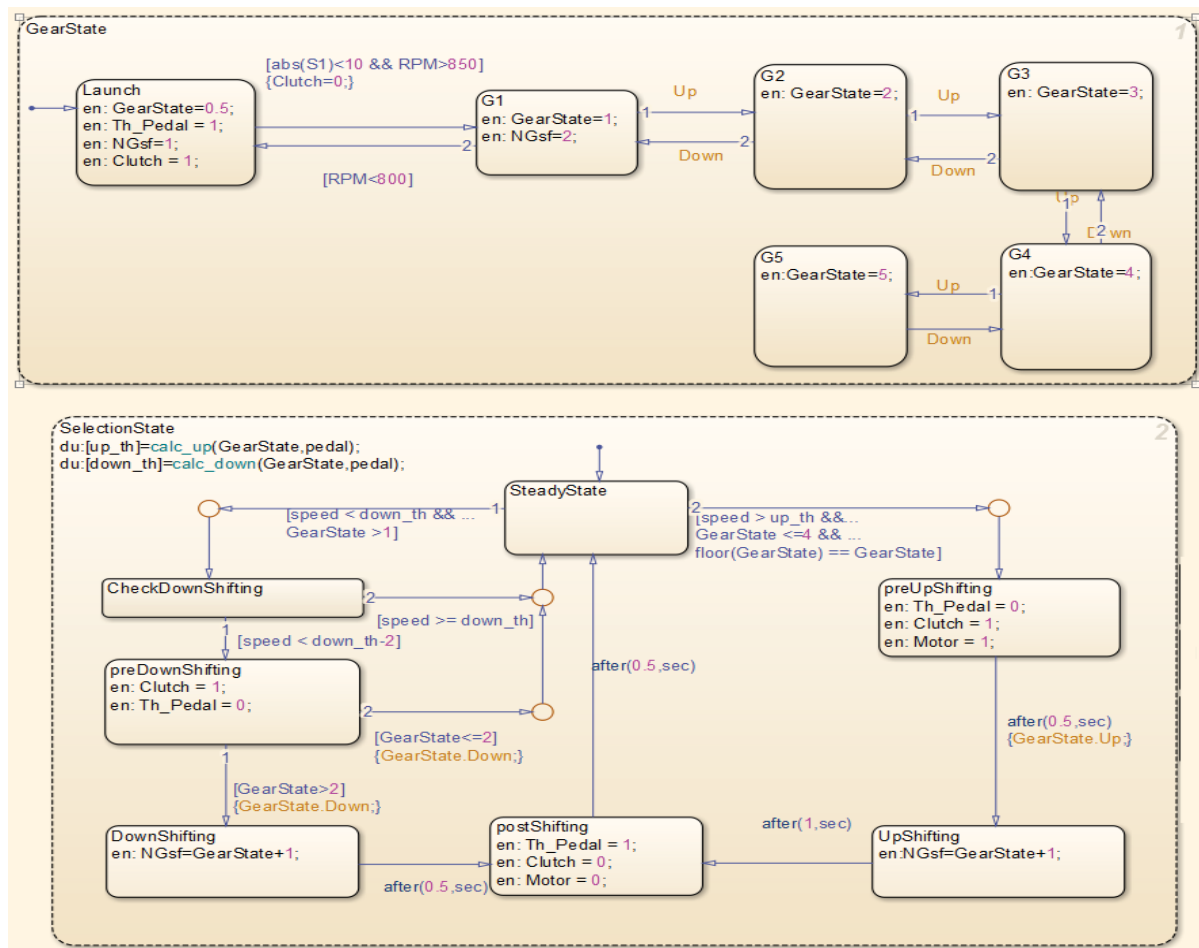


Figure 5-8: Transmission control unit (TCU).

The Stateflow chart, shown in Figure 5-8 is a realisation of the conceptual framework of manual transmission logic modelled with state flow (shift state) discussed above. While very similar to the conceptual framework, the Stateflow chart has two notable differences. The shifting processes states have been grouped to form the “SelectionState” superstate, and the gear states have been grouped together to form the “GearState” superstate. This grouping helps organise the mode logic into a hierarchical structure that is simpler to visualise and

debug. However, the inclusion of time delays in shift control must be considered to achieve best possible driveability (vibration) performance, as this allows torque disturbances caused by each event in the control algorithm to be absorbed by the powertrain, allowing the vehicle occupant more time to perceive the step in torque. This reduces the perceived aggressiveness of the shift event.

5.2.3 Energy management strategy

The EM functions as either an EM or a generator, depending on vehicle operating conditions, which are monitored and controlled using an energy management controller (EMC). EMC is known as the energy management strategy (EMS). EMC plays a critical role in the driving performance and vehicle efficiency [79]. The motor is controlled in four quadrants of operation, and together with the ICE can either drive the vehicle or be driven. A rule-based energy management strategy described broadly in Figure 5-9, was deployed on the EMC. The amount of energy that remains in the battery pack influences the most suitable driver mode for the driving conditions currently presented. This is determined by understanding more about the current, related to the State of Charge (SOC). This information is transmitted to the energy management system controller. Depending on the battery SOC and the power demand, the EM may be used as a generator driven by the ICE or by the kinetic energy of the vehicle (regenerative braking). It may also be used to power the vehicle either independently or in conjunction with the engine. Because of the relatively small energy demands of the system as compared to a full hybrid, the regenerative braking function is vitally important, as it may be used to obtain a significant portion of these energy demands. The energy wasted in braking can easily exceed 50% during daily peak-hour driving, especially in metropolises [80]. By utilising the EM extensively under all favourable conditions, system benefits can be maximised. Energy storage and power requirements are determined by considering the

demands placed by motive assistance, and the energy capture possible through regenerative braking and ICE-generator.

There are six rule-based operating modes, which may be summarised as follows:

- A. Regenerative braking (Recuperation Mode): The EM functions as a generator when the vehicle is braking, and SOC is less than maximum. The braking torque of the generator determines the maximum and minimum electric brake force applied to the wheels. It is used to recover the energy that is consumed in braking to charge the battery.
- B. EM as a generator: The EM functions as a generator when the vehicle is accelerating, SOC is low (<40%), and engine load point without generator load is inefficient.
- C. Torque assist: The EM is driven in motoring mode when SOC is not low (>40%) and delivers torque that complements the engine based on the requirement, especially during acceleration conditions.
- D. Electric-only mode: Under certain low-speed light-load conditions and when SOC is high (>80% SOC), the EM may supply all of the motive force required. This mode is developed for implementation with an AMT.
- E. Torque-hole Mode: During gear change and when SOC is not low (>40%), the EM provides a tractive force that is synchronised to the gear change. Low SOC is defined as <40% SOC.
- F. Idle mode: In this mode, the EM runs in idle condition. That is, it does not act as a generator nor does it act as a motor. This mode is often observed when the battery is fully charged, and the vehicle is cruising at high speeds and avoids loading the engine unnecessarily.

The powertrain model with a special EMC is numerically simulated in the Matlab/Simulink environment for different analysis in terms of fuel economy, emissions, electrical consumption, operation cost and total lifetime cost.

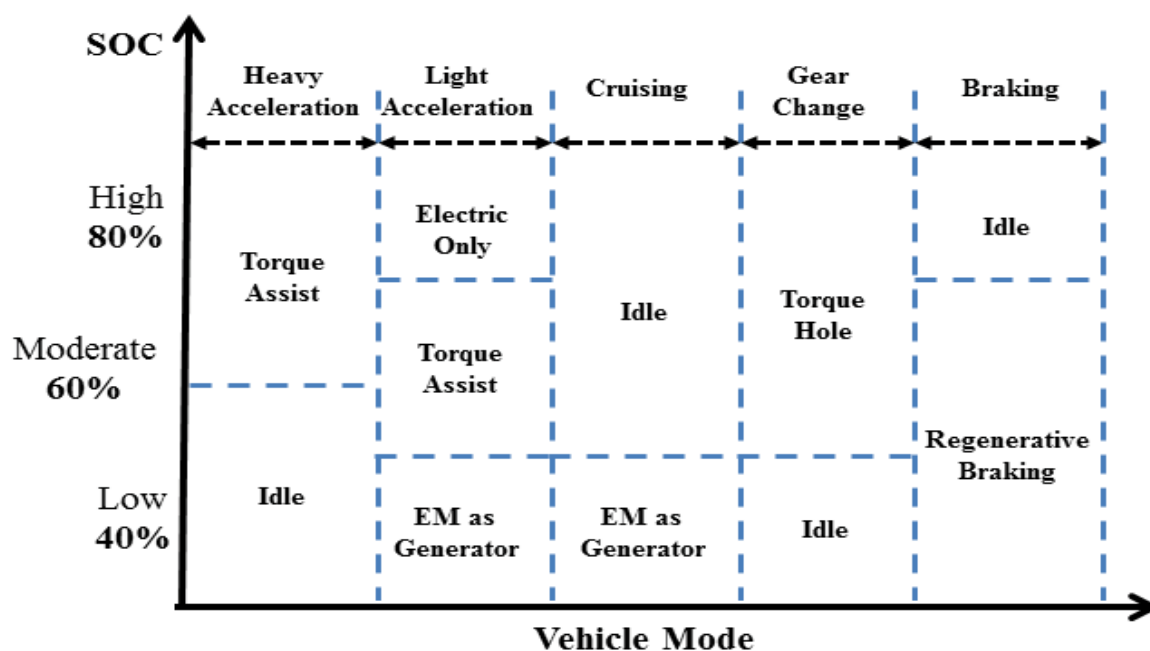


Figure 5-9: EM modes of operation.

The controller operates in a less simplistic way when the vehicle is cruising. ICE will drive vehicle propulsion while simultaneously charging energy storage devices in ICE recharge mode, in the presence of light acceleration and a decreased SOC value. This mode can be defined by the optimization scheme as the most optimum point of operation for ICE. In this mode, ICE delivered increased efficiency and decreased emissions by using specified weighting coefficients. The energy units are charged with determining the variance between power demand and maximum ICE power. In the presence of increased vehicle acceleration, the ICE can only operate the vehicle, not allowing the battery to be charged. Increased emissions would result in this mode when both high torque and low speed are used to start up the vehicle, demonstrating the worst possible operating condition for the powertrain.

To reduce this aforementioned drive mode, the EMC has been designed to increase the reliability of the overall powertrain system. In the instance where the EMC has a moderate SOC during vehicle cruising, the ICE may be engaged to recharge the battery. In the case of light acceleration and conjunction with a high SOC level, EM only mode is engaged and drives the vehicle until a point where the SOC has reached a middle point. An exception to

this is when the demand for power has reached the upper limits of the EM, in which case the ICE and EM work simultaneously to meet the vehicles power requisites.

The above can be seen in a situation where the vehicle is ascending a hill, and there is a requirement for full acceleration, resulting in more of a power demand than the EM can provide. In this case, the ICE and EM work hand in hand to provide a combined power for adequate vehicle propulsion. The required power can be delivered solely by the ICE, and the EM is disabled when there is less demand for power. When the EM and ICE function together, the EM delivers a compromise between both the power demand and maximum power of the ICE. In this combined mode, the ICE is able to operate with increased fuel efficiency and reduced emissions.

During the deceleration process, the vehicle generates the kinetic energy to produce electricity that can be stored in the battery pack using the EM as an electric generator. This process is known as a regenerative braking event. If the SOC level of the battery is low to make sure that the battery SOC is always at a high level.

The implementation of an appropriately configured battery pack improves the suitability of the system in recovering braking energy under saturated load conditions (i.e. high speed or high braking demand). By sizing the battery for peak charging as well as peak discharging demands, the back electromotive force (EMF) generated by the motor may be efficiently harnessed to charge the battery pack if battery SOC permits. The SOC is further defined in Chapter 7.

5.2.4 Other drive conditions

There are many different and combination paths for power to flow in the vehicle. It is important to have a good power flow distribution in the vehicle during the plugging-in to the standard power outlet, waiting for the traffic light or traffic jam and when the vehicle is

totally stopped for optimum working conditions. A good distribution of power flow leads to a good EMC of the vehicle. The power flow in the vehicle while waiting for the traffic light or traffic jam when the vehicle speed is zero while waiting for a change in signal, the ICE is turned on to take this opportunity to recharge the battery pack using the EM as an electric generator. During the stop event, when the vehicle is totally stopped, both the EM and ICE are not operating. All the accessory loads like radio, light and air conditioner in the vehicle will be powered by the battery pack.

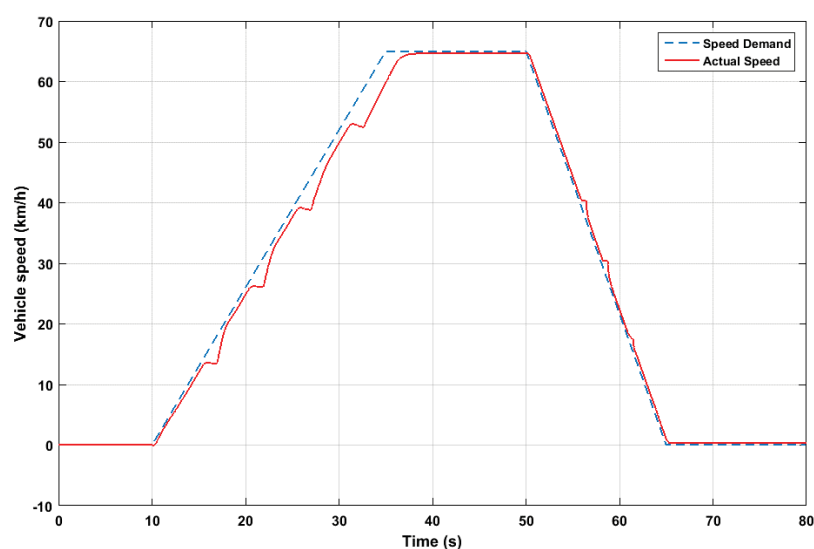
5.3 Mass constraints

The development of efficient and compact HEV powertrains for low-cost constraints requires consideration of numerous, often competing factors. One such factor is vehicle mass, which is constrained by three competing parameters. Namely, these are the total stored energy in the vehicle, against the impact on vehicle emissions, against the purchase and ongoing operational costs. The motor chosen for this study has a mass of 16 kg. Estimation of the mass of other componentry was conducted to estimate the weight penalty as compared to an otherwise identical ICE-only vehicle. The battery was estimated to be 40 kg, power electronics and controller 10 kg, wiring harness including high-power cabling of 10 kg, and housings, powertrain components, and bracketry of 20 kg. Therefore, the nominal mass of the EPS is 96 kg. The mass of components that could be downsized or eliminated included the starter motor and ring gear (2.5 kg), 12 V battery (5 kg). This calculation leads to a net weight penalty of approximately 88.5 kg, or approximately 108% of the ICE-only vehicle weight. This figure was deemed to be an acceptable outcome.

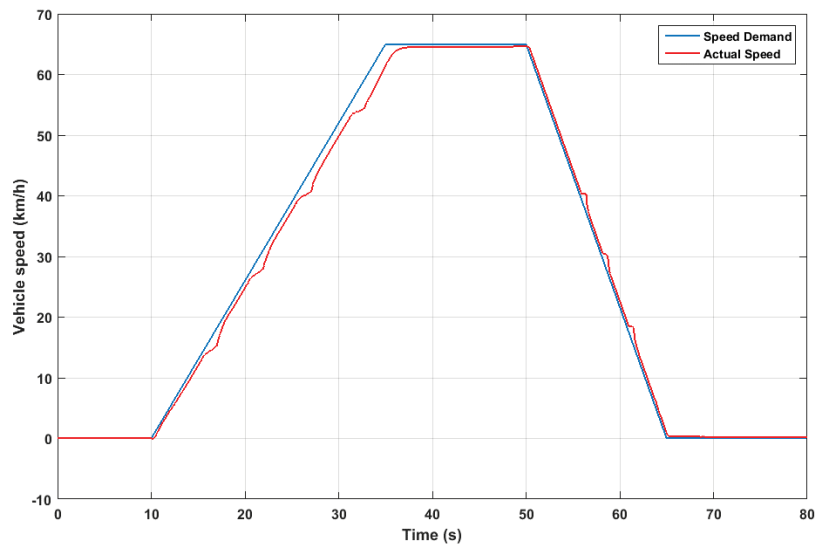
5.4 Simulation results

Before building a prototype, model simulation is the most appropriate tool for evaluating and analysing the performance of vehicles, particularly hybrid electric vehicles. Moreover, model simulation is a major step for the validation and calibration of such systems and has therefore

attracted interest from both industry and academics. The powertrain model discussed herein was built in the Matlab/Simulink environment as a mild HEV model. The Simscape simulation was performed using the ODE23t element from the ODE suite with a maximum time step of 10^{-1} for the powertrain model; relative tolerance is set to 10^{-3} . State flow event functions were used to determine lockup conditions and move between powertrain models. The results mainly focus on the electric drive mode part and comparison of the transient response of drivetrains. For initial data comparison with between models, a single cycle of the Rural Driving cycle (RDC) Figure 5-10 was used. It was selected for its simplicity and utilises five up-shifts over its duration. The RDC is a dynamometer drive schedule that is used to benchmark vehicle performance in a controlled manner. The RDC does not include any simulated incline changes and is intended to test a vehicle as it might perform in a rural setting. It was selected as an initial benchmark for its simplicity and its ability to highlight gearshift characteristics consistently. It features a single acceleration event, a cruise, and a deceleration and utilises five up-shifts over its duration. Each up-shift results in a large hole in the output torque and decreasing acceleration. Figure 5-11 represents the output shaft torque of the conventional and torque-fill drivetrain when upshifting from 3rd to 4th gear.



(a) Conventional vehicle Manual Transmission simulation on the RDC drive cycle.



(b) Mild Hybrid vehicle simulation on the RDC drive cycle.

Figure 5-10: (a)-(b). Rural Drive Cycle simulation for both conventional and mild hybrid vehicles.

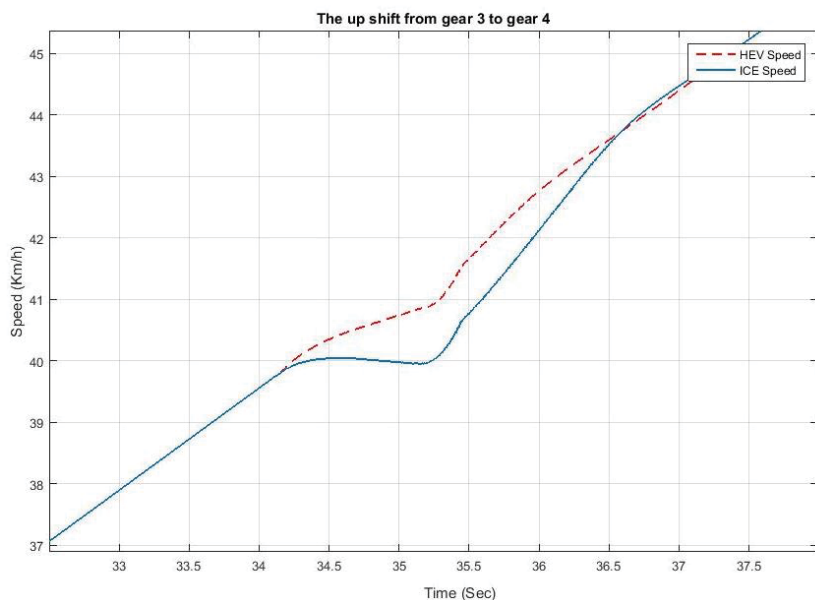


Figure 5-11: Shift process analysis.

The speed of the input shaft (i.e. engine speed) during the gear change event is related to the initial gear ratio and road speed in the first instance. When the clutch is disengaged, the engine speed becomes independent of the selected gear and road speed and is instead solely dependent on throttle angle. When the target gear is selected, and the clutch is engaged, the engine speed is proportional to the new gear ratio and the road speed. The gearshift process results in a large hole in the output torque and a decrease in speed during both the clutch disengagement and gear selection processes during shifting. This torque hole can be reduced

by bringing the electric motor into motive contact with the final drive throughout the control process, so long as the clutch hydraulic pressure is greater than zero. Simulations were conducted using both a conventional and a torque-fill drivetrain. These were modelled for comparison. The result shows the difference in magnitude of the torque hole between the different powertrains. The results mainly focus on the variation in shaft speed due to different gear ratios and compare the transient response.

Figure 5-12 shows the velocity of the vehicle during an acceleration event 0-100 km/h under maximum throttle conditions. This simulation was conducted to gauge the performance improvement in this vehicle benchmark as compared to the conventional powertrain. During gear changes, the torque-fill control method was implemented. Other than during gear changes, the throttle was held fixed at 100% open. The results of this simulation show acceleration time is reduced by approximately 1.5 seconds using the torque-fill drivetrain, and the deceleration during each gearshift is reduced markedly.

Figure 5-13 represents the output shaft torque of the conventional and mild HEV drivetrain when upshifting from 2nd to 5th gear, following the 0-100 km/h drive cycle shown in Figure 5-12. For clarity, the data after the 4-5 gear change is truncated. In each upshift event, there are three discrete torque oscillation responses. Disengaging the clutch causes the first torque excitation. When the clutch is opened, the engine and flywheel inertia are decoupled from the transmission. This sudden change in inertia causes excitation of torque response. Synchronising gears causes a second, smaller excitation. When the previous gear is desynchronized, and the next gear is locked to the output shaft, this causes a variation in layshaft speed due to the energy absorbed by the synchroniser as well as windage and bearing losses. The third spike occurs when the clutch is re-engaged. Torque overshoot can occur due to different rotational speeds between the flywheel and clutch disc [81]. The torque excitations on the output shaft are illustrated. The torque profiles of original drivetrain and

the torque-fill drivetrain are compared. When the system is operating in torque fill-in mode, it is shown that the torque hole is reduced, as well as a marked reduction in the oscillatory peak, by approximately 175 Nm.

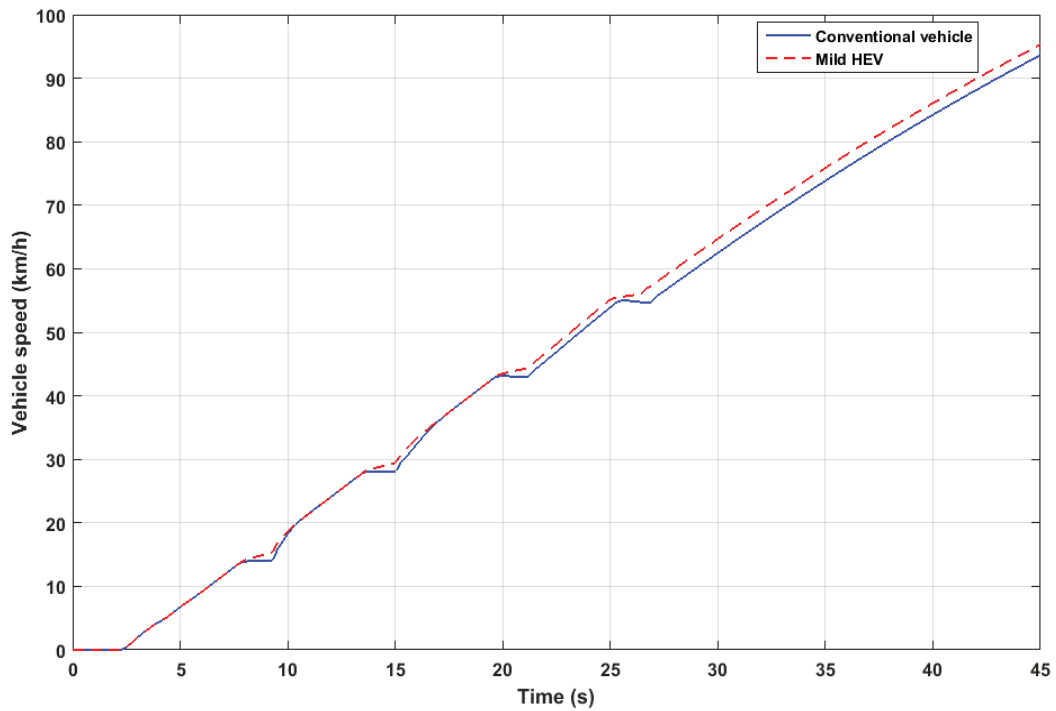


Figure 5-12: 0-100 km/h acceleration in ICE and Mild HEV models.

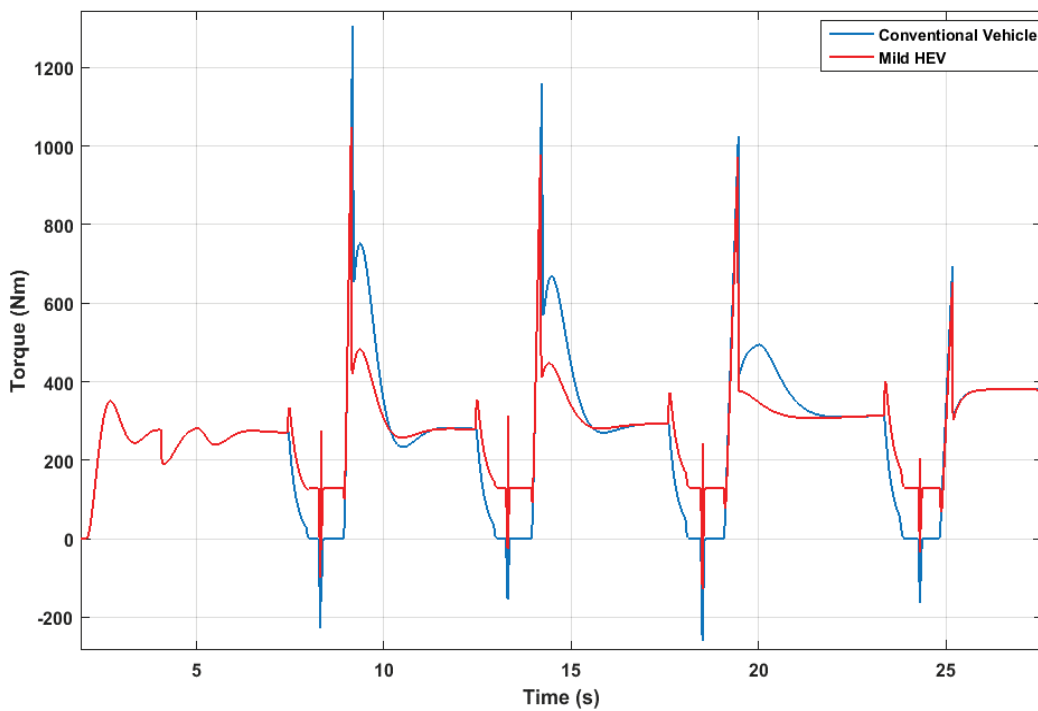
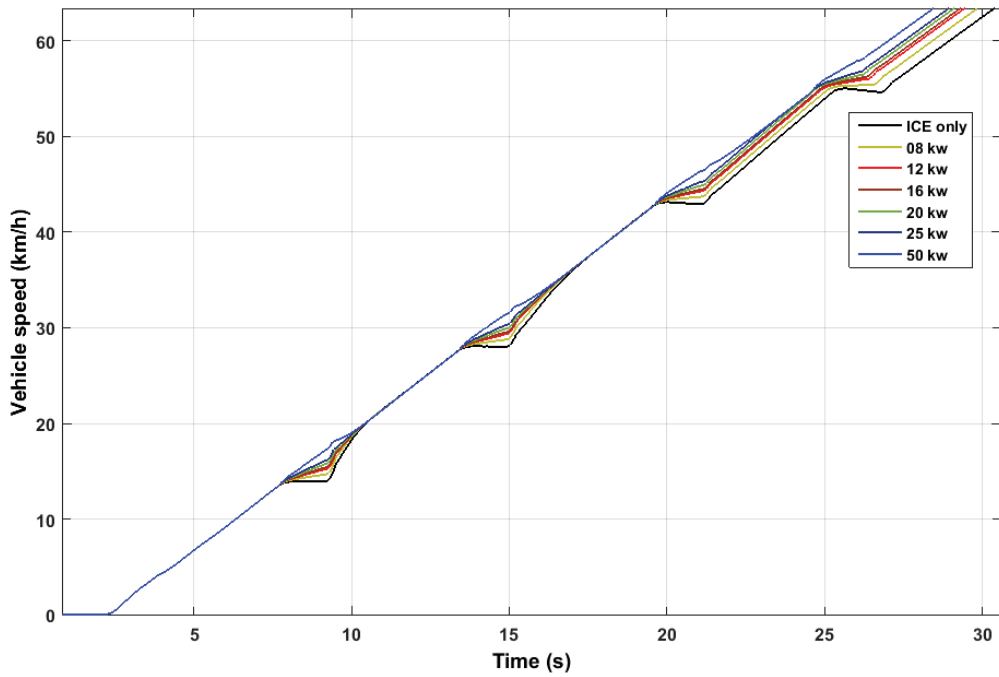


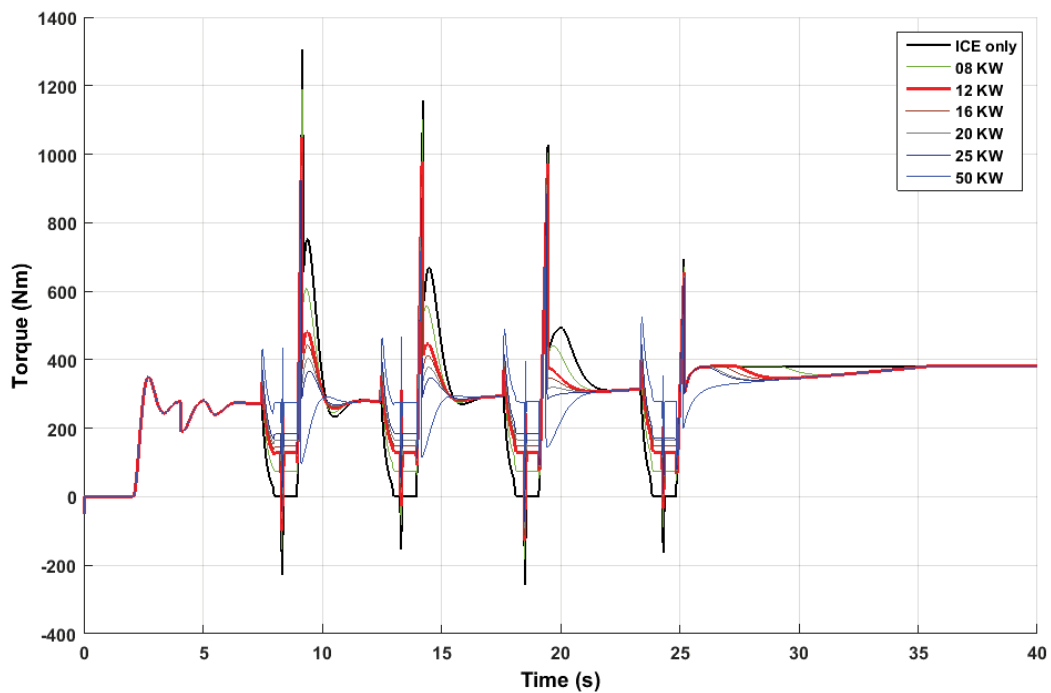
Figure 5-13: Output shaft torque profile during 0-100km/h acceleration cycle.

5.5 Motor selection

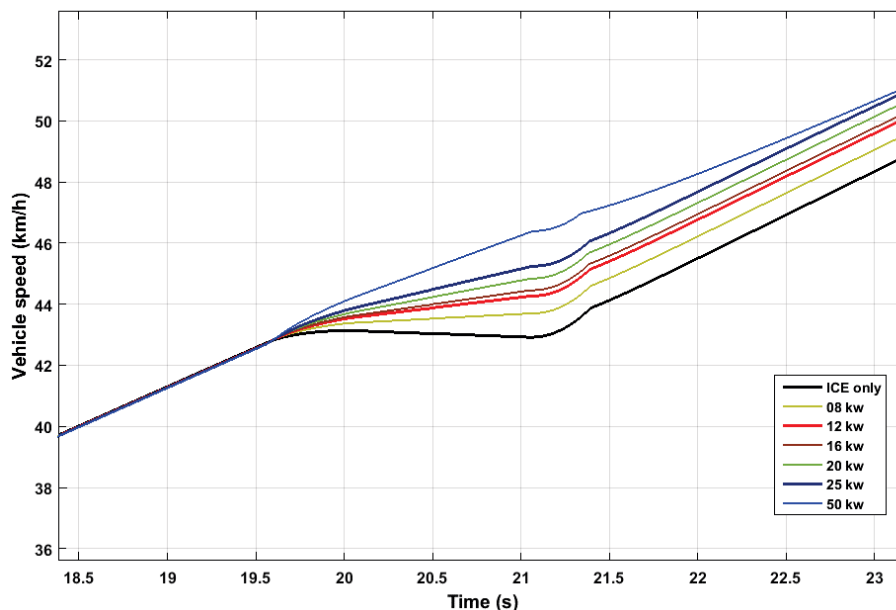
Other motor options were simulated to validate this selection, ranging from 8 kW (a sub-mild hybrid) to 20 kW electrical power in 4 kW increments. 25 kW and 50 kW simulations were also conducted to investigate the difference between a low-powered mild-hybrid, and a higher-powered electric motor as would be installed in a full-hybrid vehicle. The hypothetical motors were characterized by scaling the torque/speed characteristics of the ME0913 that was physically available for testing. A partial throttle acceleration test was simulated using each hypothetical motor, consistent with a typical gradual acceleration to cruising speed and using time-based shift events. The output results were examined. Summary results are presented in Figure 5-14. From the investigation of different motor characterizations, the hypothetical 20 kW motor had a noticeable effect in decreasing the oscillation excited by the gear synchronisation (the second and smallest oscillation observed in each gearshift event). However, the other two, larger oscillations showed an increasing trend in magnitude with decreasing motor size. Torque-fill effectiveness was similar for the hypothetical 16 kW and 20 kW motors. The ICE-only powertrain achieved a maximum vehicle velocity of 94 km/h at the end of the 30-second test. The hypothetical 20 kW and 16 kW motors achieved the same speed 36% faster. The ME0913 was approximately 6% slower than these on a 30-second acceleration test, and the hypothetical 8 kW motor was approximately 9% slower again. This difference indicates that the ME0913 is somewhat under-specified, which is consistent with the previous analysis. It also indicates that the hypothetical 20 kW motor offers no significant benefit compared to the 16 kW option.



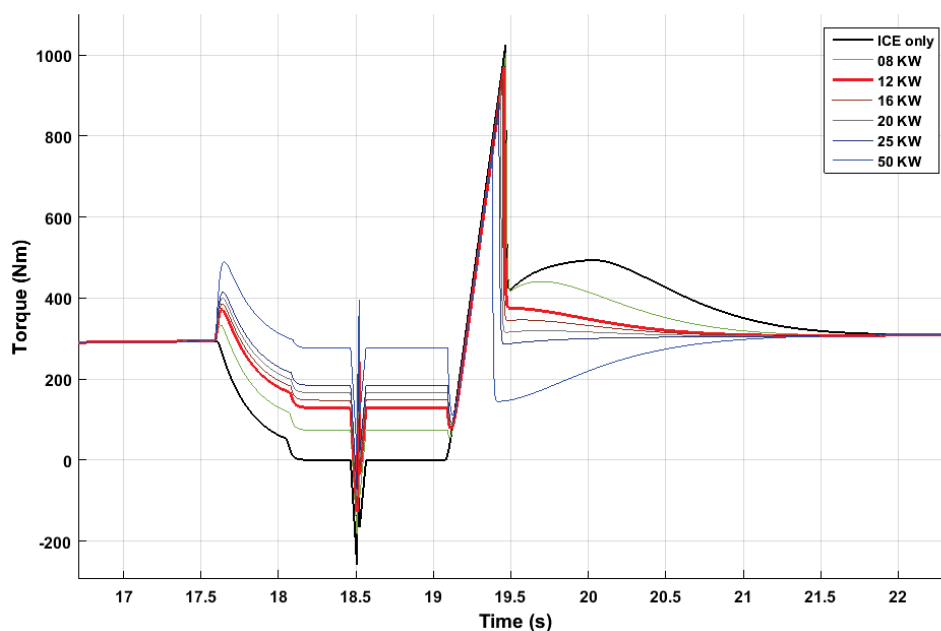
(a) Vehicle performance study: 0-60km/h.



(b) Vehicle propshaft torque during the study performed above.



(c) Detail of the 3-4 shift, showing variation in vehicle speed.



(d) Detail of the 3-4 shift, showing variation in propshaft torque.

Figure 5-14: (a)-(d). Mild hybrid manual transmission performance study with different motor powers.

5.6 Shift quality

One of the most important performance characteristics of automobiles is shift quality. Disruption of driveline torque during gear ratio changes can result in noise, vibration, and harshness issues that can negatively impact the customer's perception of the vehicle's drivability and quality. Loud clunks and jerkiness do not translate into customer satisfaction.

Vibration Dose Value (VDV) has been used to quantify human reaction to vibration in many fields, including NVH in the automotive industry [16, 82]. Because VDV correlates well with human perception, it has become somewhat of an industry standard objective metric for transmission shift quality [83]. It is, in essence, an integration of the fourth power of a band-pass filtered acceleration signal over the shift event. When the technique is applied to longitudinal acceleration data collected during a transmission shift, the calculated VDV is representative of the driver's physical perception of the harshness of the shift. The VDV is obtained from a suitably filtered vehicle acceleration signal, as shown in equation (21). Because of the bandpass filtering applied to the acceleration signal, the figure obtained is independent of other acceleration events.

To calculate the full VDV to which the vehicle occupants are subjected, it is necessary to include calculations for acceleration in the three axes. However, because our focus is on the use of VDV as a shift-quality metric, it is not necessary to include vertical or lateral vibrations. VDV is calculated according to equation (5.8) below.

$$VDV = \sqrt[4]{\int_{t_0}^{t_f} \hat{a}^4(t) dt} \quad (m/s^{7/4}) \quad (5.8)$$

In the equation (5.8), $\hat{a}(t)$ is the vehicle longitudinal acceleration, filtered according to the Butterworth Band-pass filter with a 32 Hz cut-off. The range 0-32 Hz is used to calculate VDV values due to human sensitivity to this range of frequencies. t_0 is the time at the start of the gearshift and t_f is the time at the end of shift. VDV was used to parameterize improvement in comfort. Following the method outlined in [84, 85], VDV was calculated for the ICE and mild hybrid cases presented in this study. Because VDV is time-dependent, it was used as a comparative tool, to analyse the VDV arising from the test scenario of a single gear change of three-second duration. The result from a single gear change can be used to

inform a trend over a whole drive cycle. Table 5-1 shows how VDV varies with gear the shift in both the ICE vehicle and the mild hybrid. As expected the shift quality improved approximately 16% when a torque-fill strategy was used, without any change in clutch actuation profile. Better transient control of the clutch and motor power ramping profile will yield further improvement in VDV, by minimising the torque excitation peaks shown in Figure 5-13.

Figure 5-15 shows VDV calculated for each gearshift in the simple drive cycle (shown in Figure 5-12). The simple drive cycle features four sequential upshifts, from gear 1 to gear 5. For each upshift, VDV was calculated for no in-fill torque, as well as in-fill using 8, 12, 16, 20, 25, and 50 kW hypothetical motors. The control strategy was kept constant. The curves obtained represent interpolations of results obtained by testing the six mild HEV configurations. The minimum VDV was observed at a motor power of 15-20 kW. This result agrees well with the simple acceleration test, in which the 16 kW motor option presented the best results, and further agrees with the analyses presented previously.

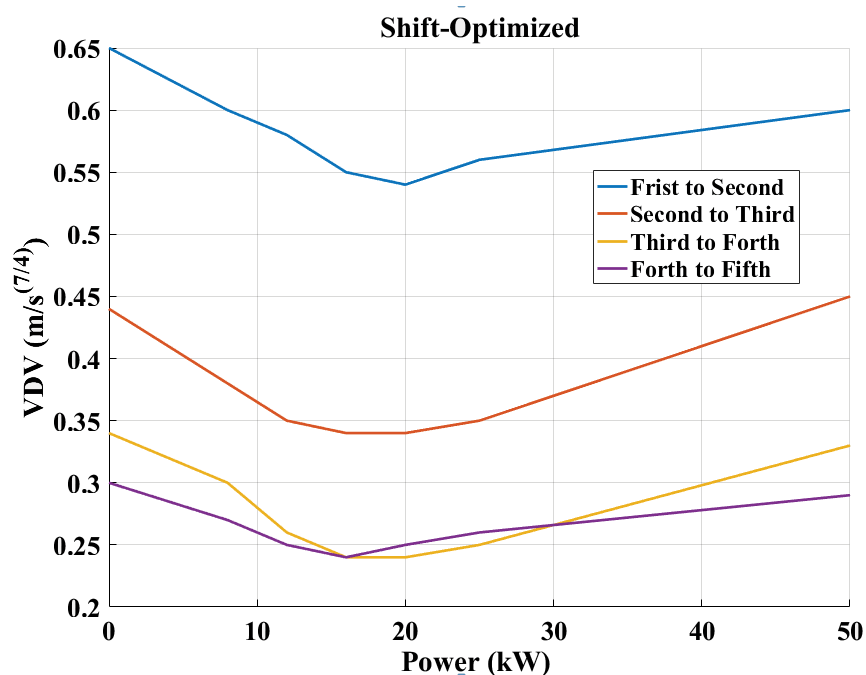


Figure 5-15: Shift-optimized

Table 5-1: VDV profile

	VDV of mild HEV (Motenergy ME0913 motor) ($m/s^{7/4}$)	VDV of ICE vehicle (no electric motor) ($m/s^{7/4}$)
1 st to 2 nd gear	0.58	0.65
2 nd to 3 rd gear	0.35	0.44
3 rd to 4 th gear	0.26	0.34
4 th to 5 th gear	0.25	0.30

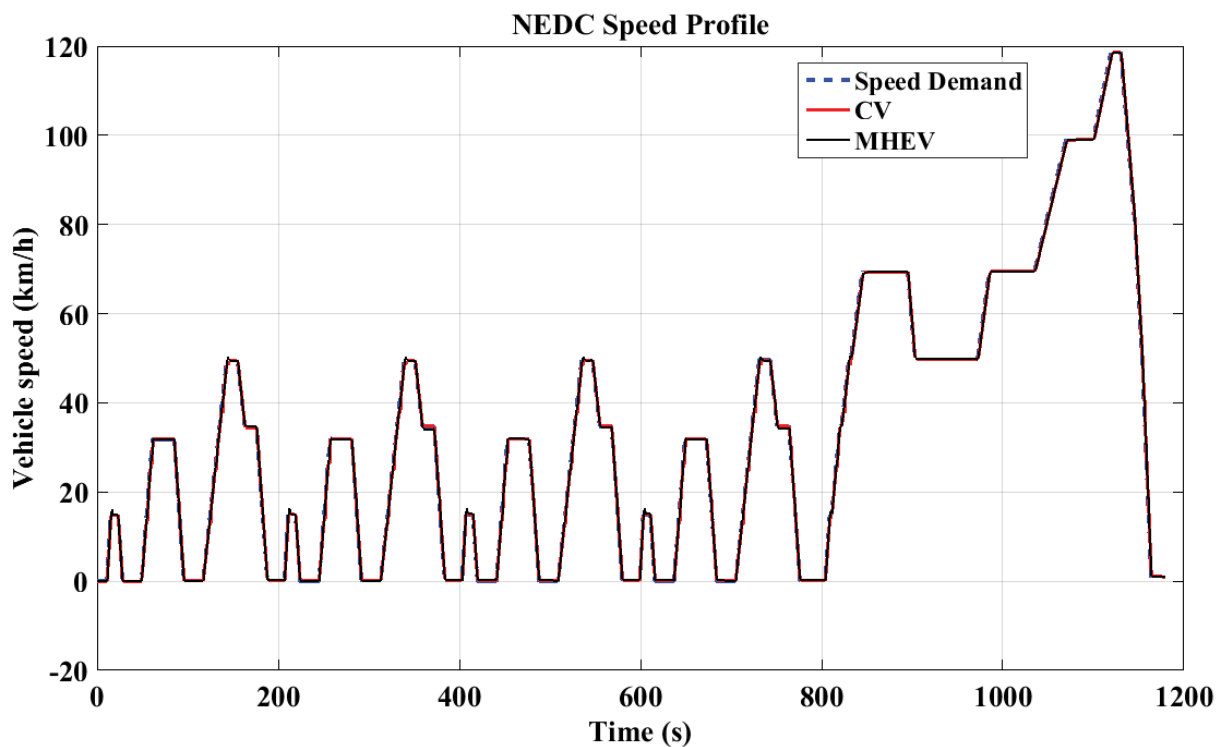
5.7 Drive cycles

The drive cycle profile model contains a time history data for the desired vehicle speed, where several standard drive cycles profile. These drive cycles consist of multiple accelerations and braking events for a particular range of time depending on the type of the drive cycles profile. The drive cycles used for the simulation are New York City Drive Cycle (NYCC), Urban Dynamometer Drive Schedule (UDDS) and the New European Drive Cycle (NEDC). These are illustrated in Figure 5-16. Table 5-2 shows some characteristic parameters of the selected drive cycles, according to these parameters the cycles can be classified into different driving patterns [86, 87]. The NEDC was utilised primarily to provide a better comparison with the literature, as it has been adopted as a standard in many developed regions. However, the UDDS and NYCC were selected owing to their low average speed and frequent stops, which are more representative of the typical urban driving conditions that were being replicated. The NYCC has an average speed of less than 20 km/h, but speed fluctuation is high. It is also characterised by frequent stops, representing the high levels of heavy traffic that would be seen in developing metropolises. In comparison, the NEDC average speed and speed fluctuation are both moderate, representing typical driving conditions in a suburban area. The cycle is characterised by fewer idle times and includes high-speed cruising. A highway cycle is not representative of real-world driving in the target market and is not considered useful to this study. This is validated by prior literature, e.g., [88], which establishes that the percentage improvement in fuel economy by adopting mild

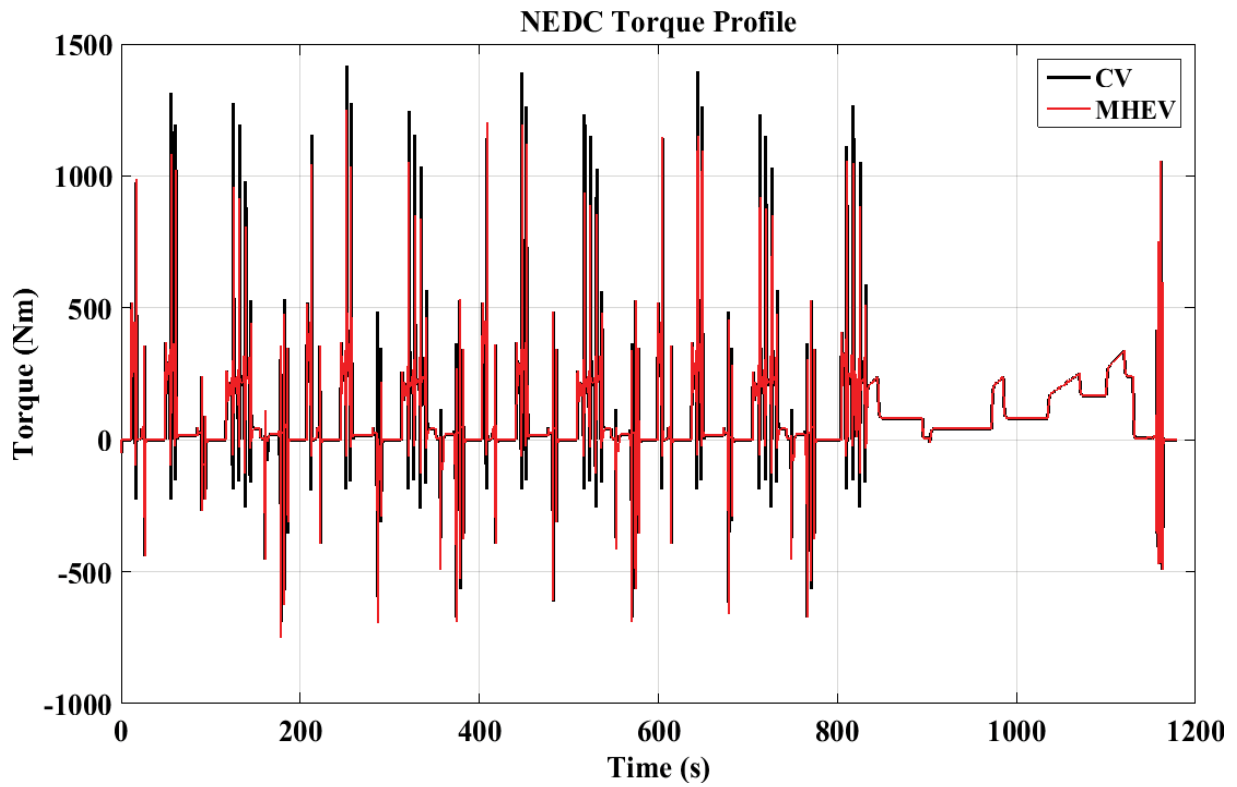
hybrid configurations for highway cycles is significantly less than for city driving. The block outputs of drive cycle profile model in the Simulink is vehicle speed based on the current simulation time.

Table 5-2: Characteristic parameters of different driving cycles.

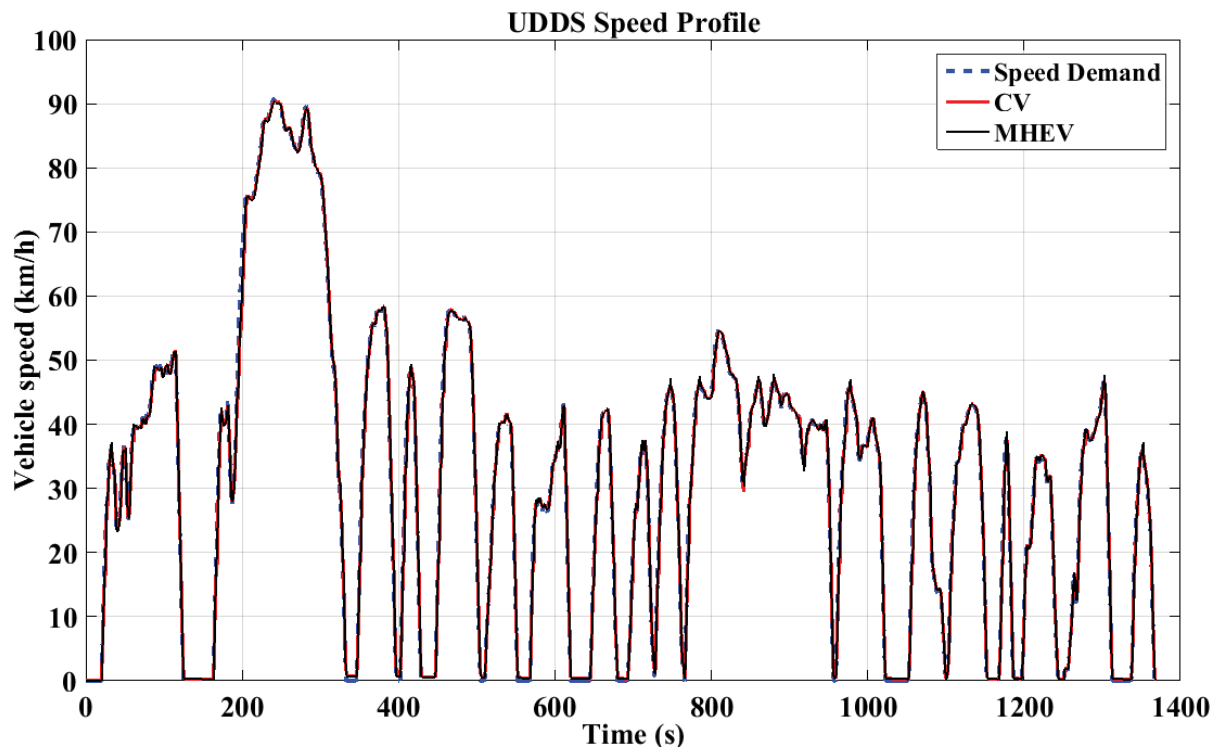
	Distance (km)	Time (sec)	Idle Time (sec)	Max Speed (km/h)	Avg Speed (km/h)	Avg Acc (m/s ²)	Avg Dec (m/s ²)	Max Acc (m/s ²)	Max Dec (m/s ²)
NEDC	10.8	1184	298	120	33.21	0.54	-0.79	1.06	-1.39
UDDS	11.9	1369	259	91.25	31.51	0.5	-0.58	1.48	-1.48
NYCC	1.87	598	210	44.58	11.41	0.62	-0.61	2.68	-2.64



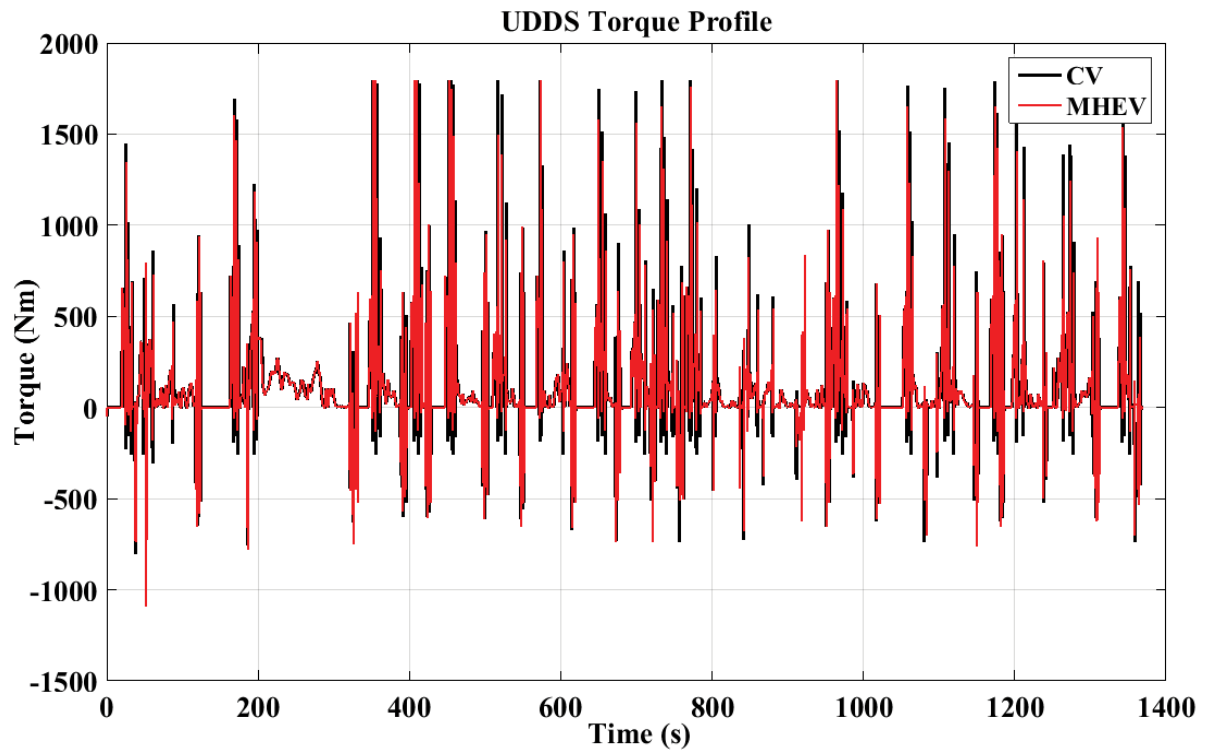
a. NEDC speed profile in CV mode and MHEV mode.



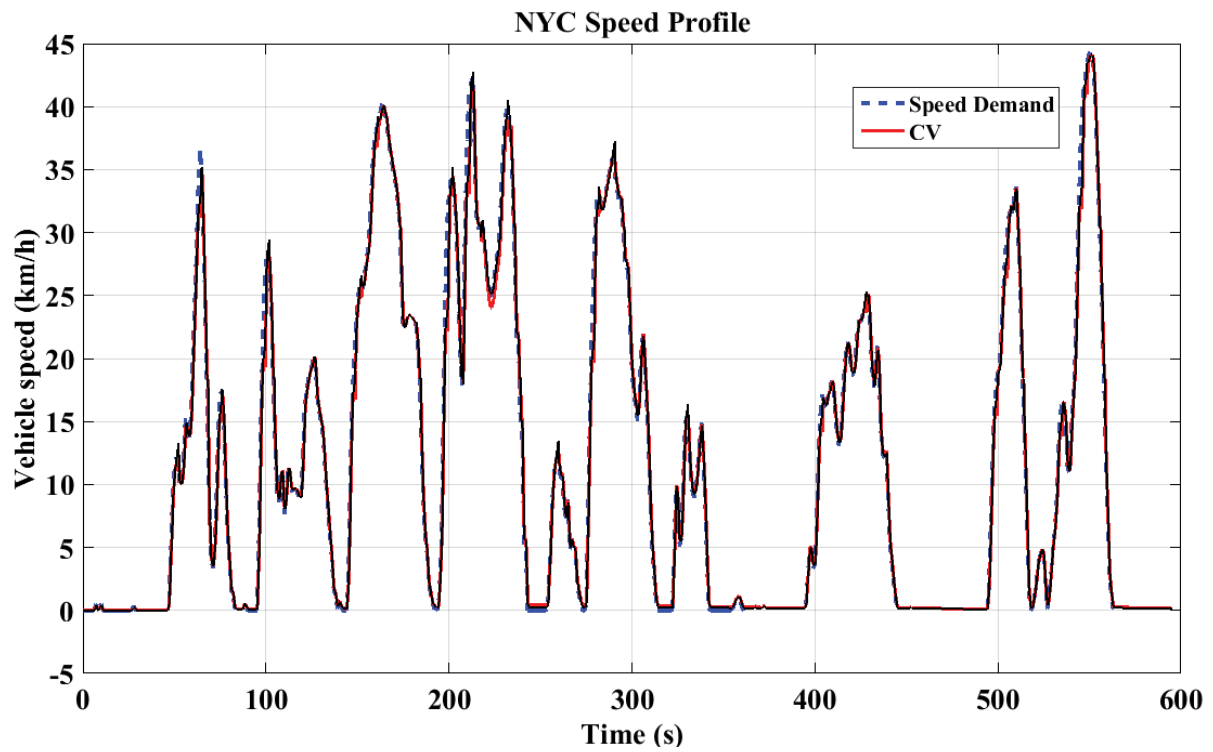
b. NEDC torque profile in CV mode and MHEV mode.



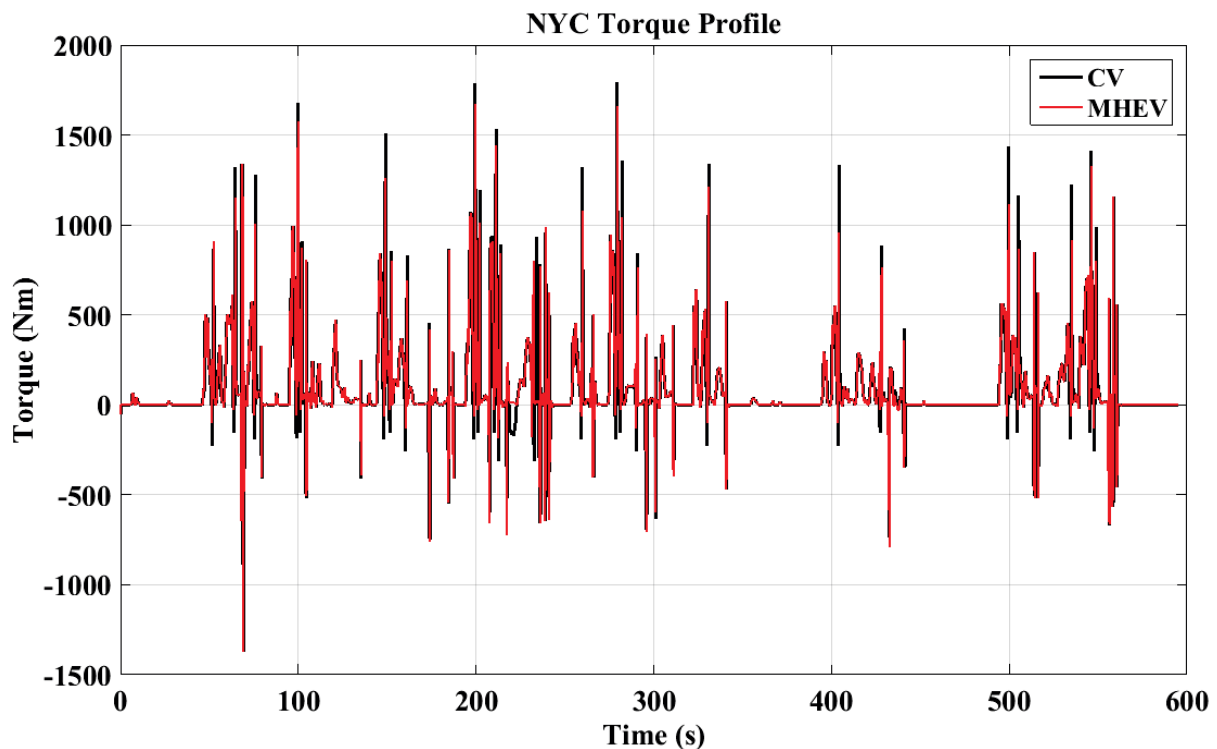
c. UDDS speed profile in CV mode and MHEV mode.



d. UDDS torque profile in CV mode and MHEV mode.



e. NYC speed profile in CV mode and MHEV mode.



f. NYC torque profile in CV mode and MHEV mode.

Figure 5-16: Speed and Torque profile for the NEDC, UDDS and NYCC.

5.8 Summary

This chapter gave an overview of the Mild HEV powertrain model development, which includes detailed modeling of each vehicle component and the overall structure in Matlab/Simulink environment. It has presented a strategy for up-shifting that employs the increased EM functionality to decrease the torque hole. The torque-fill drivetrain can be used equally successfully with automated manual, and traditional manual gearboxes, and the limited motor power and duty cycle limit the size and cost of other system components. Due to the intermittent operation, it is also possible to safely operate the components beyond their rated continuous output and yield greater benefit.

Through investigation of power needs of the motor using the NYC driving cycle, it was established that only a limited number of shifts would require more than approximately 10 kW of power for the duration of the gearshift. This information was used to guide a study of the degree of torque hole compensation required. It was further established that a minimum

power of less than 8 kW was necessary to prevent deceleration of the vehicle. These bounds were utilised for parametric investigation of alternative motor sizes and the impact on vehicle acceleration and vibration. These results demonstrated that while it is possible to compensate completely for any torque hole during shift changes, a minimum VDV is achieved with only partial torque compensation. This result leads to the conclusion that the analysis can consider the trade-off between additional cost requirements for the vehicle and driver comfort.

This chapter gives an overview of the powertrain EMC development, which includes detailed modeling of modes of operations as the braking and cruising drive conditions. The developed EMC is integrated into the overall structure of the powertrain model in Matlab/Simulink environment in order to implement various analyses. Then, in the next chapter, a few tests, such as acceleration, fuel consumption and a comparative study on components simulation results between the ADVISOR and MHEV are presented.

Chapter 6: Model verification with fuel and emissions analysis

For conventional vehicles equipped with manual transmission (MT) transmissions, a characteristic of the gear selection process is the introduction of a sudden change in the engine operating point, due to a stepped shift in the transmission ratio. With highly non-linear characteristics for fuel consumption (FC) and maximum torque of the internal combustion (IC) engine, a change in the engine operating point due to a gearshift can result in fuel-inefficient operation states and/or poor-drivability conditions. Either of these has the effect of increasing greenhouse gas (GHG) emissions. Typically, these drawbacks have been overcome using more complex or less fuel-efficient transmission technologies. These technologies include AT, DCT, AMT and CVT. However, compared to an MT each of these technologies is generally more expensive, and/or causes increased fuel consumption. Overcoming these drawbacks whilst retaining the MT's cost advantage is therefore essential to successfully designing a hybrid vehicle for developing markets.

Mild hybrid vehicles have been explored as a potential pathway to reduce vehicle emissions cost-effectively. The use of manual transmissions to develop novel hybrid vehicles provides an alternate route to producing low cost electrified powertrains. In this research, a comparative analysis examining a conventional vehicle and a Mild HEV is presented. The analysis considers fuel economy, capital and ongoing costs, and environmental emissions, and includes developmental analysis and simulation using mathematical models. Vehicle emissions (nitrogen oxides, carbon monoxide and hydrocarbons) and fuel economy are computed, analysed, and compared using a number of alternative driving cycles and their weighted combination. Different driver styles are also evaluated. Studying the relationship between the fuel economy and driveability, where driveability is addressed using fuel-

economical gearshift strategies. The simulation suggests the hybrid concept presented can deliver fuel economy gains of between 5% and 25%, as compared to the conventional powertrain. This chapter presents a comparative study on the fuel economy, emissions, and electrical consumption using different standard drive cycles and differently developed low and high-density traffic patterns and real-world drive cycles. Using two different charge tests, which are fully and partially charged, the fuel economy and emissions are computed, analysed and compared to the different standard drive cycles for the MHEV and conventional vehicle powertrains. In this chapter, the energy usage (fuel and electrical) for both the conventional and the hybrid vehicle configurations will be estimated. To do this, the conventional vehicle on which the hybrid is based (Mazda MX-5 MY90) is modelled as the base vehicle scenario. Its model is run through simulations that are validated using legislated drive cycles. These drive cycles focus on urban environment simulation, where fuel consumption can often be up to 50% higher than free-flowing (highway) environments. These environments represent the greatest possibility of improvement [89, 90]. In the second step, the electric side of the powertrain is added to the baseline vehicle model, and the simulation is run otherwise identically. This step provides a second set of results which can be benchmarked against the baseline. This chapter describes the performance analysis and sensitivity study of the powertrain model and performs model verification of selected subsystems between the ADVISOR and the powertrain.

6.1 Survey and discussion of the choice simulation tool for verification

Computer modeling, and simulation can reduce the expense and length of the design cycle of hybrid vehicles prior to the prototyping stage. A number of different software platforms have been developed to enable the accurate simulation of HEVs including Powertrain Systems Analysis Toolkit (PSAT) and The Advanced Vehicle Simulator (ADVISOR). These software solutions are either forward-looking in nature or backwards-looking modeling approach,

respectively. In the forward-looking approach, the driver module provides the input to the model, which reacts to the driver commands to follow a defined speed profile. In contrast, the backwards-looking approach uses the vehicle speed as an input to define the parameters that are required to meet the input demand. ADVISOR and PSAT do not allow any modification to its vehicle model it cannot be adapted to simulate the proposed MHEV powertrain. In order to simulate the proposed MHEV, a model has been derived and compiled in Matlab/Simulink code.

PSAT has been developed in the Matlab/Simulink environment to simulate various vehicle powertrain architectures. However, the main advantages of the forward-looking model, which are better in capturing the dynamics of the system transient component behaviour, vehicle response and at testing the performance of an actual control system, become the main factors in selecting this modeling approach. It is a better modeling approach if the objectives are to accurately model and simulate the systems and to develop an optimal control algorithm for the system. Once the control algorithm is tested and verified in the simulation mode, a physical controller can be developed rapidly by interfacing the controller with the simulation model using Hardware-in-the-loop (HIL) simulation methodology.

To ensure the accuracy and validity of comparison in regards to the fuel efficiency study in this work, the ADVISOR modeling tool was adopted. It has been developed and validated at the American National Renewable Energy Laboratory (NREL) [91, 92], which has been adopted by many researchers previously and later acquired by AVL company. ADVISOR uses a backwards-looking approach to provide realistic fuel economy results over a wide range of vehicles [93, 94]. It allows the user to perform rapid analysis of vehicle drive performance, emissions and fuel economy of conventional. This modeling approach does not require a model of driver behaviour. The torque that has to be supplied by the component directly upstream is translated by this required force. Similarly, the vehicle's linear speed is

translated into a required rotational speed. The calculation is performed component by component in a backward-looking approach, against the tractive power flow direction, until fuel use or electrical energy use, which is required to meet the trace, is found.

The disadvantages of the backwards-looking approach come from its assumption that the trace is met and from the use of efficiency or loss maps. This approach is not well suited to computing best-effort performance, which occurs when the accelerations of the speed trace exceed the capabilities of the drivetrain due to the assumption that the trace is met by the backward-looking approach. In addition, since efficiency maps are generally produced by steady-state testing, dynamic effects are not included in the maps or in the backwards-looking model's estimate of energy use. The fact the backwards-looking model does not deal in the quantities measurable in a vehicle is another related limitation. One such example is when control signals like throttle and brake position are absent from the model, further hindering dynamic system simulation and control system development. The ADVISOR model has been validated and used as a reference model benchmark for the CV powertrain model.

6.2 Validation conventional vehicle model

There lies a contrast between the ADVISOR and CV powertrain model. This is highlighted by ADVISOR employing the backward-looking simulation, as opposed to a forward-looking vehicle simulation used by the CV powertrain model. The study was performed by the CV on Simulink and ADVISOR, where one drive cycle NEDC, NYC and UDDS were performed. Instantaneous fuel consumption is based on a three-dimensional lookup table defined by engine operating point (speed and torque). Integrating instantaneous fuel consumption provides a fuel consumption figure. Key vehicle specifications were inserted into the model based on values shown in Appendix C. The instantaneous fuel lookup table is a modified base map prebuilt into ADVISOR. To accelerate the development process for the ADVISOR model, existing components within the ADVISOR component library which approach the

requirements of the CV vehicle model were implemented. These components are then modified as required to meet the specifications available with regards to fuel economy, power, and tailpipe emissions.

Table 6-1 presents the cumulative cycle fuel consumption for each simulated cycle. The figures are sufficiently close to the reported consumption by ADVISOR to indicate that the model is accurate for the purpose of the financial analysis presented herein.

Table 6-1. The reported consumption L/100 km.

	NEDC	UDDS	NYCC
ADVISOR Model	8	8.1	18
Simulation Model	7.84	8.1	17.8

6.3 Analysis of fuel economy and electricity consumption

For both the hybrid and the conventional vehicle configurations presented above, energy consumption (petrol and electricity) can now be evaluated. For comparison, the energy consumption is calculated over three legislative cycles, NEDC, UDDS and NYCC, which are all urban cycles. The urban cycles are deliberately selected because they represent well the typical conditions in the densely populated metropolises of developing regions. The stop-start behaviour of traffic flow in these cities is one of the most significant contributors substantially to fuel use [95]. The purpose of using multiple cycles is to provide a more diverse set of driving conditions, reducing bias of the results to a particular drive cycle. Fuel economy was calculated for both the baseline and the hybrid vehicle; the results are summarised in Table 6-3. Substantial differences in fuel economy are observed when comparing different drive cycles. As expected, a saving of approximately 3 - 8% fuel consumption represents a consistent improvement in fuel economy over the conventional powertrain. While the quantum of fuel saving is dependent on the drive cycle, the trend clearly shows improvement. To compensate for the change in SOC over once cycle, see Capacity in Table 6-2, an adjustment to the fuel consumed is made in accordance with [96]. In [96] an equivalent fuel

consumption is required to evaluate the equivalent economy of conventional, hybrid and electric vehicles. This type of regulation provides equivalency between various vehicle types so as to standardise the fuel consumption rates. The conversion of energy battery energy to energy in gasoline (petrol) is 34.2 MJ/L [97]. It is adopted for this research, to allow compensation for energy consumption in the battery and directly compare fuel savings between both vehicles.

Table 6-2. Comparison chart for all vehicles tested Fuel and electricity consumption of the modelled vehicles.

Drive Cycle	NEDC		UDDS		NYCC	
Drivetrain	CV	MHEV	CV	MHEV	CV	MHEV
Fuel Economy (L/100 km)	7.841	7.645	8.158	7.485	17.6	16.98
Fuel Consumption L	0.849	0.825	0.969	0.885	0.328	0.316
Capacity Ah	-	0.9	-	2	-	0.7

Table 6-3. Fuel Economics for conventional and Mild HEV.

Drive cycle	Motor			Fuel Economy (L/100 km)			CV	Fuel saving (%)
	MHEV			Motor	ICE	Total		
	Ah	kW·h	Equivalent MJ					
NEDC	0.9	0.0864	0.31104	0.00909	7.645	7.654	7.841	2.38
UDDS	2	0.192	0.69120	0.02021	7.485	7.505	8.158	8.1
NYCC	0.7	0.0672	0.24192	0.00707	16.98	16.987	17.6	3.48

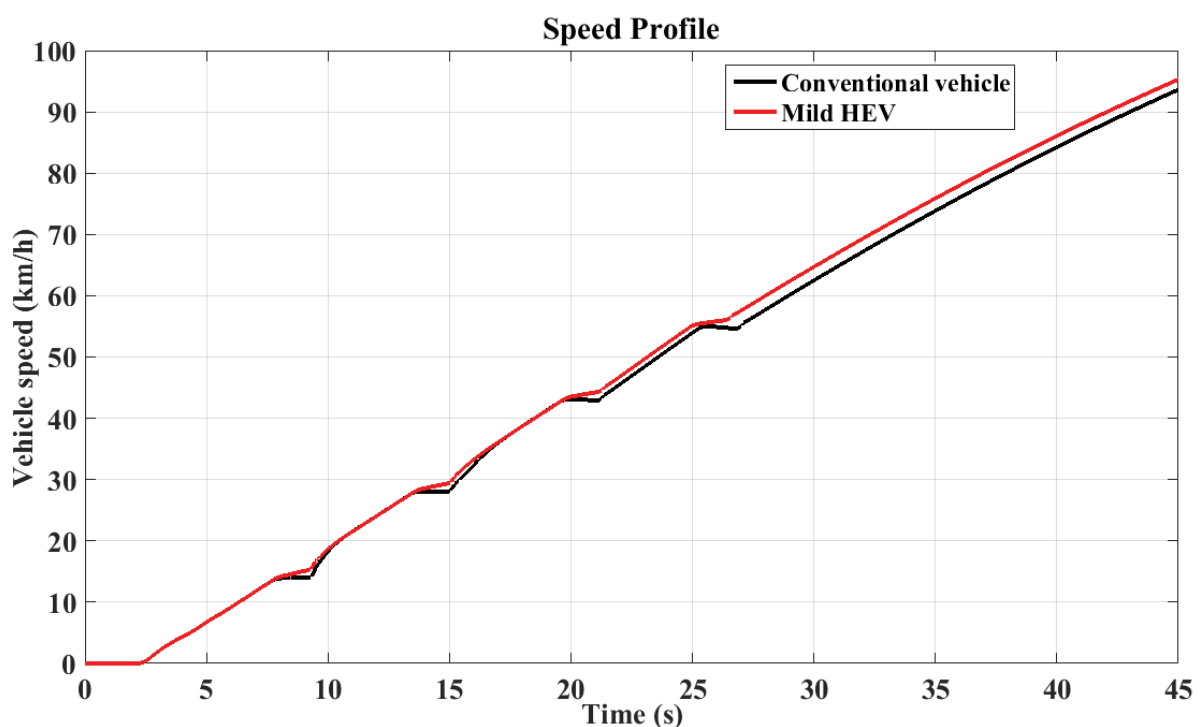
From the simulation output, it can be concluded that the mild HEV powertrain plays a noteworthy role in enhancing fuel economy. The requirements for motor capacity and torque under acceleration are much higher than that for other requirements (e.g., cruising). In other words, most of the motor capacity is wasted in the daily-use. Therefore, a design trade-off has to be made between acceleration time, energy consumption, and motor cost.

6.3.1 Physical performance benchmarking and torque-hole elimination

To benchmark vehicle performance, a 0-100km/h test was adapted from the first section of the Rural Drive Cycle (RDC,

Figure 6-1). This test is modified to keep shift points at the optimal engine speed for fuel economy, and both the baseline and the hybrid vehicle were tested. The primary functionality of this HEV arrangement, torque-fill system, is not the dominating factor for improving fuel economy. It is, however, a side benefit. The use of regenerated electrical power to perform shifts is expected to have an impact on fuel economy as the gearshift performance is improved and less energy wasted during these events. To demonstrate this the torque fill-in configuration is compared to a conventional ICE powertrain (shown in

Figure 6-1). Results are presented in Table 6-4. results are presented in Table 6. A 4.2% improvement in fuel economy is demonstrated through these simulations over the conventional vehicle, and the overall acceleration time from stand still is reduced by about 2.5s when using torque fill-in. This is a result of the continual delivery of tractive load to the road during gearshift by the electric motor drive, note that deceleration during gearshifts is significantly reduced.



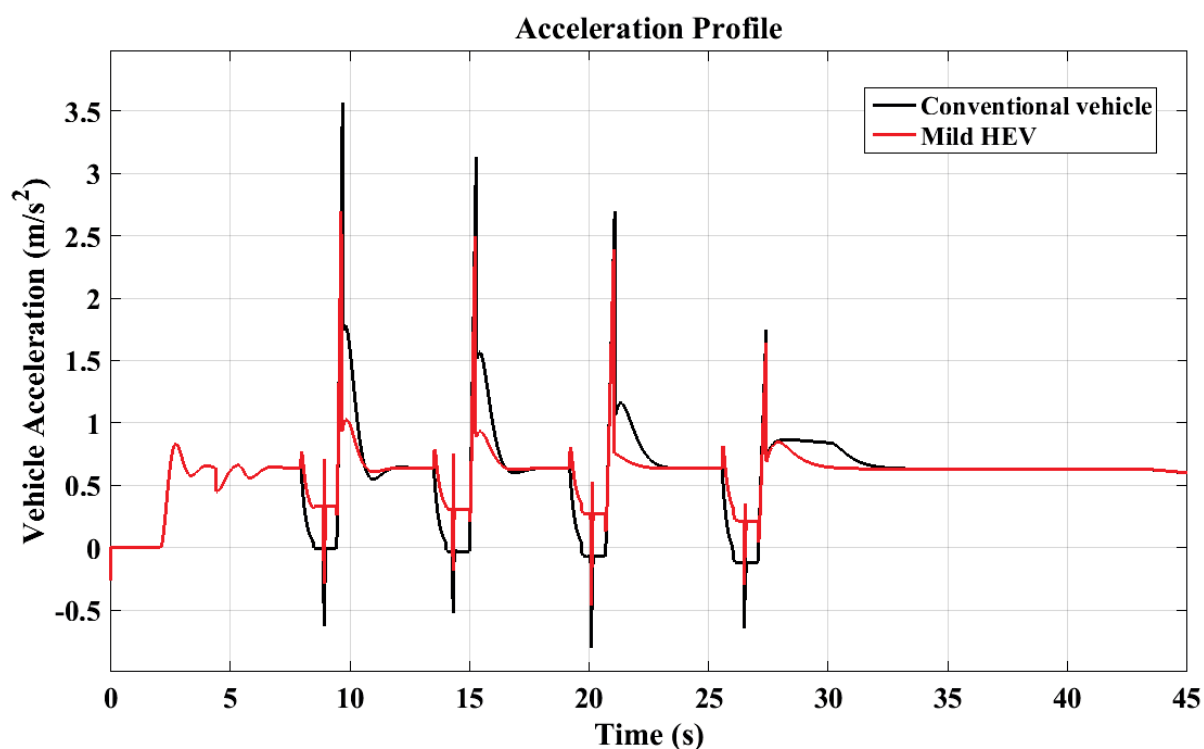


Figure 6-1: Benchmarking test: vehicle speed and acceleration profile.

Table 6-4. Comparison chart for configurations tested through the acceleration event 0-100 km/h

Vehicle Model	Distance Travelled km/L	Fuel Economy L/100 km
Conventional	12.98	7.702
Mild HEV	13.54	7.381

6.4 Direct emissions

Vehicles' emissions represent the main source of our era's pollutions. It is predicted [75, 98] that in the next decade mild hybrid electric vehicles will become a leading automotive growth sector. Electrified vehicles offer the promise of reduced emissions when compared with conventional vehicles, due to the more efficient use of combustion power and resultant emissions. Emission rates were calculated in the model as an average of the values measured over each drive cycle and measurement set. They were normalised by the fuel flow rate. The fuel ratio is a crucial factor that has a dominant effect on the emissions characteristics of an SI engine [99]. Exhaust gas components measured were nitrogen oxides (NO_x), carbon

monoxide (CO) and unburned hydrocarbons (HC) [100, 101]. Simulations of the vehicle configurations over the drive cycles resulted in vehicle performance as given in Table 6-5. There is a clear trend describing Mild HEV pollutant emissions which are lower than those of the conventional vehicle. Of note is the mild hybrid vehicle's performance in the reduction of tailpipe HC emissions compared to the conventional vehicle, which indicates that the engine is operating more efficiently and achieving complete combustion more frequently. This result correlates well with the results achieved in Table 6-2. For the MHEV powertrain, the EMC plays a critical role to manage the power flow properly in order to achieve excellent electric drive performance and high energy efficiency and also to optimize the power and energy demands throughout the system.

Table 6-5. GHG Emissions for conventional and Mild HEV.

Vehicle	Emissions (grams/km)								
	NEDC			UDDS			NYCC		
	HC	CO	NO _x	HC	CO	NO _x	HC	CO	NO _x
Conventional drivetrain	0.565	1.62	0.729	0.54	1.637	0.718	2.966	9.558	3.758
Mild Hybrid drivetrain	0.518	1.54	0.716	0.503	1.57	0.693	2.576	8.249	3.223
Improvement (%)	8.3%	4.9%	1.7%	6.8%	4.1%	3.5%	13.1 %	13.7%	14.2%

According to the obtained results of fuel economy based on a different drive cycles weighting percentage, the MHEV powertrain is more efficient in situations where a higher percentage of miles driven in the UDDS drive cycle. In the UDDS drive cycle, where the traffic is moving slow, and the driving style is cautious for most of the time travelled, the MHEV can save significant amounts of energy used and reduce harmful emissions. It can be concluded that the MHEV powertrain is more suitable for city driving cycle compared to the highway because there are more opportunities to recover the regenerative braking energy during stop-and-start events and most of the energy used to move the vehicle comes from the power grid, which minimizes the ICE running time, fuel consumption and emissions.

6.5 Low and high-density traffic patterns drive cycles

In this study, the fuel consumption and emissions for each vehicle configuration developed are presented. A discussion of the impact of traffic patterns is based on standard and author-developed traffic patterns and drive cycles. These cycles simulate low and high-density traffic. The Indian urban driving cycle (INDIAN URBAN) and highway fuel economy test (HWFET) were used as the basis for this study. These cycles are illustrated in Figure 6-2 and Figure 6-3. The HWFET drive cycle is a high-speed cruising testing cycle. Thus, required torque is usually small except in some accelerating sections. The HWFET drive cycle is a high-speed drive cycle, covering 16.5 km (10.26 miles) at an average speed of 77.6 km/h (48.5 mph). It is characterized by a mild initial acceleration from zero to reach highway speed. This acceleration takes 100 seconds. Speed then varies between 70 and 80 km/h. At 300 seconds cycle time, speed drops steeply to 45 km/h and increases again to 96 km/h. Finally, the drive cycle ends at 765 seconds with a linear deceleration to zero. The INDIAN URBAN drive cycle is recorded under typical city driving conditions, and it lasts for 2689 sec covering a distance of 17.4 km (10.8 miles) with an average speed of 23.3 km/h (14.4 mph) and a maximum speed of 62 km/h. Table 6-6 shows some characteristic parameters of the selected drive cycles, according to these parameters the cycles can be classified into different driving patterns [86, 87].

Table 6-6: Characteristic parameters of different driving cycles.

	INDIAN URBAN	HWFET
Distance (km)	17.4	16.5
Duration (sec)	2689	765
Max Speed (km/h)	62.2	96.4
Average Speed (km/h)	23.3	77.6
Average Acc (g)	0.3	0.19
Idle Time (sec)	267	6
Number of stops	52	1

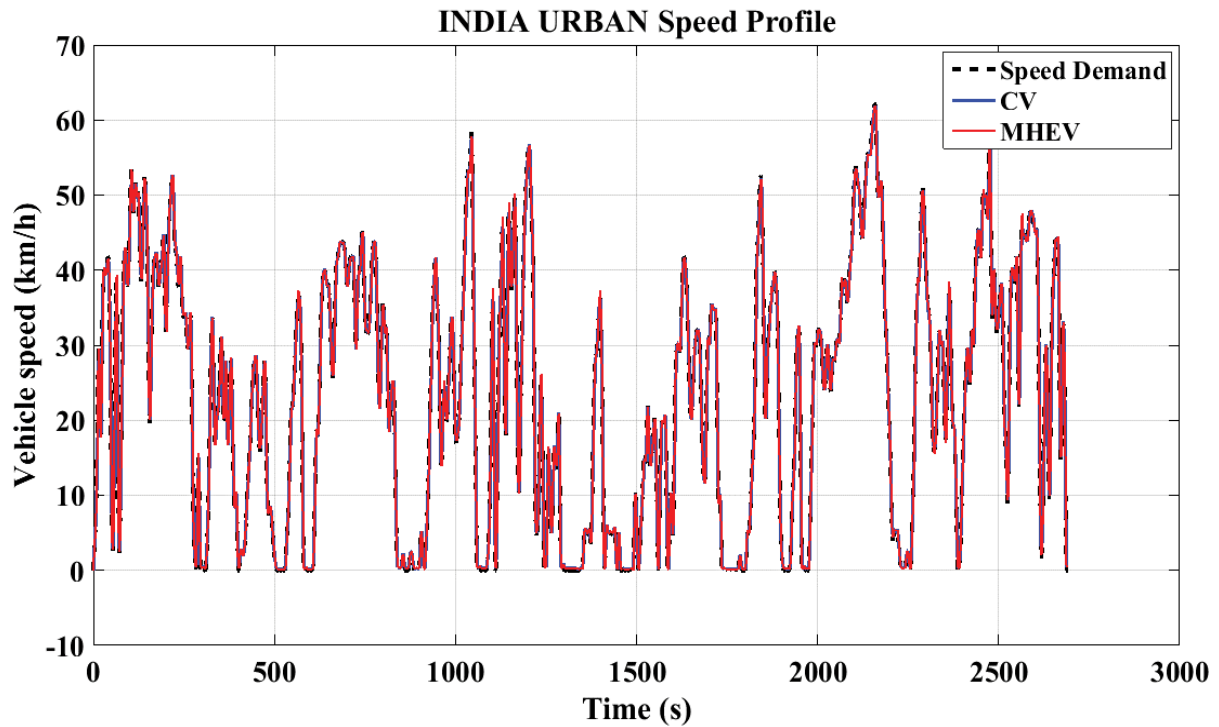


Figure 6-2: The speed profile of INDIAN URBAN Drive Cycle.

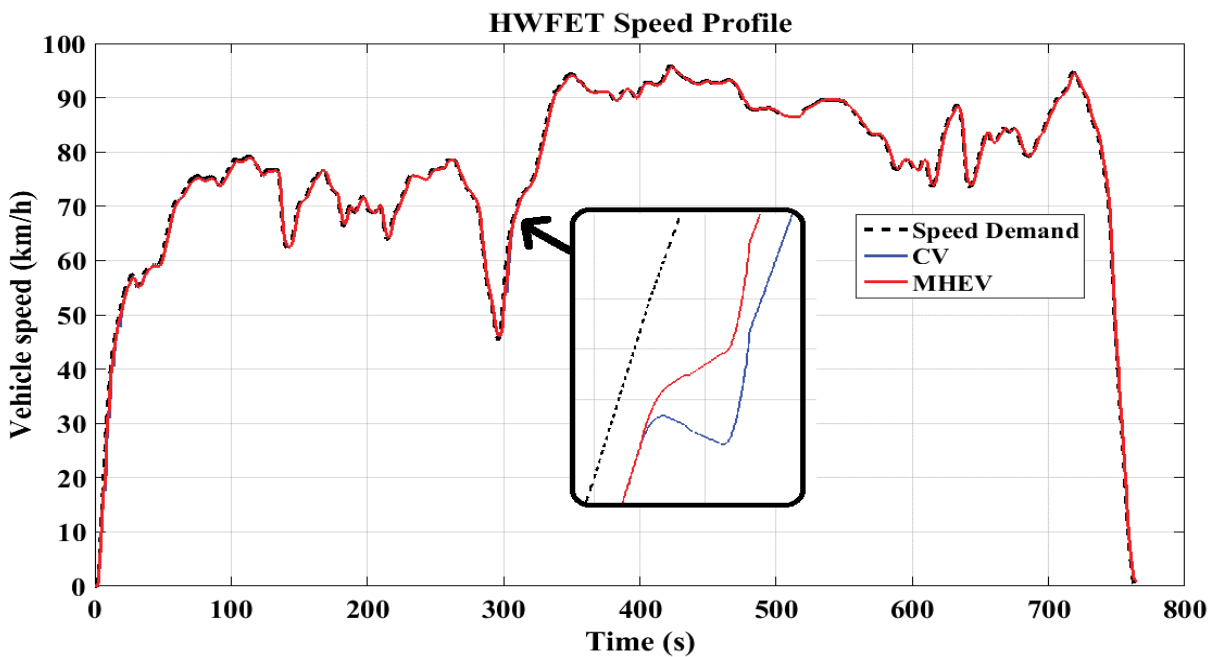


Figure 6-3: The speed profile of the HWFET Drive Cycle.

The fuel economy and emissions for different drive cycles are given in Table 6-7 and Table 6-8. The results shown in these tables demonstrate the equivalent fuel economy of both powertrains varies greatly dependent upon driving environment. As expected, the fuel

economy and emissions of the MHEV are better compared to a conventional powertrain. An improvement of approximately 10% is observed in INDIAN URBAN, and a smaller improvement of 2% is measured in HWFET. Fuel and emissions indicators improve when the drive cycle is completed using a cautious driving style and with increased “urbanisation” of the cycle. The ‘stop-start’ conditions and high level of speed fluctuation represent the ideal conditions for maximising utilisation factor of the electrified powertrain. This is because the powertrain is particularly adapted to be used in low-power acceleration at low speed, and as torque-fill during gear changes. So, the behaviour of traffic flow proves to be a major contributor influencing fuel consumption in urban regions. The result of this is enhanced fuel economy with mild hybrid configuration implementation, with a significantly smaller improvement in highway cycles than city driving.

The combined drive cycle is determined by weighting the city at 55% and the highway at 45% as the following equation [48]. Results are outlined in Table 6-9. The fuel economy for the combined drive cycle is 6% better than can be achieved by the conventional vehicle (CV).

$$FE_{\text{combined}} = \frac{1}{\frac{0.55}{FE_{\text{city}}} + \frac{0.45}{FE_{\text{highway}}}} \quad (6.1)$$

Table 6-7: Fuel economy and emissions for INDIAN URBAN drive cycle.

	INDIAN URBAN				
	Fuel		Emissions (grams/km)		
	Fuel Consumption (L)	Fuel Economy (L/100 km)	HC	CO	NOx
CV	1.9	11.1	0.45	1.9	0.69
MHEV	1.7	10	0.42	1.2	0.57

Table 6-8. Fuel economy and emissions for HWFET drive cycle.

	HWFET				
	Fuel		Emissions (grams/km)		
	Fuel Consumption (L)	Fuel Economy (L/100 km)	HC	CO	NOx
CV	0.95	5.8	0.43	1.59	0.62
MHEV	0.93	5.7	0.41	1.43	0.57

Table 6-9. Fuel economy and emissions comparison for the composite drive cycles.

COMPOSITE DRIVE CYCLE FUEL ECONOMY (L/100 km)	
CV	7.9
MHEV	7.4

There is an identified need for new drive cycles and combination cycles other than those that are used today, due to changes in traffic conditions and infrastructure. Drive cycles can vary considerably from drivers' real-world experiences. As areas become more densely populated and developed, a drive cycle developed for a specific application is not routinely updated, and as a result drive cycles lose relevance over time. This issue is particularly clear outside the USA and Europe, where more regional drive cycles may not be updated for decades. Some efforts have been made to create uniform worldwide regulation. These efforts often constitute smaller regions adopting the US or European emissions regulations. However, conversely, to the intended outcome, this harmonization can result in adverse emissions outcomes, as the drive cycles that form the basis of emissions legislation are not representative of typical local driving patterns. To combat this, a world-harmonized light vehicle test procedure has been developed, and moves toward "real world" testing utilizing portable emissions measurement systems (PEMS) are in advanced stages. In the absence of significant real-world data and analysis protocols, drive cycles still represent the most practical means of modeling emissions and fuel performance for researchers [102].

In Australia, where this study is being conducted, most commuters drive an average of less than 50 km as a daily commute. As shown in Figure 6-4, in Sydney these commuters represent 64% of drivers and in Adelaide, 83%. In many developing regions representative of the hypothetical markets, these figures are much higher. This is often because poor road conditions, severe congestion, and cost of transportation does not allow for practical long-distance daily commuting. In order to accurately model typical driving patterns, a

comparative study was conducted utilising a 40 km distance travelled under both low and high-density drive cycles. The low and high-density traffic patterns are developed from the standard drive cycles in order to capture the demands of the different traffic conditions and are the result of analysis of a range of existing drive cycles and comparison against typical expected driving conditions. The high-density drive cycle was developed using a combination of Urban Dynamometer Driving Schedule (UDDS), INDIAN URBAN and city-suburban heavy vehicle route (CSHVR) drive cycles in order to represent a typical daily trip on busy roads. The low-density drive cycle was been developed using the combination of the New European Driving Cycle (NEDC), HWFET and INDIAN HIGHWAY drive cycles in order to represent a typical daily trip on busy roads. The objective of this analysis is to compare the fuel economy, emissions of the MHEV and a conventional powertrain for the author-developed low and high-density traffic patterns. The cycles are arranged in this way to deliver more diverse simulated driving conditions. Because the cycles are each have their own characteristics and biases not linked to a single method of development, this method reduces bias in the results that may be present in a particular drive cycle, or developed under different traffic conditions.

Table 6-10 and Table 6-11 shows the characteristics of the author-developed cycles. As with previous simulations, these author-developed cycles reinforce that traffic density is one of the main influences on fuel economy and emissions. The results consistently show that the fuel economy of the MHEV is highly affected by the traffic, wherein a low density may yield worse fuel economy than a high one. This demonstrates the suitability of the MHEV topology described for urban environments. Other influencing factors include the chosen route and environmental effects including temperature and wind vector. The author-developed low- and high-density traffic drive cycles are shown in Figure 6-5 and Figure 6-6.

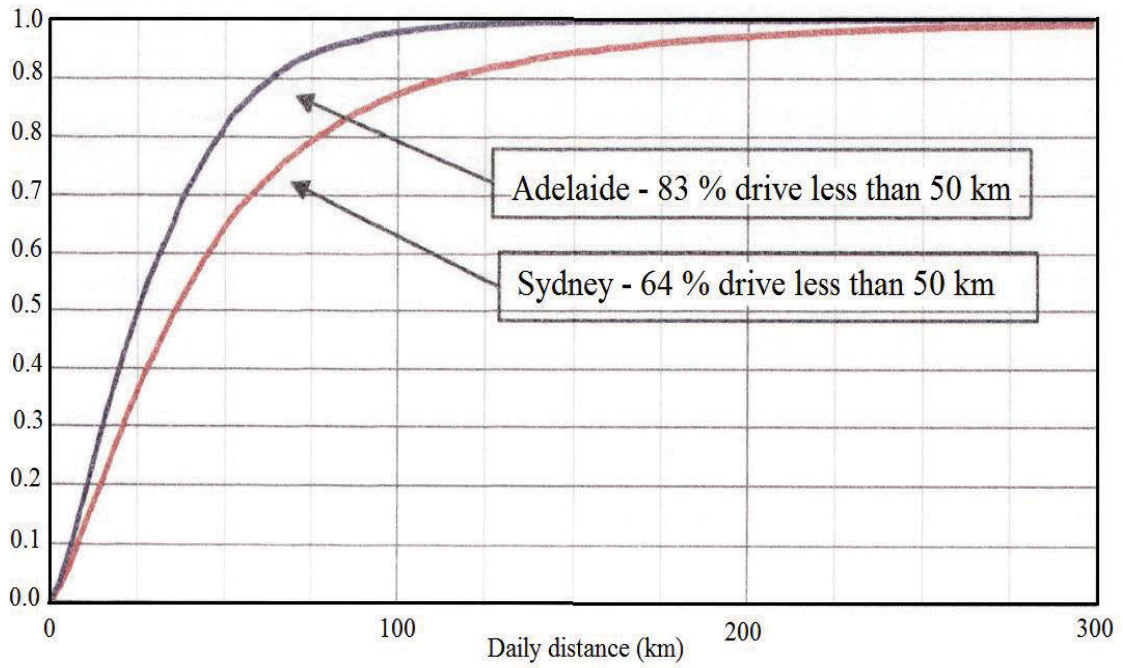


Figure 6-4. Cumulative distribution of daily driving distance in Australia [103].

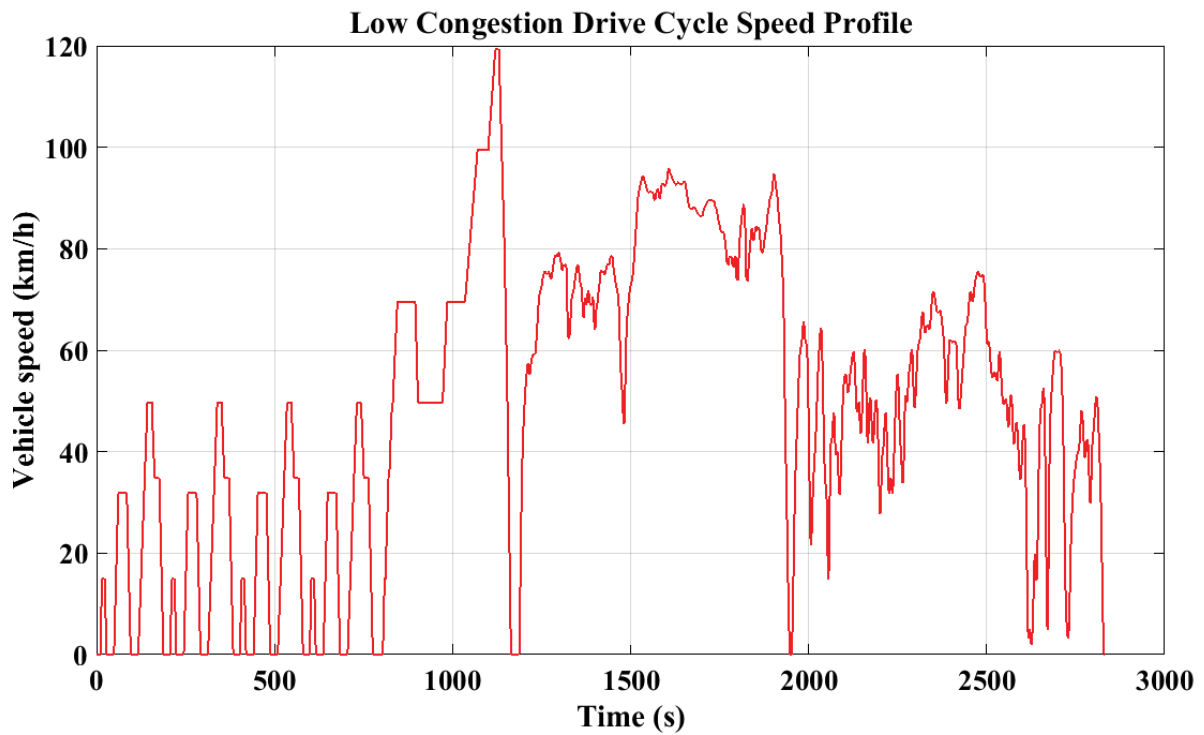


Figure 6-5: The low-density traffic pattern drive cycle.

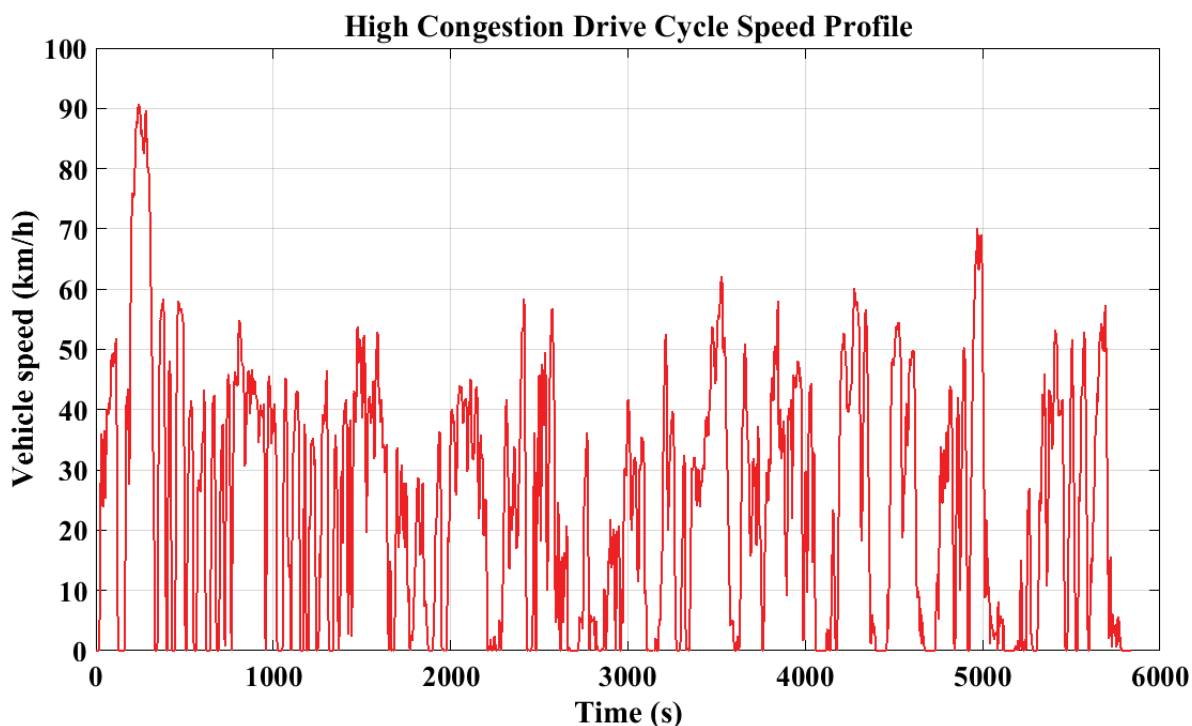


Figure 6-6: The high-density traffic pattern drive cycle.

Table 6-10. The characteristics of low and high-density traffic patterns drive cycles.

Density traffic patterns	High	Low
Drive cycle	UDDS + INDIAN URBAN+ CSHVR	NEDC + HWFET + INDIAN HIGHWAY
Distance (km)	40	39.1
Time (s)	5840	2832

Table 6-11. Fuel economy and emissions during the developed low and high-density traffic patterns drive cycles.

		MHEV		CV	
		Low	High	Low	High
Fuel economy (L/100km)		5.8	8.5	6.5	11.1
Emissions (grams/km)	HC	0.19	0.23	0.22	0.27
	CO	0.56	0.62	0.61	1.2
	NO _x	0.32	0.36	0.35	0.49

Table 6-11 lists the vehicles fuel economy and emissions of the MHEV and a conventional vehicle (CV) during drive cycles featuring low and high-density traffic patterns. The objective of this analysis is to determine the characteristics of each powertrain. As expected, the MHEV powertrain obtains higher fuel economy in high-density traffic compared to the CV under the same conditions. This is due to the higher proportion of time in traffic in which

the electrified powertrain can be utilised either as motor or brake. Regenerative braking energy is captured during stop events in the high-density traffic pattern drive cycle and can be re-used for motive power under acceleration. However, based on the fuel economy analysis results, the low-density traffic combined with an aggressive driving style achieves lower fuel economy even with the MHEV powertrain. This is because more energy is required to repeatedly accelerate the vehicle, thereby lowering the utilisation factor of the electrified powertrain. A fuel improvement of approximately 23.5% is shown in high-density traffic and 10.7% in low-density traffic.

According to the simulation results, the MHEV powertrain has a significant improvement in the fuel economy and emissions for both driving styles compared to a conventional vehicle. This is because the MHEV powertrain provides somewhat improved load management for the internal combustion engine (ICE), but also recovers significant braking energy. The use of the electric machine to propel the vehicle during gearshifts results in disproportionate improvements in emissions performance – this is because the load factor during acceleration is much higher, and therefore any electric propulsion has significant emissions and fuel savings, thus reducing the harmful emissions from the ICE. At the same time, the MHEV powertrain also has the advantages of ultracapacitors, which can absorb significant regenerative braking energy and provide more peak power during hard acceleration. This technology is well-suited to the torque-filling function, which prioritises peak power over energy density.

Improvement in comfort and driveability can be achieved through the reduction of torque-holes during gearshifts. This can be implemented by the use of a Mild Hybrid Vehicle (MHEV) powertrain, with minimal changes compared to a conventional vehicle with manual transmission. The traditional manual gearbox is the ideal platform for development and successful implementation of the torque-fill drivetrain, owing to its' simplicity and low cost.

Values attained for both low and high traffic drive cycles fall within a predicted systemic pattern of behaviour. A realistic approach is taken in regards to sizing of the components of the vehicle subsystems, with the resultant performance output dictated by the desired benchmarking goals. The use of the MHEV as has been proposed is feasible and shows great potential. There is an observable improvement in the values yielded for GHG emissions and fuel economy for the drive cycles. The MHEV also achieves desired performance with a simpler architecture than many full-hybrid vehicles, which is essential in reducing cost. Therefore, implementation of the MHEV configuration is seen to be of great benefit.

In both the single drive cycle assessment and density traffic (drive cycles). Regardless of the type of drive cycle assessment used, the actual usage will generally comprise a mixture of city and highway driving. However, the model does shine a light on the performance of mild hybrid powertrains to their application, in a way which is seldom presented to the consumer. The model potentially offers significant reductions in the fuel and emissions of GHGs, but is highly dependent on operating condition and may also produce very modest reductions if any. The important overriding finding is that emissions savings are seen under almost all conditions, and so the adoption of MHEV must be considered a positive step for the environment. The investment will actually realise significant savings in running costs, as well as significant environmental benefits.

6.6 Driver classification

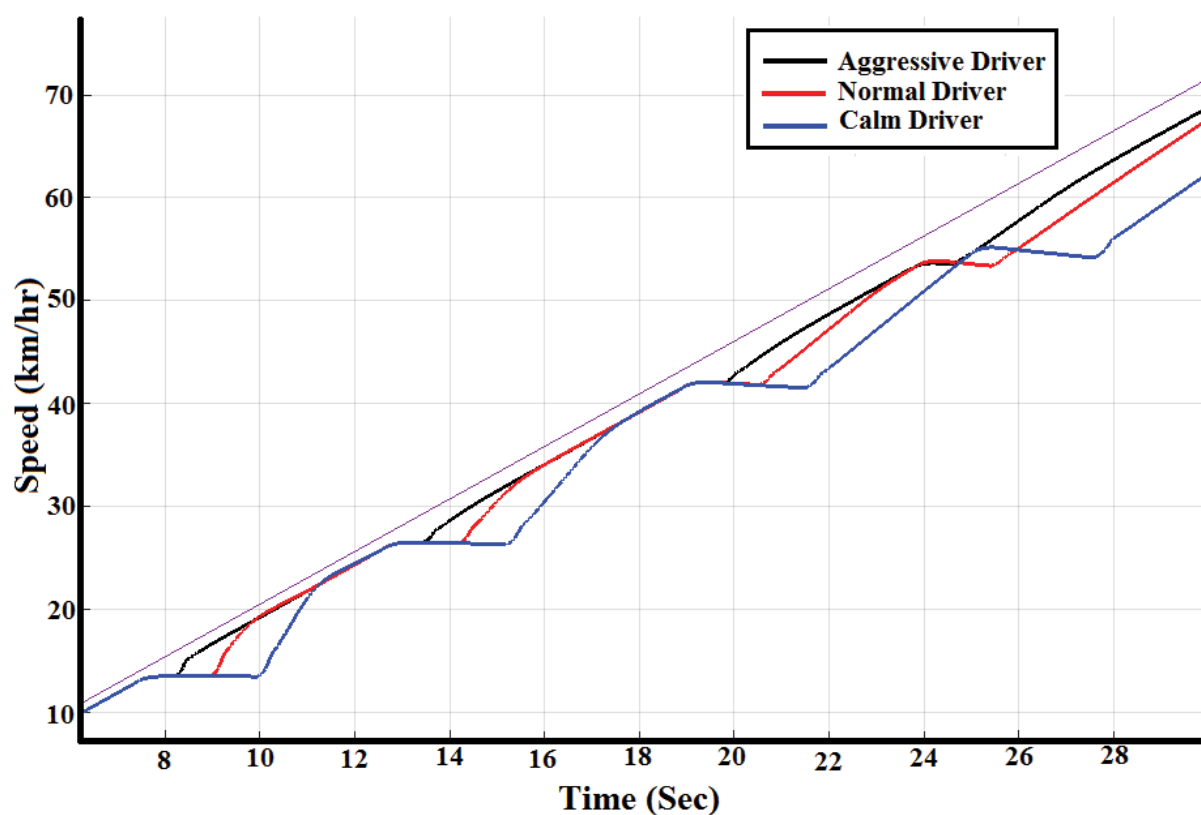
The purpose of this analysis is to investigate the influence of driver behaviour or aggressiveness at different levels and to investigate the impact of low and high developed density traffic patterns for the MHEV and conventional powertrains with regard to fuel economy. Driving technique is one of the main influences on fuel economy and emissions. Fuel economy of an MHEV is highly affected by the driver's tendencies, wherein an aggressive driver may yield worse fuel economy than a calm one. Other influencing factors

include the chosen route and environmental effects including temperature and wind vector. The driver's behaviour is a controllable factor which would have the largest effect on fuel economy, as other parameters are largely dependent on external influences. Thus the driver can be classified quantitatively based on vehicle fuel consumption alone [104].

Driving style relates to the dynamic behaviour of a driver on the road. Different drivers navigate the same route using different styles. It is widely understood that aggressive, slow, and moderate driver modulation of the primary vehicle controls (throttle and brake) will each have different effects on the fuel consumption. The effects of later shift points and larger-than-necessary throttle openings on fuel consumption are well-understood and do not change depending on vehicle configuration. In an MT equipped vehicle, driving style can also be classified using the measure of the speed of gear changes. In this section, the analysis will show that using the shifting time alone, in the hybrid vehicle model a demonstrable change in vehicle performance could be observed. This variable alone can be used to characterise the driver. Because of the focus of the mild hybrid system on torque-filling, this variable was found to have a significant impact.

In this method, driver style classifications are defined using the average time to complete a gear change. This information is extracted from the speed profile. An average gear change time of less than one second is used to define an aggressive driver. Average times of between one and three seconds define normal driver styles, and more than three seconds define calm drivers [105, 106]. For the purpose of this analysis, the gear change start is defined by the initial clutch pedal actuation, and the gear change end is defined as the application of steady-state throttle demand following the return of the clutch to its engaged position. Figure 6-7 shows the three different driver classifications graphically, presenting the speed and torque profile with different gear change period to define different driver style.

Simulations are conducted on the previously used driving cycles. In these simulations, the drive cycle was kept constant and driver parameters varied. These parameters correspond to the shift time. Shift time was changed by varying the clutch aggressiveness, and the throttle aggressiveness. The aggressiveness of each element may be controlled by varying the rate of change of the actuation, which has a direct effect on system settling time. The parameters were varied to achieve driver behaviour consistent with the three classifications. The results are shown in Table 6-12, and illustrate that using the metric of gearshift time, the driver classified as calm was the most fuel efficient, and the aggressive driver was the least. This is consistent with other results and shows that the gear change time metric is a valid method for predicting driver influence on fuel economy. It also provides guidance for the development of a robotized gearshift in an AMT application, which is a longer-term goal of this body of work.



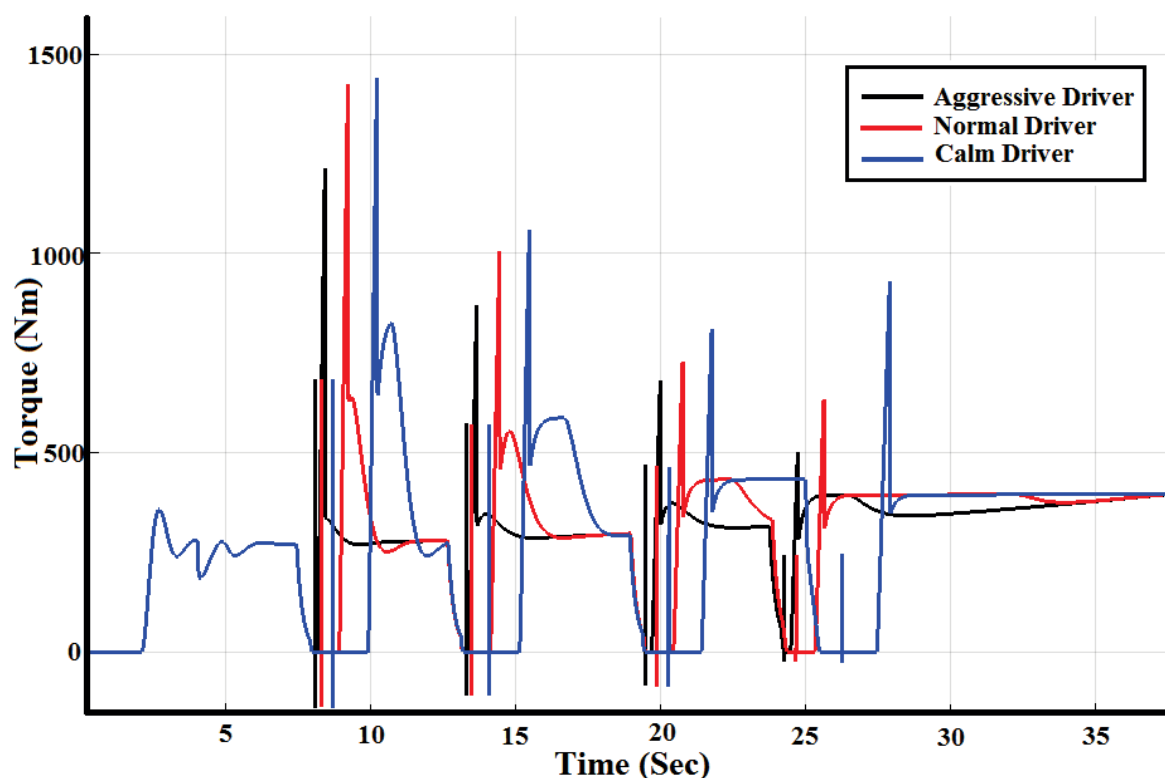


Figure 6-7: Speed and torque profile depending on drive style.

Table 6-12. Fuel Economics for conventional and Mild HEV by three driver styles.

Drive cycle	Fuel Economy (L/100 km)								
	Aggressive Driver			Normal Driver			Calm Driver		
	CV	MHEV	%	CV	MHEV	%	CV	MHEV	%
NEDC	7.9	7.6	3.8	8.3	7.9	4.8	9.1	8.2	10
UDDS	8.1	7.4	8.6	8.6	7.7	10.5	10.3	8.6	16.5
NYCC	17.6	16.98	3.5	19.8	18.8	5.1	21.2	20.3	4.2

6.7 Summary

This chapter gave an overview of the MHEV powertrain performance analysis and sensitivity study, and model verification between the CV and ADVISOR codes. The sensitivity study was conducted to investigate the effect of driving patterns, electrical consumption, fuel economy, emissions. The subsystems results of the MHEV code for both NEDC, NYC and UDDS drive cycles have been compared with the results from other vehicle simulation programs, ADVISOR code and the results are within reasonable and expected range of the actual typical behaviour of these subsystems.

Results and discussion indicate that the vehicle design goals specified are reasonable in a production setting. Benchmarking and Simulation suggest that fuel economy is mildly improved in line with expectations and that emissions are reduced, in some cases significantly. This potential for significant reductions in emissions as well as the achievement of low operating and manufacturing costs reinforces the view that such a vehicle design has the potential for significant socio-environmental impact in the target market.

The fuel economy and emissions also depend on the driver's behaviour when handling the vehicles and traffic density of a drive cycle. Comparing the simulation results, the MHEV powertrain uses less fuel energy, which has improved the fuel economy, emissions and electrical consumption.

Based on the fuel economy and emissions comparison for the tests during the UDDS, NYC, NEDC and combined drive cycles, the MHEV powertrain fuel economy is improved, and the emissions are reduced significantly compared to the conventional vehicle. The fuel economy, emissions of the MHEV and a conventional powertrain are different during the different standard and developed low, and high-density traffic patterns drive cycles. This is because the energy consumption and regeneration of the vehicle are different for every applied drive cycle.

The analysis of the influence for developed low and high-density traffic patterns drive cycles on the fuel economy, emissions, electrical consumption, the cost of operation and total lifetime cost is carried on each powertrain model. The different density traffic patterns drive cycles, being low and high levels are used in order to demonstrate the different level of aggressiveness or driving style of different traffic conditions.

Vehicle models can be classified depending on the direction of calculation: Forward Models make calculations starting from the engine toward the wheels. This model is preferred when

dynamics is under analysis and for control strategy development. Backward Models start with the driving force required at the wheel (in order to match a velocity profile) and then work backwards to the engine. In forward models, a set of differential equations are generated; whereas in standard backward models, only static equations are solved, thus making these latter models much faster to run, while their accuracy is reduced.

Contrast can be seen between the ADVISOR and CV powertrain model. This is highlighted by ADVISOR employing the backward-looking simulation, as opposed to a forward-looking vehicle simulation used by the CV powertrain model. The differences were assessed by performing one drive cycle for NEDC, NYC and UDDS. The results of these simulations were observed, presented and conclusions made about their results. By using both recommended and measured values as inputs, the ADVISOR is able to assess the necessary drivetrain torque, speed and power. This does not yield a practical result. CV/MHEV models utilize a PI controller as a driver model. By doing this, the controller either accelerates or brakes in close response to the drive cycle. The controller is able to result in a better correlation between the theoretical and measured values depending on the drive cycle. It is also more practical, as it incorporates within it the existing error (e.g. overshoot in the model) and allows for its inclusion in the model. For these reasons, the PI controller for MHEV configuration was determined to be the best choice for use.

Taking into account previous considerations, it was determined that the outcomes of the CV/MHEV code were accurate. As well as this, the constituents of the vehicle subsystems were sized accurately. When a target velocity is set, the vehicle is able to attain the required level of performance.

Chapter 7: A comparative study of battery and ultra-capacitors

The energy storage system (ESS) (the battery or ultracapacitors) is a crucial problem in the development and market penetration of HEV and EV. The key parameters for a comparison of batteries are the energy density, the power density, the cycle life, calendar life, and the cost per kWh. Volume and safety are also mentioned. To a lesser extent, energy efficiency and self-discharge are also considered. Each technology and each battery is designed following a trade-off between energy and power density. It must be noted that the relationship between car range and battery capacity is not linear as the important additional weight of the battery reduces the efficiency on the road. This is why it is important to compare batteries according to their energy and power densities. Figure 7-1 illustrates the range of specific power and specific energy for different battery technologies. It can be noted that they differ greatly from one technology to another and that for a given technology the design allows for additional trade-offs between power and energy.

A number of alternative forms of energy storage are considered for HEVs, i.e. batteries, supercapacitors hydraulics, or flywheels. To be cost-effective, the system herein uses batteries. The sizing of the energy storage can be investigated using power flow needs, regenerative braking capacity, and cycle life. The motor power demand is calculated based on benchmarking simulations of the vehicle and physical characteristics.

For energy management purposes, the SOC is used to judge the most suitable driving mode for the vehicle and provides information as to the residual power available. This is reported as the magnitude of instantaneous energy storage within the battery, which is used by the Energy Management Controller (EMC) to determine the most suitable drive mode under the current driving condition. The residual battery capacity (in amp-hours, Ah) remaining

available for discharge is calculated by the SOC calculation block. [48]. Note also that the capacity and battery efficiency temperature are dependent.

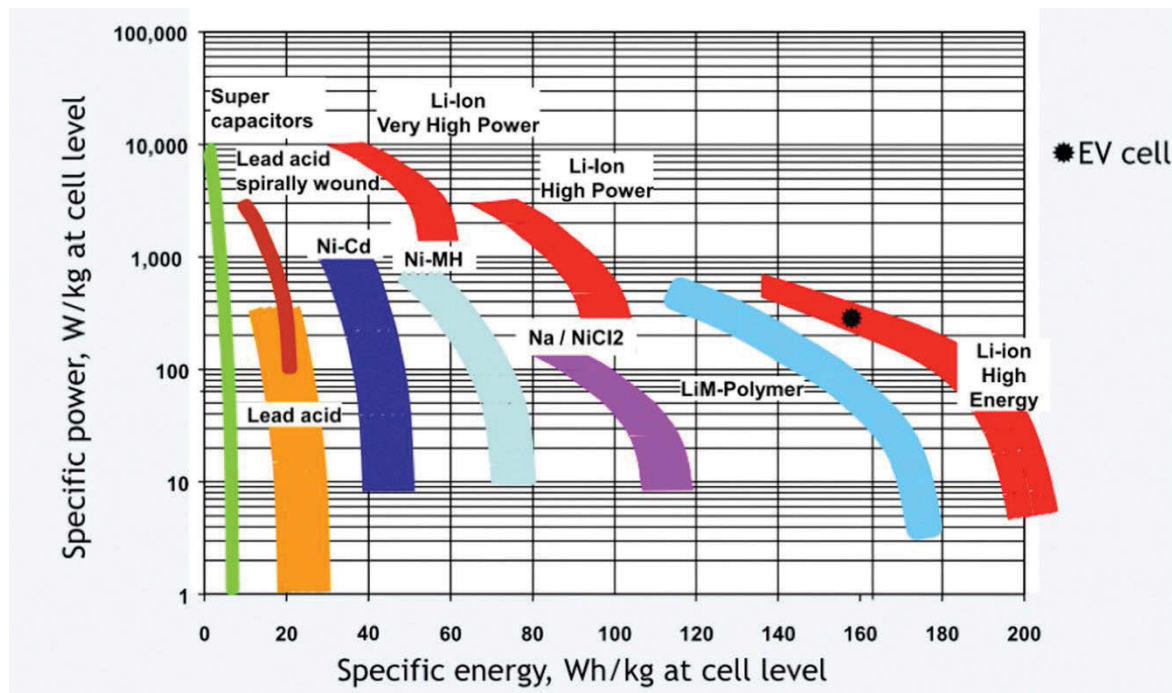


Figure 7-1. Specific energy and power of the main battery technologies [107].

The MHEV configuration proposed simplifies the vehicle architecture over and above that described in the prior literature, to achieve desired performance using only one EM. This is achieved through the application of a superior EMC that balances driving needs with SOC and other conditions. Depending on the vehicle operation condition, the electric machine (EM) functions as either an electric motor or a generator. This is monitored by an EMC in four quadrants of operation. Alongside with the ICE, the EMC can drive the vehicle or can be driven by the operator. Figure 5-9 demonstrates a rule-based energy management strategy implemented in the EMC. Both the ICE or kinetic energy of the vehicle (regenerative braking) can turn the EM into a generator capable of powering the vehicle on its own. However, this is dependent on the ultracapacitors/battery charging and power demand. Regenerative braking proves to be a vital part of the system, providing a significant influence on the small energy demands of the system. Commuters driving during peak hours, especially in metropolises, can see an energy wastage due to braking of up to 50% [80].

7.1 NiMH battery

Nickel Metal Hydride (NiMH) battery technology has been recently used in Hybrid Vehicles (such as Toyota Prius for instance). It is less expensive than Lithium-ion (Li-ion) batteries. NiMH battery technology is considered a mature technology, however, which has reached its best potential, both in cost reduction and characteristics. As seen in Figure 7-1, its energy density is between 60 and 80 Wh/kg.

In determining the battery capacity and size, the intent of the mild hybrid is to provide some of the benefits of hybrids at a low incremental cost. This intent is accomplished using a small battery pack [108, 109]. Battery sizing may be calculated by assuming the vehicle is only operating in charge-sustaining mode. Charging is accomplished by selecting optimum times to run the engine at a higher load point than road-speed requires, using the excess power to drive the BLDC motor. 80% of the battery capacity is assumed to be available for tractive power. The component efficiency of the system was calculated at 85% for the motor and controller in Chapter 9, and 81% coulombic efficiency was estimated. Multiplying these figures results in 69% total efficiency applied to both the charge and discharge cycles. Battery sizing is calculated using a discharge rate of 15C and a charge rate of 10C [108, 109], both of which are within the capabilities of typical NiMH batteries. Tractive power demands of 10 kW maximum results in a required battery capacity of 0.968 kWh to achieve 15C discharge. Using the NYC cycle, a maximum required the regenerative braking power of 9.2 kW is calculated. The latter figure results in a required battery capacity of 0.633 kWh for charging at 10C. The larger calculated value should prove sufficient to power the vehicle under ideal conditions, but nominally 1.2 kWh is used, to account for temperature effects and other losses in the absence of battery model specifications (Table 7-1).

Table 7-1. Battery Specifications

Battery	Type	NiMH
	Capacity	1.2 kWh / 12.5 Ah
	Discharge/Charge rate	15C / 10C

7.2 Battery SOC

The SOC can be calculated by equations (7.1) and (7.2). The SOC under different driving cycles is shown in Figure 7-3. The simulation begins with the initial SOC of 0.9.

$$SOC = \frac{(MC - Ah_{used})}{MC} \quad (7.1)$$

$$SOC = \left(1 - \frac{\int_0^{time(s)} I(A)}{3600 \times MC(Ah)} \right) \times 100\% \quad (7.2)$$

Where I is Current and MC is Battery Max Capacity. When running the cycle simulations, if the SOC value drops at the completion of a driving cycle (i.e., there is a net discharge), then the magnitude of the discharge must be taken into account when calculating fuel economy. The controller in Figure 5-9 prevents the SOC of the battery from dipping under the “low” threshold, which can be modified in the model. By setting the threshold and running the simulation iteratively, the simulation allows us to arrive at an optimal battery size. The proposed control strategy is capable of maintaining the balance of SOC and illustrates the SOC accumulated deviation at the end of each cycle.

7.2.1 SOC battery model

To define the most suitable drive mode for the current driving conditions, the SOC gives an indication of the energy stored in the battery pack. This information is passed on to the energy management system controller. The SOC is derived from the SOC calculation, giving an idea of the charge that is available for discharge from the battery. This value is defined by

units of ampere-hours (Ah). A block diagram of the SOC calculation within the Matlab/Simulink environment can be observed in Figure 7-2.

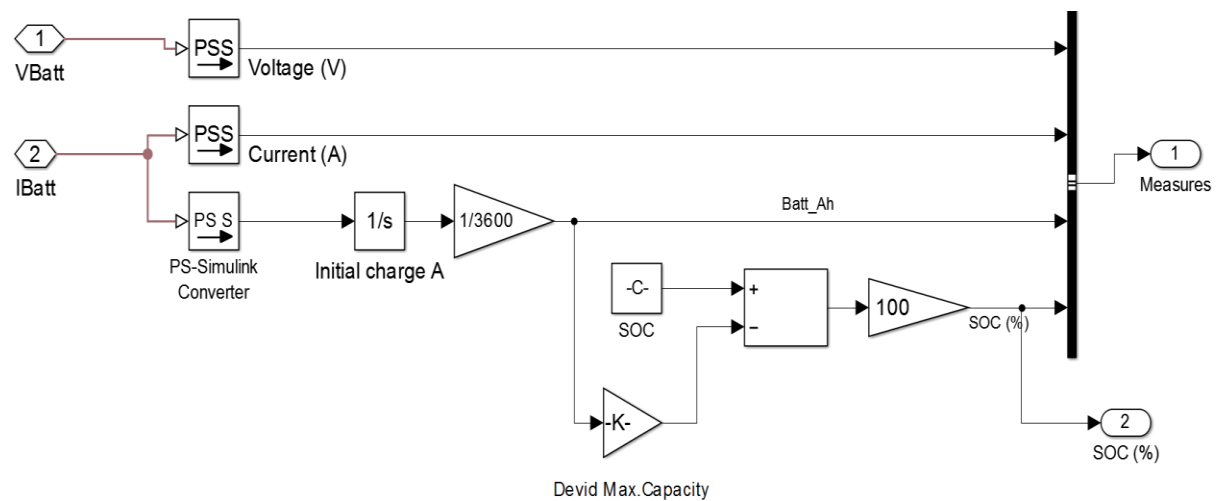


Figure 7-2: Battery SOC calculation in the Simulink environment

The SOC variations under the NYCC, NEDC, and UDDS drive cycles are presented in Figure 7-3 and Figure 7-4. The simulations are conducted with an initial SOC = 0.9 and 0.5. In both simulations, 0.5 is set as the low threshold. The results show the proposed control strategy is capable of maintaining the balance of SOC and illustrates the SOC accumulated deviation at the end of each cycle. Referring to the battery SOC graph, it can be seen that regenerative braking results in increases and high current discharge (such as when the test conditions call for high electrical drive power from EM) result in decreases in SOC. The regenerative braking during the deceleration is in the recuperation mode when the driver is either presses the brake pedal or at low accelerator pedal position.

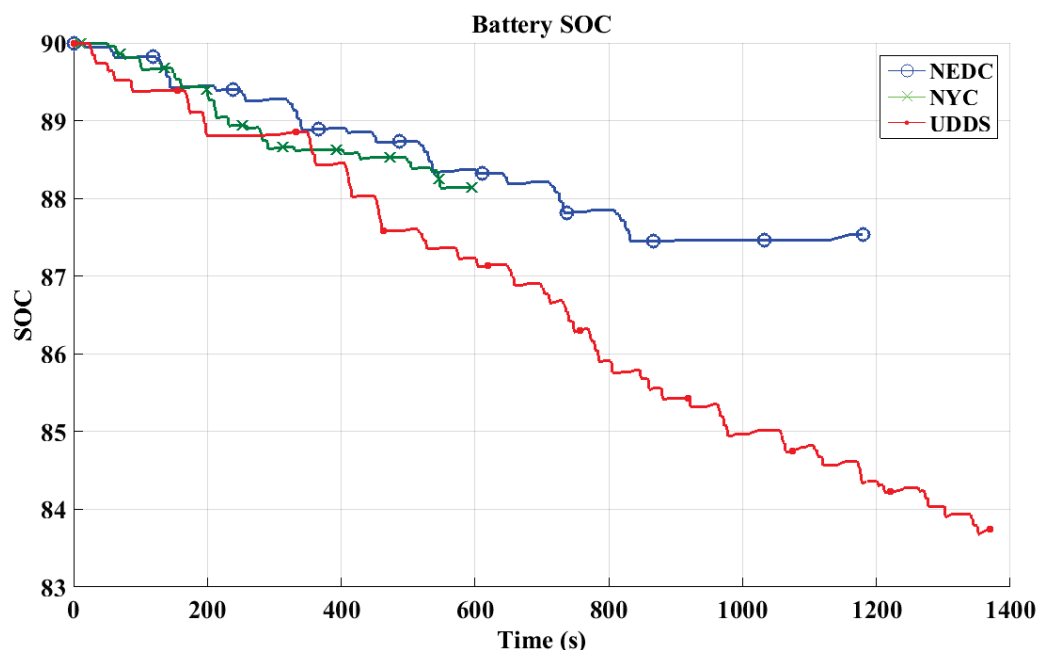


Figure 7-3. SOC profile.

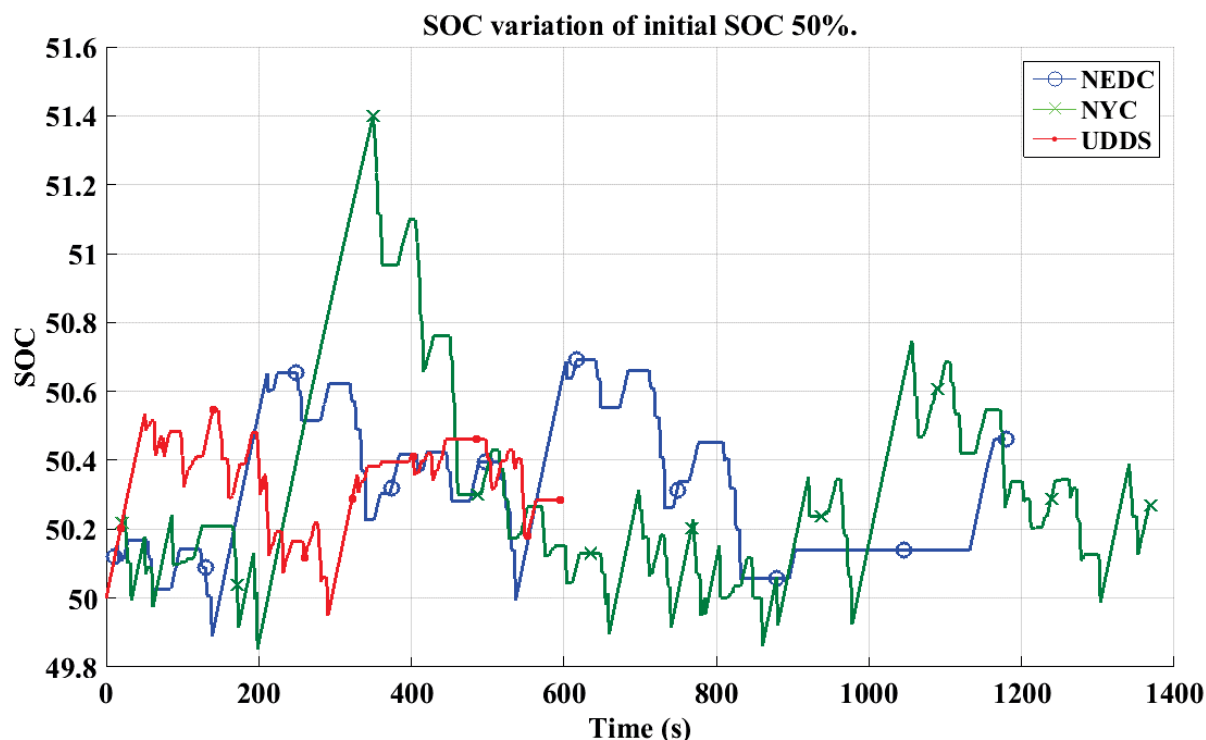


Figure 7-4. SOC 50% profile.

7.3 Impact of regenerative braking on the SOC of the battery during the example of high congestion drive cycle

This study is focused on the effects of regenerative braking on the SOC of the battery on the MHEV powertrain during the example of high congestion drive cycle as shown in Figure 7-5.

The example of High Congestion Drive Cycle has been developed with the combination of Urban Dynamometer Driving Schedule (UDDS), INDIAN URBAN and city-suburban heavy vehicle route (CSHVR) drive cycles in order to represent a typical daily trip on busy roads. Figure 7-5 plots the battery SOC history and vehicle speed over the example of high congestion drive cycle.

For the analysis of the vehicle, regenerative braking enabled mode and disabled. Before the start of the MHEV powertrain test without the regenerative braking subject to high congestion drive cycle, the battery was charged to a high SOC level; each test is started with a high 90% SOC. The vehicle was determined low SOC at 68 %, was reached. The test is repeated with regenerative braking enabled mode. The SOC during the example of high congestion drive cycles was reached at 85%.

The figure and results show the significant difference between the initial and the reached SOC for the different modes of regenerative braking. As a conclusion, the regenerative braking has significant effects on the battery.

Based on the simulation results of power requirements between the battery and MHEV powertrain, it can be concluded that different drive cycles have different driving style characteristics according to the acceleration and deceleration events during the driving schedule. In this study, the High Congestion Drive Cycle can be considered as a cautious driving condition because more power was handled significantly by the battery pack in order to capture regenerative braking energy. Based on this analysis, it can be concluded that the MHEV powertrain is more suitable for city driving cycle, where the traffic is moving slow, and there are more opportunities to recover the regenerative braking energy during the stop-and-start events and most of the power used to move the vehicle comes from the EM, which is a lot cheaper compared to the fuel price.

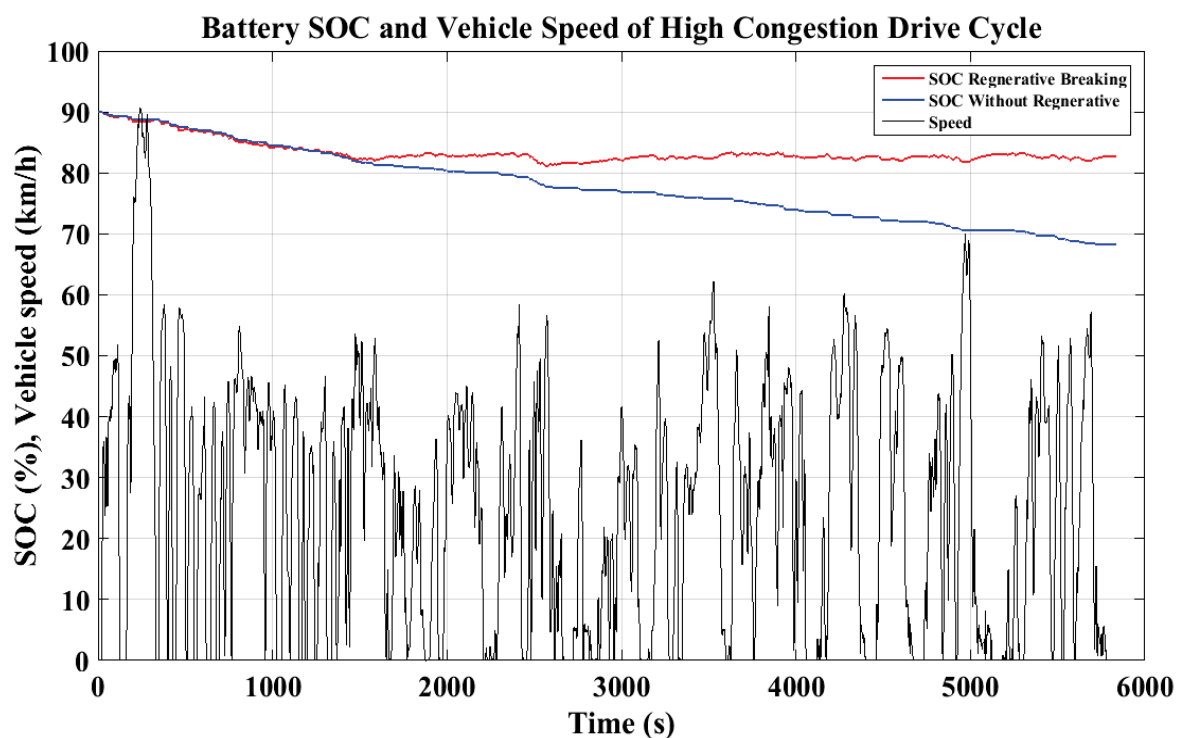


Figure 7-5: Battery SOC and Speed of High Congestion Drive Cycles.

7.4 Ultracapacitor SOC

This part discusses the development of a mild hybrid system for such markets with a focus on improving drive performance and efficiency. To achieve this, high power density ultracapacitors are used based on their fast charging and discharging characteristics, together with intelligent drivetrain control taking advantage of the ultracapacitors' characteristics to deliver smooth torque delivery during gear change (torque-filling). This part specifically investigates the role of ultracapacitors in this vehicle.

The traditional implementation of a battery pack in mild hybrids sees improved suitability to recover braking energy under low or medium load torque conditions at high speed. When the motor operates within the lower rpm range, the back EMF generated by the motor is not enough to charge the high-voltage battery pack. In saying this, there is observable heat loss due to higher charging conditions from conventional electrochemical battery cells, with most battery manufacturers regulating the charging current to under 3C for safety. Deterioration in performance and lifecycle is seen when batteries are provided with high power.

The electrical energy storage was parametrized to allow the easy reconfiguration between battery and supercapacitor, the main changes related to a raised regenerative braking threshold before brake blending was required, and the ability to provide greater electric-only assistance under higher torque demands – although for a shorter period due to the lower energy density. Figure 7-6 presents the layout of a mild hybrid, ultracapacitor-equipped powertrain.

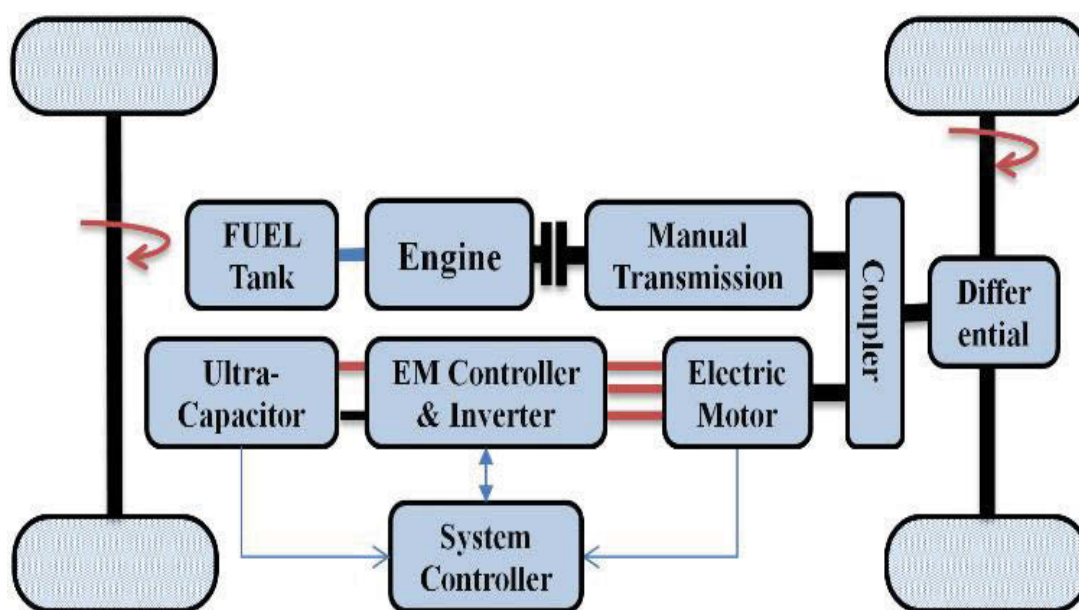


Figure 7-6: General Powertrain layout with an ultracapacitor.

The use of ultracapacitors (UC) (also known as supercapacitors), while retaining many beneficial aspects of electrochemical batteries, appears to be an alternative solution. They have shown potential for improved regenerative braking performance. UC has a longer life cycle and a very high-power density, allowing a higher charge rate than is achievable with a battery pack and thus more energy can be recouped during regenerative braking. However, they also have a very low energy density relative to batteries, making them only really suited to the minimal energy storage requirements of Mild Hybrid powertrains [26, 110]. Some of the advantages of the implementation of SC include fast charge and discharge time, large capacity, long cycle life and other characteristics. SC can reduce peak battery currents with no chemical variations on the electrodes. This results in a noticeable improvement in the life

cycle when compared to batteries. In addition to this comparison, there is an improvement power generation and consumption, based on the SC ability to supply power demand in a shorter time. The primary storage is the SC bank, which captures the energy from regenerative braking and to supply peak current for fast acceleration, which cannot easily be handled by the battery. The SC's terminal voltage is also directly proportional to State of charge (SOC). SOC is calculated by measuring the energy according to maximum energy with respect to time in equation (7.3).

$$SOC = \frac{E}{E_{max}} = \frac{V^2}{V_{max}^2} \quad (7.3)$$

7.4.1 Capacity calculation

The purpose of the mild hybrid is to provide some of the benefits of hybrids at a low incremental cost, which has placed limitations on choosing the UC capacity and size. Assuming the vehicle is operating in charge-sustaining mode allows the UC sizing to be determined. Selecting optimal periods for running the engine at higher load points than road-speed requirements achieves charging. Excess power is used to drive the PM motor.

A 1.2 kWh battery module was used in place of the ultracapacitors discussed here. The relatively large size was due to battery chemistry limiting tractive power availability to 80% of the battery capacity, and 85% component efficiency of the system for both the motor and controller. In contrast, a bank consisting of two UC cells of 165 Farad capacity (Maxwell UC BMOD0165 P048 B0110) each rated at 48V (Figure 7-7) was used to replace the 96 V / 1.2 kWh NiMH battery module as an energy source. This choice was reached after consideration of the packing constraints, and relevant energy calculations performed to justify the selection.

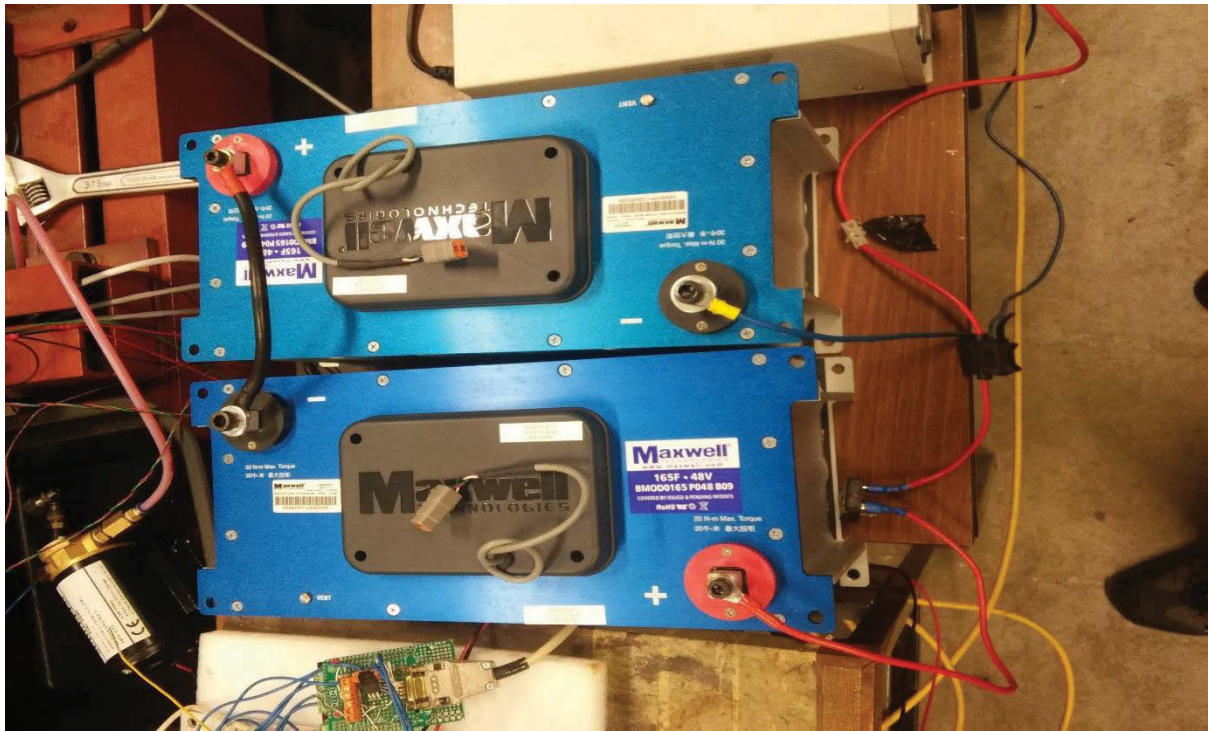


Figure 7-7: Supercapacitor bank.

Total usable electrical energy is where V_2 represents the fully charged DC voltage of the UC bank, for two cells, equals to 96 V and V_1 , its cut-off voltage, for two cells to be 89 V. The overall bank capacitance is 82 Farad as both cells are connected in series. The overall usable electrical energy is seen by using (7.4) and (7.5) is 53095 J, which is good to provide approximately 5 sec continuous power when the motor is operating at its rated 10 kW output power. It is worth mentioning that the cut-off voltage is limited by the maximum input current of motor and controller, discussion of these parameters is saved for further research.

$$E = P \times T \quad (7.4)$$

$$E = \frac{1}{2} C (V_2^2 - V_1^2) \quad (7.5)$$

The SOC variations under the NEDC drive cycle are presented in Figure 7-8 with the regenerative braking effective. The simulations are conducted with an initial SOC = 0. In both simulations, the results show the proposed control strategy is capable of maintaining the balance of SOC.

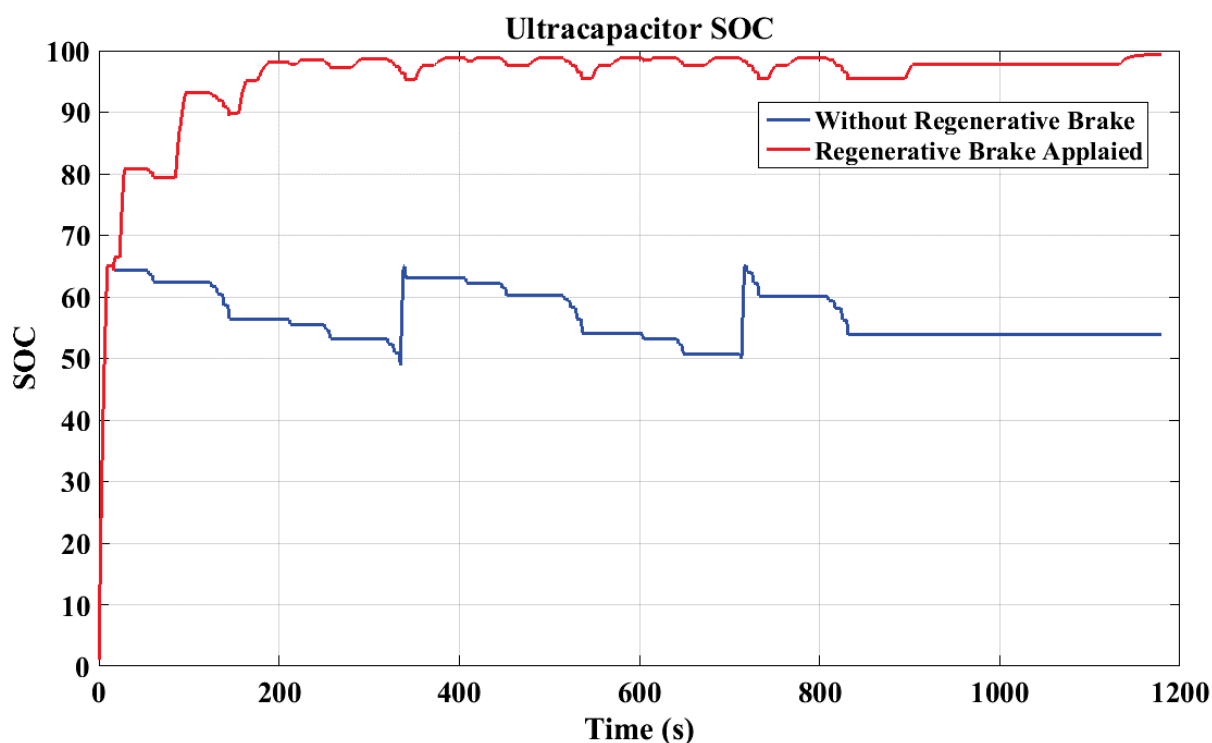


Figure 7-8: SOC of ultracapacitors with regenerative braking on the NEDC Drive Cycle.

As the power demand from the EM reaches its highest point, the SOC follows a trend of increase during regenerative braking and decreases throughout high current discharge. This can be observed in the ultracapacitors SOC graph. Along with this, both the usage and generation of energy of the ultracapacitors compare much more rapidly to the battery bank. This is resultant of the ultracapacitors ability to deliver demanded power in a smaller time span. The benefits provided by the ultracapacitors pack are to derive energy from regenerative braking and providing energy for peak acceleration which would otherwise not be within the battery pack's handling capabilities.

7.5 Summary

Based on the analysis of the effectiveness of batteries / ultracapacitors on power and energy demands during the different standard driving characteristics drive cycles, it was observed that the EMC plays an important role on the power requirement of the EPS of the vehicle. Lastly, the influence of different initial and target SOC's of the battery on electrical

consumption during the developed real-world drive cycle is tested using the MHEV powertrain.

In the total comparison of the simulation results of MHEV powertrain subject to drive cycles of different density traffic patterns, one can readily conclude that the SOC of high-density traffic pattern drive cycle is significantly better than that for the drive cycles at low-density traffic pattern. Because of the effective regenerative braking, the MHEV powertrain uses less energy than the conventional vehicle.

Under regenerative braking, the braking split (between friction braking and electrical/regenerative braking) is allocated depending on two principal variables. These are the brake pedal position and the battery SOC. By adding ultracapacitors the ability to sink rapid charge current into storage is improved, allowing a greater range of regenerative braking. This results in better energy efficiency and allows the system to meet large electric power demands better.

The results of the regenerating braking using the motor and battery/supercapacitors are almost perfect (without energy loss). This could be due to the assumptions that made in the simulations. Prior work comparing the implementation of electrochemical batteries and supercapacitors has been published by the team in another thesis [111]. In that work, they have shown some potential improvements over batteries.

Chapter 8: Cost analysis

This chapter presents a study on the MHEV powertrain production cost and total payback period. Firstly, the cost of the developed energy management controller (EMC) on the conventional vehicle is studied by using the real-world drive cycle. Partial drivetrain electrification is a cost-effective means of improving fuel economy. By utilising an EM to supplement the ICE, varying power demands may be more efficiently met without sacrificing vehicle performance [4, 112, 113]. In order to validate design decisions, a payback period must be calculated, taking into account the increased purchase price over the base vehicle. Manzie [89] accomplishes this using the total cost of ownership (TCO) methodology. In this case, this approach is not feasible for a number of reasons. Primarily there is significant regional variability in the published information that is available. For instance, to estimate operating costs, it is important to include government charges and service costs. However, the cost of labour and government regulation vary significantly from region to region, so it is difficult if not impossible to defend any estimation as accurate. Likewise, residual vehicle value depends on many variable parameters, such as new car tariffs, average national fleet age, and foreign exchange rate. Often in developing regions, the national average vehicle fleet age far exceeds that of Western countries. For instance, nearly 70% of vehicles registered in Egypt are over 15 years old [114], making residual value calculations based on the net present value method unreliable.

In general, a number of considerations are made with respect to the vehicle type, system configuration, annualised driving range, maintenance, and so on [89, 115, 116]. The result of this type of calculation procedure is an estimate of the lifecycle costs of a particular vehicle configuration. This has become a critical factor in the vehicle electrification debate as such vehicles typically have a much higher upfront cost than conventional internal combustion

engine equivalents. For the purpose of this research, however, the considerations are significantly simplified. A particular vehicle configuration has already been adopted for the overall analysis (see section 1.1). Consequently, the baseline vehicles are identical, with the exception of the additional electrification equipment. Such Relative Cost of Ownership (RCO) models are typically applied to the comparison of alternative configuration arrangements[116] and are applicable here.

Specific to this research, the relative cost of ownership can be calculated as follows:

$$RCO = \{SPF \times (G + E + Tx + B + M + I)_{HEV} + M_{HEV} + T + C_{HEV} - R_{HEV}\} - \{SPF \times (G + E + Tx)_{ICEV} + M_{ICEV} + T + C_{ICEV} - R_{ICEV}\} \quad (8.1)$$

Where SPF is sale price factor, G is a glider, E is the engine, Tx is the transmission, B is a battery, M is motor, I is Inverter, T is Total Range, C is Consumption, R is Residual, and M is Maintenance. As stated, identical vehicle configurations are used, with exception to the electrification components. Therefore, the net vehicle cost between both configurations can be used. Also, as this is a mild hybrid vehicle, maintenance costs are assumed to be identical. Net fuel consumption can also be considered. Finally, based on the vehicle fleet profile of the target markets, it is reasonable to assume the vehicle will be held by the owner until it has no residual value. Therefore, the cost analysis simplifies to a payback period calculation. RCO can be simplified to:

$$RCO = SPF \times (B + M + I)_{HEV} + T \times (C_{HEV} - C_{ICEV}) \quad (8.2)$$

8.1 Production Cost

The production cost may be calculated by developing pricing using the power ratings of each element of the mild-hybrid powertrain, in line with [117, 118]. This cost is then added to the cost of the base (ICE only) vehicle. Because the base vehicle is substantially identical to the

mild hybrid version without the electric powertrain, it is not necessary to consider the cost of the base vehicle in the payback period calculation.

It is necessary to multiply the price difference by a ‘sale price factor’, which includes both the retail mark-up and government charges that would be added to the sale price of a vehicle. In most cases, the retail mark-up is adjusted up or down by market forces to maintain parity with global prices despite total government charges. Therefore, the use of a single factor is considered appropriate. The literature [89] cites 1.71 as a reasonable approximation.

The development of a low-cost electric hybrid drive system for small vehicles was conducted as a proof of concept with an aim to target developing markets which see a correlation with elevated environmental pollutant levels [119, 120]. The development of a hybrid vehicle will have a focus on improving drive (including shift) characteristics with low-cost hardware, for implementation in an automatic vehicle. In recognising the market forces acting as a barrier to entry, a 5% cost limit on the net manufacturing cost increase over the base vehicle is a primary design criterion. This value has been chosen as being representative of the typical variation that may be acceptable to the end consumer. The value covers the total cost of hybridization, included motor, inverter, and battery. The cost estimates for these components are presented below.

8.1.1 Electric propulsion system (EPS) Cost

Drive cycle analyses were conducted to select the minimum practical electric motor and battery characteristics in order to enhance both performance and operating efficiency. The drive cycle analyses allowed the identification of typical energy requirements, which were used to minimise the cost and size of the electric powertrain components. An extensive design study was conducted to select an appropriate electric motor. The motors studied had a very wide operating range and are a higher efficiency power source when compared to

internal combustion engines (ICE), as they typically range from 65% to 95% round-trip efficiency [121, 122]. The design study suggested that the most suitable EM for the low-cost HEV is a Brushless DC Motor (BLDC), with a rated continuous mechanical power output of 10 kW (30 kW peak). Because the intended use profile involves short pulses of high power for torque-filling, the peak mechanical power figure is as significant in consideration as the continuous output. BLDC drive is widely used for EV and HEV applications [52, 55, 56]. A 10 kW EM was found to satisfy most requirements for torque-fill in during gear change, and also has sufficient power to be able to be used for improving vehicle efficiencies under high demand or low engine efficiency conditions [59, 123]. However, many mild hybrid vehicles characterised by a low degree of hybridization operate at relatively higher voltages. These include Honda models fitted with Integrated Motor Assist, which operate on 144 V [26]. Despite the high voltage compared to current trends, the vehicle as presented is characterized by 14.2% degree of hybridization.

Various methods have been proposed for approximating the manufacturing cost based on physical performance requirements. McKeever [124] gives original equations (8.3) and (8.4) for both the inverter and motor cost, however, because of the technological and scale improvements in the intervening period, they cannot be considered realistic in the current term.

$$\text{Inverter cost} = \$418 + \$7.60 \times kW \text{ peak} \quad (8.3)$$

$$\text{Motor Cost} = \$33.33 + \$10.6 \times kW \text{ peak} \quad (8.4)$$

Hadley [117] proposes a near-term cost of US\$41 per rated kW for total motor and inverter cost. Wu [118] provides a compound annual growth rate (CAGR) for the capital cost of HEV components. For the motor/controller, the CAGR is -4.4%. By applying the CAGR to the figure proposed by Hadley [117], we arrive at a 2016 figure of US\$31.30/kW. The motor and

controller are therefore expected to add approximately US\$375.60 to the cost of the base vehicle.

8.1.2 Battery cost

From [109], Based on the available literature the cost of a 1.2kWh battery(Table 7-1) is estimated at US\$60, the total system cost is, therefore, US\$436. The cumulative cost of the motor, controller and battery results in an overall additional cost of \$435.60. The cost of producing a simple B-segment vehicle varies depending on the specification and production region, however typically falls between \$8000-\$12000. In this case, the overall additional cost fulfils the goal of providing a system with the low-cost implementation of mild hybrid vehicle benefits. Suitability for mass-market vehicles sold in pre-mature stage markets is taken into consideration, with the aim of reducing atmospheric particle pollutants in urban regions [26]. It will also reduce dependency on fossil fuels for such regions. However, as these costs breach the pre-defined upper limits, further study of overall costs and cost-saving measures is required to reach the goal.

8.2 Payback period

The cost difference of US\$435.60 is multiplied by the sale price factor of 1.71 to arrive at a retail price difference of US\$744.86. This figure was used as the basis for the payback calculation. An average fuel price of US\$1.50 per litre was also used, as was an annual distance travelled of 15,000 km [125].

The results shown in Table 6-12 were then used to calculate a payback period in years, which is shown in Table 8-1. The calm driver yielded the shortest payback period, of 2-4 years, whereas the aggressive driver yielded a much greater payback period of 5.5 to 11 years, dependent upon the drive cycle used for the analysis. Using a weighted average of 40% NEDC and 60% NYCC cycles, which may be more representative of a realistic driving

pattern, the calm driver broke even in 3.6 years whereas the aggressive driver broke even in 6.8 years. In every case, however, the payback period does not exceed the typical vehicle lifetime, which is greater than 15 years. The results suggest that the low-cost mild-hybrid powertrain is effective, though particularly susceptible to driver influence.

Table 8-1: Payback period of years.

	Payback 15,000 km		
	Aggressive Driver	Normal Driver	Calm Driver
NEDC	11	8.2	3.6
UDDS	4.7	3.6	1.9
NYCC	5.5	3.3	3.6
Weighted average years	6.8	4.3	3.6

8.3 Ultracapacitor cost

The cost for the UC was approximated at a value of \$450, resulting in a total additional manufacturing cost of \$825.60. In comparison, the identical system with a battery module replacing the UC resulted in a net additional manufacturing cost of \$435.60. The UC, therefore, represents an almost 90% cost increase over the battery system, and it is necessary to question whether the benefits justify the cost difference. There is a target to reduce atmospheric particle pollutants in urban regions, and the appropriateness of these vehicles introduced into pre-mature stage markets is taken into account [26]. Whilst both the UC and the battery are effective in reducing emissions output, the UC offers weight benefits, life cycle and power density improvement over the battery, as well as improved energy recapture. However, in the absence of significant fuel economy and emissions reductions over the battery system, financial considerations are a strong influence. There remains potential for costs to be reduced further. However, more research in the area is required to determine how to achieve this.

8.4 Vehicles daily and annual operation cost

The purpose of this comparative study between the MHEV, a conventional vehicle is to optimize the vehicle energy efficiency and electric drive performance throughout the system. Table 8-2 lists the vehicle and components parameters and specifications for each powertrain. The analysis of the influence of developed low and high-density traffic patterns drive cycles on the fuel economy, and the annual cost is carried on each powertrain model. The different density traffic patterns drive cycles, being low and high levels are used in order to demonstrate the different level of aggressiveness or driving style of different traffic conditions.

Table 8-2: Vehicle and components parameters and specifications.

	ICE powered vehicle	MHEV
ICE	1.6 L, 70 kW@ 5000 rpm	
EM	-	12 kW BLDC
Battery	Lead-acid battery 12 V	NiMH, 1.2 kWh / 12.5 Ah
Vehicle mass	1100 kg	1200 kg
Transmission	5-speed Manual	

For further analysis, a comparative study on a daily and annual operation cost was conducted during a 40 km distance travelled under the developed low and high-density traffic patterns drive cycles. The low and high-density traffic patterns drive cycles are defined in Chapter 6. The reasonable daily trip is assumed as 40 km distance covered from house to workplace and back to the house. The assumptions used to generate the annual energy cost estimate was fuel costs of US\$1.50 per litre and an annual driving distance of 15,000 km.

Based on the vehicle daily and annual operation cost listed in Table 8-3, since the MHEV powertrain uses less fuel to travel the same distance, it can save about 11% and 25% annually for the low and high-density traffic patterns drive cycles, respectively, compared to a conventional Vehicle. Based on this analysis, it can be concluded that the MHEV powertrain is more suitable for city driving cycle, where the traffic is moving slow, and there are more

opportunities to recover the regenerative braking energy during the stop-and-start events, which is a lot cheaper compared to the fuel price.

Table 8-3: Vehicles daily and annual fuel cost under same distance.

Page 203	MHEV		CV	
	Low	High	Low	High
Fuel economy (L/100km)	5.8	8.5	6.5	11.1
Fuel used daily (L)	2.2	3.4	2.5	4.5
Daily fuel cost (\$)	3.3	5.1	3.75	6.75
Annual fuel cost (\$)	1204	1861	1369	2465

8.5 Summary

This chapter has introduced a cost-effective mild hybrid electric powertrain for an MT vehicle, integrating an EM to provide improved fuel economy, drivability and comfort by reducing torque holes during gearshifts. The adoption of the motor has required the development of vehicle control strategies to manage power split under a range of driving conditions, and a gearshifting strategy to control transient vibration during and after gearshift.

Our stated goal in undertaking this design study is to develop an ultra-low-cost mild hybrid drive system for B-segment, light-duty vehicles offered in less sophisticated markets, due to the correlation these markets share geographically with areas affected by high atmospheric pollutant levels [119, 120]. In developing a product for these markets, key design characteristics have been identified (in particular, driving characteristics such as shift quality, commercial characteristics contributing to manufacturing cost) that should be met, and ways of maximising the fulfilment of these goals have been investigated. The MHEV configuration proposed simplifies the vehicle architecture over and above that described in the prior literature, to achieve desired performance using only one EM. This is achieved through the application of a superior EMC that balances driving needs with SOC and other conditions. This simplification reduces overall weight and cost. Despite a focus on minimising added cost, any increase in cost over the cost to produce the equivalent ICE-powered vehicle must

be compensated through other means, such as fuel or tax savings. Inherent cost of ownership savings made by adoption of the mild hybrid drive has been quantified.

This analysis concluded that the MHEV powertrain is able to reduce the operation cost of the vehicle besides of improving its fuel economy, emissions and electrical consumption.

A low-cost ultracapacitor-based HEV targeted toward developing regions has been proposed.

The production cost analysis shows the system is affordable within the typical B/C segment price range, although there is significant scope to refine the initial work in this area to find further cost-efficiencies.

Chapter 9: Model-Based design of an automotive MHEV

As automotive systems become more complex, achieving software validation to a high degree of fidelity and confidence becomes increasingly important and challenging. Software validation and simulation must be able to handle the inherent complexity and non-linearity whilst being cost-effective and catering to industry needs. Model-based design (MBD) is the current industry standard which is used to meet validation needs from conceptual simulation through to final system acceptance, as shown in Figure 9-1. MBD, sometimes called model-in-the-loop (MIL) is generally used by first creating an initial design investigation, then adding greater and greater detail until final parameters may be tuned using built-in optimization tools. Software-in-the-loop (SIL) is used to build and simulate the control algorithm software with the plant model as a step in the verification process, which is then transferred to a processor-in-the-loop (PIL), which uses a production microcontroller to control the plant model in a non-real-time environment. This allows debugging and stability testing. Finally, the model is substituted with real hardware and production controller in a step known as hardware-in-the-loop (HIL) to verify the system in a real-time testbed environment. Because the HIL environment operates in real-time, it is the most challenging step to achieve. It relies on acceptable model simplifications and selection of robust fixed-step solvers for implementation and simulation of complex physical models.

The validation process is multi-stage and begins from non-real-time environments where the model is created (MBD/MIL) in software, and controlled using another software application (SIL). This stage is useful for requirements analysis. The second PIL stage is optional and is only typically required where the processor requires verification prior to moving to the target ECU. PIL is often used as a design assurance tool. The final (HIL) stage is a fully real-time

environment where both the target ECU and the physical hardware are embedded into a model for real-time verification. It is the principal method of formal verification and validation.

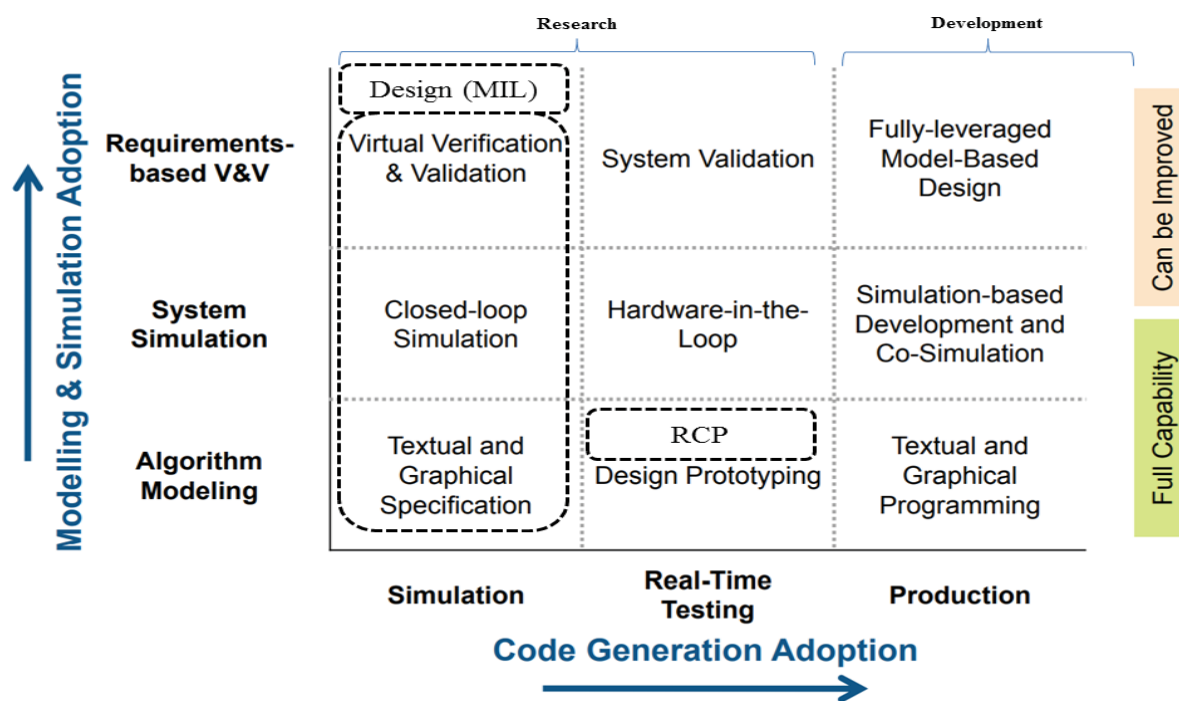


Figure 9-1: Model-Based Design Adoption Grid.

This chapter presents the development of the Electric Propulsion System (EPS) which has been deployed in the mild hybrid vehicle test bed. The presentation is developed in the context of the well-established V-cycle development process, which is a commonly used standard process throughout the automotive industry for technological development. This is a real-time process, which requires specific real-time implementation techniques to process the model, interface with the electrical hardware and manage power requirements.

The major phases of the V-cycle are shown in Figure 9-2 Throughout the chapter the different process steps will be discussed with reference to the MHEV development work undertaken [126, 127].

The vehicle simulation will be addressed and discussed. Two main techniques make up the vehicle simulation: simulation without time limitations, and real-time simulation. The latter is

broken down into Rapid Prototyping (RP), and Hardware-in-the-loop (HIL) [128]. By implementing these simulation phases, there is an observable improvement in development time and prototyping iterations. Overall, this improves the quality of the developed systems [129].

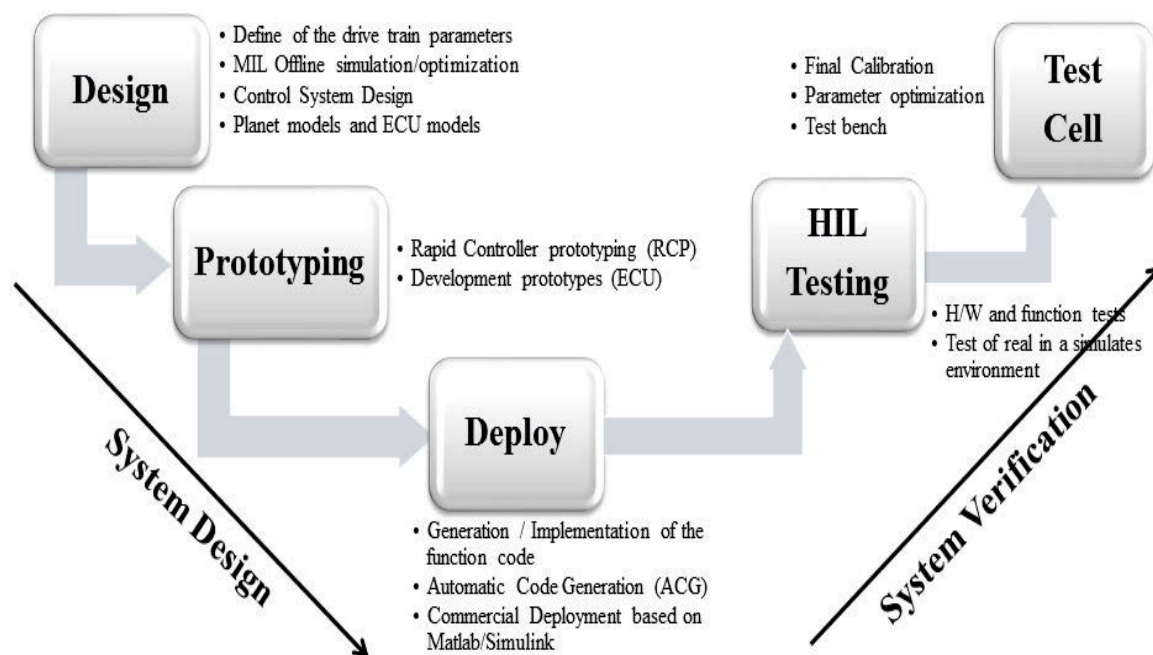


Figure 9-2: V-Cycle for automotive system design.

9.1 Design and system definition

The One primary goal of the system is to eliminate the hole in driving torque (“torque hole”) which is output from the MT during gear change processes. The torque hole is caused by the momentary disconnection of propulsion, caused by clutch actuation, required to successfully execute a gear change. This goal is achieved by deploying the EPS as a torque modifier in the model by using the concept of a mild hybrid electric powertrain as shown in Figure 9-3 as a torque gap filler. The specifications for the ICE, PMSM/BLDC, battery and transmission are listed in Appendix C and detailed in Chapter 3.

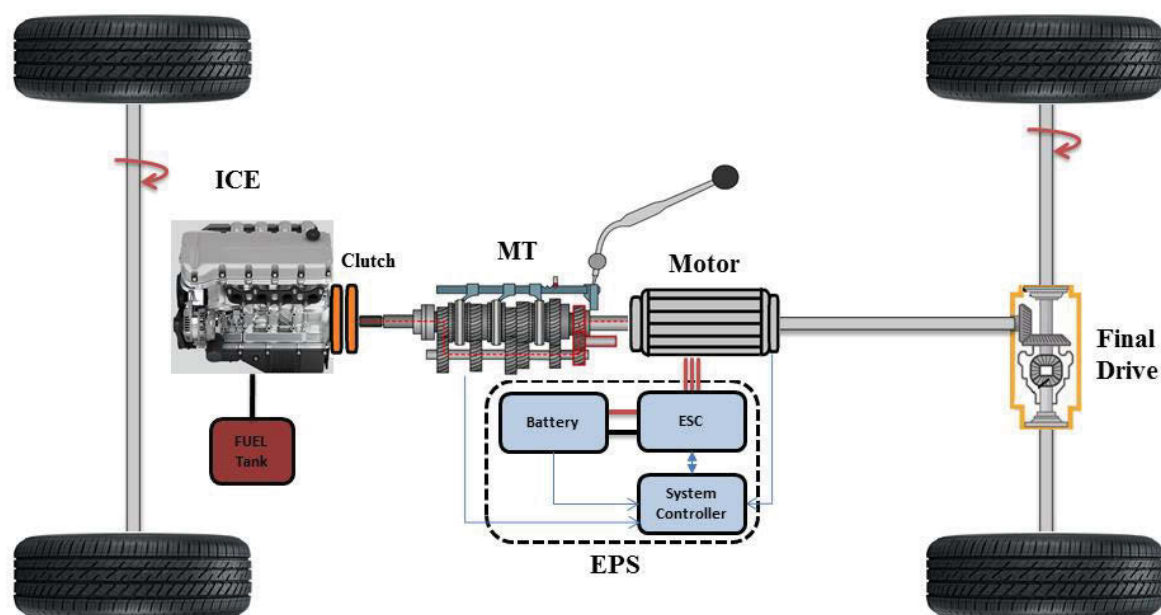


Figure 9-3: MHEV Powertrain.

Vehicle model development is based on libraries of individual components that have been previously developed and can be modified and deployed to suit individual needs. Some vehicle modeling tools use the effect-to-cause method, which is a feed-forward simulation: A driving cycle is used as an input. From this, the operating points of the individual components are calculated, and from there the overall fuel consumption and battery depletion/charge can be obtained. This method is not very useful for controller design and optimization, but can be used for the fast comparison of different hybrid drivetrain structures and configurations. The more common approach is The cause-effect method of vehicle modelling, which is the basis for nearly all hybrid vehicle simulation tools, uses a driver model to follow a driving cycle (task: speed control) or a simulated track (task: speed and direction control). It is very useful for controller design and optimization. Many of these tools are based on Matlab/Simulink or at least have an interface to Simulink or a Simulink model export capability (e. g. IAV VeLoDyn, PSAT by Argonne Nat. Lab., dSPACE ASM and NI VeriStand & LabVIEW Model Interface Toolkit). Other environments, such as Dymola, SimulationX, LMS Amesim, CarSim etc. often use their own simulation environment and corresponding solvers or support code export to Simulink [126].

HIL is used to create system-level test environments by utilising multiple real-time software environments that interact with commercial hardware. Simulation testing is used to evaluate performance and analyse interactions between the EPS and transmission output. The simulated system parameters can be easily modified in the software, making it more effective [93, 130].

9.1.1 Simulation model

MODEL-IN-THE-LOOP (MIL) is step in the development process that is characterised by the presence of mathematical models of the entire vehicle; i.e., the detailed physical models of the engine, transmission and chassis components, controllers (ECU), and connecting hardware. A detailed analysis and overview of modeling approaches for the non-real-time simulation of Mild hybrid vehicle (MHEV) components are provided in chapter 5. Many of the model components are based on pre-existing components in Matlab/Simulink/Stateflow by using Simscape and SimDriveline libraries. A general structure of a plant model is shown in Figure 9-4. Stability is ensured by simplifying the model, ensuring that physical validity is sufficient for the application. After the offline validation, the real-time model is implemented as an HIL system.

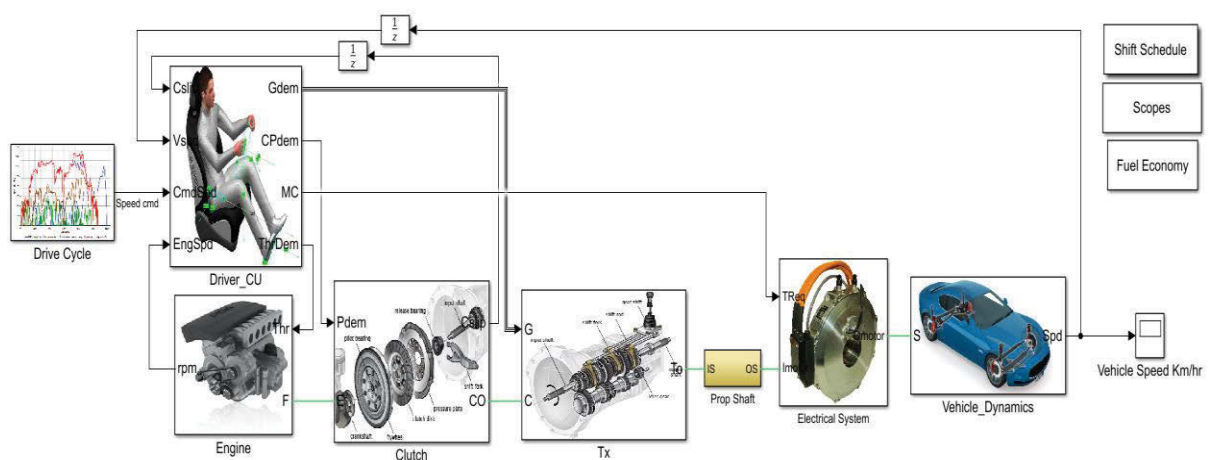


Figure 9-4: A high-level view of the powertrain of the mild HEV model in Simulink.

The EPS model is integrated as a pure Simulink model in the offline/desktop simulation. The high-level Simulink model wraps Stateflow component models to complete the simulation environment (model-in-the-loop). In the section, the use of Simulink for EPS design is discussed, including the compilation of the Simulink model into hardware code that can be used for real-time implementation. The software architecture design tools used for this process include RTI by dSPACE, as well as NI LabView. The workflow of the control development process is shown in Figure 9-5.

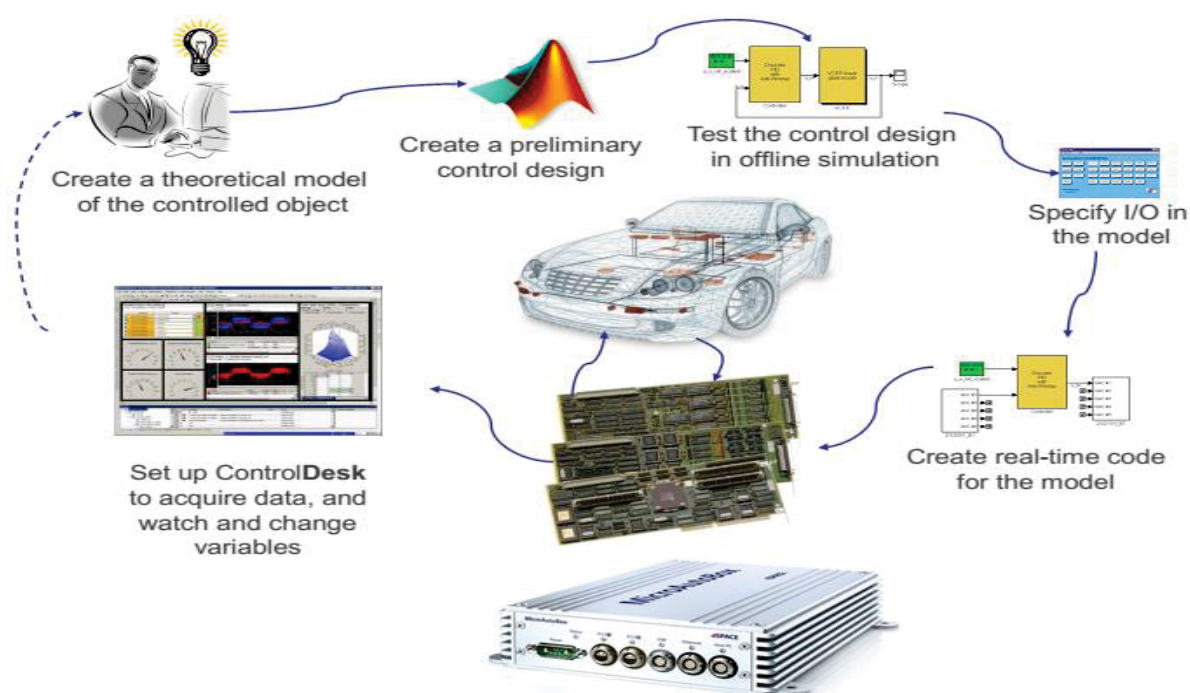


Figure 9-5: Automotive Development Process.

9.2 Prototyping and deployment

Application of Rapid Control Prototyping (RCP) technology significantly reduces the time-to-market for new products and saves the cost of new product development and model manufacturing. RCP has become a standard method for developing and optimizing algorithms in automotive applications [131]. Designing the most appropriate EPS for hybrid vehicles depends on many factors, including the driver's expectation, vehicle and project

constraints, energy source and more. Other target requirements may include noise, vibration and harshness (NVH), drivability, or other quality characteristics. There is extensive literature in the field of designing EPS to particular constraints [53]. The research presented herein focuses on simplification of the design architecture and criteria to provide RCP and validation functions. It is part of a broader research project aimed at delivering a low-cost hybrid electric vehicle (HEV) suitable for deployment in developing regions.

The specific implementation of interfaces, along with model processing in real-time with electrical hardware functionality and mathematically modeling the motor for simulations is outlined in this section. The advantages seen include an emulation of EPS behaviour, a decrease in time required for both development and testing, and negating the requirement for expensive vehicles with EPS for testing. Desktop simulations are 10-20 times slower than real-time, causing the controls development process to become tedious. The successful real-time simulation requires careful consideration of the vehicle models used for simulation. The models must be sufficiently detailed to accurately depict the dynamics of the powertrain, but also sufficiently simple to minimize computing time to be able to run in real-time. When executed successfully, the entire environment, including the model and hardware, is able to emulate the dynamic behaviour of the system with sufficient fidelity. This reduces development and testing time and also eliminates the imperative for expensive real-world testing using built physical models. A number of verification and testing systems are readily available from a variety of manufacturers, including dSPACE and National Instruments (NI).

9.2.1 EPS architecture

A representation of the EPS is outlined in Figure 9-6. The parts that make up the EPS include the electric motor, KHB1260124 power converter (used to supply the Mars 0913 motor with electric power) and the Electronic Speed Control (ESC) to provide efficient and comfortable

controls [132]. The current supplied to each phase, polarity, the position of the rotor through Back-EMF, speed monitoring, Hall-effect position sensors are managed by the ESC. It controls the operation of the electric motor to produce the required torque and speed, according to the command from the supervisory controller through the CAN network [133]. It is also used to read the physical motor's speed and temperature. dSPACE MicroAutoBox II provides supervisory control to the motor controller by reading information through the CAN-bus into a feedback control loop and issuing commands to the motor controller using analog and digital signals through the interface circuitry. The interface circuitry is made up of a custom-designed relay board and wire connections. The interface combines the output ports, e.g. sensor signals, CAN bus signals and motor driver command signals. Relays are responsible for controlling system power, throttle, brake enable, and motor direction. Other functions are effected by analog control signals and CAN-based feedback. Due to safety issues associated with battery storage and discharge in the laboratory environment, the motor is powered by a grid-connected 157 kW variable DC power supply to demonstrate proof-of-concept. In brief, The PM motor is controlled using a supervisory controller and an electronic speed controller. The speed control is provided by a Kelly Controls KHB126014, which receives its control signal from a dSPACE MicroAutoBox II, acting as the supervisory controller.

Important considerations must be made toward the selection of step size, solver choice, and a number of solver iterations [134]. Fast and stable control of the full model in this research was determined by the process of trial and error. Based on this, the following simulation set-up was selected: step size is 0.1 msec fixed step. Previous research has determined the validity of the system.

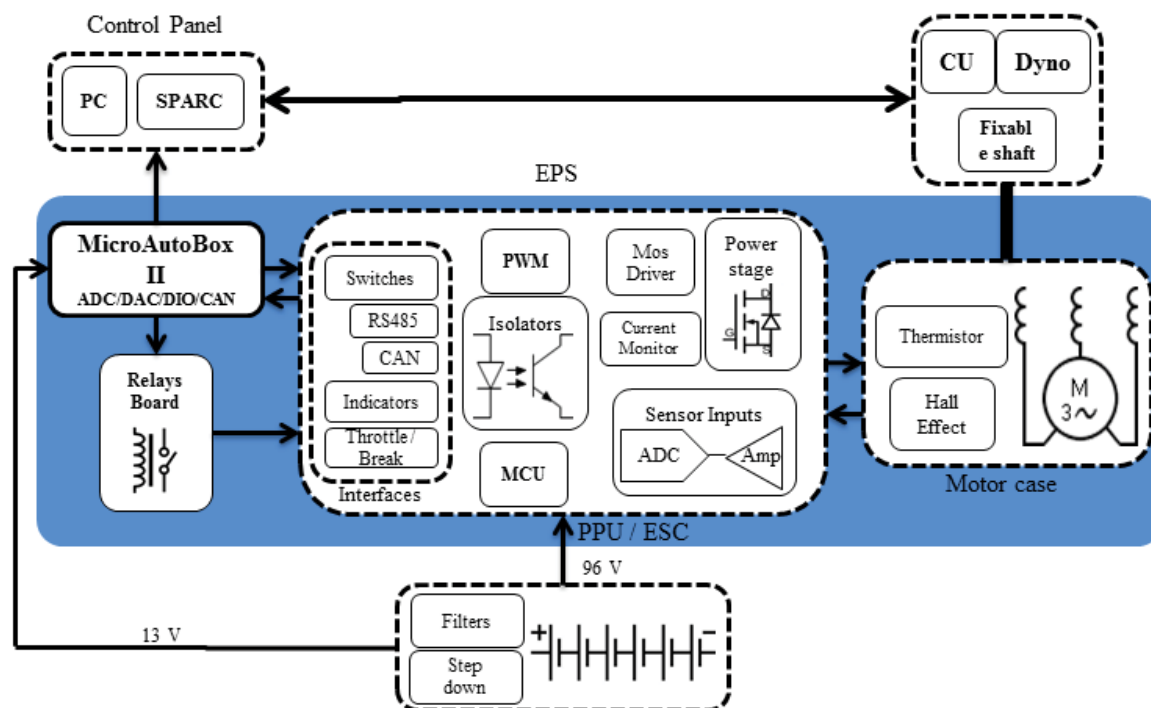


Figure 9-6: The functional block diagram of an electric propulsion system.

In this section, all the components and subsystems of the model and their interactions are described. The architecture of the system is shown in Figure 9-6 and Figure 9-7. It consists of electric motor controller KHB1260124 as the power converter, used to supply the Mars 0913 Brushless electric motor with electric power and the Electronic Speed Control (ESC) to provide efficient, smooth and quiet controls. The BLDC motor operates on three phases. The ESC controls the operation of the electric motor to produce the required torque and speed, according to the command from the supervisory controller. The ESC supports serial network communication. For this, use is made of the Control Area Network (CAN) protocol, with a data rate of 1 Mbps.

BLDC

A preliminary control design (Block Diagram)

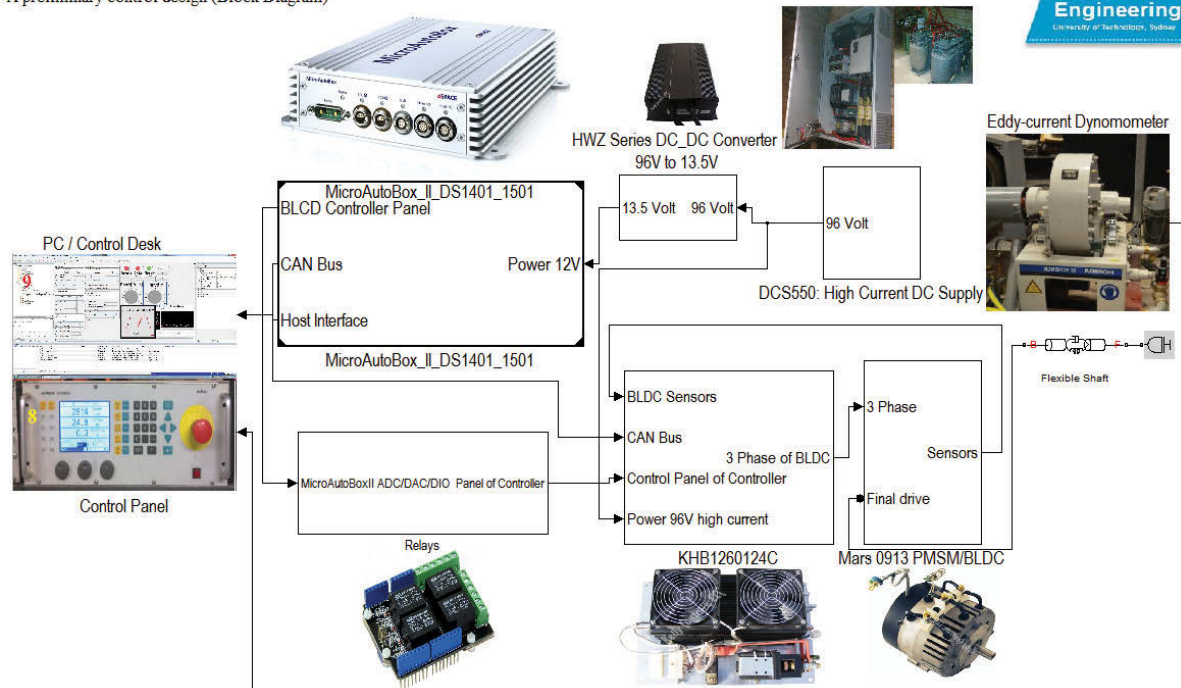


Figure 9-7: System architecture of an electric propulsion system.

9.2.2 Traction motor

Based on the NYC cycle analysis described in Chapter 3, a 10 kW cts/ 30 kW pk. electric motor was found to satisfy requirements. The Motenergy ME0913 (12 kW / 30 kW pk. electrical input) motor was selected as a suitable off-the-shelf motor for initial testing. The motor is configured as a three-phase, Y-connected motor with 3 Hall sensors at 120 degrees electrical timing and an axial air gap. It has a four-pole motor (8 magnets) and two stators. It is rated by the manufacturer to 30 kW peak at 96 V with a continuous current of 125 A of AC (180 A of DC into the motor control) [135].

9.2.3 Supervisory controller

Commercial controllers used in Rapid Control Prototyping are produced by various manufacturers. They include MicroAutoBox II from dSPACE and CompactRIO from National Instruments (NI). dSPACE MicroAutoBox II is suitable for special tasks such as development or verification and the plant model is executed in real-time on system's

processor. This is a prototyping platform typically used for a gateway or bypassing applications when developing or rapid prototyping electronic control units. The model is downloaded directly to a dSPACE Rapid Prototyping system via auto-code generation using RTI [136, 137]. The validation process also includes design processes for handling real-time simulation using Simulink, dSPACE RTI & ControlDesk environments. The real-time simulation running in dSPACE ControlDesk was hosted on a local computer within the laboratory. This software provides the user with complete control over the dSPACE hardware (MicroAutoBox II) and enables the user to change simulation parameters during runtime [138]. The host computer and MicroAutoBox II together form the supervisory controller of the testing apparatus.

MicroAutoBoxII 1401 is a self-contained real-time controller environment which is able to operate in a similar manner to an ECU without intervention by the user. It is used for a wide variety of rapid control prototyping (RCP) scenarios, performing both bypass and full pass fast function prototyping. The hardware is based around an IBM PowerPC microprocessor running at 900MHz. It includes a real-time processor unit (RTP), as well as interfaces providing functionality for typical automotive I/O functions for connection and control of sensors and actuators including digital I/O and A/D conversion.

The MicroAutoBoxII connects to a host PC using a host interface cable. The host PC serves multiple functions, including the development and design in Matlab/Simulink, data collection to verify the software-in-the-loop (SIL) models, and providing control interfaces for the commands sent to the MicroAutoBox, including simulation start, stop, observation of outputs during simulation, and post-simulation analysis[139].

The supervisory controller is used to determine the distribution of torque across the engine and the permanent-magnet motor (PM). It coordinates the control of the two power plants using information derived from other controllers and sensors, such as the engine control unit,

transmission control unit, and motor control unit. It then commands each subsystem controller separately to ensure the output torque from the entire powertrain meets the driver commanded output, in a manner that is imperceptible to the driver. In its physical embodiment, the supervisory controller is responsible for the following tasks:

- Providing motor torque commands to the motor control unit to provide motoring or regenerating torque
- Providing throttle position commands to the engine control unit
- Providing clutch position commands to the Vehicle Systems control unit

It makes these commands based on information reported on the communication bus including: current motor power, the driver requested torque, battery voltage, battery state of charge, engine clutch position, current gear selected, vehicle speed, gearshift status, among others.

9.2.4 EPS control panel

Model-Based Design (MBD) of embedded control systems has been widely adopted in the automotive industry. MBD that brings great efficiencies is the use of Auto Code Generation (ACG) technology. Control Algorithms developed in model-based graphical languages such as Simulink can be converted to production code for implementation in hardware (ECU) very effectively. Even more importantly, as revisions to the algorithms due to design changes are developed, the code can be regenerated in minutes versus weeks as is often the case where ACG is not used. The dSPACE software provides a graphical programming environment for the development of control strategies and modeling. The control models are designed in Simulink platform. The real-time interface (RTI) blockset provides function blocks to associate Simulink models with real hardware (MicroAutoBoxII). The main objective of this model was to establish the control system. The signal “Throttle analog input” is provided as

one example to indicate how to conduct adaptation of signal between KHB controller and controller model concerning RTI blocks. The throttle changes according to a 0-5 volt signal. In order to output these values, one DA conversion of RTI block is used as one output port of model as shown in Figure 9-8. Another example of signal adaptation is related to the CAN Bus. The KHB controller has default ID 0x6B, so only the data frame with ID 107 can be received by KHB controller. To read the different parameters a frame must be sent with one ID and a data field, which has the command relating to that parameter. However, commands can be set by trigger multiplexer to switch between commands. This trigger multiplexer is created by making a new model within Simulink and adding a MATLAB Function block to it from the User-Defined Function library to edit function.

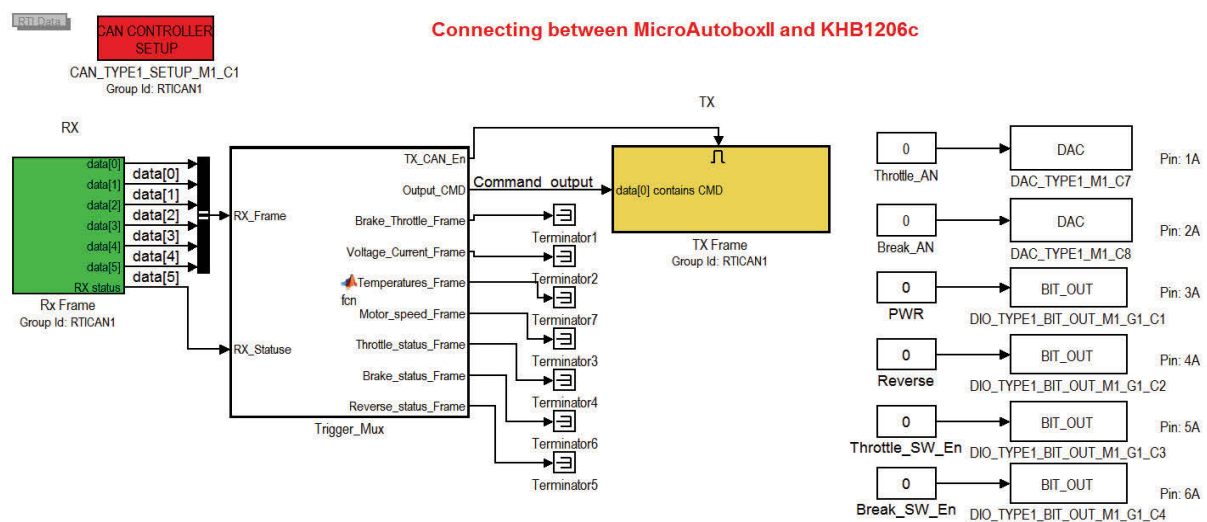


Figure 9-8: Modeling control design.

The model was developed and programmed into the MicroAutoBox II boot. It is automatically converted to code, using the automatic code generation function of the real-time interface. The real-time simulation runs in dSPACE ControlDesk, which allows logical configuration of simulation runs. Figure 9-9 shows the cockpit layout of the real-time simulation. The layout is used for setting up relevant parameters during experimentation. The MicroAutoBox II controller receives commands from ControlDesk through a host interface cable. The commands control the parameters including Throttle, Brake, Reverse motor

direction and KHB power switch. These commands were interpreted by the controller logic and applied to the KHB motor driver (responsible for managing the speed and position and working as data acquisition through CAN bus). The ControlDesk dashboard was configured to allow control of power, throttle, brake, and direction. Indicators were configured to display controller and motor temperatures, motor speed, direction, motor current, voltage, CAN-Bus activity, power status, and a speed histogram.

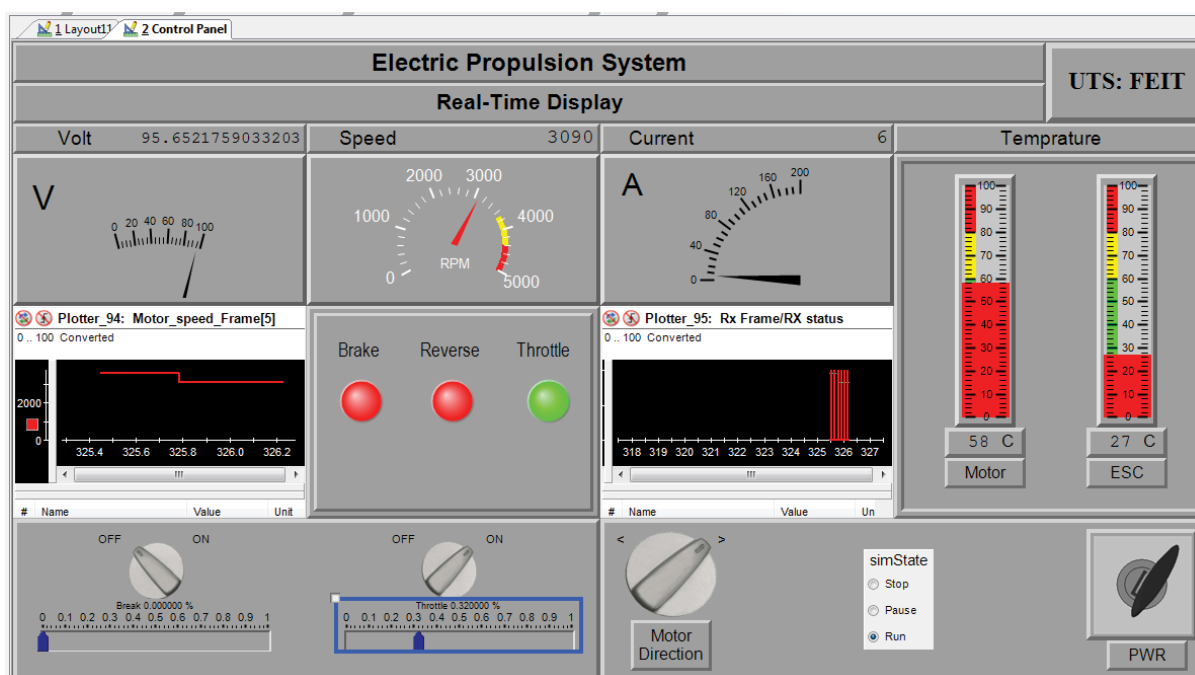


Figure 9-9: EPS control panel.

The setup is configured this way to allow the MicroAutoBox to act as the virtual driver, which is programmed into ControlDesk and deployed to the dSPACE Real-time Interface (RTI). The combination of the RTI and the MicroAutoBox is required to translate driving commands into motor control and allows for the rapid build of scenarios for testing. A CAN gateway is installed between the motor controller and the MicroAutoBox. This is used to provide feedback signals including motor speed and temperature and is used in the RTI to generate correcting commands to meet the virtual driver input. The motor is mechanically connected to an eddy current brake through a gearbox, simulating vehicle load and reduction. The ICE engine is omitted in this HIL setup. Experimental conditions may be obtained by

operating the motor to reach initial test conditions, then switching the required load in using the eddy current brake and initiating the test in the RTI.

9.2.5 Motor control

The important component of HEV and EV is power electronics. However, they represent an important share of the total cost of the vehicle, almost as important as the battery. This area has a high potential for cost reduction. Power electronics are the intermediate between the battery, a DC current source, and the AC motor. It is composed of a DC/AC inverter, which controls the voltage fed to the engine through switching devices. Control algorithms specific to each type of motor ensure that it operates at the highest efficiency. Brushless motors, in contrast to brushed DC motors, require an Electronic Speed Control (ESC) for constant control and position feedback to operate, due to the time-varying voltages on three phases required to produce constant rotating motion. This ESC poses a challenge when using an inverter to power the motor by appropriate high-power high-frequency switching is required by the electric motor to produce torque for the vehicle's propulsion, which can cause efficiency and heat dissipation to be a concern. The controller that was implemented for the EPS was a KHB1260124. It is listed in Table 9-1.

Table 9-1: KHB1260124

Parameter	SI Units
Controller voltage range	10 to 30 V (24 V preferred)
Configurable battery voltage range	18 to 136 V
Continuous current	300 A
Peak current	600 A
Feature:	
<ul style="list-style-type: none"> • CAN Bus for reading parameters • Opto-isolated for stability • Main Contactor Coil Driver 	

9.2.6 Protoshield kit and relay shield board

MicroAutoBoxII works like an ECU to send, receive and process signals. The relay shield board works between the MicroAutoBox and the motor controller as an auxiliary switch, to provide power and overcurrent protection. By using Proto Shield kit to connect with cables and relay board. The relay shield is an add-on board that allows control of high current is switching that the MicroAutoBoxII cannot directly control through its digital I/Os. It consists of four relays (both normally open and normally closed) that are controlled by the MicroAutoBoxII. Indicators show the state of each relay, and the form factor is a standard “shield” type board to allow smooth connections with the motor controller.

9.2.7 Mechanical coupling

Mechanical couplings were required for three purposes. In the initial stage, a coupling was required to connect the motor to the eddy current dynamometer for investigation of the motor characteristics as shown in Figure 9-10. The dynamometer is a Horiba-WT190 system. The basic parameters of the rated torque are 600Nm. The rated power is 190kW. The maximum speed is 10000 rpm, and the base speed is 3030 rpm.

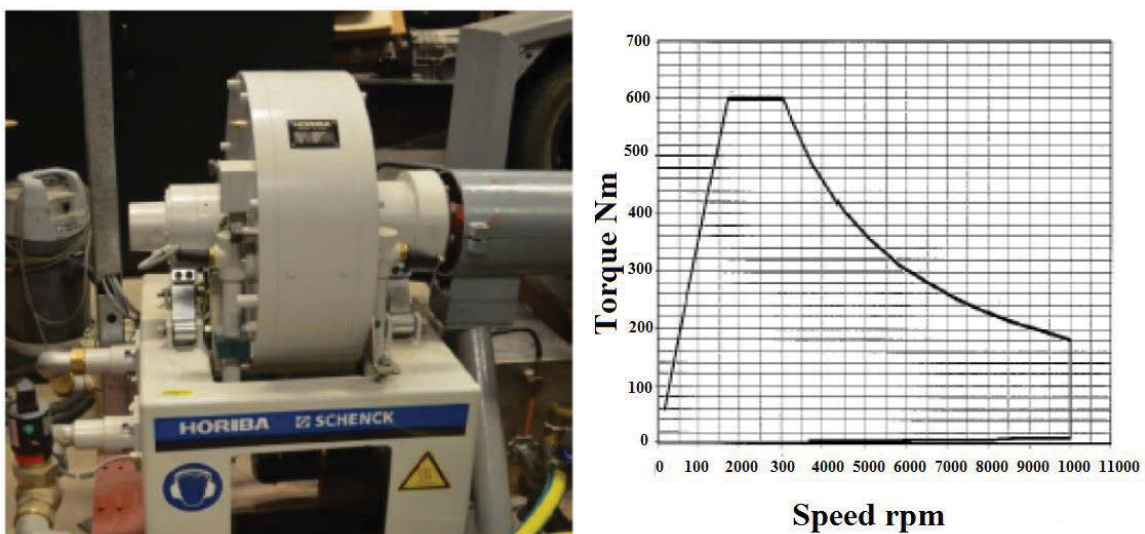


Figure 9-10: Eddy-current dynamometer and its characteristic curve [140].

In the second stage, another coupling was required for connection to the Mercedes powertrain for testing and development of the torque-hole elimination device. Finally, a mechanical coupling would be required to connect the completed torque-hole elimination prototype to the dynamometer for testing and validation. They include a motor mount bracket and plate, shaft selection, and the design of three mating (companion) flanges.

A. Mount

The motor mount was designed using SolidWorks, with reference to the drawings supplied with the ME0913 motor. The mount consists of a welded steel bracket bolted to a slotted steel plate to allow infinite X-Y adjustability within a 400mm range in the longitudinal direction and 100mm adjustability in the lateral. The slotted plate was bolted to the UTS dynamometer stand, and in turn, the bracket was loosely bolted to the plate. The motor was then screwed into the vertical section of the mounting bracket, and the shaft was attached. The face was squared off with reference to the dynamometer to minimize angular and axial misalignment in the lateral direction. As there was no adjustability in the vertical axis, the bracket was designed such that a small angular misalignment would be evident ($<5^\circ$), as is required to prevent bearing flat-spotting.

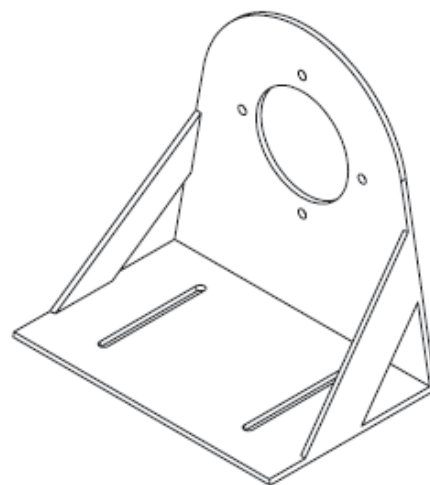


Figure 9: 9-11: Motor Mount

9.2.8 Shaft

The shaft selected for connection between the dynamometer and the motor was a Dana Gelenkwellenbau (GWB) Model 473.10. It is a double-cardan shaft specified with a slip assembly permitting operating lengths between 300 and 450mm. It was selected for its high torque limit of 195N.m. as well as its compact dimensions and lightweight.

The shaft was designed such that it could be placed in service between the dynamometer and the motor for the initial examination of motor characteristics and then placed into service between the output shaft of the Mercedes powertrain and the geartrain/ME0913 assembly when testing and developing the torque-hole elimination system.

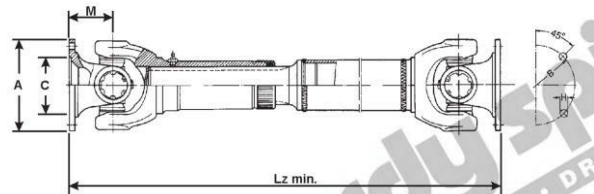


Figure 9-12: Shaft installation and line drawing (Hardy Spicer, 2014).

9.2.9 Companion flange

Two companion flanges were designed. The first companion flange was designed for mating to the Horiba-Schenk WT190 eddy current dynamometer. It consisted of a 150mm diameter steel 8-bolt flange located with an H7 (hole basis) tolerance. The flange has a thickness of 10mm and a negligible weight in comparison to the eddy-current dynamometer.

The second flange is a five-bolt flange with a 153.2 mm diameter. The flange locates using the centre lip provided on the outboard end of the front wheel hub, again using an H7 fit. The flange is designed to butt against the brake rotor after removal of the wheel. This allows suspension articulation, retains braking ability whilst testing, and simplifies removal for

maintenance or repair. This method of assembly was chosen for its simplicity and low cost. However, the efficiency of the mechanism is less than could be achieved by direct connection to either the output shaft of the gearbox (bypassing the differential) or the output of the differential, because of the reduction and then multiplication ratios required, as well as the increased shaft length and associated bearing losses.

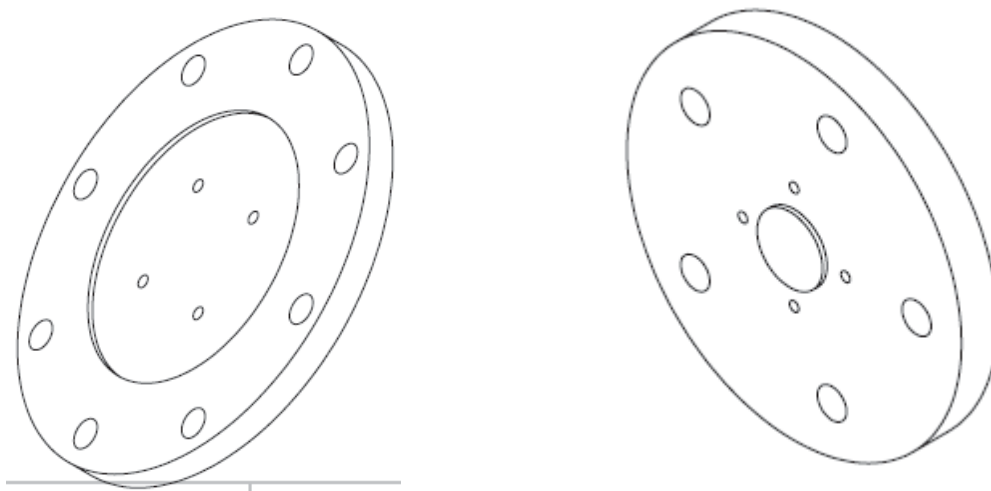


Figure 9-13: Companion Flange

9.2.10 Validation

Motor dynamometer test cycles were used to investigate and validate motor characteristics. The cycles are designed to test the motor at all speeds including very low-speed operation, transient speed and load testing. The PMSM was subjected to iterative cycles in the laboratory. Low-speed steady-state controllability of the dynamometer presented issues. Therefore, an investigation was undertaken to determine whether speed and current measurements could be used to predict power output accurately over a range of input voltages and voltage profiles, by understanding motor losses.

A. Data Acquisition Methodology

A Data Acquisition Interface (DAI) module, integrated into the MicroAutoBox II was used for data collecting and recording. The DAI was programmed from within ControlDesk. Torque was measured using the SPARC dynamometer controller, and efficiency computation completed within MATLAB. The DAI module was programmed to measure and record the necessary parameters (current, speed and temperature) of the motor while it was running on the dynamometer. The complete experimental procedure required several iterations. To create the efficiency map, the motor was set to a fixed no-load speed (voltage) starting from the maximum speed down to 1000 rpm in steps of 500 rpm. At each speed interval, the load torque was increased from zero in steps of 0.5 Nm and maintained for 10 seconds. The maximum developed motor torque was determined when the brake torque applied by the dynamometer resulted in a non-stable operating point (that is, the motor speed could not be stabilized constant). At this point, brake torque was released, and the next no-load speed was set. The sampling frequency used for the preliminary data acquisition was 0.5 Hz. Once the whole load range of the motor was measured, the parameters were analysed and validated in Matlab.

At high torque/low rpm conditions, the control limit of the dynamometer was reached. As a result, the accuracy of these conditions is poor [141]. To complete testing as comprehensively as possible, when the control limit was reached, the dynamometer was controlled for a speed of zero, which is not practically possible using the eddy current brake dynamometer available and results in a system speed of around 15 rpm. This speed allows us to approximate speed/torque characteristics of the motor at close to zero rpm. However, this test could not be sustained for long periods due to the possibility of mechanical failure of the motor. The current supplied to the motor did not exceed 105 A in these results, despite the motor being

rated to 180 A peak/125 A continuous. At this load, the elevated case temperatures indicated that mechanical failure was likely at higher loads. Because of the air-cooled design of the motor, this was a significant limitation.

Figure 9-14 shows the three-dimensional efficiency map for the motor. The low-efficiency regions are a low-speed, high load conditions. The average efficiency is about 85% for the system, which includes power loss in the motor, controller, and mechanical losses. The manufacturer-rated power of the motor could not be reached during testing. Specifically, this was 12 kW continuous and 30 kW peak. However, the rated peak efficiency of 92% was demonstrated, and a peak efficiency of 95.4% was observed during testing. Rated peak torque of 90 N.m (stall) could not be observed, due to limitations of the apparatus. A maximum torque of 52.5 N.m was measured at 50 rpm. It is doubtful that the rated peak torque can be practically achieved due to mechanical limitations in the construction of the motor.

The test facilities at UTS that were used in this study are shown in Figure 9-15 They consist of an electric propulsion system, and a Horiba Schenck WT190 water-cooled eddy-current dynamometer (dyno). The motor is connected with the dyno through a custom-machined companion flange and shaft adapter, as well as a Dana Spicer GWB473-series Cardan shaft. An ABB DCS550 DC drive provides the DC power. The supply is capable of supplying up to 157.5 kW at 450 VDC. For testing constant-duty power levels, it was set to 96 V, and up to 120 A, the test was controlled through the Horiba Schenck SPARC controller and the dashboard in ControlDesk. Parameters including torque, voltage, temperatures, and current are all data logged for later analysis in Excel and Matlab.

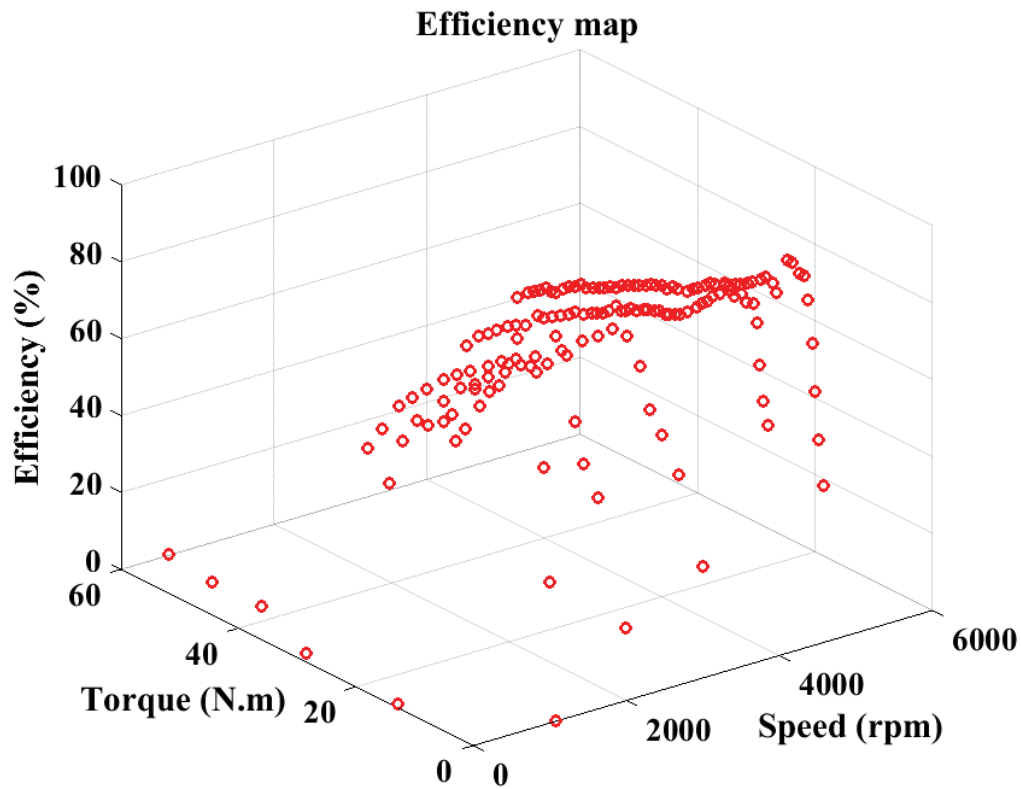


Figure 9-14: Efficiency map of the electric propulsion system.

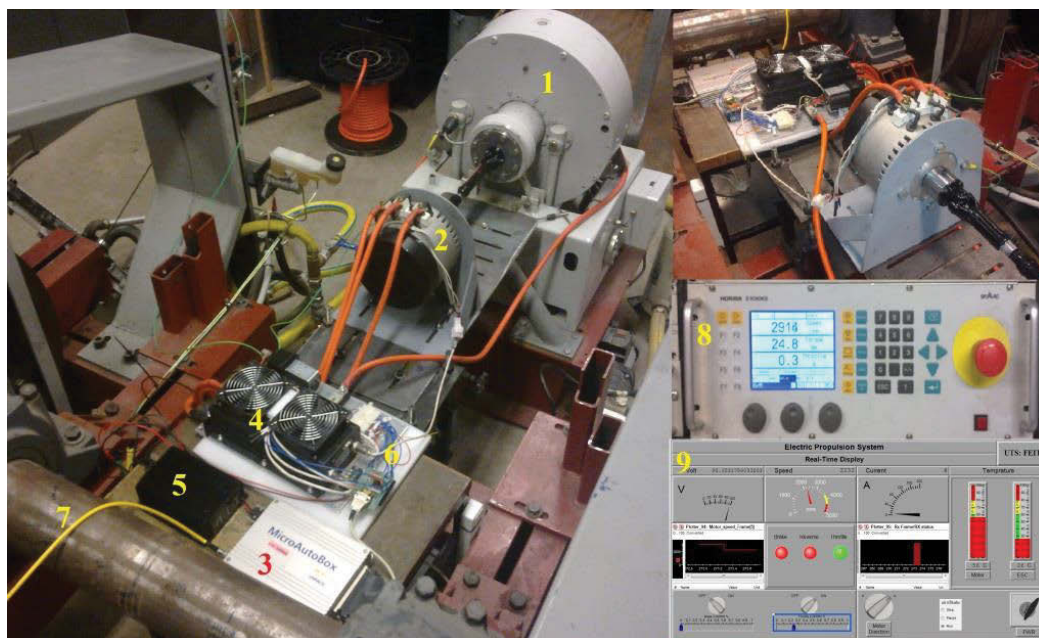


Figure 9-15: EPS test facility at UTS.

1-Dynamometer WT190. 2- Mars 0913 PMSM/BLDC. 3-MicroAutoBoxII. 4-KHB1260124. 5-Step-down 96 V/13.5 V. 6-Relays Board. 7-PC host interface. 8- SPARC control (Dyno stand controller). 9-Control Desk.

9.2.11 Testing results

The experimental validation procedure consisted of various steady state and transient tests ranging from maximum torque runs to the continuous power of the motor. Table 9-2 shows the results obtained for some of the tested parameters. Our results show that maximum power of 9.8 kW was obtained in the region of 2600-3000 rpm. Figure 9-16 shows the upper limit of torque and power available from the motor. The motor efficiency was calculated using a numerical method, by dividing the mechanical output power measured by the AC electrical input power supplied to the motor from the controller. The AC input power was not measured directly. Instead, it was approximated by measuring the DC input power to the controller directly and dividing it by the manufacturer-supplied inverter efficiency of 98%. This was deemed acceptable as the inverter efficiency does not vary significantly over a wide range of operating conditions [142]. Likewise, the mechanical output power was calculated by measuring the output torque and speed and taking the product thereof.

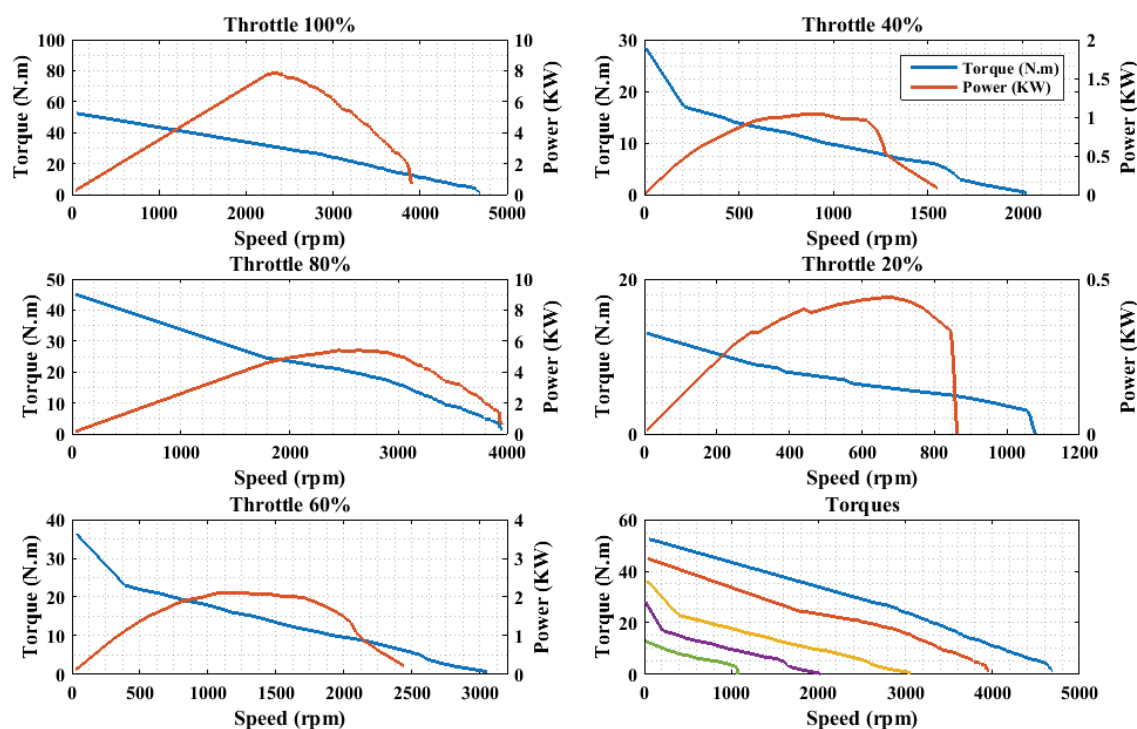


Figure 9-16: Torque and Power vs Speed of the motor at different throttles.

Table 9-2: EPS test results

Peak Power	9.8 KW
Peak Torque	54 Nm
Continuous Power	8 KW @ 2800 RPM
Continuous Torque	28 Nm @ 2800 RPM
Continuous Power (2 mins)	4 KW @ 4000 RPM
Continuous Torque (2 mins)	10 Nm @ 4000 RPM
Peak Efficiency	95.4%
Average Efficiency	85%

The mechanical power is the product of torque and speed of the motor. Equation (9.1) was used to calculate the efficiency of electric motors directly (IEEE 112-B, CSA-390).

$$Motor\ Eff = \frac{Output\ mechanical\ power}{AC\ Input\ electrical\ power} \times 100\% \quad (9.1)$$

Therefore, it is necessary to measure both the mechanical output power and the electrical input power. The mechanical power is given by the equation:

$$Mechanical\ Power = Torque \times Angular\ Speed \quad (9.2)$$

The average efficiency is 82%. Although our testing could not validate manufacturer claims, it shows that this motor can nevertheless meet our design target. The losses were not calculated individually, but can be classified as electrical losses, magnetic losses (core loss, iron power and copper loss), mechanical losses, and stray load losses, previously investigated in [143, 144].

9.3 HIL phase

Hardware-in-the-loop (HIL) simulation has been established as a development step in the automotive industry. Unlike test drives in a real vehicle, these tests are performed in the lab, so that errors that occur can be reproduced at any time. The HIL test system replaces the real environment of the EPS (ECU, Motor, etc.) and the tests can be executed in any test scenario. HIL testing is a standard step in rapid control prototyping [145]. HIL has been described in

the literature for different user applications to test and validate vehicle drivetrains under specific driving cycles [146-148].

The goal, in this case, is to fill torque holes in conventional vehicles (CV) equipped with manual transmission, using commercial hardware. The study focuses on control during the shift. The BLDC motor (or ‘hardware’) is integrated into a comprehensive virtual system. A real BLDC motor is fixed to an accurate real-time driver, with an eddy brake simulating the virtual vehicle model. A virtual vehicle model is simulated, and its output is manifested through the shaft output from the induction motor which is connected to an eddy brake.

This system creates a foundation for a wide range of HIL-testing functions. It is vital that the simulation capture the bi-directional interactions between its actual and virtual components so that a real system in the simulation can be appropriately tested.

Figure 9-17 summarizes the structure of a motor-in-the-loop simulator. The setup uses a control unit and real-time control tools (dSPACE) and implements a fixed step-size routine to ensure continuous synchronization between the virtual simulator and real-time. This is implemented within the Matlab real-time workshop. Real-time simulation is ensured by using a control unit and real-time tools (dSPACE). The real-time tools allow for the rapid prototyping of different vehicle driveline options without the need to install vehicle components. In addition to this, it makes it possible for the driveline model to command motor speed and measure torque through the eddy brake. The mild HEV hardware-in-loop setup provided in this section is fully integrated, with the ability to emulate the required vehicle, drivetrain, and driver simultaneously in real-time [149, 150].

Referring to Figure 9-17, the EPS is central to the HEV. It consists of an electric motor, a power converter, and electronic controllers. The Induction Motor (IM) is the tool that is used to emulate the real output of the manual transmission. The IM is controlled by an ABB motor

controller. Both the ABB and the electronic controller in the EPS are commanded by a supervisory controller. The supervisory controller is based on dSPACE ControlDesk and is implemented on a dSPACE MicroAutoBox II control unit. The supervisory controller is programmed with a vehicle model, which is used to generate torque commands for both the IM and the EPS. A shaft connects the IM and the eddy brake, emulating the propshaft in a real vehicle. The eddy brake acts as a brake based on a road load model, to simulate rolling, aerodynamic, and inertial resistance loads. The supervisory controller runs a model based on real data acquired from a vehicle, which gives the torque profile, vehicle speed, and gear changes.

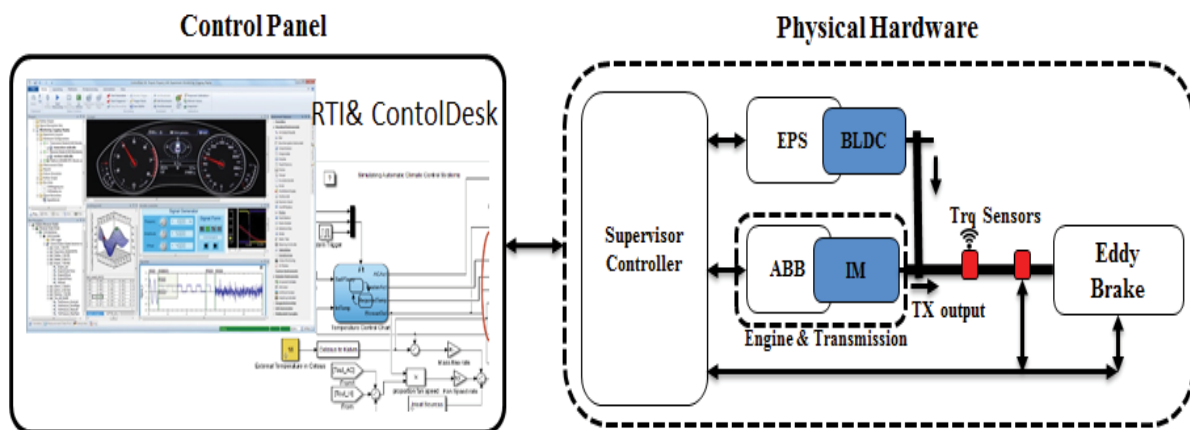


Figure 9-17: System structure schematic.

9.3.1 System structure and integration

Figure 9-18 & Figure 9-19 demonstrate the structure and components of the powertrain test rig. An offline tested MHEV powertrain control model can be loaded into MicroAutoBox to acquire data, watch and change variables, through setting up an interactive window in PC as monitoring software interface. dSPACE ControlDesk environment was used to develop a real-time interface (RTI) in the host PC, permitting user control of the simulator.



Figure 9-18: Plan view of the test rig.

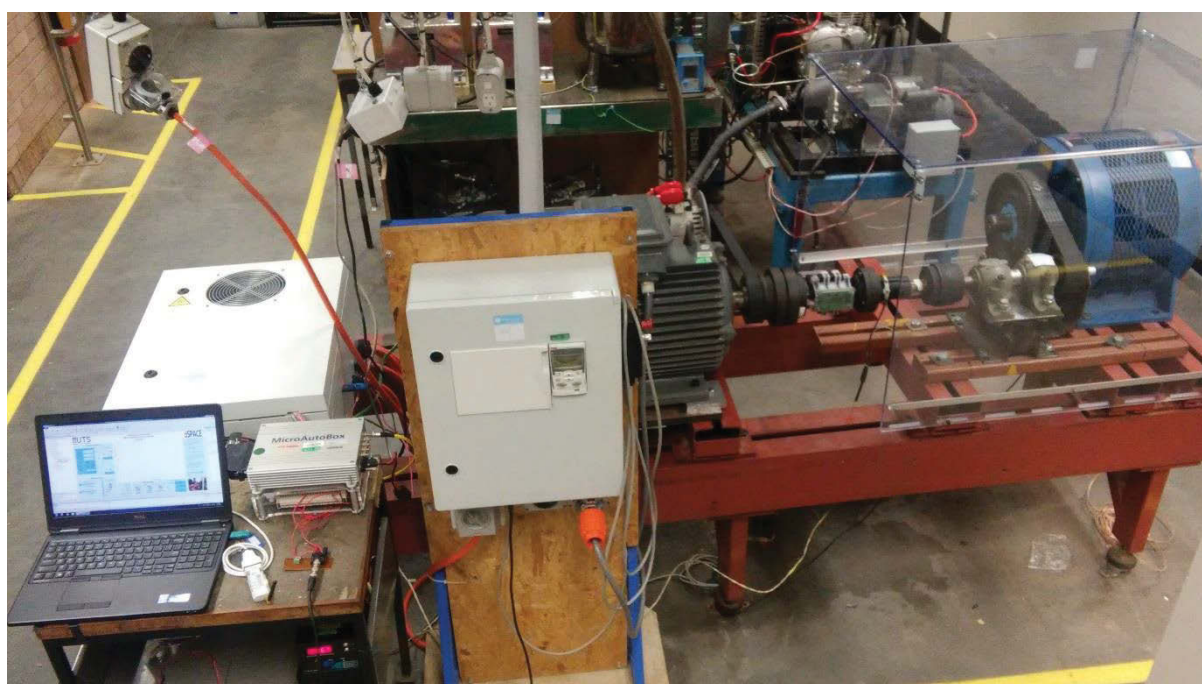


Figure 9-19: System in the loop.

1. Torque sensors calibration for transmission efficiency testing

To investigate the transmission efficiency, two wireless torque sensors are installed on the shaft of the transmission respectively (as shown in Figure 9-20).

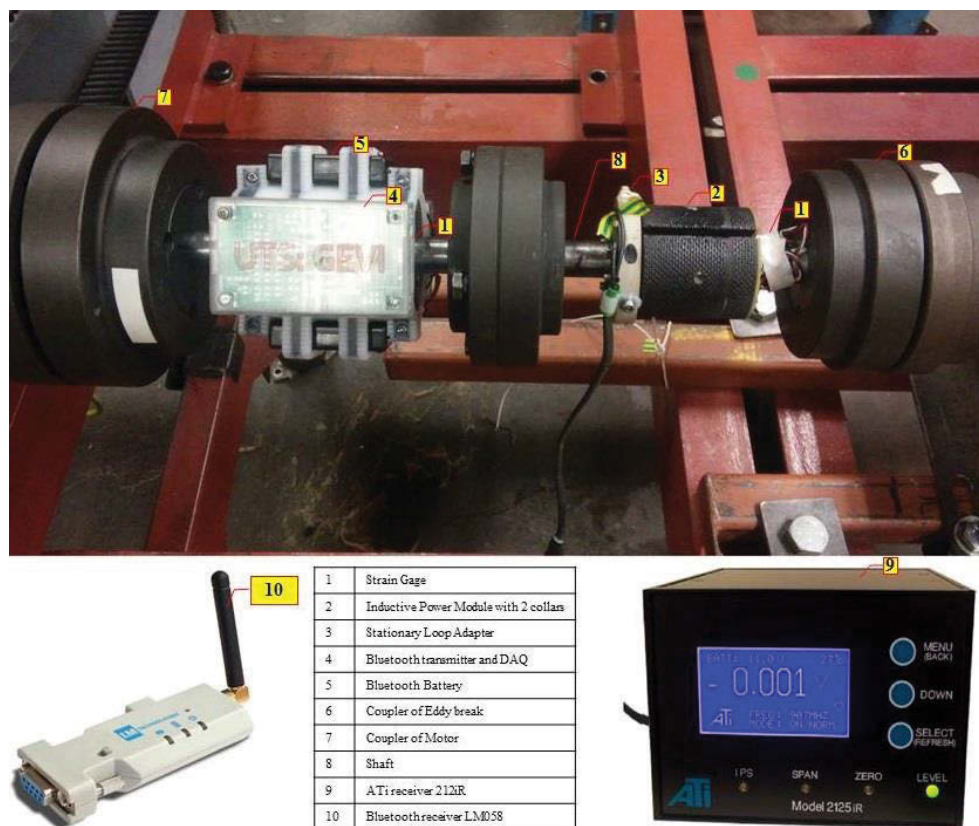


Figure 9-20: Torque sensors.

A. Torque sensor (B-DAQ)

To measure and facilitate investigation of the gearshift characteristic in a manual transmission, a wireless torque sensor is installed on the output shafts of the IM motor (emulating the propshaft of a manual transmission). A Bluetooth data acquisition board with strain gages (B-DAQ) is selected in this study to transmit data from rotating shafts to a stationary receiver using Bluetooth communication. The system includes two torque sensors at the propshaft, an eddy current brake functioning as a load for the system, Bluetooth data acquisition (B-DAQ), NI LabVIEW, the IM motor functioning as the vehicle propulsion device, and the BLDC motor under test. As shown in Figure 9-21, a strain gage is adhered to the shaft to transmit shaft torque, while the system is running. Power is supplied to the transmitter by an internal battery for continuous, non-interrupted measurements.

Because the torque related-elastic deformation of strain gage in sensors is displayed in terms of digital voltage, the relationship of torque applied to the shaft and the voltage from the sensor display should be calibrated before implementation (Shown in Figure 9-22). The calibration is used in the program code for B-DAQ in LabVIEW.



Figure 9-21: B-DAQ Torque Sensor Calibration.

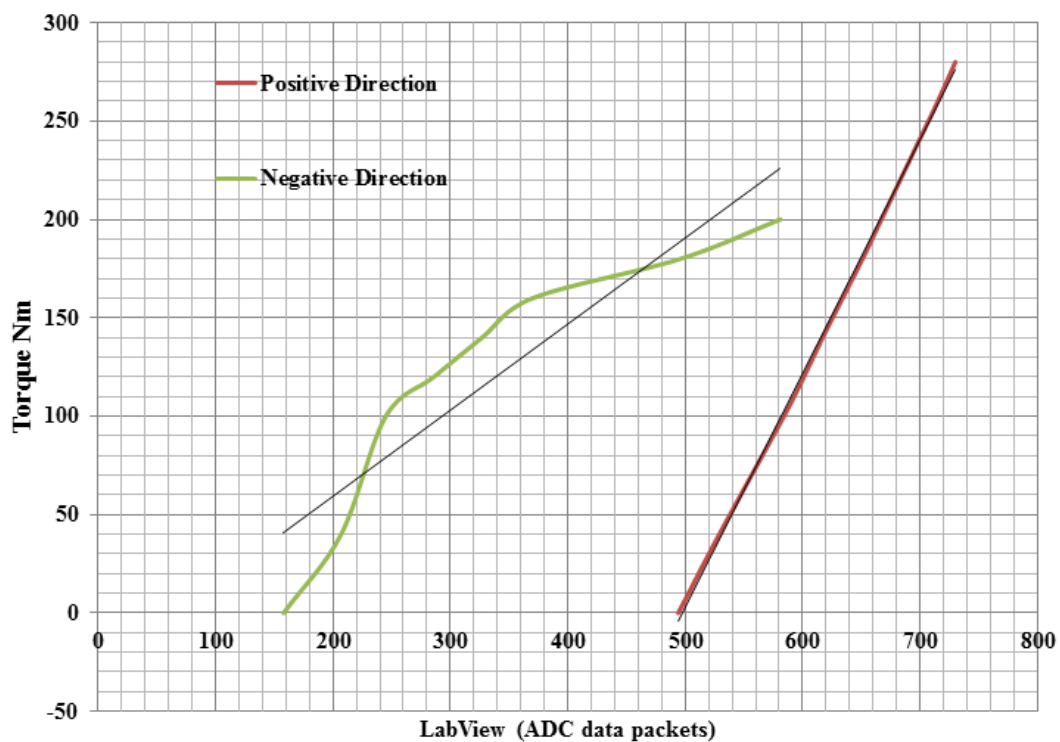


Figure 9-22: Real torque on the shaft VS Labview display Bluetooth DAQ.

B. ATi 2000 series

ATi 2000 series is selected in this study to transmit data from rotating shaft to a stationary receiver by using telemetry transmitter. As shown in Figure 9-20, a miniature strain gage has adhered to the shaft in order to transmit shaft torque, while the system is running. No batteries are required because the power is supplied to the transmitter Stationary Loop Adapter inductively for continuous, noninterrupted measurements. 2025iR Digital Receiver with a built-in induction power supply.

C. IM motor and ABB controller

The rig has a 3-phase induction motor drive (McCOLL 180M) with ABB drive controller (ACS355-03E-44A0-4) as torque control. The Induction Motor (IM) is the tool that is used to emulate the real output of the manual transmission. The motor is listed in Table 9-3. The characteristics of the selected motor in combination with the matching inverter ACS355 are demonstrated in Figure 9-23.

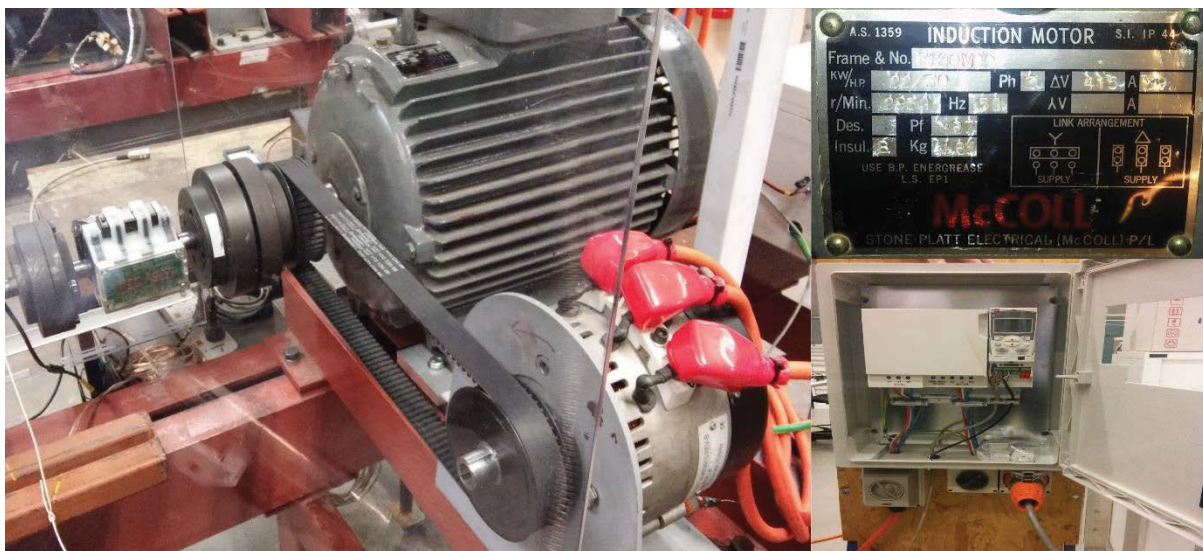


Figure 9-23: Induction Motor and ABB ACS355 assembly.

Table 9-3: McCOLL 180M IM motor.

Parameter	SI Units
Power	22 KW
Frequency	50 Hz
Power factor	0.87
3-phase	ΔV 413 – A 39
Weight	185 Kg

2. Eddy current brake

Eaton Dynamic MODEL 0M0-1M0020-0706 (DSI-AS706) is an eddy current brake. It is an air-cooled brake, used in the powertrain testing to supply additional EPS load and driving dynamic resistances to simulate vehicle aerodynamic resistance, rolling resistance, and acceleration resistance. It designed to simulate the inertia of a vehicle with a mass of 1200 kg. An eddy current brake is an adjustable speed drive system that is simple to operate, as shown in Figure 9-24. Essentially the eddy current controls work by sending a varying voltage to an inductive coil (whether it be for a clutch or for a brake). An increased voltage causes an increased torque. By increasing the output of the control, increasing the torque on the brake.

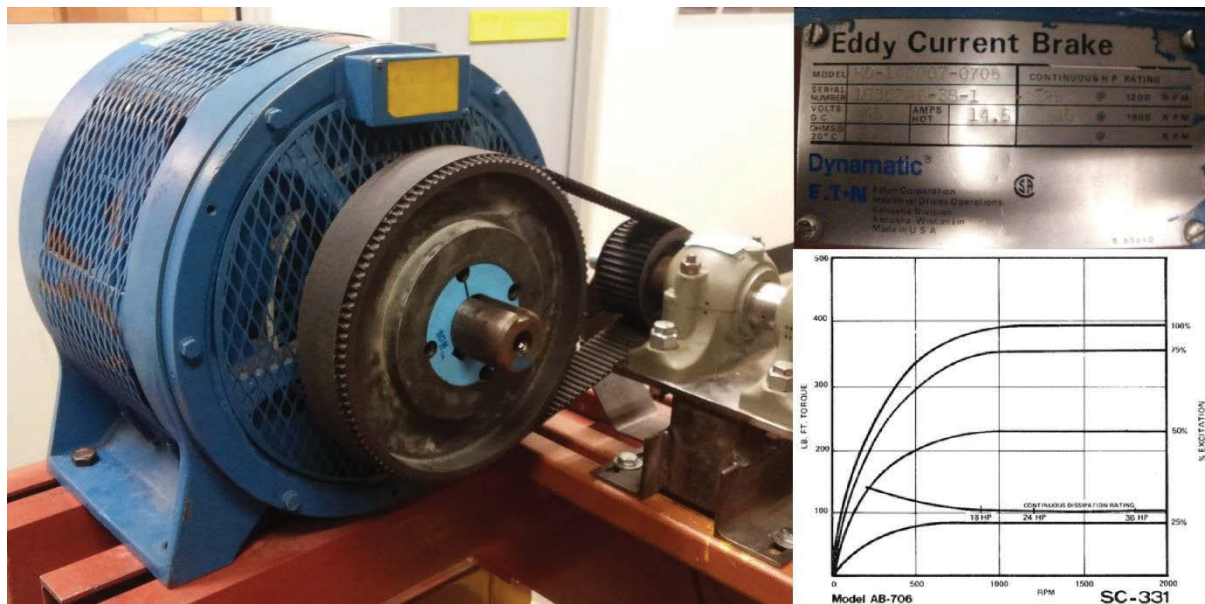


Figure 9-24: Eddy current brake Eaton Dynamic.

3. Incremental encoder

To avoid noise on the speed and position signals which coming by CAN from ESC, a very high resolution is required, which can only be obtained by high-resolution incremental encoders. Kubler-05.2400.1122.1024 is an encoder connected to the shaft through “Housing Bearing SN510” as shown in Figure 9-25 and monitored with MicroAutoBox and power/ground connections added.

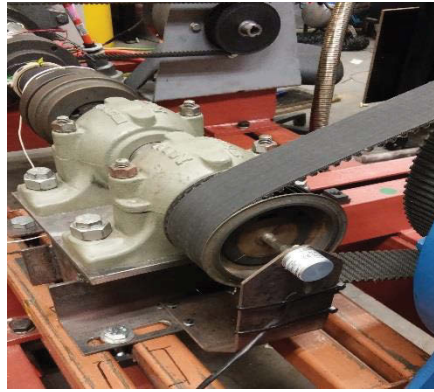


Figure 9-25 Kubler Encoder.

4. DC supply

By using a standard laboratory power supply, there is no battery in the test rig; a high-power DC supply is used and is shown in Figure 9-26. In this case, batteries were not included as the experimental powertrain was bench tested using a fixed AC power supply (three-phase), and an AC/DC inverter drive. The chosen power supply is capable of 157kW using an ABB DCS550 (S02-0300-06-00-00) 4-quadrant thyristor drive with 96 V to provide power to drive the EPS of the powertrain.

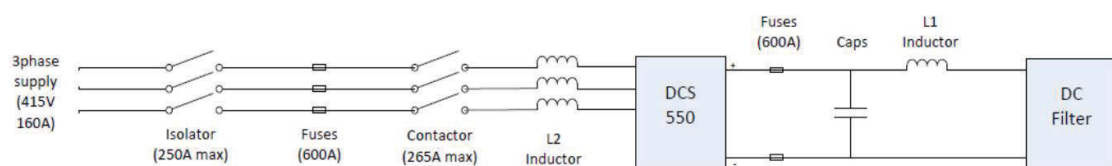


Figure 9-26: Power supply assembly.

9.3.2 Test rig model

The top level of the RTI-Simulink blocks used for the test rig is shown in Figure 9-27. It is divided into the following sub-systems: drive cycles, control units, EPS of BLDC, ABB for IM, torque, and encoder as shown in Figure 9-28. For real-time implementation, every block contains I/O, ADC, DAC, encoder, and CAN blocks from the RTI (dSPACE) library. The ESC block illustrated in the previous section on the EPS control panel. The Controller block uses the feedback from the Torque sensor and Kubler encoder to track the speed and torque and compute the required power to the ESC to become closed-loop HIL.

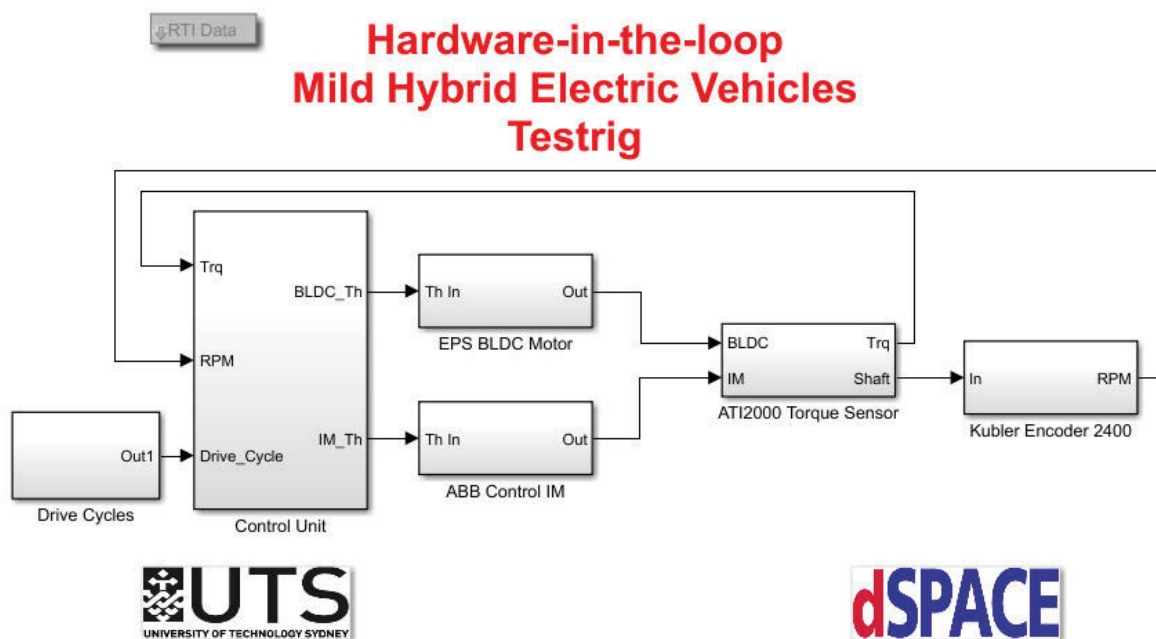


Figure 9-27: The top level of the RTI-Simulink blocks used for the Test Rig.

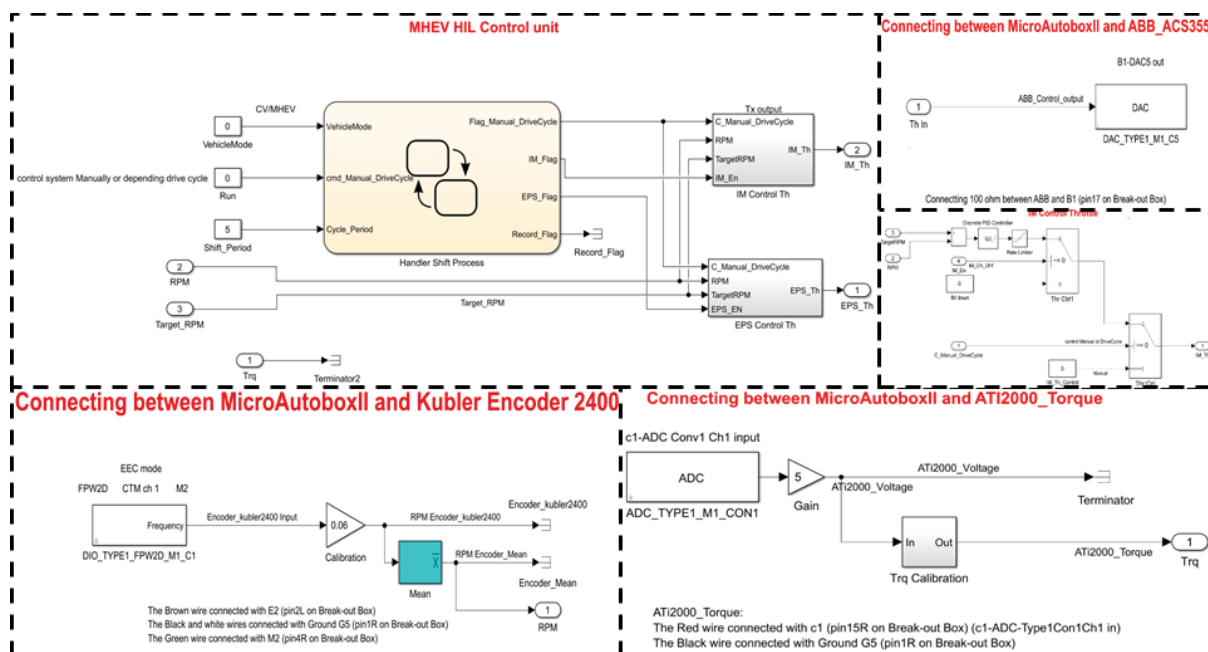


Figure 9-28: Test rig modeling control design.

9.3.3 Control panel

Figure 9-29 shows the control panel of the real-time test rig simulation for setting up important parameters such as IM speed, ESC parameters, and so on. The simulation results, such as ESC data, output shaft torque and speed, can be displayed and plotted through the instruments in the layout. The operating condition of the vehicle is updated in real-time based on the input. The simulation results can also be logged using recorders. Recorded data can be exported to Matlab for further analysis.

It is the vehicle monitoring interface for the real model car driving instrument display and driver throttle, brake and key input control signal. MicoAutobox works like an ECU to send, receive and process the signal. During the experiment, the simulation runs in parallel with the hardware and communicates with MicroAutoBox II at a frequency of 1 MHz.

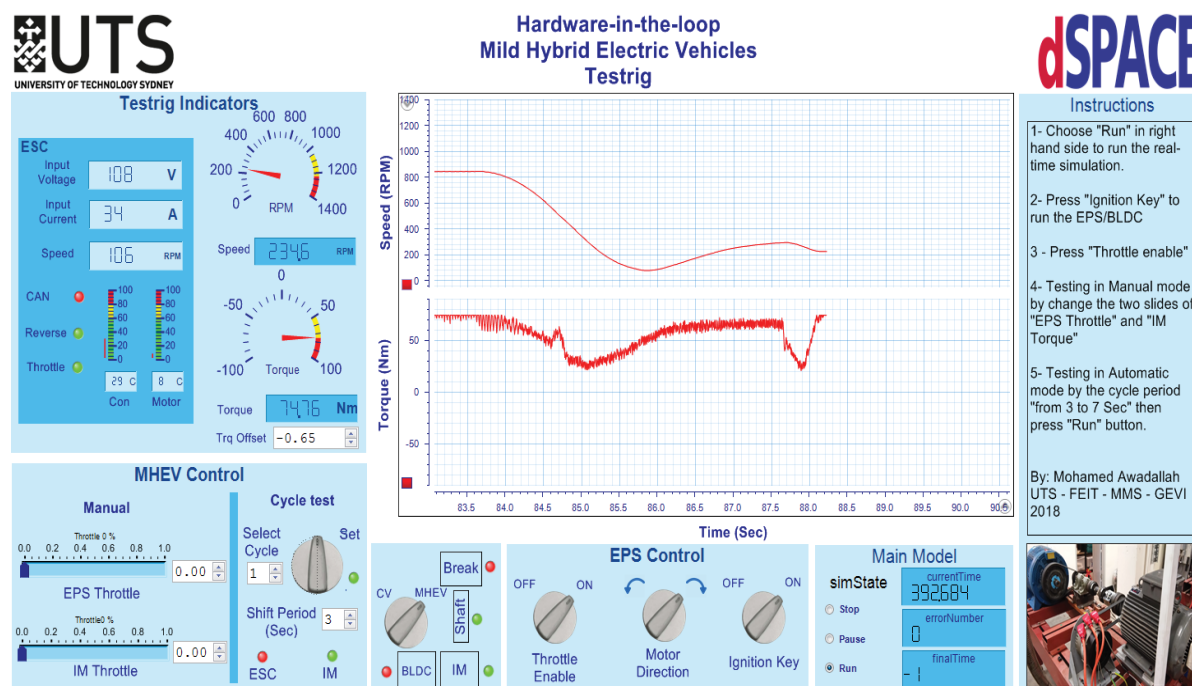


Figure 9-29: PC display panel for data acquiring, variables changing in ControDesk.

In this manner, the setup as detailed allows gear change events to be fully integrated into the simulation. Signal analysis and speed profiles are interactively available in Real-time while the simulation is running, allowing monitoring and evaluation functions during the experiment. The HIL method allows almost any check and validation function to be integrated to verify the functionality of the model.

9.3.4 Electric drive interface levels

To deeply analyse the integration of different power sources and components and their behaviour under real operating conditions. Due to their potential for high-power component damage and needs for critical safety operations, electric drive control systems need to be validated on an HIL test bench, prior to system integration. There are different interface levels between the supervisor controller (MicroAutoBox), and the HIL system can be established for electric drive test systems. HIL can be interfaced with a control system at 3 different levels of integration that allow software and hardware testing in a safe environment

as shown in Figure 9-30. All characteristics of both the power electronics and mechanical motor can be simulated and parameterized for performance and diagnostic determination [145, 149, 151].

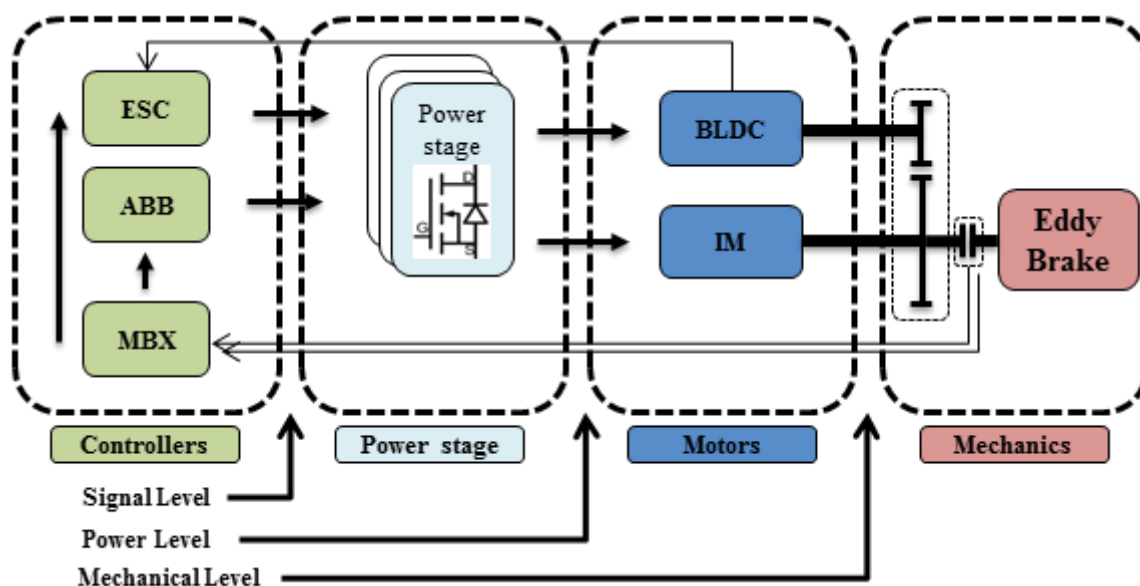


Figure 9-30: HIL Interface Levels.

1. Signal level interface

The standard I/O of the controller, such as interfaces to a motor position sensor or the communication interfaces (CAN). The interface signals to the test bench can be discrete analog and digital signals, though protocol-based interfaces: to the input signals of the gate drivers and to the output signals of the current transducers at a very high rate to ensure the accuracy and timing of the captured signal. For precise measurements of (angular) position, speed or torque, there are no power or safety restrictions.

2. Power level interface

It is the level of power electronics components of the system. The biggest difference is the power stage output interface, where dynamic loading depends on the electric motor type (e.g. BLDC and IM). The ESC controller monitors the voltage characteristics during this phase to synchronize position and speed.

3. Mechanical level interface

It is mechanical test bench which is capable of applying mechanical load torques or forces to those parts of the real system to translate these into a suitable mechanical load to be applied to the motor shaft which are physically incorporated into the HIL environment. Using a mechanical test bench can be considered state-of-the-art testing of electric drives in many cases.

9.4 Test scenario

In the case of our mild HEV hardware-in-the-loop setup, the hardware and software are fully integrated. The software controls the emulation of the output of manual transmission and EPS concurrently in real-time [149]. The BLDC motor command comes from the power management module (Kelly controller) via the virtual driver handled by the MicroAutoBox II, rather than directly. The test scenario is setup as follows. A constant torque and speed is achieved (Cruising) where the IM motor is initially rotating at 800 RPM with constant torque. A gear change is then commanded, which is simulated by a drop to zero torque output by the IM motor. The torque sensor recognises the drop-in torque and commands the BLDC motor such that the torque hole is filled. Once torque resumes, the BLDC motor is de-energized. The resulting data can then be acquired and analysed for calibration of the system and enhancement of the emulation fidelity. From a control perspective, the control signals are passed to MicroAutoBox II and processed into a command that is sent to the ABB controller of the Induction Motor. The updated vehicle velocity is subsequently translated to the IM motor, based on change states in the transmission by a virtual driver, and this request is sent to the model through MicroAutoBox II. With a change in target torque simulating gear change, the virtual driver integrated into the simulation assesses the difference in actual motor speed and reacts to increase the speed position as required. MicroAutoBox II receives

the speed position signal, processing the signal to the IM motor through the ABB Control interface. Concurrently, the updated vehicle velocity is also provided to the EPS Model, which again compares this value to the driving schedule and determines the torque hole for the following step. When the desired vehicle velocity profile starts to fall, the EPS model sends an appropriate command to the BLDC motor to eliminate the torque hole, which is measured by using a shaft-mounted transducer (B-DAQ). The values gained from the measured torque are input to the simulation module, which can assess the impact of the supplied torque on BLDC motor velocity. The resulting motor velocity is consequently converted to motor speed. The simulation is run simultaneously with the hardware and communicated with MicroAutoBox II throughout the testing duration. The updated speed and torque are provided to the model, which again compares this value to the old data without EPS to show the torque elimination.

Upshifting from 2nd to 3rd gear was selected for its simplicity and utilises that test scenario was selected as an initial benchmark for its simplicity and its ability to highlight gearshift characteristics consistently. Up-shifting control can be finished in 4 Seconds. During the inertial phase, motor torque drop down close to zero and then recover. As predicted in simulations, a large hole in the output torque and a corresponding decrease are evident during the gearshift process, shown in Figure 9-31(a). The results demonstrate the shaft speed variation resulting from the selection of varying gear ratios, as well as the transient system response. When operating in torque-fill mode, the resultant shows marked reduction in oscillation amplitude and a reduced torque hole magnitude. The torque oscillation is of particular interest, showing a reduction of 40 Nm (see Figure 9-31(b)). Based on transmission output shaft sensors.

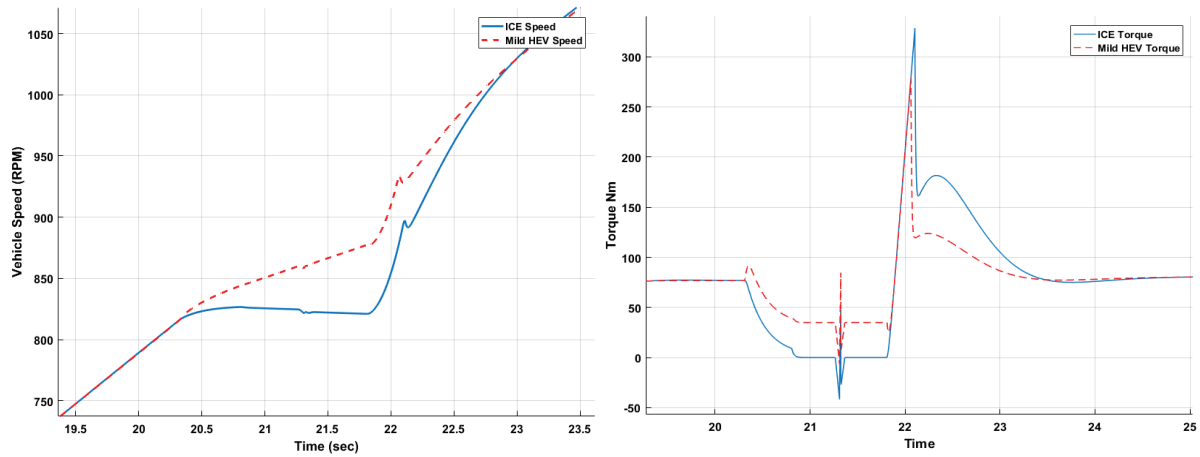
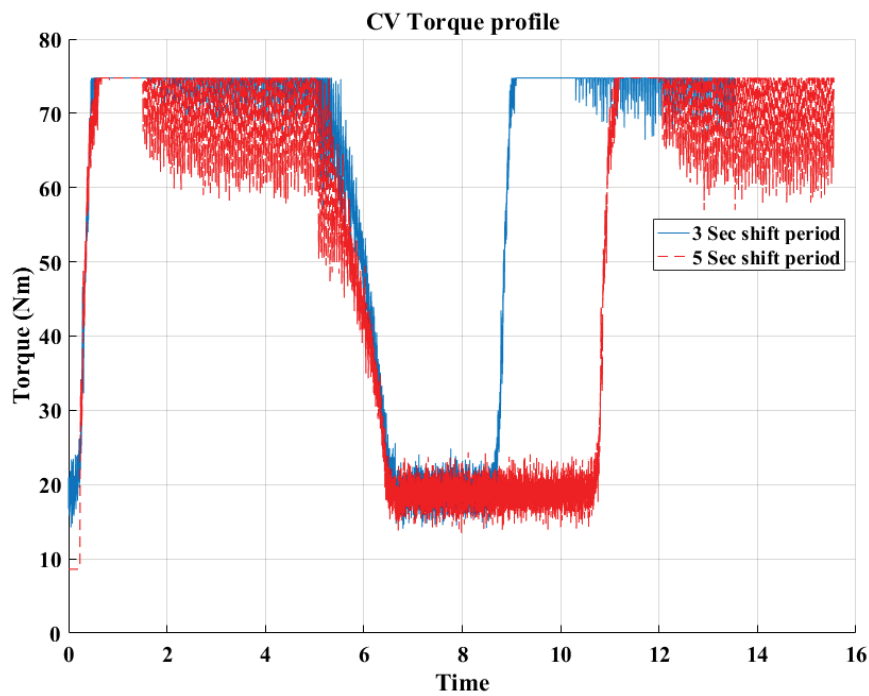


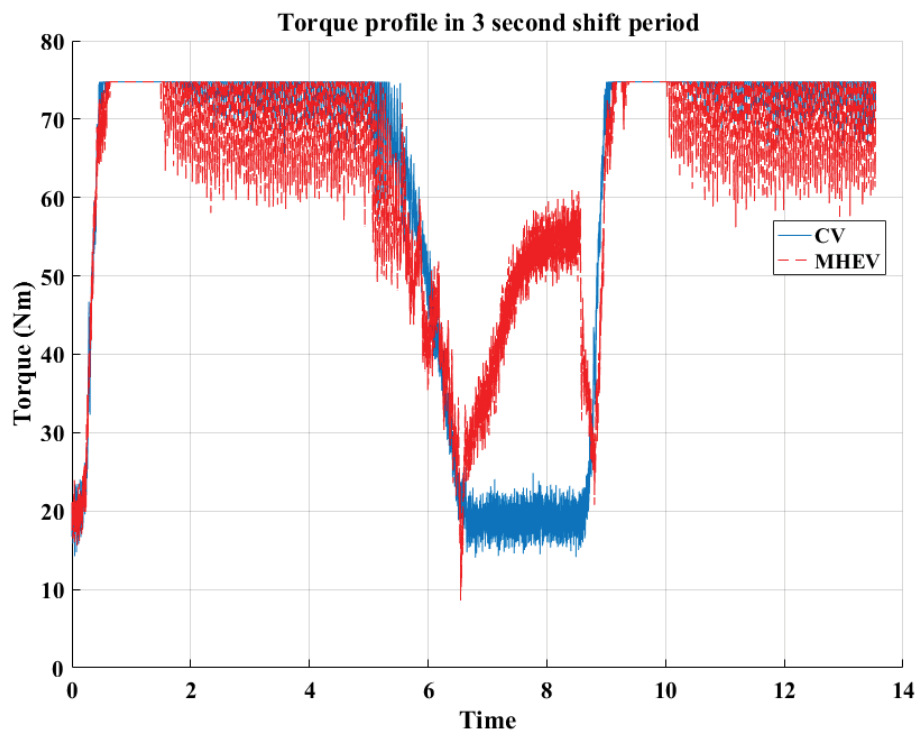
Figure 9-31: shows the torque and rotation speed output of a gearshift from 2nd to 3rd gear.

The difference between experimental and simulation results is largely due to the variation of PID-control strategies. The differences result in variations in the demand requirements between the two scenarios. The experiment results of the torque hole, it is shown in MHEV Torque profile in 3 second shift period with PID enhancement.

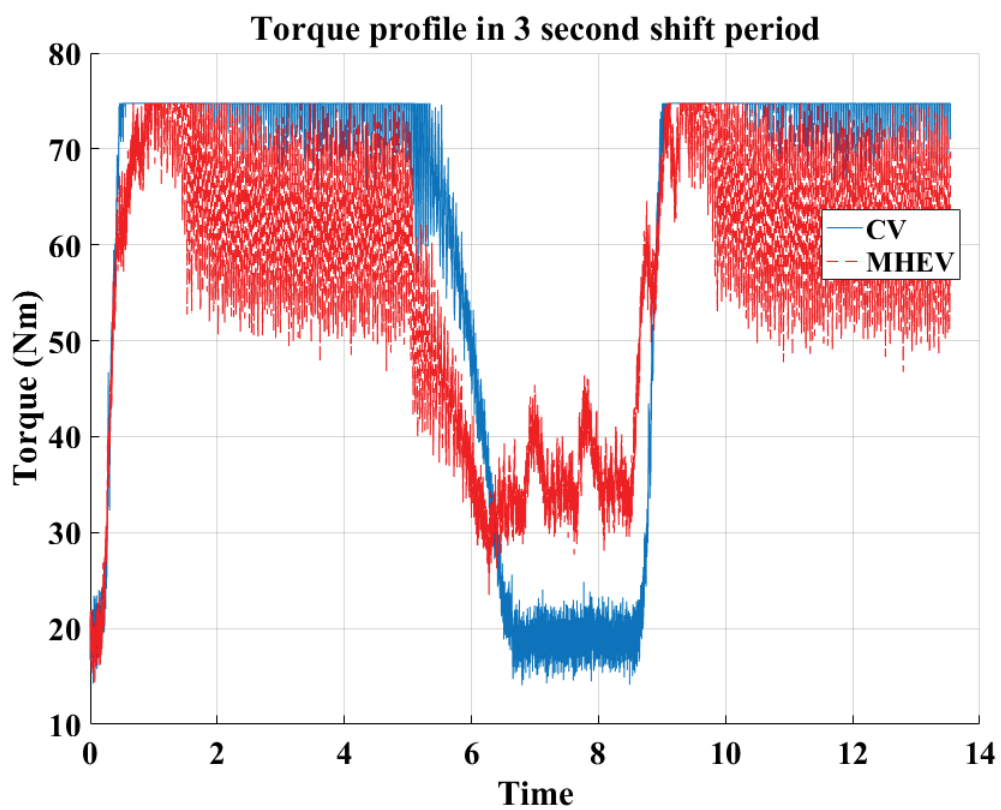
Figure 9-32, The results demonstrate the capability of the HIL model to simulate the behaviour of the real system.



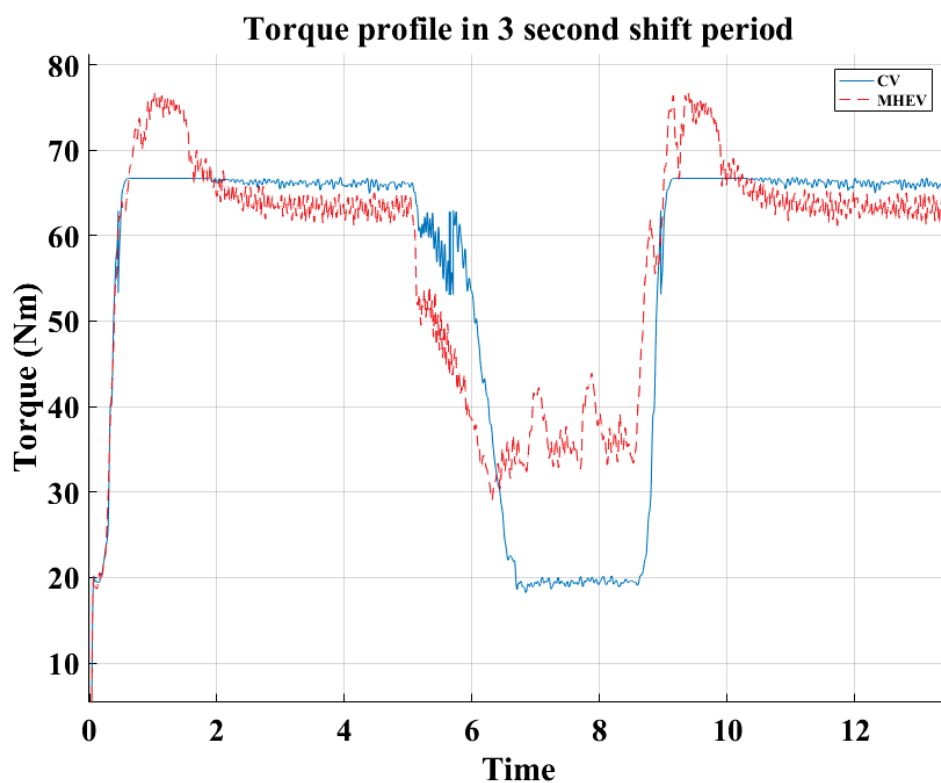
a. CV Torque in different shift period



b. MHEV Torque profile in 3 second shift period



c. MHEV Torque profile in 3 second shift period with PID enhancement.



d. Torque profile after filtration

Figure 9-32: HIL torque profile.

9.5 Summary

The presented rapid prototyping was developed to address the growing importance of electric propulsion system development in the automotive field, wherein hardware-in-the-loop testing is a standard step in modern development processes [152]. The control architecture and the detailed functionalities of the system are discussed. This system allows for the integration of the electric machine (BLDC) in highly detailed HIL systems, including simulations of vehicle dynamics or even whole-of-vehicle virtual environments. It is often used in a wide range of situations as the basis for HIL testing purposes.

An experimental validation of the rated characteristics of a BLDC electric machine was conducted. The experimental validation used HIL techniques implemented on a dSPACE MicroAutoBox II supervisory controller, which controlled a motor controller and, in turn, the BLDC motor. The HIL system was designed and implemented in the Matlab/Simulink environment and transferred directly into dSPACE ControlDesk. The rated torque and power

characteristics could not be achieved in the current testing, although it was found that the motor could still achieve design parameters set for use in a Mild Hybrid Electric Vehicle. The motor exceeded the manufacturer-rated peak efficiency of 92%, achieving a peak efficiency of 95.4%.

The HIL technique with Motor-in-the-loop allows the same control setup to be used after validation for control of the motor when it is deployed in the prototype vehicle. Developing an HIL control system at this stage dramatically reduces the prototyping cycle time as no further design work is required for building a control environment within the prototype vehicle.

The real-time modeling completed using HIL principles has allowed rapid validation of fundamental system design decisions made for this HEV system, as the initial data generated has validated aspects of the ADVISOR simulation. The HIL simulation could be further refined by replacing the eddy current brake with a DC motor controlled in four quadrants and adding a simulated engine. However the authors consider this development work to be of limited benefit considering the HIL simulation itself needs further validation using the aforementioned future work on a physical prototype. More refinement on the HIL would negate its advantages in development time, and reduce the resources available for the development of the future prototype.

The process is described by the V-cycle, which represents a series of development challenges that have been met using state-of-the-art tools. The EPS Model is designed using a combination of high-level programming languages and graphical environments. Draft control algorithms are developed and optimized using a process referred to as rapid control prototyping which utilizes a specialised development EPS containing many features to allow flexible, efficient, and quick prototype evaluations. The last and often most expensive step in

embedded control development is EPS Calibration, which incorporates the fine-tuning of system and control parameters in the vehicle or on a test bench.

Chapter 10: Thesis conclusions

In this chapter, a summary of the main contributions of this research and future direction to extend the research is presented.

Vehicles' emissions represent one of the primary sources of air pollution, and improvements in vehicle fuel economy are a constant and significant challenge to powertrain designers as they seek to conserve fossil fuel and limit environmental damage. Hybrid Electric Vehicles (HEVs) are one particularly promising solution to this concern. Where other incremental changes have cumulative effects (for instance, downsizing, lightweighting, and improving vehicle resistance), the HEV represents another order of magnitude of change. Whilst HEVs themselves are not a new concept, the advanced technology implemented in this field in recent years allows far greater potential than in the past. This has led to exponential increases in the number of HEVs produced for the worldwide market, as well as marked increases in studies of the benefits and drawbacks of such vehicles.

The research presented herein has introduced a mild hybrid powertrain for a manual transmission vehicle, integrating an electric machine to provide drivability and comfort by reducing torque holes during gearshifts. The adoption of an electric motor has required the development of vehicle shift-control strategies to improve the performance of powertrain system damping, by actively controlling the electric motor output during the transient vibration results from gearshifting. Moderately successful results are achieved regarding fuel economy, torque-hole reduction, and acceleration performance, providing a significant improvement over the conventional vehicle. The results suggest further development of the concept would be beneficial.

The Electric-propulsion system (EPS), made of the electric motor, energy storage, power management and control system is designed taking into consideration the limitations of the

existing equipment whilst exploiting the capabilities to meet performance requirements. The design takes advantage of motor characteristics and uses them to meet gearshift requirements and improve energy performance. Matlab/Simulink is used to build the vehicle model as well as calculate energy efficiency and flows. Detailed comparisons between the simulations of the conventional vehicle (CV) and MHEV, in different testing cycles, is presented.

It shows that the MHEV has a significant improvement in economic performance relative to the conventional vehicle with manual transmission. At the same time, better dynamic performance is attained, particularly with respect to acceleration. The performance of the EPS was experimentally verified in an integrated powertrain testing bench in the lab.

Initial manufacturing and ongoing ownership cost are analysed to ascertain whether the Automatic transmission (AT) is a worthwhile alternative to the MHEV proposed from the customer perspective. The analysis considers fuel savings and increased capital cost. The outcomes show that the conventional vehicle with manual transmission has the lowest retail price, where the MHEV based on the same vehicle costs a less than the automatic gearbox-equipped version. The small retail price difference obviously signals that it is a smart choice to consider the MHEV version. From the viewpoint of a lifetime costing, thousands of dollars saving is expected by minimizing fuel consumption. The MHEV not only improves dynamic performance as compared to the CV with little additional initial cost but is also cost-effective in the long term.

The vehicle on which the simulation is based is a 1990 Mazda MX-5 (Miata). As the car uses a low-tech four-cylinder engine with power output characteristics typical of most B- and C-segment vehicles, this vehicle was deemed most suitable. In addition to this, the lightweight and simple body and rear drive powertrain made this vehicle choice appropriate as a basis for research, because of the simplicity of modifying the rear-drive powertrain for hybridization. The implementation of the system was underpinned by a low-tech B/C-segment passenger

car. This was selected for two reasons: these vehicles are very common in most regions, developing or otherwise. Also, such a common vehicle will allow future development, including laboratory testing, to continue using a readily available vehicle that matches well with physical characteristics used in simulations. Benefits of the system were shown to be favourable in software, showing improvement in fuel economy.

Further development of the system may realise an anti-jerk control in addition to the torque hole fill-in. This could be executed using the same electric machine, yielding further driveability improvement. With an AMT instead of a traditional manual, the system could operate completely automatically without driver intervention. Finally, since the model utilised in the MATLAB and Simulink model is based on a simple calculation, it is recommended that further work be performed to increase the accuracy of the model.

The torque-fill drivetrain is not designed to be a full-featured hybrid vehicle. It is intended for price-sensitive markets dominated by vehicles equipped with manual transmissions. These markets typically have a high number of aspirational new-vehicle buyers and are also often geographically located in cities with a high level of air pollution. A low-cost hybrid vehicle utilizing a driveline as proposed could be successful in such a market.

The torque-fill drivetrain can be used equally successfully with automated manual, and traditional manual gearboxes, and the limited motor power and duty cycle limit the size and cost of other system components, such as batteries and converters. Due to the intermittent operation, it is also possible to safely operate the components beyond their rated continuous output and yield greater benefit.

The advantages of the proposed design are that a single electric machine may be used in many modes, filling torque-hole during gearshifts, anti-jerk control, regeneration, ICE assist, and electric vehicle mode at low speeds to enable ICE stop-start. When coupled with a clutch

and gearshift actuator, the operation of the powertrain will be fully automatic, requiring no driver intervention and achieving superior driveability measures. A 12 kW torque-fill drivetrain will improve vehicle drivability and comfort by reducing torque holes during gearshifts. Because the vehicle reaches its cruising speed quicker, it is possible to yield a small but measurable improvement in fuel economy. The greater economy may be realized at the same hardware cost by including operating modes to assist the internal combustion engine or regenerate electricity from the front axle.

The mild hybrid powertrain discussed herein is a low-cost option developed for implementation in highly price-sensitive markets. The development work presented, including the development of the physical system specifications, as well as the control and simulation discussed arises out of the need to deliver a suitable option for pre-mature markets that do not yet support significant electrification. This thesis has introduced a powertrain concept incorporating a manual transmission and a low-power BLDC electric motor, the aim of which is to deliver superior drivability and comfort, improved emissions and performance over conventional powertrains. The predominant method for these gains is by delivering fill-in torque during gearshifts.

Based on the model verification analysis with the ADVISOR code, the obtained results of the MHEV powertrain subsystems code with a proposed 5-speed MT for different drive cycles are found to be within the typical range of reported results for these subsystems. A conclusion may be drawn from the results obtained as well as previous discussions, insofar as the MHEV code is demonstrated to be realistic and promising.

Based on the fuel economy and emissions comparison between the MHEV and conventional powertrain, the fuel economy for the HWFET, UDSS and combined drive cycles with different weighting percentage is improved, and the emissions are reduced significantly. This work lays a foundation for the optimization of a powertrain using the energy management

controller (EMC/EMS) developed for this application. Comparing the simulation results of fuel economy, emissions and electrical consumption of the MHEV and a conventional powertrain are subjected to different standard cycles, and specifically-developed low and high-density traffic patterns drive cycles. The simulation results readily conclude that the fuel economy, emissions and electrical consumption all vary according to the vehicle powertrain, EMC, drive cycle characteristics and the driver's behaviour. A significant improvement in fuel economy, emissions and electrical consumption of the MHEV powertrain is achieved based on the obtained results. This is because of regenerative braking and the EMC which effectively manages and controls the power flow in the system. According to the drive cycle analyses, the regenerative braking function has a marked effect on the battery energy and driving cycles implemented. From a further analysis on the influence of different initial and target battery SOC's on electrical consumption, fuel economy and emissions during the example of the high congestion drive cycle, the selected initial and target SOC's are found to have an impact on the battery life and performance.

The developed EMC plays an important role in the power balance requirements between both of the energy sources of the vehicle. From the analysis of the MHEV powertrain operation cost of fuel and electricity consumption for different battery characteristics during the example of the high congestion drive cycle, it can be concluded that the MHEV powertrain is able to reduce the operation cost of the vehicle energy besides improving its fuel economy and emissions such as HC, CO and NOx. Finally, from the obtained results of the impact of driving distance on the MHEV powertrain fuel consumption analysis, the amount of the MHEV fuel consumption also depends on the driving distance and driver's aggressiveness.

Alternatively, adding the ultracapacitor pack in this powertrain in place of the battery was found to more effectively capture the regenerative braking energy, resulting in better energy efficiency, and meeting large power demand from the motor, resulting in better dynamic

vehicle drive performance. The increased initial cost of the ultracapacitor unit does result in a slightly negative effect on the cost of ownership in comparison to the battery-powered option.

The 5MT was selected because it offers much lower manufacturing cost, much higher transmission efficiency, and much higher in-service reliability than CVT. This is particularly important in the selected target market which is price-sensitive and in which fleet age is relatively higher than western markets.

A strategy for shifting is presented, utilising the hybridised powertrain to decrease the torque hole. The torque fill drivetrain may be applied equally successfully to both AMT and MT gearboxes. The cost of the system is limited by the deliberate downsizing of the continuous motor power, and the simultaneous reduction in duty cycle to allow the possibility of safe momentary overload if required, yielding greater benefit. The flow-on effect of this is that other components, such as batteries, converters, and power electronics are also positively limited in size and cost.

10.1 Contributions

The specific research objectives of this thesis were achieved as follows.

Determine the parameters and specifications of each of the EPS components based on the sizing and selection processes in order to design an MHEV based on a conventional vehicle using typical vehicle parameters, specifications and performance requirements according to the Mazda MX-5 (Miata) specifications, This was achieved by sizing the EPS correctly in order to achieve most of the vehicle drive performance and efficiency based on the design specifications and requirements of the vehicle, and calculating the power requirements for gear change and another condition.

Mathematical models of both conventional and mild hybrid powertrain are developed and used to compare the dynamic system performance of the two systems. This mathematical

modeling is used to run different simulations for gear-shift control algorithm design during system development, allowed to evaluate the achievable performance and its dependency on system properties. This research presented a brief treatment of shift quality and metrics using the Vibration Dose Value (VDV) approach, which provides a metric for occupant comfort. One of the project goal to fulfil our stated aim of bringing hybrid technology to developing nations is to show the occupant comfort of a vehicle equipped with our manual-transmission hybrid powertrain approaches the comfort of an identical vehicle with fully automatic ICE powertrain. The amount of motor torque applied and the length of time it is applied are optimised by minimising the VDV.

Derive a detailed model of the CV and MHEV powertrain components and the overall structure, and simulate the behaviour of the proposed powertrain in the Matlab/Simulink/Stateflow environment using a forward-looking modeling approach for different types of analysis, This was achieved by conducting a number of analysis of the vehicle fuel economy, emissions, electrical consumption, operation cost and total lifetime cost during the standard and developed drive cycles.

Verify the powertrain by conducting a performance analysis, sensitivity study and comparing the simulation results of the selected components and acquired and required velocities for both the CV and MHEV. This was achieved by comparing CV simulation results with the ADVISOR under various standard and developed drive cycles, especially in the low and high-density traffic patterns characteristics drive cycles.

Analyse a comparative study on the MHEV and CV powertrains fuel economy, emissions during the standard drive cycles and developed low and high-density traffic patterns and example of high congestion drive cycles in order to investigate the influence of the battery characteristics, initial and target SOC of the battery and effectiveness of the developed EMC.

This was achieved by design of an EMC for the MHEV powertrain in order to optimize the power management in terms of the all-electric drive performance and energy efficiency by improving the vehicle fuel economy.

Develop a new hybrid powertrain by introducing a novel MHEV powertrain, which consists of only one EM to function as an electric motor or generator at different time intervals, and performing a comparative investigation of two different energy sources in the ESC, which are the battery, and an ultracapacitor bank which captures more regenerative braking and boosts the peak power during fast acceleration.

Introducing an efficient and novel contribution to society, benefiting the environment and the economy by developing the low-cost MHEV powertrain, which reduces dependence on oil and reducing the effect of global warming in parts of the world which are economically and environmentally vulnerable.

One of the most important parts of the works is the HIL system development. This was developed using the dSPACE MicroAutoBox II. The control hardware, software and electrical schematics were developed.

Although the MHEV showed a satisfactory result in dynamic and economic performance, it has some drawbacks as well. The disadvantages may include additional vehicle weight from the integration of the EPS components. Issues in system control in the lightly-damped EPS system, where the precise estimation of clutch torques, and consideration of engine torque control and influences of time delay are likely to significantly impact on the capability to achieve high-quality shifting. These all contributions are discussed in the thesis and presented in earlier papers [153-163].

10.2 Future research

The capability of power management for the MHEV powertrain can be further enhanced by incorporating some new features and methods to overcome certain drawbacks. The recommendations for future study would be useful to continue to provide more improvements in optimizing the power management, energy efficiency and all drive performance powertrain.

It is suggested the powertrain model is expanded to include a detailed acceleration control in order to improve the vehicle response to driver's demand during shifting. A more sophisticated control design method is needed to obtain better tracking.

The overall structure of the MHEV powertrain can be further improved if consideration is given to the transient analysis in the model, including higher-fidelity models of subsystems that were simply approximated (including components such as step-up and step-down converters, a detailed energy management controller). Further development of the ultracapacitor model would also be beneficial, as the study presented herein is only designed to demonstrate proof-of-concept. A further recommendation is to revise and validate the simulation results from the MHEV powertrain with the experimental data when the test data from an actual vehicle is available. The future extension of this research will be the implementation of these control strategies in experimental facilities available at the University of Technology, Sydney.

This work paves the way for future research to develop the EPS for real CV powertrain, which would be practically viable for implementation.

APPENDICES

Appendix A : Internet multimedia

The below URL contains:

- A.1 **Simulink model**
- A.2 **Thesis softcopy**
- A.3 **Presentation**
- A.4 **Thesis figures**
- A.5 **Lab videos and photos**

URL: <https://sites.google.com/view/mohamedawadallah/thesis>



Appendix B : List of publications and achievements

B.1 Journal Papers

- 1- Comparative fuel economy, cost and emissions analysis of a novel mild hybrid and conventional vehicles, Proceedings of the Institution of Mechanical Engineers, Part D: Journal of Automobile Engineering, ISSN 0954-4070, DOI 10.1177/0954407017736116, 2017.
- 2- Dynamic modeling and simulation of a manual transmission based mild hybrid vehicle, Mechanism and Machine Theory, ISSN 0094-114X, DOI 10.1016/j.mechmachtheory.2017.02.011, 2017.

B.2 Journal papers under reviewing

- 3- Mild Hybrid Electric Vehicle (MHEV) Powertrain Development Using Model-Based Design Principles
- 4- Impact of Automotive Emissions and Influence of High and Low Congestion Traffic Patterns on a P3 HEV

B.3 Conference proceedings

- 1- Hardware-In-The-Loop Simulation For The Design And Testing Of Motor In Advanced Powertrain Applications, IEEE International Symposium on Industrial Electronics (ISIE), IEEE, Cairns, Australia.
- 2- Impact of Low and High Congestion Traffic Patterns on a Mild-HEV Performance, in SAE 2017 International Powertrains, Fuels & Lubricants Meeting, Beijing, China, DOI 10.4271/2017-01-2458, 2017.
- 3- A Comparative Fuel Analysis of a novel HEV with a conventional vehicle, in Vehicular Technology Conference (VTC Spring), 2017 IEEE 85th, Sydney, Australia, ISBN 978-1-5090-5932-4, 2017.

- 4- A Low-Cost and Novel Approach in Gearshift Control for a Mild-Hybrid Powertrain, in IEEE Transportation Electrification Conference and Expo (ITEC), Chicago, Illinois, USA, ISBN 978-1-5090-3953-1, DOI 10.1109/ITEC.2017.7993364, 2017.
- 5- A System Analysis and Modeling of an HEV based on Ultracapacitor Battery, in IEEE Transportation Electrification Conference and Expo (ITEC), 2017 IEEE, Chicago, Illinois, USA, ISBN 978-1-5090-3953-1, DOI 10.1109/ITEC.2017.7993370,2017.
- 6- An innovative control strategy for a hybrid energy storage system (HESS), in 2017 IEEE International Conference on Mechatronics (ICM), Gippsland, Victoria, Australia, ISBN 978-1-5090-4539-6, DOI 10.1109/ICMECH.2017.7921146, 2017.
- 7- Selection and Characterisation of PMSM motor for mild HEV Applications, in 29th Electric Vehicle Symposium 2016 (EVS29), Montréal, Québec, Canada, ISBN 9781510832701, 2016.
- 8- Eliminating the torque hole: Using a mild hybrid EV architecture to deliver better driveability, in 2016 IEEE Transportation Electrification Conference and Expo, Asia-Pacific (ITEC Asia-Pacific), Busan, South Korea, ISBN 978-1-5090-1272-5, DOI 10.1109/ITEC-AP.2016.7512943, 2016.
- 9- Comparative System Dynamic Modeling of a Conventional and Hybrid Electric Powertrain, in Power Engineering - International conference on Power Transmissions (ICPT 2016), Chongqing, China, ISBN 978-1-138-03267-5, DOI 10.1201/9781315386829-36, 2016.
- 10- Rapid Prototyping and Validation of Mars 0913 Brushless Motor to Develop Mild HEV, in The 7th TM Symposium China (TMC2015), Shanghai, China, 2015.
- 11- An Electric Scooter with Super-Capacitor Drive and Regenerative Braking, in SAE 2014 World Congress & Exhibition, Detroit, Michigan, USA, DOI 10.4271/2014-01-1878, 2014.

B.4 Special sessions

- Innovative Vehicle Technologies, in 2017 IEEE International Conference on Mechatronics (ICM), Gippsland, Victoria, Australia, 2017.

B.5 Awards

- Presentation Competition, IEEE Australia New Zealand Student and Young Professionals Congress (ANZSCON 2017), Sydney, NSW, Australia, 2017.
- IEEE-IES Student Paper competition, "IEEE-ISIE 2018 Australia" from "IEEE IES-SYPA", Carins, Queensland, Australia, 2018.

Appendix C : Vehicle parameters

Vehicle global specifications

Component	Parameter	SI Units
Vehicle	Mass	1100 kg
	Frontal area	3 m ²
	Drag coefficient	0.4
	Distance from CG to front axle	1.4 m
	Distance from CG to rear axle	1.6 m
	CG height	0.5 m
	Air density	1.2 kg/m ³
	Gravitational acceleration	9.81 m/s ²
	Tire rolling radius	0.312 m
	Rolling resistance coefficient	0.015
	Mass as hybrid	1200 kg
Engine	Type	Spark-Ignition
	Maximum power	70 kW
	Speed at maximum power	5000 rpm
	Maximum speed	7000 rpm
	Idling speed	800 rpm
	Cylinders	4
	Swept volume	1.6 L / 1598 cc
Gear ratio	Type	Manual, 5 forward 1 reverse, fully synchronised
	First	3.581
	Second	2.022
	Third	1.4
	Fourth	1.03
	Fifth	0.94
	Final drive ratio	4.06
Clutch	Type	single dry-plate clutch
	Friction coefficient	0.3
Motor (MHEV only)	Model	MARS ME0913 Brushless DC 24 Pole
	Type	BLDC
	Voltage	96 V
	Maximum power output	10 kW
	Torque	30 Nm
	Maximum torque	54 Nm
Battery	Type	NiMH
	Capacity	1.2 kWh / 12.5 Ah
	Discharge/Charge rate	15C / 10C

Appendix D : HIL test rig

D.1 EPS

Item	Model number with description
Supervisor controller	MicroAutoBox II 14014/1501
Motor controller with an inverter	KHB1260124
BLDC motor	Mars 0913
DC converter	HWZ Series 96 to 13.5 volt
DC supply driver Driver	ABB DCS550

D.2 IM and ABB

Item	Model number with description
Induction Motor (IM)	McCOLL 180M 3-phase
IM Driver	ACS355-03E-44A0-4
Software interface	ABB DriveWindow light

D.3 Sensors

Item	Model number with description
Encoder	Kubler-05.2400.1122.1024
Torque sensor	ATi 2000 (2025iR Digital Receiver)
RX of Bluetooth torque sensor	LM058 Bluetooth to RS232 Serial Adapter
TX Bluetooth Schematic	

OFFSET ADJUSTMENT RANGE
 $c2 = V_{ref} * ((1-B) * R_{ref} + (B-1) * R_i - R_{hd}) / (R_{ref} + 2B * (1-B) * R_i - 2R_{hd})$
 B: 0-B:1 Potentiometer wiper position
 V_{ref}: excitation voltage
 R_i: gauge resistance
 R_{ref}: gauge resistance

Gain = 2 * (R13/R14)

Desired gain	R14	R13/C18
100	4k	200k/0.1uF
1000	2k	1M/0.1uF
5000	2k	2M/0.05uF
10,000	2k	5M/0.05uF
	2k	10M/0.01uF

*ENA326 datasheet, pg 9

ARF7044AF Serial Number
0018 B302 1C92

D.4 Eddy brake (AS706)

Data		
Maximum Torque Lb. Ft.	1800	420
	1200	410
	900	388
Dissipation Maximum Continuous Horsepower	1800	35
	1200	25
	900	17.5
Inertia - Lb. Ft.	16.0	
Maximum Torque Transmitted Through Shaft	1258 lbs. ft.	
Volts DC	45	
Amps	14.5	

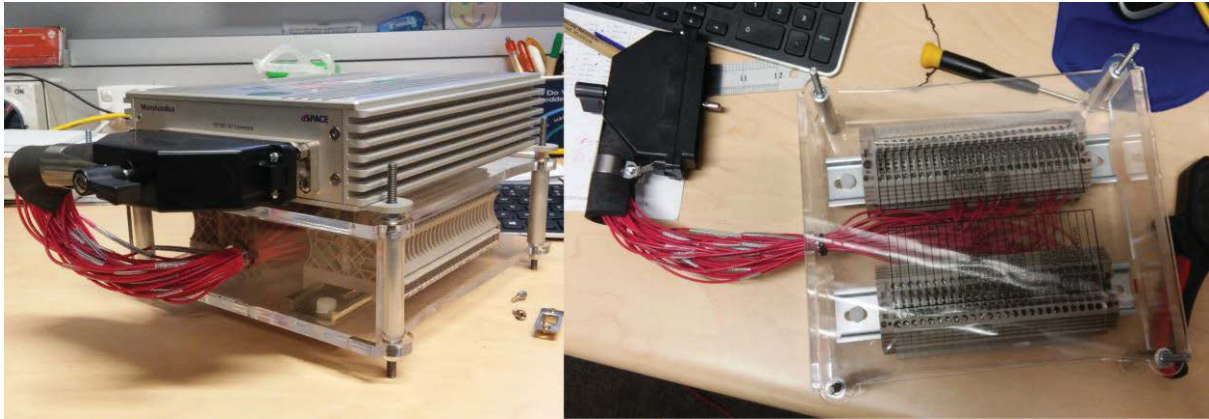
D.5 Couplers

Item	Model number with description
Coupler between torque sensor and Housing Bearing	FLANG Coupling HRC TYPE H SZ 110H 1610 HRC Spider: HRC COUPLING SIZE 110 (100)
Pair Housing Bearing	SN510
Coupler between IM and torque sensor	FLANG Coupling HRC 150H 2012
Belt between IM and BLDC	HTD 1280 8m
Belt between eddy brake and bearing	GT3 1200 8MGT

D.6 Break-out box

Item	Model number with description
DIN Rail Mount Terminal Block	102000 WDU2.5 - DIN Rail Mount Terminal Block, 2 Ways, 30 AWG, 12 AWG, 4 mm ² , Screw, 24 A
END CLAMP	1061200000 - MOUNTING BRACKET
End Cover	WAP2.5/10
Wire 20 AWG	3053 RD005 - Wire, Stranded, Hook Up, PVC, Red, 20 AWG, 0.51 mm ² , 100 ft, 30.5 m
DIN Mounting Rail	0514500000 - DIN MOUNTING RAIL, 35MM X 7.5MM

Pin on right-hand-side	MicroAutoBox pins	Pin on left-hand-side	MicroAutoBox pins
01	F3-GND	01	G5-GND
02	E2-Vsens out	02	c2-VBAT in
03	E1-Vdrive in	03	M5-DI-Pullup-PWM in
04	A1-DAC7 out	04	M2-DI-CTM in
05	A2-DAC8 out	05	M4-DI-CTM in
06	A3-DO out	06	P1-DI-Pullup in
07	A4-DO out	07	P2-DI-Pullup in
08	A5-DO out	08	R5-DI in
09	A6-DO out	09	R6- DI in
10	V5-CAN1-LOW i/o	10	X5-CAN2-LOW i/o
11	V6-CAN1-HIGH i/o	11	X6-CAN2-HIGH i/o
12	F2-DO out	12	Y3-DI in
13	G1- DO-PWM out	13	Y4-DI in
14	D3-DO-PWM out	14	a1-ADC-Type1Con1Ch2 in
15	C4-DO-PWM out	15	c1-ADC-Type1Con1Ch1 in
16	C3-DO-PWM out	16	U5-TXD-RS232 out
17	B1-DAC5 out	17	U6-RXD-RS232 in
18		18	
19		19	
20		20	
21		21	
22		22	
23		23	
24		24	
25	G3-GND	25	G5-GND



Break-out box of MicroAutoBox.

Appendix E : Internal combustion engine (ICE) Data

```
clear;  
clc;  
fc_map_spd =  
[52.3598775598299,104.719755119660,157.079632679490,209.439510239320,261.7993  
87799149,314.159265358979,366.519142918809,418.879020478639,471.238898038469  
,523.598775598299,575.958653158129,628.318530717959];
```

```
fc_map_trq =  
[15.6000000000000,31.2000000000000,46.8000000000000,62.4000000000000,78,93.60  
0000000000,109.200000000000,124.800000000000,140.400000000000,156,171.60000  
000000];
```

```
fc_max_trq =  
[112.320000000000,134.160000000000,146.640000000000,158.340000000000,165.3600  
000000,162.240000000000,159.120000000000,159.900000000000,165.360000000000  
,164.580000000000,160.680000000000,151.320000000000];
```

```
fc_fuel_map =  
[0.138858395288669,0.200936266123603,0.252395553789404,0.300587585095471,0.34  
7145988221672,0.426376954945207,0.480286684880808,0.588106144752009,0.588106  
144752009,0.653451271946677,0.718796399141345;  
0.277716790577338,0.365932712290139,0.458232704452607,0.558700837514409,0.64  
5283131047344,0.779240641796412,0.897678684836748,1.03245300967575,1.1762122  
8950402,1.30690254389335,1.43759279828269;  
0.416575185866007,0.553799952974809,0.705727373702411,0.833150371732013,0.95  
5672485222015,1.07329371417242,1.21272387932404,1.34284236385042,1.543778629  
97402,1.96035381584003,2.15638919742403;  
0.539097299356008,0.718796399141345,0.911564524365614,1.09126362415095,1.249  
72555759802,1.41145474740482,1.55521402723309,1.77738745969496,2.02896619939  
443,2.38509714260537,2.87518559656538;  
0.633030919698343,0.865822935329347,1.09044681006102,1.29056626209469,1.5111  
0606637669,1.67855295481303,1.94401753404136,2.22173432461870,2.499451115196  
04,2.89969001926338,3.59398199570672;  
0.710628258242011,0.994879561538816,1.27177953802622,1.51927420727602,1.7888  
2285695403,2.08777681386963,2.36712723262684,2.66608118954244,2.999341338235  
25,3.52863686851206,4.31277839484807;  
0.743300821839345,1.08064504098182,1.37224767108802,1.78392197241443,2.20131  
397237037,2.54895004904600,2.88172010928485,3.15616964350245,3.5506908489402  
6,4.17391999955940,5.03157479398941;  
0.947504344322682,1.29383351845442,1.72903206557091,2.20866529917977,2.56479  
624239071,2.99934133823525,3.33913599964752,3.68546517377926,4.2931748566896  
7,4.83553941240541,5.75037119313076;  
1.10269902141002,1.60258924444923,2.15246848979235,2.58766703690884,2.995665  
67483055,3.41836696637105,3.88517621876796,4.41079608564007,5.01507514937276  
,5.62376500919109,6.46916759227210;  
1.55194677087336,2.09104407022937,2.57296438329004,3.02221213275338,3.471459  
88221672,3.87169878628406,4.49982882144280,5.06424735758675,5.77814287218849  
,6.45283131047344,7.18796399141345];
```

```

1.88684054774603,2.55172721695177,3.15371920123265,3.64789172564232,4.088154
52011640,4.42059785471927,5.22025884876402,5.89413047295903,6.55003218717550
,7.23288876635978,7.90676039055479;
2.05837150663203,2.88172010928485,3.52863686851206,4.07753593694726,4.557822
62182807,5.11652345934248,5.69482783501529,6.42996051595530,7.14548965873691
,7.84141526336012,8.62555678969614];

```

```

fc_fuel_lhv = 42600;
fc_spd_scale = 1;
fc_trq_scale = 0.73624;
fc_eff_scale = 1;
%-----

```

```

figure;
ylabel('Torque (Nm)')
xlabel('Speed (rpm)')

```

```

% compute efficiency map
trq=[];
for x=1:length(fc_map_trq)
    if fc_map_trq(x)>0
        trq=[trq fc_map_trq(x)];
    end;
end;
spd=[];
for x=1:length(fc_map_spd)
    if fc_map_spd(x)>0
        spd=[spd fc_map_spd(x)];
    end;
end;
diff_trq=length(fc_map_trq)-length(trq);
diff_spd=length(fc_map_spd)-length(spd);
[T,w]=meshgrid(trq,spd);
fc_map_kW=T.*w/1000;
fc_eff_map=fc_map_kW*1000./(fc_fuel_map(diff_spd+1:length(fc_map_spd),...
    diff_trq+1:length(fc_map_trq))*fc_fuel_lhv);

```

```

% plot efficiency map and torque envelope
hold on
plot(fc_map_spd*30/pi*fc_spd_scale,fc_max_trq*fc_trq_scale,'k-')
plot(fc_map_spd*30/pi*fc_spd_scale,fc_max_trq*fc_trq_scale,'kx')
c=contour(spd*30/pi*fc_spd_scale,trq*fc_trq_scale,(fc_eff_map*fc_eff_scale));
clabel(c);

```

```


grid;

```


Appendix F : Dynamics Calculations

drive Train - motor									
I	θ_e	θ_f	θ_{c1}	θ_{c2}	θ_{g1}	θ_{d1}	θ_w		
	I_e							θ_e	
		I_f							θ_f
			I_{c1}						θ_{c1}
				I_{c2}					θ_{c2}
					$I_{g1} + I_{g2}$				θ_{g1}
						$I_{d1} + I_{d2}$			θ_{d1}
						I_w		θ_w	
K	k_e	k_f	k_{c1}	k_{c2}	k_{g1}	k_{d1}	k_w		
	$-k_e$	$-k_e$						k_e	
	$-k_e$	$k_e + k_f$	$-k_f$						k_e
		$-k_f$	k_f						k_{c1}
				k_{c1}	$-k_{c1}$				k_{c2}
				$-k_{c1}$	$k_{c1} + I_{c1}^2 k_{c2}$	$-I_{c1} k_{c2}$			k_{g1}
					$-I_{c1} k_{c2}$	$k_{c2} + I_{c2}^2 k_{d1}$	$-I_{c2} k_{d1}$		k_{d1}
					$-I_{c2} k_{d1}$	k_{d1}		k_w	
C	b_e	b_f	b_{c1}	b_{c2}	b_{g1}	b_{d1}	b_w		
								b_e	
		c_f	$-c_f$						b_f
		$-c_f$	$c_f + c_{c1}$	$-c_{c1}$					b_{c1}
			$-c_{c1}$	$c_{c1} + c_{c2}$	$-c_{c2}$				b_{c2}
				$-c_{c2}$	$k_{c1} + I_{c1}^2 c_{c2}$	$-I_{c1} c_{c2}$			b_{g1}
					$-I_{c1} c_{c2}$	$c_{c2} + I_{c2}^2 c_{d1}$	$-I_{c2} c_{d1}$		b_{d1}
					$-I_{c2} c_{d1}$	c_{d1}		b_w	

drive Train + Motor									
I	θ_e	θ_f	θ_{c1}	θ_{c2}	θ_{g1}	θ_{d1}	θ_w	θ_m	
	I_e								θ_e
		I_f							θ_f
			I_{c1}						θ_{c1}
				I_{c2}					θ_{c2}
					$I_{g1} + I_{g2}$				θ_{g1}
						$I_{d1} + I_{d2}$			θ_{d1}
						I_w		θ_w	
							I_m	θ_m	
K	k_e	k_f	k_{c1}	k_{c2}	k_{g1}	k_{d1}	k_w	k_m	
	$-k_e$	$-k_e$							k_e
	$-k_e$	$k_e + k_f$	$-k_f$						k_e
		$-k_f$	k_f						k_{c1}
				k_{c1}	$-k_{c1}$				k_{c2}
				$-k_{c1}$	$k_{c1} + I_{c1}^2 k_{c2}$	$-I_{c1} k_{c2}$			k_{g1}
					$-I_{c1} k_{c2}$	$k_{c2} + I_{c2}^2 k_{d1}$	$-I_{c2} k_{d1}$		k_{d1}
					$-I_{c2} k_{d1}$	k_{d1}		k_w	
							k_m	k_m	
C	b_e	b_f	b_{c1}	b_{c2}	b_{g1}	b_{d1}	b_w	b_m	
									b_e
		c_f	$-c_f$						b_f
		$-c_f$	$c_f + c_{c1}$	$-c_{c1}$					b_{c1}
			$-c_{c1}$	$c_{c1} + c_{c2}$	$-c_{c2}$				b_{c2}
				$-c_{c2}$	$k_{c1} + I_{c1}^2 c_{c2}$	$-I_{c1} c_{c2}$			b_{g1}
					$-I_{c1} c_{c2}$	$c_{c2} + I_{c2}^2 c_{d1}$	$-I_{c2} c_{d1}$		b_{d1}
					$-I_{c2} c_{d1}$	c_{d1}		b_w	
							c_m	b_m	



Eliminating the Torque Hole: Using a Mild Hybrid EV Architecture



Mohamed Awadallah¹, Peter Tawadros², Paul Walker³, Nong Zhang⁴
 Mohamed.M.Awadallah@student.uts.edu.au¹, Peter.Tawadros@uts.edu.au², Paul.Walker@uts.edu.au³, Nong.Zhang@uts.edu.au⁴
 School of Electrical, Mechanical and Mechatronics Systems, University of Technology Sydney - UTS

Introduction

Hybrid vehicle engineering has mainly focused on fuel economy benefits and emissions reductions. Although the transient power delivery benefits of hybrid powertrains are well-understood, these are not always a primary focus for research and development efforts. The approach to this problem is to deliver a low-cost, low-tech mild-hybrid powertrain with unique power delivery features designed to appeal to aspirational consumers.

The powertrain is a simple post-transmission parallel hybrid configuration. It works by utilizing a low-powered four-cylinder engine coupled to a four-speed manual transmission through a robotically-actuated clutch. A low-voltage BLDC motor is directly connected to the transmission output shaft, before the final drive.


The aim is to design a mild hybrid powertrain that does not exceed 5% of the expense of the base vehicle as manufacture cost for hybridization.

Experimental Design

Simulink and Matlab were used to model a driveline that has a four-speed manual transmission.


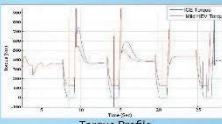
The modeling was established based on a typical ICE powertrain with manual transmission, equipped with an electric motor at the prop shaft.

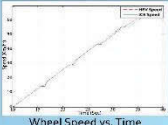
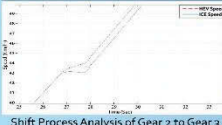
Based on the NYC cycle analysis, the Motenergy ME0933 (12 kW/30 kW pk.) motor was selected as a suitable motor for initial testing.



Results

The diagram below shows the schematic of the drivetrain designed for torque-hole elimination. The electric motor is mounted on the output shaft of the transmission as it is required to provide continuous output torque to the wheels. The graphs below compare both the conventional and mild hybrid powertrains. The results show that the torque hole is reduced in the mild hybrid design.

Conclusion


By reducing torque holes during gear shifts, a 12 kW mild hybrid powertrain will improve vehicle drivability and comfort. Since the vehicle reaches its cruising speed quicker, it is possible to yield a small but measurable improvement in fuel economy.

The mild hybrid drivetrain can be used as successfully with both automated and traditional manual gearboxes. The limited motor power and duty cycle limits the size and cost of other system components such as batteries and converters. Due to the intermittent operation, it is also possible to safely operate the components beyond their rated continuous output to yield greater benefit.


Although the mild hybrid powertrain is not designed for full-featured hybrid vehicles, it could be implemented in price-sensitive markets dominated by vehicles equipped with manual transmissions. The utilization of this powertrain in a low-cost hybrid vehicle could be successful in such a market.

References

- [1] Barasz, R. and S. Cikanek. Torque fill-in for an automated shift manual transmission in a parallel hybrid electric vehicle. In American Control Conference, 2002. Proceedings of the 2002. IEEE.
- [2] Glielmo, L., et al., Gearshift control for automated manual transmissions. *Mechatronics, IEEE/ASME Transactions on*, 2006, 11(1): p. 17-26.
- [3] Zeraouli, M., M.E.H. Benbouzid, and D. Diallo, Electric motor drive selection issues for HEV propulsion systems: A comparative study. *Vehicular Technology, IEEE Transactions on*, 2006, 55(6): p. 1756-1764.



Selection & Characterisation of PMSM motor for mild HEV Applications



Mohamed Awadallah¹, Peter Tawadros², Paul Walker³, Nong Zhang⁴
 Mohamed.M.Awadallah@student.uts.edu.au¹, Peter.Tawadros@uts.edu.au², Paul.Walker@uts.edu.au³, Nong.Zhang@uts.edu.au⁴

Introduction

Mild hybridization is a compromise that minimizes conceptual changes to vehicle systems while enhancing fuel efficiency. By definition, a mild hybrid system is used to assist the internal combustion engine (ICE). This paper discusses a mild-hybrid system in which the electric motor is inserted between the transmission output and the differential. Selecting the most appropriate electric propulsion system (EPS) for hybrid vehicles depends on many factors, including the driver's expectation, vehicle and project constraints, energy source and more. There is a focus on simplification of architecture to provide rapid prototyping and validation functions. This is part of a broader research project aimed at delivering a low-cost hybrid electric vehicle (HEV) suitable for deployment in developing regions.

Experimental Design

For the Traction Motor, both a Cost and Selected Motor analysis were conducted. Motor and Plant modelling were also undertaken within the mathematical model. Considerations to vehicle weight were studied, with an acceptable net weight of 88.5kg.

Motor dynamometer test cycles validated motor characteristics. The PMSM was subjected to iterative cycles. Low-speed steady-state controllability of the dynamometer presented issues. Speed and current were used for understanding motor losses to measure power output over a range of input voltages and voltage profiles.

The model was programmed into the MicroAutoBox II boot, with an automatic code generation function of the real-time interface. The real-time simulation ran in dSPACE ControlDesk to configure simulation runs. The ControlDesk controlled parameters like Throttle, Brake, Reverse motor direction and KHB power switch which were applied to the motor driver. The ControlDesk dashboard controlled power, throttle, brake, and direction. Indicators displayed controller and motor temperatures, motor speed, direction, motor current, voltage, CAN-Bus activity, power status, and a speed histogram.

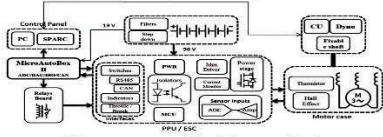


Figure 1: Functional Block diagram of EPS.

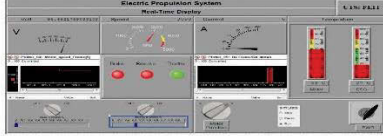


Figure 2: EPS Control Panel

Specification	Result
Peak Power	9.8 kW
Peak Torque	54 Nm
Continuous Power	8 kW @ 2800 rpm
Continuous Torque	28 Nm @ 2800 rpm
Continuous Power (2 minutes)	4 kW @ 4000 rpm
Continuous Torque (2 minutes)	10 Nm @ 4000 rpm
Peak Efficiency	95.4%

Table 1: EPS Validation results

Results

The results show a maximum power of 9.8 kW obtained in the region of 2600-3000 rpm. Motor efficiency was calculated numerically as the output mechanical power of the motor divided by the AC power supplied to the motor by the controller. AC power was determined by multiplying the DC power supplied to the inverter by a fixed efficiency value of 98%. The average efficiency was 82%. This means that the motor can nevertheless meet the design target. The losses were not calculated individually, but can be classified as electrical, magnetic, mechanical, and stray load losses.

Conclusion

An experimental validation of the rated characteristics of a PMSM electric machine was conducted. The experimental validation used HIL techniques implemented on a dSpace MicroAutoBox II controller, which controlled a motor controller and consequently the PM motor. The rated torque and power characteristics could not be achieved in the current testing, although it was found that the motor could still achieve design parameters set for use in a Mild HEV. The motor exceeded the manufacturer-rated peak efficiency of 92%, achieving a peak efficiency of 95.4%. A HIL simulation allowed for the integration of the motor in a comprehensive virtual system. The facility comprised of a real PM motor coupled to the accurate real-time driver and virtual vehicle model simulated through the dynamometer. It was the basis for a broad range of HIL-testing functions.


HIL with Motor-in-the-loop allows the same control setup to be used after validation for control of the motor when it is deployed in the prototype vehicle. Developing an HIL control system at this stage dramatically reduces the prototyping cycle time as no further design work is required for building a control environment within the prototype vehicle.

References


- [1] M. Ehsani, Y. Gao, and A. Emadi, "Electric Propulsion Systems," In *Modern electric, hybrid electric, and fuel cell vehicles: fundamentals, theory, and design*, 2 ed: CRC press, 2009.
- [2] M. Zeraouli, M. E. H. Benbouzid, and D. Diallo, "Electric motor drive selection issues for HEV propulsion systems: A comparative study," *Vehicular Technology, IEEE Transactions on*, vol. 55, 2006, pp. 1756-1764.
- [3] B. C. Chan, "The state of the art of electric, hybrid, and fuel cell vehicles," *Proceedings of the IEEE*, vol. 95, 2007, pp. 704-718.
- [4] H. Fathy, Z. Filipi, J. Hagena, and J. Stein, "Review of hardware-in-the-loop simulation and its prospects in the automotive area," *Ann Arbor*, vol. 2001, 2006, pp. 48109-2125.

Biography



 Mohamed Awadallah received BSc Eng. degree in communications and electronics engineering from Modern Academy for engineering, Cairo, Egypt in 2006 and the Diploma in Embedded Systems from Information Technology Institute (ITI), Cairo, Egypt, in 2007. He is embedded systems engineer in research Centre Green Energy and Vehicle Innovations (GEVI), Australia. He is currently pursuing the PhD degree at University of Technology Sydney (UTS), Australia and a member of Engineers Australia, SAE and IEEE. Awadallah has a mixed background, covering a variety of roles in both academia and industry. Research topics include areas of hybrid and control of automotive systems. Specialities: Matlab/Simulink modeling, dSPACE, Hardware-in-the-loop, hybrid and electric vehicles, powertrains.



 Dr. Paul Walker (Co-supervisor) is a Senior Lecturer at UTS, focusing research on innovative drivetrain and powertrain technologies. His current research includes dynamics and control of vehicle powertrains and development of novel hybrid and electric vehicle powertrain architectures, including design, integration and transient dynamic analysis. Research topics include vibration analysis, powertrain dynamics and control, powertrain hybridization and electrification, vehicle integration, hybrid energy storage systems, electrification and hybridization of two-wheelers and ultra-compact vehicles, toroidal continuously variable transmissions, traction drives, and novel hybrid technologies.



<https://orcid.org/0000-0002-2317-4527> Prof. Nong Zhang (Supervisor) received the B.E. degree from the Northeastern University, Shenyang, China, in 1982, the M.E. degree from Shanghai Jiao Tong University, Shanghai, China, in 1984, and the PhD degree from the University of Tokyo, Tokyo, Japan, in 1989. He has been with several prestigious universities in China, Japan, the United States, and Australia, respectively. In 1995, he joined the UTS, NSW, Australia, where he has been a Professor of mechanical engineering with the School of Mechanical and Mechatronic Systems since 2009. For more than 30 years, he has been involved in research in areas of dynamics and control of automotive systems including powertrains with various types of transmissions, hybrid propulsion systems, vehicle dynamics, passive and active suspensions, and mechanical vibration including experimental modal analysis, rotor dynamics, cold rolling mill chatter, and machine condition monitoring.

References

- [1] J. Hansen *et al.*, "A closer look at United States and global surface temperature change," *Journal of Geophysical Research: Atmospheres*, vol. 106, no. D20, pp. 23947-23963, 2001.
- [2] J. Hansen, R. Ruedy, M. Sato, and K. Lo, "Global surface temperature change," *Reviews of Geophysics*, vol. 48, no. 4, 2010.
- [3] M. Ehsani, Y. Gao, and A. Emadi, "Environmental Impact and History of Modern Transportation," in *Modern electric, hybrid electric, and fuel cell vehicles: fundamentals, theory, and design* Second ed.: CRC press, 2009.
- [4] C. Chan, "The state of the art of electric and hybrid vehicles," *Proceedings of the IEEE*, vol. 90, no. 2, pp. 247-275, 2002.
- [5] H. S. Das, C. W. Tan, and A. Yatim, "Fuel cell hybrid electric vehicles: A review on power conditioning units and topologies," *Renewable and Sustainable Energy Reviews*, vol. 76, pp. 268-291, 2017.
- [6] S.-i. Jeon, S.-t. Jo, Y.-i. Park, and J.-m. Lee, "Multi-Mode Driving Control of a Parallel Hybrid Electric Vehicle Using Driving Pattern Recognition," *Journal of Dynamic Systems, Measurement, and Control*, vol. 124, no. 1, pp. 141-149, 2000.
- [7] M. A. Miller, A. G. Holmes, B. M. Conlon, and P. J. Savagian, "The GM "Voltec" 4ET50 Multi-Mode Electric Transaxle," *SAE Int. J. Engines*, vol. 4, no. 1, pp. 1102-1114, 2011.
- [8] M. Carello, P. Bonansea, and M. D'Auria, "Driveline Optimization for a Hybrid Electric City Vehicle to Minimize Fuel Consumption," 2014. Available: <http://dx.doi.org/10.4271/2014-01-1090>
- [9] R. R. Semel, "Fuel Economy Improvements through Improved Automatic Transmission Warmup - Stand Alone Oil to Air (OTA) Transmission Cooling Strategy with Thermostatic Cold Flow Bypass Valve," 2001. Available: <http://dx.doi.org/10.4271/2001-01-1760>
- [10] S. F. Tie and C. W. Tan, "A review of energy sources and energy management system in electric vehicles," *Renewable and Sustainable Energy Reviews*, vol. 20, pp. 82-102, 2013.
- [11] OrganisationforEconomicCo-operationandDevelopment, *The Cost of Air Pollution*. Paris: OECD Publishing, 2014.
- [12] W. H. Organization, "WHO's Ambient Air Pollution database: Update 2014," *Ginebra, Suiza: World Health Organization (WHO)*, 2014.
- [13] B. Bilgin *et al.*, "Making the case for electrified transportation," *IEEE Transactions on Transportation Electrification*, vol. 1, no. 1, pp. 4-17, 2015.
- [14] S. T. Anderson, I. W. Parry, J. M. Sallee, and C. Fischer, "Automobile fuel economy standards: Impacts, efficiency, and alternatives," *Review of Environmental Economics and Policy*, p. req021, 2011.
- [15] W. Enang and C. Bannister, "Modelling and control of hybrid electric vehicles (A comprehensive review)," *Renewable and Sustainable Energy Reviews*, vol. 74, pp. 1210-1239, 2017.
- [16] K. Govindswamy, T. Wellmann, and G. Eisele, "Aspects of NVH Integration in Hybrid Vehicles," *SAE Int. J. Passeng. Cars - Mech. Syst.*, vol. 2, no. 1, pp. 1396-1405, 2009.
- [17] E. P. Kasseris and J. B. Heywood, "Comparative analysis of automotive powertrain choices for the next 25 years," in *SAE World Congress & Exhibition, USA, 2007*: SAE Technical Paper.
- [18] A. Emadi, K. Rajashekara, S. S. Williamson, and S. M. Lukic, "Topological overview of hybrid electric and fuel cell vehicular power system architectures and configurations," *IEEE Transactions on Vehicular Technology*, vol. 54, no. 3, pp. 763-770, 2005.
- [19] A. Emadi, Y. J. Lee, and K. Rajashekara, "Power electronics and motor drives in electric, hybrid electric, and plug-in hybrid electric vehicles," *IEEE Transactions on industrial electronics*, vol. 55, no. 6, pp. 2237-2245, 2008.
- [20] M. Nikowitz, *Advanced Hybrid and Electric Vehicles: System Optimization and Vehicle Integration*. Springer, 2016.
- [21] M. Ehsani, Y. Gao, and A. Emadi, *Modern electric, hybrid electric, and fuel cell vehicles: fundamentals, theory, and design*, Second ed. CRC press, 2009.
- [22] E. Karden, S. Ploumen, B. Fricke, T. Miller, and K. Snyder, "Energy storage devices for future hybrid electric vehicles," *Journal of Power Sources*, vol. 168, no. 1, pp. 2-11, 2007.
- [23] C. Mi and M. A. Masrur, "Advanced HEV Architectures and Dynamics of HEV Powertrain," in *Hybrid electric vehicles: principles and applications with practical perspectives* 2 ed.: John Wiley & Sons, 2017.
- [24] R. Bao, V. Avila, and J. Baxter, "Effect of 48 V Mild Hybrid System Layout on Powertrain System Efficiency and Its Potential of Fuel Economy Improvement," in *SAE World Congress Experience, USA, 2017*, p. 11: SAE Technical Paper.
- [25] N. Ding, K. Prasad, and T. Lie, "The electric vehicle: a review," *International Journal of Electric and Hybrid Vehicles*, vol. 9, no. 1, pp. 49-66, 2017.
- [26] T. Hutchinson, S. Burgess, and G. Herrmann, "Current hybrid-electric powertrain architectures: Applying empirical design data to life cycle assessment and whole-life cost analysis," *Applied Energy*, vol. 119, pp. 314-329, 2014.
- [27] K.-L. Kuo, "Simulation and Analysis of the Shift Process for an Automatic Transmission," *World Academy of Science, Engineering and Technology*, vol. 52, pp. 341-347, 2011.
- [28] Z. Sun and K. Hebbale, "Challenges and opportunities in automotive transmission control," in *American Control Conference, 2005. Proceedings of the 2005*, 2005, pp. 3284-3289: IEEE.

- [29] P. D. Walker and N. Zhang, "Active damping of transient vibration in dual clutch transmission equipped powertrains: A comparison of conventional and hybrid electric vehicles," *Mechanism and Machine Theory*, vol. 77, pp. 1-12, 2014.
- [30] X. Zhou, P. Walker, N. Zhang, B. Zhu, and J. Ruan, "Numerical and experimental investigation of drag torque in a two-speed dual clutch transmission," *Mechanism and Machine Theory*, vol. 79, pp. 46-63, 2014.
- [31] G. Wagner, "Application of transmission systems for different driveline configurations in passenger cars," SAE Technical Paper2001.
- [32] E. Galvagno, M. Velardocchia, and A. Vigliani, "A model for a flywheel automatic assisted manual transmission," *Mechanism and Machine Theory*, vol. 44, no. 6, pp. 1294-1305, 2009.
- [33] R. C. Baraszu and S. R. Cikanek, "Hybrid electric vehicle with motor torque fill in," in *Ford Motor Company*, ed: Google Patents, 2003.
- [34] P. Tona, P. Gautier, and R. Amari, "Modeling and control of a mild-hybrid city car with a downsized turbo-charged CNG engine," in *Proceedings of Advanced Vehicle Control Symposium AVEC*, 2008.
- [35] E. Galvagno, M. Velardocchia, and A. Vigliani, "Analysis and simulation of a torque assist automated manual transmission," *Mechanical Systems and Signal Processing*, vol. 25, no. 6, pp. 1877-1886, 2011.
- [36] R. C. Baraszu and S. R. Cikanek, "Torque fill-in for an automated shift manual transmission in a parallel hybrid electric vehicle," in *Proceedings of the 2002 American Control Conference (IEEE Cat. No.CH37301)*, 2002, vol. 2, pp. 1431-1436 vol.2: IEEE.
- [37] B. Gao, Q. Liang, Y. Xiang, L. Guo, and H. Chen, "Gear ratio optimization and shift control of 2-speed I-AMT in electric vehicle," *Mechanical Systems and Signal Processing*, vol. 50, pp. 615-631, 2015.
- [38] H. Liu, Y. Lei, Z. Li, J. Zhang, and Y. Li, "Gear-Shift Strategy for a Clutchless Automated Manual Transmission in Battery Electric Vehicles," *SAE International Journal of Commercial Vehicles*, vol. 5, no. 1, pp. 57-62, 2012.
- [39] A. Sornioti *et al.*, "A novel clutchless multiple-speed transmission for electric axles," *International Journal of Powertrains*, vol. 2, no. 2-3, pp. 103-131, 2013.
- [40] Z. Rahman, K. L. Butler, and M. Ehsani, "A comparison study between two parallel hybrid control concepts," *Development*, vol. 1, p. 0978, 2000.
- [41] K. Aoki, S. Kuroda, S. Kajiwara, H. Sato, and Y. Yamamoto, "Development of integrated motor assist hybrid system: development of the 'insight', a personal hybrid coupe," Honda R and D Co., Ltd.(US)2000.
- [42] G. Wu and Z. Dong, "Design, analysis and modeling of a novel hybrid powertrain system based on hybridized automated manual transmission," *Mechanical Systems and Signal Processing*, vol. 93, pp. 688-705, 2017.
- [43] J. Horn, J. Bamberger, P. Michau, and S. Pindl, "Flatness-based clutch control for automated manual transmissions," *Control engineering practice*, vol. 11, no. 12, pp. 1353-1359, 2003.
- [44] W. Wang, Q. Wang, and X. Zeng, "Automated manual transmission shift strategy for parallel hybrid electric vehicle," *Training*, vol. 2014, pp. 02-24, 2009.
- [45] L. Glielmo, L. Iannelli, V. Vacca, and F. Vasca, "Gearshift control for automated manual transmissions," *Mechatronics, IEEE/ASME Transactions on*, vol. 11, no. 1, pp. 17-26, 2006.
- [46] E. Chen, "Manual Transmission with Electric Torque Assist for Torque Gap Compensation," MD Thesis, Mechatronics Engineering Department, University of Technology Sydney, Sydney, 2013.
- [47] D. Jung, S. Cho, S. Park, and K. Min, "Application of a modified thermostatic control strategy to parallel mild HEV for improving fuel economy in urban driving conditions," *International Journal of Automotive Technology*, vol. 17, no. 2, pp. 339-346, 2016.
- [48] S. Abdul Rahman, N. Zhang, and J. Zhu, "A comparative analysis of fuel economy and emissions between a conventional HEV and the UTS PHEV," *IEEE Transactions on Vehicular Technology*, vol. 60, no. 1, pp. 44-54, 2011.
- [49] K. Takao and H. Toshihiko, "Vehicle Development through "Kansei" Engineering," SAE Technical Paper0148-7191, 2003.
- [50] C. Chan and Y. Wong, "Electric vehicles charge forward," *Power and Energy Magazine, IEEE*, vol. 2, no. 6, pp. 24-33, 2004.
- [51] Z. Rahman, M. Ehsani, and K. Butler, "An investigation of electric motor drive characteristics for EV and HEV propulsion systems," *SAE transactions*, vol. 109, no. 6, pp. 2396-2403, 2000.
- [52] M. Zeraoulia, M. E. H. Benbouzid, and D. Diallo, "Electric motor drive selection issues for HEV propulsion systems: A comparative study," *Vehicular Technology, IEEE Transactions on*, vol. 55, no. 6, pp. 1756-1764, 2006.
- [53] M. Ehsani, Y. Gao, and A. Emadi, "Electric Propulsion Systems," in *Modern electric, hybrid electric, and fuel cell vehicles: fundamentals, theory, and design* Second ed.: CRC press, 2009.
- [54] B. C. Chan, "The state of the art of electric, hybrid, and fuel cell vehicles," *Proceedings of the IEEE*, vol. 95, no. 4, pp. 704-718, 2007.
- [55] S. Sharma and V. Kumar, "Optimized Motor Selection for Various Hybrid and Electric Vehicles," SAE Technical Paper2013.
- [56] L. Chang, "Comparison of AC drives for electric vehicles-a report on experts' opinion survey," *Aerospace and Electronic Systems Magazine, IEEE*, vol. 9, no. 8, pp. 7-11, 1994.
- [57] A. Serrarens, M. Dassen, and M. Steinbuch, "Simulation and control of an automotive dry clutch," in *American Control Conference, 2004. Proceedings of the 2004*, 2004, vol. 5, pp. 4078-4083: IEEE.

- [58] M. M. Corporation, *1990 Mazda MX-5 Workshop Manual*. HIROSHIMA, JAPAN, 1989.
- [59] U. Wagner and A. Wagner, "Electrical Shift Gearbox (ESG) - Consistent Development of the Dual Clutch Transmission to a Mild Hybrid System," 2005. Available: <http://dx.doi.org/10.4271/2005-01-4182>
- [60] A. Crowther and N. Zhang, "Torsional finite elements and nonlinear numerical modelling in vehicle powertrain dynamics," *Journal of Sound and Vibration*, vol. 284, no. 3, pp. 825-849, 2005.
- [61] A. R. Crowther, R. Singh, N. Zhang, and C. Chapman, "Impulsive response of an automatic transmission system with multiple clearances: Formulation, simulation and experiment," *Journal of Sound and Vibration*, vol. 306, no. 3, pp. 444-466, 2007.
- [62] S. S. Rao, *Mechanical Vibrations*, 5th ed. Upper Saddle River, N.J. : Prentice Hall, 2011.
- [63] M. De la Cruz, S. Theodossiades, and H. Rahnejat, "An investigation of manual transmission drive rattle," *Proceedings of the Institution of Mechanical Engineers, Part K: Journal of Multi-body Dynamics*, vol. 224, no. 2, pp. 167-181, 2010.
- [64] E. Honey and I.-S. Suh, "A feasibility study of an electric-hydraulic hybrid powertrain for passenger vehicles," *Proceedings of the Institution of Mechanical Engineers, Part D: Journal of Automobile Engineering*, vol. 229, no. 14, pp. 1894-1906, 2015.
- [65] H. A. Borhan, A. Vahidi, A. M. Phillips, M. L. Kuang, and I. V. Kolmanovsky, "Predictive energy management of a power-split hybrid electric vehicle," in *American Control Conference, 2009. ACC'09.*, 2009, pp. 3970-3976: IEEE.
- [66] K. Hartani, Y. Miloud, and A. Miloudi, "Improved direct torque control of permanent magnet synchronous electrical vehicle motor with proportional-integral resistance estimator," *Journal of Electrical Engineering and Technology*, vol. 5, no. 3, pp. 451-461, 2010.
- [67] Z. Zhou, J. Zhang, L. Xu, and Z. Guo, "Modeling and simulation of hydro-mechanical continuously variable transmission system based on Simscape," in *Advanced Mechatronic Systems (ICAMechS), 2015 International Conference on*, 2015, pp. 397-401: IEEE.
- [68] S. Mahapatra, T. Egel, R. Hassan, R. Shenoy, and M. Carone, "Model-based design for hybrid electric vehicle systems," SAE Technical Paper0148-7191, 2008.
- [69] A. V. D. Heijden, A. Serrarens, M. Camlibel, and H. Nijmeijer, "Hybrid optimal control of dry clutch engagement," *International Journal of Control*, vol. 80, no. 11, pp. 1717-1728, 2007.
- [70] M. BĂȚĂUȘ, A. MACIAC, M. OPREAN, and N. VASILIU, "Automotive Clutch Models for Real Time Simulation," *Proceedings of the Romanian Academy, Series A: Mathematics, Physics, Technical Sciences, Information Science*, 2011.
- [71] F. Vasca, L. Iannelli, A. Senatore, and G. Reale, "Torque transmissibility assessment for automotive dry-clutch engagement," *IEEE/ASME transactions on Mechatronics*, vol. 16, no. 3, pp. 564-573, 2011.
- [72] B. Mashadi and M. Badrykoochi, "Driveline oscillation control by using a dry clutch system," *Applied Mathematical Modelling*, vol. 39, no. 21, pp. 6471-6490, 2015.
- [73] E. Rabeih and D. Crolla, "Intelligent control of clutch judder and shunt phenomena in vehicle drivelines," *International journal of vehicle design*, vol. 17, no. 3, pp. 318-332, 1996.
- [74] P. C. Sen, *Principles of electric machines and power electronics*. John Wiley & Sons, 2007.
- [75] K. L. Butler, M. Ehsani, and P. Kamath, "A Matlab-based modeling and simulation package for electric and hybrid electric vehicle design," *IEEE Transactions on vehicular technology*, vol. 48, no. 6, pp. 1770-1778, 1999.
- [76] J. Gong, D.-x. Zhao, Y. Chen, and N. Chen, "Study on shift schedule saving energy of automatic transmission of ground vehicles," *Journal of Zhejiang University Science*, vol. 5, no. 7, pp. 878-883, 2004.
- [77] G. Lucente, M. Montanari, and C. Rossi, "Modelling of an automated manual transmission system," *Mechatronics*, vol. 17, no. 2, pp. 73-91, 2007.
- [78] C.-Y. Tseng and C.-H. Yu, "Advanced shifting control of synchronizer mechanisms for clutchless automatic manual transmission in an electric vehicle," *Mechanism and Machine Theory*, vol. 84, pp. 37-56, 2015.
- [79] J. Torres, R. Gonzalez, A. Gimenez, and J. Lopez, "Energy management strategy for plug-in hybrid electric vehicles. A comparative study," *Applied Energy*, vol. 113, pp. 816-824, 2014.
- [80] J. Ruan, P. Walker, N. Zhang, and G. Xu, "The Safety and Dynamic Performance of Blended Brake System on a Two-Speed DCT Based Battery Electric Vehicle," *SAE International Journal of Passenger Cars-Mechanical Systems*, vol. 9, no. 2016-01-0468, pp. 143-153, 2016.
- [81] J. Fredriksson and B. Egardt, "Nonlinear control applied to gearshifting in automated manual transmissions," in *Decision and Control, 2000. Proceedings of the 39th IEEE Conference on*, 2000, vol. 1, pp. 444-449: IEEE.
- [82] X. Wei, "Modeling and control of a hybrid electric drivetrain for optimum fuel economy, performance and driveability," The Ohio State University, 2004.
- [83] T. W. Megli, M. Haghgoie, and D. S. Colvin, "Shift Characteristics of a 4-Speed Automatic Transmission," 1999. Available: <http://dx.doi.org/10.4271/1999-01-1060>
- [84] M. J. Griffin, "Methods for Measuring and Evaluating," in *Handbook of human vibration*: Academic press, 2012.
- [85] T. D'Anna, K. Govindswamy, F. Wolter, and P. Janssen, "Aspects of shift quality with emphasis on powertrain integration and vehicle sensitivity," SAE Technical Paper0148-7191, 2005.
- [86] J. Ruan and P. Walker, "An Optimal Regenerative Braking Energy Recovery System for Two-Speed Dual Clutch Transmission-Based Electric Vehicles," 2014. Available: <http://dx.doi.org/10.4271/2014-01-1740>

- [87] Z. Wei, J. Xu, and D. Halim, "HEV power management control strategy for urban driving," *Applied Energy*, 2016.
- [88] F. Chiara and M. Canova, "A review of energy consumption, management, and recovery in automotive systems, with considerations of future trends," *Proceedings of the Institution of Mechanical Engineers, Part D: Journal of Automobile Engineering*, vol. 227, no. 6, pp. 914-936, 2013.
- [89] R. Sharma, C. Manzie, M. Bessede, M. Brear, and R. Crawford, "Conventional, hybrid and electric vehicles for Australian driving conditions—Part I: Technical and financial analysis," *Transportation Research Part C: Emerging Technologies*, vol. 25, pp. 238-249, 2012.
- [90] M. Amrhein and P. T. Krein, "Dynamic simulation for analysis of hybrid electric vehicle system and subsystem interactions, including power electronics," *IEEE transactions on vehicular technology*, vol. 54, no. 3, pp. 825-836, 2005.
- [91] T. Markel *et al.*, "ADVISOR: a systems analysis tool for advanced vehicle modeling," *Journal of power sources*, vol. 110, no. 2, pp. 255-266, 2002.
- [92] A. C. Baisden and A. Emadi, "ADVISOR-based model of a battery and an ultra-capacitor energy source for hybrid electric vehicles," *IEEE Transactions on Vehicular Technology*, vol. 53, no. 1, pp. 199-205, 2004.
- [93] S. C. Oh, "Evaluation of motor characteristics for hybrid electric vehicles using the hardware-in-the-loop concept," *IEEE transactions on vehicular technology*, vol. 54, no. 3, pp. 817-824, 2005.
- [94] C. Manzie, H. Watson, S. Halgamuge, and K. Lim, "A comparison of fuel consumption between hybrid and intelligent vehicles during urban driving," *Proceedings of the Institution of Mechanical Engineers, Part D: Journal of Automobile Engineering*, vol. 220, no. 1, pp. 67-76, 2006.
- [95] C. Manzie, H. Watson, and S. Halgamuge, "Fuel economy improvements for urban driving: Hybrid vs. intelligent vehicles," *Transportation Research Part C: Emerging Technologies*, vol. 15, no. 1, pp. 1-16, 2007.
- [96] P. Weissler, "Many factors figure in fuel-economy calculation for electric vehicles," *Automotive Engineering International*, 2009.
- [97] K. Mazloomi and C. Gomes, "Hydrogen as an energy carrier: prospects and challenges," *Renewable and Sustainable Energy Reviews*, vol. 16, no. 5, pp. 3024-3033, 2012.
- [98] T. R. Hawkins, O. M. Gausen, and A. H. Strømman, "Environmental impacts of hybrid and electric vehicles—a review," *The International Journal of Life Cycle Assessment*, vol. 17, no. 8, pp. 997-1014, 2012.
- [99] G. Ao, J. Qiang, H. Zhong, X. Mao, L. Yang, and B. Zhuo, "Fuel economy and NO_x emission potential investigation and trade-off of a hybrid electric vehicle based on dynamic programming," *Proceedings of the Institution of Mechanical Engineers, Part D: Journal of Automobile Engineering*, vol. 222, no. 10, pp. 1851-1864, 2008.
- [100] V. H. Johnson, K. B. Wipke, and D. J. Rausen, "HEV control strategy for real-time optimization of fuel economy and emissions," *SAE transactions*, vol. 109, no. 3, pp. 1677-1690, 2000.
- [101] G. Fontaras, P. Pistikopoulos, and Z. Samaras, "Experimental evaluation of hybrid vehicle fuel economy and pollutant emissions over real-world simulation driving cycles," *Atmospheric environment*, vol. 42, no. 18, pp. 4023-4035, 2008.
- [102] L. Rubino, P. Bonnel, M. Carriero, and A. Krasenbrink, "Portable Emission Measurement System (PEMS) For Heavy Duty Diesel Vehicle PM Measurement: The European PM PEMS Program," *SAE International Journal of Engines*, vol. 2, no. 2, pp. 660-673, 2009.
- [103] S. Abdul Rahman, "Optimal power management for the UTS plug-in hybrid electric vehicle," University of Technology Sydney, Australia, 2011.
- [104] J. Thomas, S. Huff, B. West, and P. Chambon, "Fuel Consumption Sensitivity of Conventional and Hybrid Electric Light-Duty Gasoline Vehicles to Driving Style," *SAE International Journal of Fuels and Lubricants*, vol. 10, no. 2017-01-9379, 2017.
- [105] Y. L. Murphey, R. Milton, and L. Kiliaris, "Driver's style classification using jerk analysis," in *Computational Intelligence in Vehicles and Vehicular Systems, 2009. CIVIS'09. IEEE Workshop on*, 2009, pp. 23-28: IEEE.
- [106] S. Lee, J. Choi, K. Jeong, and H. Kim, "A Study of Fuel Economy Improvement in a Plug-in Hybrid Electric Vehicle using Engine on/off and Battery Charging Power Control Based on Driver Characteristics," *Energies*, vol. 8, no. 9, pp. 10106-10126, 2015.
- [107] A. M. Andwari, A. Pesiridis, S. Rajoo, R. Martinez-Botas, and V. Esfahanian, "A review of Battery Electric Vehicle technology and readiness levels," *Renewable and Sustainable Energy Reviews*, vol. 78, pp. 414-430, 2017.
- [108] R. Sharma, M. Bessede, C. Manzie, M. Brear, and R. Crawford, "An Economic and In-Service Emissions Analysis of Conventional, Hybrid and Electric Vehicles for Australian Driving Conditions," *SAE International Journal of Commercial Vehicles*, vol. 5, no. 1, pp. 291-298, 2012.
- [109] P. Brown, N. Jackson, L. Sykes, J. Wheals, and M. Wiseman, "A Hybrid and Fuel Cell Vehicle Future?," SAE Technical Paper0148-7191, 2002.
- [110] Z. Liu, W. J. Ortmann, B. Nefcy, D. Colvin, and F. Connolly, "Methods of Measuring Regenerative Braking Efficiency in a Test Cycle," *SAE International Journal of Alternative Powertrains*, vol. 6, no. 1, pp. 103-112, 2017.
- [111] J. Ruan, "Design and verification of novel powertrain management for multi-gear battery electric vehicles," PhD, FEIT, University of Technology Sydney, Sydney, Australia, 2016.
- [112] M. Ehsani, Y. Gao, and J. M. Miller, "Hybrid electric vehicles: Architecture and motor drives," *Proceedings of the IEEE*, vol. 95, no. 4, pp. 719-728, 2007.

- [113] A. H. Niasar, H. Moghbelli, and A. Vahedi, "Design methodology of drive train for a series-parallel hybrid electric vehicle (SP-HEV) and its power flow control strategy," in *IEEE International Conference on Electric Machines and Drives, 2005.*, 2005, pp. 1549-1554: IEEE.
- [114] A. Waked and C. Afif, "Emissions of air pollutants from road transport in Lebanon and other countries in the Middle East region," *Atmospheric environment*, vol. 61, pp. 446-452, 2012.
- [115] M. Contestabile, M. Alajaji, and B. Almubarak, "Will current electric vehicle policy lead to cost-effective electrification of passenger car transport?," *Energy Policy*, vol. 110, pp. 20-30, 2017.
- [116] J. D. Bishop, N. P. Martin, and A. M. Boies, "Cost-effectiveness of alternative powertrains for reduced energy use and CO 2 emissions in passenger vehicles," *Applied Energy*, vol. 124, pp. 44-61, 2014.
- [117] S. W. Hadley and T. P. Cleary, "Plug-in Hybrid Electric Vehicle Value Proposition Study-Final Report," 2010.
- [118] G. Wu, A. Inderbitzin, and C. Bening, "Total cost of ownership of electric vehicles compared to conventional vehicles: A probabilistic analysis and projection across market segments," *Energy Policy*, vol. 80, pp. 196-214, 2015.
- [119] K. R. Smith, "Fuel combustion, air pollution exposure, and health: the situation in developing countries," *Annual Review of Energy and the Environment*, vol. 18, no. 1, pp. 529-566, 1993.
- [120] D. Campbell-Lendrum and C. Corvalán, "Climate change and developing-country cities: implications for environmental health and equity," *Journal of Urban Health*, vol. 84, no. 1, pp. 109-117, 2007.
- [121] Y. Li, M. Liu, J. Lau, and B. Zhang, "A novel method to determine the motor efficiency under variable speed operations and partial load conditions," *Applied Energy*, vol. 144, pp. 234-240, 2015.
- [122] F. Di Nicola, A. Sornioti, T. Holdstock, F. Viotto, and S. Bertolotto, "Optimization of a multiple-speed transmission for downsizing the motor of a fully electric vehicle," *SAE International Journal of Alternative Powertrains*, vol. 1, no. 2012-01-0630, pp. 134-143, 2012.
- [123] M. S. Rahmat, F. Ahmad, A. K. M. Yamin, V. R. Aparow, and N. Tamaldin, "Modelling and Torque Tracking Control of Permanent Magnet Synchronous Motor for Hybrid Electric Vehicles," *International Journal of Automotive and Mechanical Engineering*, vol. 7, p. 955, 2013.
- [124] J. W. McKeever, S. Das, L. M. Tolbert, L. D. Marlino, and A. Nedungadi, "Life-Cycle Cost Sensitivity to Battery-Pack Voltage of an HEV," *Life*, vol. 1, p. 1556, 2000.
- [125] P. D. Walker and H. M. Roser, "Energy consumption and cost analysis of hybrid electric powertrain configurations for two wheelers," *Applied Energy*, vol. 146, pp. 279-287, 2015.
- [126] K. Kott and P. Waeltermann, "Embedded Software Tools Enable Hybrid Vehicle Architecture Design and Optimization," presented at the SAE Convergence 2010, 2010. Available: <http://dx.doi.org/10.4271/2010-01-2308>
- [127] A. Ingalalli, H. Satheesh, and M. Kande, "Platform for Hardware In Loop Simulation," in *Power Electronics, Electrical Drives, Automation and Motion (SPEEDAM), 2016 International Symposium on*, 2016, pp. 41-46: IEEE.
- [128] R. Isermann, J. Schaffnit, and S. Sinsel, "Hardware-in-the-loop simulation for the design and testing of engine-control systems," *Control Engineering Practice*, vol. 7, no. 5, pp. 643-653, 1999.
- [129] Q.-Z. Yan, J. M. Williams, and J. Li, "Chassis control system development using simulation: software in the loop, rapid prototyping, and hardware in the loop," in *Automotive Dynamics & Stability Conference and Exhibition, 2002: SAE Technical Paper*.
- [130] T. Chung, K. Yi, J. Kim, and J. Lee, "Closed-loop evaluation of vehicle stability control (VSC) systems using a combined vehicle and human driving model," SAE Technical Paper0148-7191, 2004.
- [131] Z. Xia, F. Gao, K. Togai, and H. Yamaura, "Accelerated and Integrated Real Time Testing Process Based on Two Universal Controllers on Rapid Controller Prototyping," *SAE International Journal of Passenger Cars-Mechanical Systems*, vol. 1, no. 2008-01-0285, pp. 258-267, 2008.
- [132] K. Controls. (2008, 12/1/2015). *KHB12601,24-120V,600A,Opto BLDC Controller/With Regen*. Available: <http://kellycontroller.com/khb1260124-120v600aopto-blcdc-controllerwith-regen-p-830.html>
- [133] J. C. Gamazo-Real, E. Vázquez-Sánchez, and J. Gómez-Gil, "Position and speed control of brushless DC motors using sensorless techniques and application trends," *Sensors*, vol. 10, no. 7, pp. 6901-6947, 2010.
- [134] S. Miller and J. Wendlandt, "Real-Time Simulation of Physical Systems Using Simscape," pp. 1-13, 2010.
- [135] K. Controls. (2008, 04/1/2016). *MARS 0913(ETEK COMPARABLE)PMSM/BLDC MOTOR*. Available: <http://kellycontroller.com/mars-0913etek-comparablepmsmblcdc-motor-p-874.html>
- [136] V. Jaikamal, "Model-based ECU development—An Integrated MiL-SiL-HiL Approach," in *SAE World Congress & Exhibition, 2009: SAE Technical Paper*.
- [137] R. M. Ashby, J. Jeong, S. Y. Rao, G. J. Heydinger, and D. A. Guenther, "A Primer on Building a Hardware in the Loop Simulation and Validation for a 6X4 Tractor Trailer Model," *SAE International Journal of Commercial Vehicles*, vol. 7, no. 2014-01-0118, pp. 8-18, 2014.
- [138] S. J. Rao, M. K. Salaani, G. J. Heydinger, D. A. Guenther, and W. R. Garrott, "Modeling of a 6× 4 Tractor and Trailers for Use in Real Time Hardware in the Loop Simulation for ESC Testing," SAE Technical Paper0148-7191, 2013.

- [139] Y. Li, P. Agashe, Z. Ge, and B. Chen, "Rapid Prototyping Energy Management System for a Single Shaft Parallel Hybrid Electric Vehicle Using Hardware-in-the-Loop Simulation," *SAE International Journal of Alternative Powertrains*, vol. 2, no. 2, pp. 241-251, 2013.
- [140] X. Zhou, P. Walker, N. Zhang, B. Zhu, and J. Ruan, "Study of power losses in a two-speed dual clutch transmission," SAE Technical Paper0148-7191, 2014.
- [141] J. Song and Q. Chen, "A Study of Dynamic Electric Dynamometer Based on Separate-excited DC Generator," *Journal of Asian Electric Vehicles*, vol. 3, no. 1, pp. 673-676, 2005.
- [142] D. Hari, C. Brace, C. Vagg, S. Akehurst, L. Ash, and R. Strong, "Development and Testing of a Low Cost High Performance Hybrid Vehicle Electric Motor," SAE Technical Paper2013.
- [143] C. Cavallaro, A. O. D. Tommaso, R. Miceli, A. Raciti, G. R. Galluzzo, and M. Trapanese, "Efficiency enhancement of permanent-magnet synchronous motor drives by online loss minimization approaches," *Industrial Electronics, IEEE Transactions on*, vol. 52, no. 4, pp. 1153-1160, 2005.
- [144] A. T. De Almeida, F. J. Ferreira, J. F. Busch, and P. Angers, "Comparative analysis of IEEE 112-B and IEC 34-2 efficiency testing standards using stray load losses in low-voltage three-phase, cage induction motors," *Industry Applications, IEEE Transactions on*, vol. 38, no. 2, pp. 608-614, 2002.
- [145] A. Wagener, T. Schulte, P. Waeltermann, and H. Schuette, "Hardware-in-the-Loop Test Systems for Electric Motors in Advanced Powertrain Applications," in *SAE World Congress & Exhibition, 2007*: SAE International.
- [146] K. Athanasas and I. Dear, "Validation of complex vehicle systems of prototype vehicles," *IEEE transactions on vehicular technology*, vol. 53, no. 6, pp. 1835-1846, 2004.
- [147] H. Schuette and P. Waeltermann, "Hardware-in-the-loop testing of vehicle dynamics controllers—a technical survey," SAE Technical Paper0148-7191, 2005.
- [148] Z. Filipi *et al.*, "Engine-in-the-loop testing for evaluating hybrid propulsion concepts and transient emissions-HMMWV case study," in *SAE World Congress & Exhibition, USA, 2006*: SAE Technical Paper.
- [149] J. Allen, "Simulation and Test Systems for Validation of Electric Drive and Battery Management Systems," in *Aerospace Electronics and Avionics Systems, 2012*: SAE International.
- [150] H. Fathy, Z. Filipi, J. Hagen, and J. Stein, "Review of hardware-in-the-loop simulation and its prospects in the automotive area," *Ann Arbor*, vol. 1001, pp. 48109-2125, 2006.
- [151] F. Mocera and A. Somà, "Study of a Hardware-In-the-Loop bench for hybrid electric working vehicles simulation," in *Ecological Vehicles and Renewable Energies (EVER), Twelfth International Conference on, 2017*, pp. 1-8: IEEE.
- [152] T. Schulte and J. Bracker, "Real-time simulation of BLDC motors for hardware-in-the-loop applications incorporating sensorless control," in *Industrial Electronics, 2008. ISIE 2008. IEEE International Symposium on, 2008*, pp. 2195-2200: IEEE.
- [153] M. Awadallah, P. Tawadros, P. Walker, and N. Zhang, "Comparative fuel economy, cost and emissions analysis of a novel mild hybrid and conventional vehicles," *Proceedings of the Institution of Mechanical Engineers, Part D: Journal of Automobile Engineering*, p. 17, November 8, 2017 2017.
- [154] M. Awadallah, P. Tawadros, P. Walker, and N. Zhang, "Dynamic modelling and simulation of a manual transmission based mild hybrid vehicle," (in English), *Mechanism and Machine Theory*, vol. 112, pp. 218-239, June 2017 2017.
- [155] M. Awadallah, P. Tawadros, P. Walker, and N. Zhang, "A Comparative Fuel Analysis of a novel HEV with conventional vehicle," in *Vehicular Technology Conference (VTC Spring), 2017 IEEE 85th*, Sydney, Australia, 2017, pp. 1-6: IEEE.
- [156] M. Awadallah, P. Tawadros, P. Walker, and N. Zhang, "Impact of Low and High Congestion Traffic Patterns on a Mild-HEV Performance," in *SAE 2017 International Powertrains, Fuels & Lubricants Meeting*, Beijing, China, 2017: SAE International.
- [157] M. Awadallah, P. Tawadros, P. Walker, and N. Zhang, "A Low-Cost and Novel Approach in Gearshift Control for a Mild-Hybrid Powertrain," in *IEEE Transportation Electrification Conference and Expo (ITEC), 2017 IEEE*, Chicago, Illinois, USA, 2017, pp. 754-760: IEEE.
- [158] M. Awadallah, P. Tawadros, P. Walker, and N. Zhang, "A System Analysis and Modeling of a HEV based on Ultracapacitor Battery," in *IEEE Transportation Electrification Conference and Expo (ITEC), 2017 IEEE*, Chicago, Illinois, USA, 2017, pp. 792-798: IEEE.
- [159] M. Awadallah, P. Tawadros, P. Walker, and N. Zhang, "Selection and Characterisation of PMSM motor for mild HEV Applications," in *29th Electric Vehicle Symposium 2016 (EVS29)*, Montréal, Québec, Canada, 2016, pp. 1276-1286: Electric Drive Transportation Association (EDTA).
- [160] M. Awadallah, P. Tawadros, P. Walker, and N. Zhang, "Eliminating the torque hole: Using a mild hybrid EV architecture to deliver better driveability," in *2016 IEEE Transportation Electrification Conference and Expo, Asia-Pacific (ITEC Asia-Pacific)*, Busan, South Korea, 2016, pp. 173-179: IEEE.
- [161] M. Awadallah, P. Tawadros, P. Walker, and N. Zhang, "Comparative System Dynamic Modeling of a Conventional and Hybrid Electric Powertrain," in *Power Engineering - International conference on Power Transmissions (ICPT 2016)*, Y. S. Datong Qin, Ed. Chongqing, China: CRC Press, 2016, pp. 231-238.
- [162] M. Awadallah, P. Tawadros, and N. Zhang, "Rapid Prototyping and Validation of Mars 0913 Brushless Motor to Develop Mild HEV," in *The 7th TM Symposium China (TMC2015)*, Shanghai, China, 2015, vol. 1, pp. 92-98: SAE-China, 2015.
- [163] M. Awadallah, P. Tawadros, P. Walker, and N. Zhang, "Hardware-In-The-Loop Simulation For The Design And Testing Of Motor In Advanced Powertrain Applications," in *IEEE International Symposium on Industrial Electronics (ISIE)*, Cairns, Australia, 2018: IEEE.